IMPACT PERFORMANCE OF STEEL-CONCRETE-STEEL SANDWICH STRUCTURES

KAZI MD. ABU SOHEL

NATIONAL UNIVERSITY OF SINGAPORE
2008

IMPACT PERFORMANCE OF STEEL-CONCRETE-STEEL SANDWICH STRUCTURES

KAZI MD. ABU SOHEL

(B.Sc. Eng, BUET, M.Sc. Eng., BUET, M. Eng., NUS)

A THESIS SUBMITTED

FOR THE DEGREE OF DOCTOR OF PHILOSOPHY

DEPARTMENT OF CIVIL ENGINEERING

NATIONAL UNIVERSITY OF SINGAPORE

2008

Acknowledgements

The author wishes to express his sincere gratitude to his supervisors, Prof. Liew Jat Yuen, Richard and Prof. Koh Chan Ghee for their personal commitment, patience, interesting discussion, invaluable guidance and constructive advices throughout the course of this study. The author would also like to thank Assoc. Prof. Tan Kiang Hwee and Assoc. Prof. Wee Tiong Huan for their helpful suggestions and comments.

The author's heartfelt appreciation is dedicated to Dr. Chia Kok Seng, Dr. Lee Siew Chin, Dr. Dai Xuexin and Mr. Wang Tongyun for their contributions and continuous supports.

Sincere thanks are also extended to the Maritime and Port Authority of Singapore, and Keppel Offshore & Marine Ltd for providing the research grant through the Centre for Offshore Research & Engineering, NUS.

The kind assistance from all the staff members of the NUS Concrete and Structural Engineering Laboratory is deeply appreciated. Special thanks goes to Ms. Tan Annie, Mr. Ang Beng Oon, Mr. Koh Yian Kheng, Mr. Choo Peng Kin and Mr. Ishak Bin A Rahman for their continuous support during experimental pace of the project.

Finally, special thanks and loves go to his wife (Saima Sultana), son, parents and friends for their moral supports, mutual understanding and constant loves. Thank you for making this study possible and May God bless all of you…

TABLE OF CONTENTS

Chapter 7 Finite element analysis

Summary

The aim of this research is to assess the impact performance of Steel-Concrete-Steel (SCS) sandwich structures comprising a concrete core sandwiched in between two steel plates which are interconnected by J-hook connectors. Specifically, novel J-hook connectors that are capable of resisting tension and shear have been developed for this purpose and their uses are not restricted by the concrete core thickness (compare to Bi-Steel). The J-hook connectors are firstly welded to the two face plates which are then interlocked by filling the gap between the face plates with concrete to form composite sandwich structures. Lightweight concrete of density < 1450 kg/m^3 is used to reduce the overall weight of the sandwich structures.

Shear transfer capacity of the J-hook connectors between steel plate and concrete is similar to headed stud connectors confirmed by the push-out tests. Twelve sandwich beam specimens have been tested to evaluate the flexural and shear performance subjected to static point load. Parameters investigated include degree of composite action, concrete with and without fibres and concrete strength. Using Eurocodes as a basis of design, theoretical model is developed to predict the flexural and shear capacity considering partial composite and enable construction of sandwich structures with J-hook connectors. Compared with test results, the predicted capacity is generally conservative if brittle failure of connectors can be avoided. Test evidence also shows

that inclusion of 1% volume fraction of fibres in the concrete core significantly increases the beam flexural capacity as well as its post-peak ductility.

Impact tests were carried out by dropping free weights on to sandwich beams and slabs to investigate their structural response against impact loads. Test results revealed that the proposed J-hook connectors provide an effective means to interlock the top and bottom steel face plates, preventing them from separation during impact. The use of fibres in concrete core and J-hook connectors enhances the overall structural integrity of the sandwich beams and slabs when compared with those without such enhancement. If the impact area is small, low velocity impact by large mass on SCS sandwich slabs is more likely dominated by local punching.

Contact law for sandwich structures is proposed to predict the contact impact force and local indentation during impact. To validate this contact law, small sandwich panels (300 mm ×300 mm) were tested. The developed contact law has been used to predict the impact forces for the beams and slabs. The elastic-plastic dynamic analysis has been carried out to predict the global deformation history of the SCS sandwich structures. Combining both steel plate and shear connector tensile capacity, punching model has been proposed for designing of SCS sandwich slabs. The experimental results were used to verify the analytical solution and it was found that the analytical results agree well (about 93% of accuracy) with experimental results.

In the final part of this research, three-dimensional FE models were developed to predict the local as well as global responses of SCS sandwich structures due to low velocity impact. Using discrete beam element to model the interconnection between J-

hooks, the finite element analysis of the specimens predicted the local and global responses of the slabs and beams with reasonable accuracy. It is found that the steel plate tends to separate from concrete due to impact but the J-hook connectors prevent the separation.

The SCS sandwich structures with interconnected J-hook shear connectors can be used for structural decking purposes and they have better impact performance than SCS sandwich structures with overlapping stud connectors. The analysis methods and numerical models developed in this dissertation are the first reported research in predicting the response of SCS sandwiches with lightweight concrete under low velocity impact and static loading.

List of tables

List of figures

List of symbols

Δ	Total central deflection of a sandwich beam
Δ_1	Flexural deflection of a sandwich beam
Δ_2	Shear deflection of a sandwich beam
Δt	Time step
$\Delta\sigma_m$	Deviatoric stress limit for the maximum failure surface
δ	Indentation depth
δ_{cr}	Critical indentation depth at which steel plate become plastic
δ_m	Maximum indentation depth at maximum contact force
δ_p	Permanent indentation depth
ε_r	Radial strain
ε_θ	Circumferential strain
$\dot{\varepsilon}_d$	Dynamic strain rate
$\dot{\varepsilon}_s$	Quasi static strain-rate
ϕ	Shear modulus reduction factor for cracked concrete
γ_a	Partial material safety factor for steel
γ_c	Partial material safety factor for concrete
γ_v	Partial safety factor for stud
ν	Poison's ratio
ρ	Material density
σ	Stress
σ_c	Compressive stress
σ_0	Plastic tensile strength of steel plate
σ_t	Tensile stress
σ_y	Yield strength of steel
σ_{yd}	Dynamic yield strength of steel
σ_u	Ultimate tensile strength of steel

τ_{FRC}	Shear strength of FRC
τ_{plain}	Shear strength of plain concrete
τ_{Rd}	Design shear resistance of concrete
ω	Natural circular frequency
A_s	Cross sectional area of steel face plate or stud
A_{sw}	Total cross sectional area of the J-hook connector within the cross section
a	Radius of deformed zone at impact point
a_v	Shear span of beam
b	Width of a SCS sandwich section or beam
b_s	Length of angle connector
C	Damping coefficient
D	Flexural rigidity of SCS beam section
d	Bar diameter
E_{cm}	Secant modulus of the concrete
E_c	Modulus of elasticity of concrete
E_s	Modulus of elasticity of steel
F	Force
F_{du}	Ultimate force carrying capacity of impact damaged beam
F_{el}	Predicted static force using elastic theory
$F_{faceplat}$	Plastic membrane force in the steel plate due to local force
e	
F_m	Maximum contact force
F_p	Plastic resistance of SCS sandwich slab
F_{pl}	Predicted plastic load using plastic approach
F_t	Tensile capacity of the J-hook connectors within concrete block
f_{ck}	Characteristic compressive strength concrete cylinder
f_c	Compressive strength of concrete cylinder
$f_c^{'}$	Uniaxial compressive strength of concrete
f_{cu}	Concrete cube compressive strength
f_t	Tensile strength of concrete
G	Shear modulus
$G_c^{/}$	Effective shear modulus
h	Depth of the equivalent truss

h_c	Concrete core thickness
h_s	Height of the shear connector
h_t	Total thickness of the sandwich section
L	Span length of SCS sandwich beam or side length of SCS sandwich slab
L_h	Half length of beam
K	Contact stiffness
K_e	Elastic contact stiffness
K_p	Plastic contact stiffness
k_e	Elastic stiffness of beam
k_r	Unloading stiffness of beam
K_{sc}	Shear connector stiffness
k_t	Stiffness reduction factor for the tension steel plates
k_c	Stiffness reduction factor for the compression steel plates
M	Total mass (m_s+m_b)
$M_{pl.Rd}$	Plastic moment capacity of sandwich section
M_{ult}	Ultimate moment capacity of sandwich section
M_{Sd}	Design bending moment
m_b	Total mass of beam
m_e	Effective mass
m_p	Total mass of SCS sandwich slab
m_{pl}	Plastic moment per unit length
m_s	Mass of the projectile
N	Number of time step
$N_{c.Rd}$	Compressive force in the compression steel plate
$N_{cu.Rd}$	Ultimate compressive force in concrete
N_a	Number of shear connectors provided between maximum and zero moment
N_0	Radial force in the steel plate
N_p	Number of shear connectors between zero and maximum moment for partial composite action
N_s	Number of shear connectors between zero and maximum moment for full composite action
$N_{t.Rd}$	Tensile force in the steel plate
n	Modulus ratio between steel and concrete ($n=E_s/E_c$)
P_{cRd}	Design shear resistance of a shear connector attached to the compression plate

P_{Rd}	Design shear resistance of stud shear connector
P_R	shear resistance of the welded shear connector
P_{Rk}	Characteristic shear resistance of a welded shear connector
P_{tRd}	Design shear resistance of a shear connector attached to the tension plate
p	Pressure
R	Radius of a circular plate
R_c	Contact radius
R_i	Radius of the projectile head
R_u	Plastic resistance force of beam
S	Shear stiffness of the SCS beam section
S_s	longitudinal spacing of shear connectors
t	Time
t_c	Thickness of steel plate in compression
t_s	Thickness of steel plate
t_t	Thickness of steel plate in tension
V	Transverse shear resistance of SCS section
V_c	shear resistance of the concrete core
V_f	Fibre volume faction expressed as percentage
V_0	Impact velocity
V_p	Punching resistance
$V_{pl.Rd}$	Design shear resistance in absence of a moment
V_{Rd}	Design ultimate transverse shear resistance
V_s	Shear contribution due to the presence of J-hook connectors
V_{Sd}	Design shear force
w	deflection
w_e	Elastic displacement
w_m	Maximum deflection
w_p	Displacements of the projectile
w_{res}	Residual deflection
x	Depth of the plastic neutral axis from the inner surface of compression plate
y_{du}	Deflection at ultimate load of impact damaged beam
y_m	Distance from neutral axis to the top of compression plat
z	The position of the neutral axis (elastic)

1 Introduction

1.1 Overview

Steel-Concrete-Steel (SCS) sandwich composite construction, also known as double skinned composite, is a structural system consisting of a concrete core, sandwiched between two relatively thin steel plates, connected to the concrete by mechanical shear connectors. This form of construction combines the advantages of both steel and reinforced concrete systems to provide protection against impact and blast. It allows pre-fabrication of large panels in factory and enables rapid installation into the main structure dramatically reducing fabrication cost and construction time. The two face plates act as permanent formwork during construction providing impermeable skins, which are highly suited for marine and offshore applications. In addition, the flat steel surfaces can be readily protected, inspected and tested so that the integrity of the structure can be assured throughout its service life. The structural performance of SCS sandwich system has shown its superiority over traditional engineering structures in application requiring high strength, high ductility, as well as high energy absorbing capability (Sohel et al. 2003, Oduyemi and Wright, 1989).

The concept of SCS sandwiches began in 1970s when Solomon et al. (1976) proposed an alternative form of roadway decking for long and medium-span bridges. The innovative concept of using shear connector in SCS sandwich construction began in 1985, and this type of construction was originally devised for use in Conway river

submerged tube tunnel by a team of consultants in Cardiff, UK (Tomlinson et al., 1989). Since then this system has been considered for a variety of offshore and onshore structures including oil production, storage vessels, ship hull, caissons, core shear wall of tall buildings, and impact and blast resistance structures.

Low velocity and large mass impacts may be expected for civil, marine and offshore structures in their service life. For this reason, there is an increasing awareness of the effect of foreign object impacts termed as low velocity impacts on structures used in marine, offshore and other civil structures. In SCS sandwich structure, steel have a high fracture toughness and therefore high levels of resistance against impact loads. But concrete offer very little resistance to impact load, yet inclusion of randomly oriented discrete discontinuous fibres improves many of its engineering properties, especially against impact or abrasive loading (Shah, 1987). The concept of using fibres for such purposes is an old one and has been reported to be in existence for 3500 years (Bentur and Mindess, 1990). Use of natural fibres, namely coir, cellulose, sisal, jute, etc. for structural purposes in concrete have been studied extensively. However, due to concerns of their long-term performance (Zollo, 1997), metallic and polymer fibres are widely used in fibre reinforced concrete.

1.2 Background

The potential uses of SCS sandwich construction are diverse, including submerged tube tunnels, protective structures, building cores, basement of multi-storey building, bridge deck (Bowerman et al., 2002; Xie et al., 2007; Zhao and Han, 2006), gravity seawalls, floating breakwater, anti-collision structures, nuclear structures, liquid containment, ship hulls and offshore structures, in which resistance of impact and

explosive loads is of prime importance. However, at present, applications of this form of construction are limited by the thickness and weight of the concrete core making it less suitable for offshore uses. The present research work explores the use of lightweight concrete (LWC) materials to replace the conventional normal weight concrete for SCS construction. Lightweight concrete core of density less than 1500 kg/m^3 is found to be feasible for the construction of ship hulls, bridge decks and building floor slabs (Dai and Liew, 2006). Lightweight concrete is a good insulator; this implies better fire performance and acoustic property than conventional stiffened plate construction. SCS sandwich system can be further optimized by reducing the thickness of the core and maintaining the overall structural performance of the sandwich systems.

Currently, there are two types of mechanical connectors (Figs. 1.1 and 1.2) used in SCS sandwich construction. The first type is the conventional headed stud construction in which the studs are welded to the steel plates before concrete is cast. The resistance of the two steel face plates against tensile separation depends on the pull out strength of the headed studs. The conventional headed studs are installed on the steel plate and thus there is no restriction on the core thickness and thus making the casting of concrete easier. The second type is Bi-Steel connector in which steel round bar is rotated at high speed and opposite external force is applied to the steel face plates generating frictional heat that fuse the bar and the plates together (Bowerman et al., 2002). The Bi-Steel SCS system can only be fabricated in a factory environment, which reduces site work and improves the quality of the construction. The Bi-Steel connectors provide direct connection to the two face plates allowing effective shear transfer even without the presence of concrete core. The only disadvantage of such

method is that the core thickness must not be too thin (≥ 200 mm) to restrict the placement of the Bi-Steel cross connectors. To overcome all these disadvantages of using headed stud and Bi-Steel connectors in SCS sandwich structures, it is necessary to develop new type of shear connector which can interconnect both top and bottom steel face plates and their uses will not be restricted by the concrete core thickness.

Most of the previous studies have been focused on the strength capacity of sandwich structures under static and quasi-static loading (Oduyemi and Wright 1989; Narayanan et al., 1994; Xie et al., 2007; McKinley and Boswell, 2002). Design and construction guides for SCS sandwich with headed stud and Bi-Steel are available in the literature (Bowerman et al., 1999; Narayanan et al., 1994). However, the performance of the SCS sandwich structures under impact load has not been explored extensively. Very limited literature on impact behaviour of SCS sandwich structures is available (Sohel et al. 2003; Corbett 21993). Sohel et al. (2003) conducted impact tests on SCS sandwich beams with angle shear connectors welded on the face plates. The test specimens were failed by tensile separation of the face plates, local buckling of face plates and crushing of concrete core leading to poor impact performance.

Impact with dropping and floating objects or moorings can cause local indentation of the steel face plate, permanent compression of the underlying core material, local damage of core and formation of interfacial cracks leading to the loss of composite action. This dropping object impact is generally termed as low velocity impact and the velocity range is generally 1.0 to 10 m/s which can be simulated by mechanical drop weight or pendulum test machine (Richardson and Wisheart, 1996). During the impact of a dropping object or projectile on a sandwich structure, two types of physical

deformation occur; (1) local indentation, and (2) global structural deformation. Thus, appropriate model is needed to predict these physical deformations and impact force, which can be used for punching and shear characterization of the sandwich structures. Several researchers (Olson, 2002; Yang and Sun, 1982; Abrate, 1997; Hazizan and Cantwell, 2002) used Hertz contact law to predict the localized deformation. However, this is inappropriate for sandwich structures containing low strength core compared to face plate strength, since the indentation of a sandwich structure is predominantly a result of core crushing (Koller, 1986; Abrate, 1997; Zhou and Strong, 2004; Hoo Fatt and Park, 2001). Generally, for a specific shape of projectile, the local indentation depends on the core material and face plate properties. In SCS sandwich structure, core materials are mainly composed of cementitious material which is brittle in nature. However, when confined it shows some elastic-plastic behaviour (Lahlou et al. 1999). This behaviour needs to be considered to model the local indentation of SCS sandwich panel.

Like local indentation, appropriate dynamic model is also necessary to get the global response of the sandwich structures. Several dynamic models which include single-degree of freedom system (Lee, 1940), two degrees of freedom system (Suaris and Shah, 1982) and spring mass model (Shivakumar et al., 1985) are used to model the dynamic behaviour of beams and panels. The aforementioned models were limited to elastic impact of beams and plates. If, however, the impact load causes the structure to become plastic, then it is necessary to consider this plastic behaviour in the dynamic model and can be modeled using an elastic-plastic SDOF system (Biggs, 1964).

1.3 Objectives and Scope

In view of the preceding discussion, the objective of this research is to study the behaviour of SCS sandwich structures subject to drop weight impact loading and to evaluate the potential of SCS sandwich system with innovative J-hook connectors as impact resistant system which can be used in deck-like structures. To achieve this main objective, the specific objectives are set as follow

i) To carryout static experiments, investigating systematically the role and efficiency of J-hook connectors in enhancing the behaviour and strength of the new form of SCS sandwich beams.

ii) To develop analytical models to predict the flexural capacity of the sandwich sections under static load.

iii) To experimentally investigate the structural performance of the proposed sandwich beams and slabs under impact load.

iv) To develop dynamic models to reflect the effect of J-hook connectors on the impact response of the SCS sandwich beams and slabs.

v) To conduct finite element study to predict the local damage and global response the sandwich beams and slabs subjected to low velocity drop-weight impact.

To achieve the aforementioned objectives, the research scopes are as following.

i) One of the scopes includes concept of development of SCS sandwich system with novel shear connector and lightweight concrete infill material. This is one of the main parts of this dissertation. The concept of development of novel shear connector is based on the background study and the innovation of the author. Different types of analytical models, for example truss and tie model to explain force transfer mechanism, provide a tool to generate the novel J-hook shear connectors. In addition, the investigation is also carried out to develop a suitable mix design of structural lightweight concrete (density $\leq$ 1500 kg/m^3 and compressive strength $\geq$ 25 MPa) based on commercially available lightweight aggregate and lightweight sand.

ii) Impact tests on SCS sandwich beams and slabs are conducted to investigate the effects of different parameters on impact resistance. In addition, static tests are carried out to establish the effect of J-hook connectors on the ultimate strength and observe the possible failure modes of SCS sandwich structure. This research addresses the issue of a drop weight impact at low velocities by a relatively large object on SCS sandwich slabs and beams. In the experimental programme, the thickness of the steel plates, the spacing and the type of shear connector and material properties of the concrete are considered. The study is to also focus on the local as well as global damage effect of such an impact. The experimental results are used to verify the numerical and analytical method adopted to simulate the behaviour of SCS sandwich slab.

iii) In addition with analytical model, the commercially available finite element (FE) code LS-DYNA is used to predict the impact response of SCS sandwich structures and verify the results with those obtained from experiment.

It is expected that this research will contribute to existing literature and hopefully lead to the recommendation of design guidelines for practical use of SCS sandwich structure in marine, offshore, bridge and other deck-like structures. The analytical models (static and dynamic) can be used to evaluate the ultimate strength and dynamic response of the SCS sandwich section. In general term, this research is likely to help in developing an understanding on both local (punching) and global response of SCS sandwich structures subject to possible impact by falling objects.

1.4 Outline of the thesis

In Chapter 1, the background of development of the SCS sandwich structure is reported. This chapter also introduces the problem and identifies the need for study with a particular focus on the low velocity impact on SCS sandwich structures. Finally, the main objectives and scope of this research program conducted herein are presented.

Chapter 2 gives a comprehensive review of the available literature on sandwich structures. Major types of shear connectors currently used in composite structures are also summarized in this chapter. Different analytical approaches to analyse of impact responses are summarized highlighting the underlying principles.

The key concept of SCS sandwich structures with J-hook shear connector is described in Chapter 3. To evaluate the flexural strength of the proposed SCS sandwich

structures, analytical solutions are derived in this chapter. Experimental results of 12 beams obtained in this part of study are presented and compared with the analytical results. Test results of ten push out test specimens investigating the effectiveness of J-hook shear connector with different types of concrete are presented, and discussed in detail.

Chapter 4 addresses the local indentation behaviour of SCS sandwich panels with concrete core. This core is assumed to behave as elastic-plastic because the core under the impact point is virtually confined by the two steel plates and the surrounding concrete. Based on this assumption force-indentation relations were developed for different phases of the indentation. The experimental results are used to verify this proposed force indentation relationship.

Chapter 5 addresses the impact behaviour of SCS sandwich beams with J-hook shear connector; where lightweight concrete is used as core. The force-indentation relations developed in previous chapter are then incorporated in the global elastic-plastic dynamic model for SCS sandwich beam. The experimental investigation focuses on the performance of J-hook connector embedded in lightweight concrete core and the measured impact force and central displacement are used to validate the theoretical model.

Chapter 6 describes the impact behaviour of SCS sandwich slabs with J-hook shear connector; where both lightweight concrete and normal weight concrete are used as core. The force-indentation relations developed in previous chapter are then incorporated in the global elastic-plastic dynamic model for SCS sandwich slab. The

experimental investigation focuses on the performance of panel under very large mass impact where local punching is more dominant.

The three-dimensional FE models of SCS sandwich beam and slabs subjected to low-velocity drop-impact are discussed in Chapter 7. Particular interest is given to model the J-hook connectors into the SCS sandwich beams and slabs. The experimental data is also applied to verify the FE analyses results.

Chapter 8 completes the thesis with a set of conclusions derived from present analytical and experimental investigation, and recommendations are made for any future work in the same area.

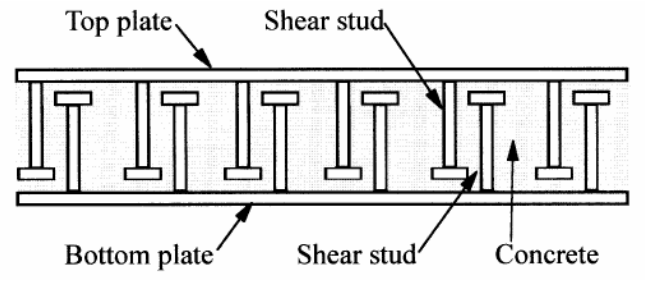

Fig 1.1 SCS sandwich construction with overlapping headed stud connectors

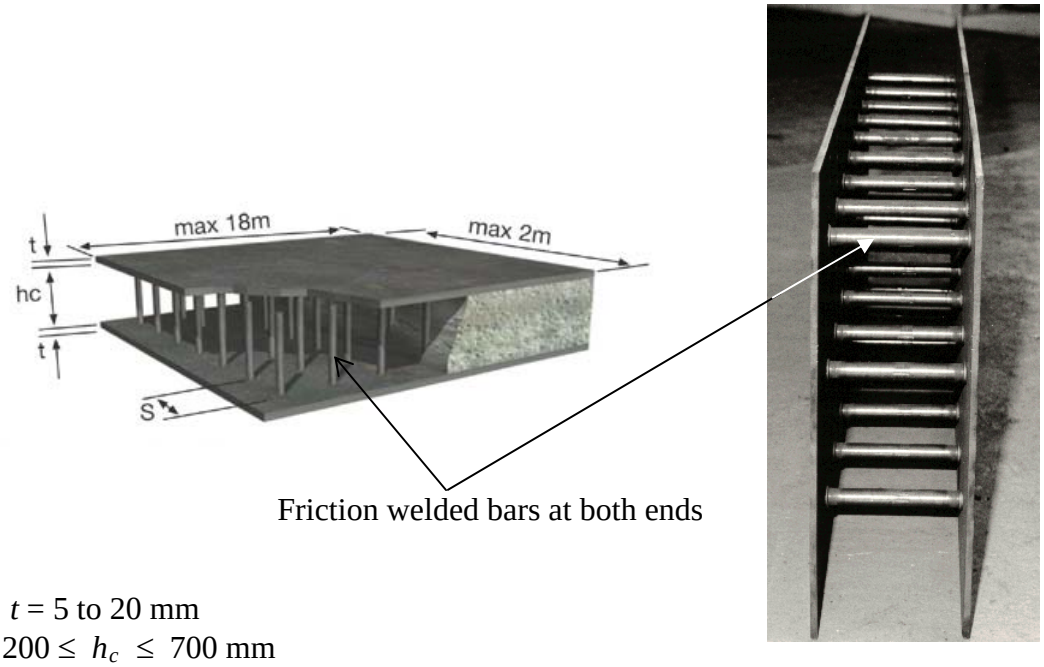

t = 5 to 20 mm
$200 \leq h_c \leq 700$ mm
Bar diameter 25 mm, min. S = 200 mm

Fig. 1.2 Bi-Steel sandwich panel

2 Literature review

2.1 General

Different forms of SCS sandwich structures are available in literature. Among them, the SCS sandwich system with shear connectors is considered for a variety of offshore and onshore structures including oil production, storage vessels, caissons, core shear wall of tall buildings, and impact and blast resistance structures. In this chapter, a concise history of the development of SCS sandwich structures is given and the common definitions and fundamental theory underlying impact loading are discussed.

2.2 Steel-Concrete-Steel (SCS) sandwich

In composite structures steel and concrete are used to form a composite unit. The first applications of this composite construction were in the USA (Bowerman et al., 2002). In these early composite constructions, the interaction between concrete and steel was provided primarily by interface bonding. However, this type of bonding was found weak and prone to failure (Bowerman et al., 2002). From 1950s, the mechanical shear connector was begun to be used in composite constructions to provide bond between the concrete and steel (Johnson, 2004). By providing shear connectors (mainly headed shear connectors), concrete slab integrates extremely well with steel to provide additional rigidity. The main application of the headed stud connector was to composite girders and floor systems, but the headed stud also found a variety of other

applications. Interest was renewed in the mid '80s when Tomtinson et al., (1989) proposed a studded form of SCS sandwich composite for an immersed tube tunnel for the Conway river crossing (Bowerman et al., 2002). Further modification in SCS sandwich construction was done by CORUS (prev. British Steel) and named their patented product as Bi-Steel (Pryer and Bowerman 1998).

2.2.1 SCS sandwich without shear connectors

The first research on SCS sandwich beams and slabs without shear connector were done by Solomon et al. (1976). This form of SCS sandwich consists of a concrete core to which flat steel plates are attached by means of epoxy resin adhesive. The behaviour of these sandwich beams was similar to reinforced concrete beams without shear reinforcement. The failure of the most beams occurred in a shear-tension mode and their proposed formula for calculation the ultimate shear resistance (SI unit) of the beam base on ACI-ASCE equations (ACI-ASCE committee 326, 1962) is as following

$$V_a = bh_c\left((0.14\sqrt{f_{cu}} + 17.2\frac{\rho h_c}{a_v}\right) \qquad (2.1)$$

where $\rho = A_s / bh_c$ in which A_s is the cross-sectional area of tensile steel plate; b is the width of the beam; h_c is the depth of the concrete core; and a_v is the shear span of the beam.

The SCS sandwich slabs with adhesive bonding showed that the failure mode was in punching. The critical factor under patch loads appeared to be the strength of the concrete in punching shear.

Bergan and Bakken (2005) proposed a concept for design of ship and other marine structures that is based on sandwich plates made of steel plates bonded with lightweight concrete core by adhesive. Special, extremely lightweight concretes were developed for this purpose. A cellular structural concept was developed for very large structures (Bergan et al., 2006). They showed that their concept comes out with no more weight than steel ships and has an important potential for savings since nearly 40 percent of the total weight is made up by relatively inexpensive concrete. Experiment on SCS sandwich beams in which lightweight concrete was used as core materials to reduce the overall weight of the sandwich beams was conducted. Without mechanical shear connector, shear failure in the concrete core was the failure mode of the SCS sandwich beams where chemical glue was the shear transfer medium between steel face plates and concrete core.

2.2.2 SCS sandwich with angle shear connectors

The performance of SCS sandwich system without shear connector was poor in shear. To improve the performance, angle shear has begun to use in SCS sandwich structures. This type of sandwich structures has been applied to port and harbour facilities since early 1980s (Malek et al. 1993). The static test on sandwich beams with angle shear connector was conducted by Malek et al. (1993) and Sohel (2003). The failure mode was shear failure in the concrete core. Steel plate separation occurs when impact was applied at the centre of the beam (Sohel et al. 2003).

2.2.3 SCS sandwich with headed shear connectors

The performance of SCS sandwich system without shear connector was poor in shear. Similar behaviour was also observed for beams with angle shear connectors (Malek et

al., 1993; Sohel et al. 2003). The system was renewed by providing overlapping shear connectors (Fig. 1.1). The concept behind using mechanical shear connector is to allow the shear transfer between concrete to the steel and vice versa, and prevent vertical separation of the concrete and steel components. The basic information and understanding of the behaviour of studded SCS sandwich beams were known by the tests conducted by Oduyemi and Wright (1989). Early pilot tests (Write et al., 1991) were carried out on individual half scale and full-scale models and used to verify analytical and design assumptions made in specific projects. Since then many tests have been reported on SCS sandwich structures with headed stud shear connectors.

Ultimate load carrying capacity of the SCS sandwich composite beam with headed stud connectors is governed by three possible failure modes: flexural failure, horizontal slip failure and vertical shear failure. These modes may or may not be preceded by local buckling of compression plate. From tests results (Write et al., 1991), it was found that the shear connection should be designed as 55% in the tension zone and 80% in the compression zone to its ultimate strength due to the requirement of sustained combined shear, axial and bending stresses plus additional stresses.

Design criterion for double skin composite immersed tube tunnels was reported by Roberts et al., (1995) and Narayanan et al., (1997). It was suggested that to determine the longitudinal forces, tunnel element could be idealised as a simple beam of closed hollow cross-section, closed structures subjected to external pressures, and the analysis performed on a unit length basis, assuming plane strain conditions. It was also recommended that the analysis of internal forces in tunnel unit should be carried out assuming linear material and linear geometric behaviour.

Roberts et al., (1996) carried out a series of quasi-static load tests on SCS sandwich beams of low and high span/depth ratios subjected to four-point loading. The primary modes of failure observed in their tests were tension plate yielding and slipping. Significant shear cracking occurred in all the short span beams but was not the primary cause of failure, indicating that the stud connectors provided adequate transverse shear resistances. The contribution of external steel plates on transverse shear is relatively small, and therefore the design ultimate transverse shear resistance V_{Rd} should be determined from the equations,

$$V_{Rd} = \tau_{Rd}\, b\, h_c \tag{2.2}$$

$$\tau_{Rd} = \frac{f_{ck}}{20\ \gamma_c} + \frac{0.5\, n_0\, A_s\, f_u}{b\, s_t \gamma_a} \tag{2.3}$$

where A_s, f_u, h_c and $s_t \leq 0.75\, h_c$ are the cross sectional area, ultimate tensile strength, depth of the concrete core and longitudinal spacing of the smallest diameter full depth or overlapping stud connectors, and n_0 is the number of such connectors across the width of the section (Fig. 2.1). τ_{Rd}, b, f_{ck}, γ_a and γ_c are the design shear resistance of concrete, width of sandwich section, concrete cylinder characteristic compressive strength, partial material safety factor for steel and partial material safety factor for concrete respectively. The factor 0.5 in the last term of Eq. 2.3 acknowledges that the full resistance of the concrete and stud connectors is unlikely to be mobilized simultaneously. They also suggested that sandwich beams subjected to combined bending and shear should be designed in accordance with generally conservative interaction equation

$$\left\{\frac{V_{Sd}}{V_{pl.Rd}}\right\}^2 + \left\{\frac{M_{Sd}}{M_{pl.Rd}}\right\}^2 \leq 1 \tag{2.4}$$

in which M_{Sd} and V_{Sd} are the design bending moment and design shear force respectively. $V_{pl.Rd}$ and $M_{pl.Rd}$ are the design shear resistance and design plastic moment resistance respectively.

The ultimate moment resistance of SCS sandwich section subjected to pure bending is developed based on the following assumptions (Narayanan et al., 1994).

(1) A rectangular stress block of depth $0.9x$ for the concrete as per BS8110-part 1: 1997 (where 'x' is the depth of the plastic neutral axis from the interface of the compression plate and the concrete).

(2) The concrete beneath the plastic neutral axis does not contribute to the resistance of the section.

(3) The forces in the steel plates depends on material yield strength and on the strength of the shear connectors to transfer the shear load from the steel plate to the concrete core (see Fig. 2.1).

The ultimate compressive force in concrete is given by

$$N_{cu.Rd} = 0.45 f_{cu} b(0.9x) \tag{2.5}$$

Where b is the width of the beam. Alternatively, concrete cube strength, f_{cu} may be replaced by $1.26 f_{ck}$ and where f_{ck} is the characteristic cylinder strength of concrete.

From equilibrium of forces

$$N_{t.Rd} = N_{c.Rd} + N_{cu.Rd} \tag{2.6}$$

The depth of plastic neutral axis can be obtained from Eqs. (2.5) and (2.6)

$$x = \frac{2.47}{f_{cu} b}\left[N_{t.Rd} - N_{c.Rd}\right] \tag{2.7}$$

If moments are taken about the plastic neutral axis, the moment of resistance of the section is:

$$M_{pl.y.Rd} = N_{c.Rd}\left[x + \frac{t_c}{2}\right] + N_{cu.Rd}(0.55x) + N_{t.Rd}\left[h_t - x - t_c - \frac{t_t}{2}\right] \qquad (2.8)$$

Similarly, if moments are taken about the centre of compression plate the moment resistance of the section is given by

$$M_{pl.y.Rd} = N_{t.Rd}\left[h_c + \frac{t_c}{2} + \frac{t_t}{2}\right] - N_{cu.Rd}\left[0.45x + \frac{t_c}{2}\right] \qquad (2.9)$$

To prevent local buckling in the compressive plate, the expression (Eq. (2.10c)) for the spacing of connectors comes from the analysis of critical buckling load for fixed ends plate and the analysis done by Roberts et al. (1996) as following

$$\sigma_{cr} = \frac{4\pi^2 EI}{(\text{area})(\text{Length})^2} = \frac{4\pi^2 E(bt_c^3/12)}{(bt_c)S_s^2} \qquad (2.10a)$$

or $$\frac{S_s}{t_c} = \sqrt{\frac{\pi^2 E}{3\sigma_{cr}}} \qquad (2.10b)$$

Assuming $E = 200\times10^3$ N/mm^2 and $\sigma_{cr} = \sigma_y = 275$ N/mm^2, the spacing of connectors should be governed by

$$\frac{S_s}{t_c} \le 40 \qquad (2.10c)$$

where S_s and t_c are the longitudinal spacing of shear connectors in the compression region and thickness of steel face plate in compression respectively. This limiting spacing for overlapping stud is also provided by the SCS design guide (Narayanan et al., 1994), because no continuous bond exists between the concrete core and steel face plates. Steel face plate therefore remains vulnerable to local buckling under compression. For efficiency and removal of the buckling problem, full composite interaction with continuous bond is required between the core and the steel face plates. This can be achieved by using steel with textured surfaces (Subedi and Coyle, 2002; Subedi, 2003). The textured surface can be prepared by welding Durbar, Expamet and Wavy wire on the steel plate. Test results (Subedi, 2003) confirmed that the

combination of textured surface and mechanical shear connectors in SCS sandwich failed in flexural mode and no local buckling and no interface shear slips were observed during the test. Expamet and Wavy wire were recommended for practical use. It should be bear in mind that inclusion of these extra materials on the steel face plates for surface preparation increases the overall weight of the structures as well as construction cost.

Similar as SCS beams, SCS sandwich panel (or double skin composite (DSC) slab) with overlapping headed shear connectors also showed very high load carrying capacity which was confirmed by both experiment and non-linear FE analysis (Shanmugam et al., 2002). These DSC slabs also exhibited good flexural characteristics and highly ductile behaviour. The test failure modes of these DSC sandwich slabs were failure of shear studs, cracking and crushing of concrete, buckling of steel face plate and punching through failures (Kumar, 2000).

Other than SCS sandwich beams and slabs, performance of SCS sandwich column, bent corner, and T-junction also investigated experimentally by Burgan and Naji, 1998. The performance of bent corner and T-junction was not satisfactory using the conventional headed stud shear connector due to tensile separation failure of tension plate. Measures should be taken to improve the connection between the tension plate and the concrete, i.e. either by increasing the length of the stud connectors or reducing their spacing or both.

2.2.4 Bi-Steel composite panel

To increase the strength and composite action between steel face plates and concrete core in SCS sandwich, further improvement was done in shear connection by providing cross bars to connect the top and bottom steel face pates (see Fig. 1.2). This improved SCS sandwich system called Bi-Steel (Fig. 1.2) is a patent owned by Corus Construction & Industrial (Pryer and Bowerman, 1998). It comprises of two steel facing plates that are fixed in their relative positions by an array of transverse bars connectors. The bar connectors are welded at each end to the steel face plate. The bars are arranged in a closely spaced regular pattern and this is achieved using a high-speed friction welding technology. In practical use, Bi-Steel panels would be welded or bolted together to form a structure which would then be filled with a structural grade concrete (Bowerman et al., 1999) which therefore plays a fundamental role in the performance of the product. Large hydrostatic pressures during concrete placing can be sustained due to the presence of closely spaced shear connectors. The composite action of the steel and concrete together in the Bi-Steel gives it very high strength. The design procedure recommended for the Bi-Steel is to ensure that the tensile plate yields before any other type of failure occurs. The main variables in achieving this are the distance between the steel plates, the thickness of the plates and the spacing of the bars. Bi-Steel panels are factory produced to tight tolerances in flat or curved form, and provide a modular system which addresses the buildability issues such as ease in construction and economical viability. Clubley et al., (2003) reported based on their experimental investigation that the Bi-Steel system has significant shear capacity and this shear strength is affected by several parameters, including plate spacing, connector spacing and shear connector diameter. They also concluded that the Bi-Steel panels have high ductility and deformation capacity.

A series of analytical solutions were presented by McKinley and Boswell, (2002) for determining the elastic and plastic load–deflection behaviour of Bi-Steel beam-type elements with equal plate thickness and loaded in three-point bending. The solutions were then later compared with experimental results. Using doubly reinforced beam concept, the elastic moment capacity of the Bi-Steel section was determined. The post-yield strength of the Bi-Steel panel was based on the plastic behaviour of the stress–strain curve for steel. Xie and Chapman (2006) and Xie et al., (2007) proposed a truss model to analyse the behaviour of Bi-Steel beam capacity. In this truss model, tapering web compression members was proposed for analysis of Bi-Steel beam member forces (Fig. 2.2). The area of concrete in longitudinal compression can be determined from equivalent steel section.

The truss model consists of pin jointed line elements in which the axial stress is uniform across a section. To achieve this, the uniform web thickness over which, according to the equivalent beam model, the stress varies, is replaced by a tapering web across which the stress is constant, with the requirement that the total compressive forces are equal to that in the equivalent beam model, and that the depths of the compression zones y_m are also equal. The depth h of the truss is equal to the distance from the mid-thickness of the bottom plate to the centroid of the compression area (Fig. 2.2 (c)); h is given by Eqs. (2.11) to (2.13).

$$h = \frac{nt_c\left(2h_c + t_c + t_t\right) + \left(y_m - t_c\right)\left[h_c - \left(y_m - t_c\right)/3 + t_t/2\right]}{2nt_c + y_m - t_c} \tag{2.11}$$

where y_m is given by $y_m = -\alpha + \sqrt{\alpha^2 - 2\beta}$ (2.12)

with $\alpha = n\left(t_c + t_t\right) - t_c$; $\beta = -\left(h_c + t_c + t_t\right)nt_t + \left(nt_t^2 - nt_c^2 + t_c^2\right)/2$ (2.13)

where $n = E_s / E_c$ is the modular ratio between steel and concrete. An inherent characteristic of this model is that the plates are connected to the concrete only at the nodal points. That is, there is no bond between steel and concrete, as in reality.

2.3 Lightweight concrete core for SCS sandwiches

Concrete mass is a big challenge in using of SCS sandwich system in marine and offshore structures. However, great advances have been made in recent years with developing special light-weight aggregates for concretes that enable significant reduction in the mass density of concrete. Early attempts to control the voids in the lightweight core by using polystyrene beads as an aggregate were developed by Parton and Shendy (1982) by the introduction of fine sawdust as filler, which was found to give stability to the mixing process, and to give the set material a degree of elastic flexibility and toughness.

Shendy (1991) used Lightweight Expanded Clay Aggregate (LECA) concrete core in Sandwich beam made of dense concrete faces reinforced with steel wire mesh. He showed that this sandwich beam constructed with LECA concrete core can have great advances in terms of the ratio of ultimate load to density, and overall weight. When shear reinforcement in the form of conventional stirrups is provided in the sandwich beams, they behave in a similar manner to dense concrete beams; they can have similar ultimate loads and similar modes of failure, the characteristic sandwich shear failure having been overcome by the reinforcement.

Bergan and Bakken (2005) proposed a concept for design of ship and other type of marine structures that is based on using sandwich plates made of steel skins with

lightweight concrete core. They claimed that special, extremely light concretes had been developed for this purpose. According to their test, strength and fatigue performance were clearly better than anticipated, and showed a real potential for maritime applications.

Another development, known as Sandwich Plate System (SPS), has been made by Intelligent Engineering in cooperation with several industrial partners. Their SPS system comprises two steel surface plates acting compositely with a compact polyurethane core, known as dense elastomer core, in between (Kennedy and Kennedy, 2004). This design has already proven to have a significant potential for lightweight internal deck-like structures and strengthening of weakened areas in ships.

2.4 Shear connectors used for SCS sandwich constructions

On a composite structure, both steel and concrete have to work together. The connection between the two materials is usually achieved by using steel connectors, which may have different shapes (Figs 2.3 and 2.4). The most widely used type of connector is the headed stud. The strength and stiffness of a composite section depends on the degree of composite action between concrete and steel components. The degree of composite action is related to the geometrical and mechanical properties of the shear connectors and the concrete.

According to Eurocode 4 (1994), the design resistance of an angle connector welded to the steel beams should be determined from

$$P_{Rd} = 10 b_s h_s^{3/4} f_{ck}^{2/3} / \gamma_v \qquad (2.14)$$

where b_s, h_s,f_{ck} and γ_v are the length, height of the angle in mm, characteristic strength of concrete in N/mm^2 and partial safety factor respectively. The partial safety factor γ_v should be taken as 1.25 for the ultimate limit state.

For headed shear stud, Eurocode 4 (1994) suggests that the ultimate strength (P_{RK}) can either be determined from push shear test or taken conservatively as the lesser of the following (EC4: Part 1:1)

(a) Stud ultimate strength criterion

$$P_{RK} = 0.8\sigma_u(A_s) \qquad (2.15)$$

(b) Concrete strength criterion

$$P_{RK} = 0.29\alpha d^2\sqrt{f_{ck}E_{cm}} \qquad (2.16)$$

The design resistance P_{Rd} is determined by $P_{Rd} = P_{RK} / \gamma_v$ where P_{Rd} = design shear resistance of the headed stud; σ_u = tensile strength of the stud material ($\sigma_u \leq 500$ N/mm^2); E_{cm} = secant modulus of the concrete; d = diameter of the stud shank; α = a coefficient; γ_v = partial safety factor and should be taken as 1.25. The coefficient α can be determined from the following expressions:

$$\alpha = 0.2(h_s/d + 1) \quad \text{for } 3 \leq h_s/d \leq 4 \qquad (2.17)$$

$$\alpha = 1.0 \quad \text{for } h_s/d > 4$$

where h_s is the welded height of the connector.

The strength and stiffness of shear connectors in SCS beams is significantly less than results from push shear tests (Robert et al., 1996) due to combine action of shear and bending moment. Therefore, the design shear resistance of the shear connector

attached to the compression and tension plates, P_{cRd} and P_{tRd} respectively, should be taken as (Narayanan et al. 1994),

$$P_{cRd} = 0.8P_{RK}/\gamma_v \quad (2.18a)$$

$$P_{tRd} = 0.6P_{RK}/\gamma_v \quad (2.18b)$$

where P_{RK} is the characteristic shear resistance of the welded shear connectors.

2.5 Impact behaviour of beams and plates

In many applications, safety considerations may make it necessary to assess the response of a structure to the expected impact loads. Hughes and Beebly (1982) suggested that a structure may be designed to withstand the expected maximum impact loads or stresses using static load design methods. However, as the structural response at higher modes of vibration and at high strain rate is different from the static load response, a different design approach for impact loading is needed (Holt, 1994). The impact creates local damage and overall dynamic structural response in the form of, for example, flexural deformations. Overall dynamic response of the target consists of flexural and shear deformations which may lead to flexural or shear failure.

Impact can be classified as soft or hard impact based on the deformation characteristics of the projectile (drop weight). When the deformability of the projectile is larger than that of target, the impact is said to be 'soft' and this deformation of the projectile during impact consumes energy and hence would result in diminishing local damage or shallower indentation depth (Bangash, 1993). In contrast, little or no deformation arises in the projectile during hard impact and most of the projectile kinetic energy is transmitted to damage the target (Lim, 1999). Hard projectile impact can be further classified as low and high velocity impact based on the velocity of the projectile. The

'low velocity impact' refers to impact in which projectile velocities in the range 1 to 10 m/s. The contact period is such that the whole structure has time to respond to the loading. High velocity impact response is dominated by stress wave propagation through the material, in which the structure does not have time to respond, leading to much localized damage. In this case, effects of boundary condition can be ignored because the impact event is over before the stress wave reached the edge of the structure (Richardson and Wisheart, 1996).

Impact damage in metals is easily detected as damage starts at the impact surface; however, damage in sandwich often begins on the non-impacted surface or in the form of internal cracks in the core (Richardson and Wisheart, 1996). Thus, the characterization of impact damage of a composite sandwich structure is difficult because of its sandwich nature (Hoo Fatt and Park, 2001). There is at present no established method for the design of SCS sandwich composites under impact loads. Furthermore, there is also no generally accepted method for evaluating the impact properties of concrete structures for design, either from the material or structural point of view. The equivalent static load approach is the most commonly accepted, as structural designers are accustomed to this method. But it is recognized and accepted that due to different material behaviour at different strain rates, a rational design approach for impact loading is desirable.

2.5.1 Contact law

To complete the formulation of the impact model, it is necessary to combine the target deformation solution with an appropriate indentation or contact law. Perhaps the biggest landmark in contact mechanics was the work of Hertz on the elastic contact of

semi-infinite solids, published in 1882. Excellent coverage of this theory is given in several books (Goldsmith, 1960; Johnson, 1985; Stronge 2000; Timoshenko and Goodier, 1970). Hertz theory predicts the stress distribution in the contact zone between two bodies having a surface of revolution. It also allows to calculate the normal and shear stress distribution inside the solid. This reveals some interesting and important facts. For example, the maximum shear stress, which is directly related to material failure, occurs below the contact surface, potentially causing undetected plastic yielding. A very commonly used result is the static force-indentation relation for a sphere to sphere contact: (Johnson, 1985):

$$F = K\delta^{3/2} \tag{2.19}$$

where F = normal force pressing the solids together

δ = approach of the two spheres, i.e. total of deformation of both surfaces

K= constant stiffness depending on the elastic and geometrical properties of the two bodies.

It is assumed that contact under an impact situation can be described by a similar law, then (Hughes and Speirs, 1982)

$$F(t) = K\delta^{3/2}(t) \tag{2.20}$$

While this is an idealized picture of impact, it has been used extensively by many researchers in modelling an elastic impact zone and the elastic approach period of an elastic/plastic impact zone.

It is important to note that Hertz formulas are only applicable to non-conformal contacts. In other words, they cannot be used when the radii of curvature at the contact point are too close, such as in journal bearings or plane to plane contact. The contact

area must also remain small compared to the bodies' dimensions and the radii of curvature at the contact point. Consequently, Hertz formulas should be used with caution on materials with large elastic strains such as rubber. Moreover, the assumption to derive this formula is based on contact between two isotropic elastic bodies with smoothed curved surface, i.e. for sandwich structures which is not isotropic along the cross section, this contact law is not valid.

Beyond the elastic loading stage, two other stages are considered, namely elastic-plastic stage and fully plastic stage. In the elastic-plastic stage, the plastic deformation is small enough to be accommodated by an expansion of the surrounding area. As the load increases, the plastic zone grows and the displaced material flows to the sides of the indenter. For this analysis, the rigid-perfectly-plastic material model is commonly used. It assumes that the elastic deformation is small enough to be negligible and the material flows plastically at a constant stress σ in tension. For sphere-sphere contact, Johnson (1985) shows that, under those assumptions, yield will initiate when the mean contact pressure p_m is 1.1σ, and the flow will become fully plastic at about p_m=3.0σ. Stronge (2000), takes the same approach to derive an expression for the restitution coefficient that reflects the dissipation due to plastic work under different conditions of friction. Based on the rigid-perfectly plastic model and Hertz theory of impact, Johnson (1985) calculates the velocity V_y necessary to initiate yield. For a sphere striking the plane surface of a large body, it is shown that:

$$\frac{\rho V_Y^2}{\sigma} = 26\left(\frac{\sigma}{E^*}\right)^4 \tag{2.21}$$

where ρ is the sphere material density and E^* is an equivalent elastic modulus. For example, for a medium hard steel, σ = 1000 N/mm^2 and V_y =0.14 m/s. Naturally, this

velocity is quite low and one should expect that most impacts between metallic bodies involve some plastic deformation.

2.5.2 Analysis of low velocity impact on beams and plates

Goldsmith (1960) provides a comprehensive source of information on analytical methods applied to impact of isotropic beams and plates. In this book, Goldsmith used the normal modes method to determine the dynamic response of an isotropic plate or beam to a rigid impactor. Timoshenko (1913) used normal modes and a Hertz contact law to analyze the deflection of a beam impacted by a projectile. The resulting nonlinear integral equations were solved by numerical integration. Keer and Woo (1984) used integral equations to calculate the pressure distribution in an isotropic circular plate impacted by a projectile with a large radius of curvature producing a large impact area. Moyer and Gashaghai-Abdi (1984) used the finite difference method to find the dynamic response of an isotropic plate subject to a prescribed initial velocity. For sandwich structures with a weak core, it is appropriate to use Reissner–Mindlin plate approximations (Zhou and Strong, 2006). However, one difficulty is that the governing equations involve integral transforms that are too complicated to solve analytically; this problem becomes particularly awkward in the range of large deflection where the effect of membrane stretching becomes significant. In this case, it is necessary to develop a simplified modelling technique to approximate the impact force and obtain an estimate of overall deflection of the structure.

In the range of low velocity impact, the sandwich plate deflection can be approximated as a quasi-static process which employs an energy-balance model together with a lumped parameter force-deflection model. An energy balance provides a simple

solution for maximum impact force but with the limitation of not providing any time dependent information; e.g. the history of the impact force or displacement. In contrast, the lumped parameter model assumes that the structure can be represented by an assemblage of springs and masses which result in a discrete system with a few degrees of freedom rather than a continuum. This representation gives the time history of impact force and deflection of the impact point on the plate. Both models have been applied extensively in the analysis of impact response of composite laminate (Abrate, 2001; Lal, 1983; Mill and Necib, 2001; Shivakumar et al., 1985). Recent investigations have applied the energy balance model to investigate impact response of sandwich beams (Mines et al., 1994; Akil Hazizan M and Cantwell, 2002).

2.5.3 Low velocity impact test on beams and plates

Different test methods like the drop-weight test, Charpy test, swinging pendulum test, explosive test, split Hopkinson bar test, etc., have been developed to carry out impact and impulsive load tests. In the field of low velocity impact, the most widely used (Aymerich et al., 1996; Banthia et al., 1987, 1989; Bentur et al., 1986; Mindess et al., 1987, 1986) impact test setup is the instrumented drop weight impact test set-up in which a mass is raised to a specified height and dropped directly on to the specimen under test, usually a beam or a slab. Dropping the hammer from different heights can vary the applied stress rate.

Impact studies on plain concrete, fibre reinforced concrete and conventionally reinforced beams were carried out extensively (Mindess et al., 1986, 1987; Banthia et al., 1987, 1989) using an instrumented drop-weight impact machine (Benture et al., 1986) capable of dropping a 345 kg mass hammer from height of up to 3m. Inertial

contribution to the recorded impact force by the load cell at high loading rate was established from their investigation. Inertial force of the beam was calculated from the recorded beam acceleration and a method of analysis to account for inertial correction to recorded impact force was developed. Basheer Khan (2000) carried out impact test on fibre reinforced cementitous composite slabs using drop weight impact test machine similar to Banthia et al., (1987). It was found that fibre reinforced concrete is a better material than plain concrete in dynamic situations because of its ductility and increased impact resistance. Gamborva and Schumm (1994) also carried out drop weight impact testing to study the strength and collapse mechanism of slabs reinforced with polyacrylonitrile (PAN) fibres and found marked increase in the punching strength with increasing fibre content. It was found that the fibre content can markedly modify the strength and collapse mechanism, with no major variation in the total energy dissipation during the cracking process. Hughes and Speirs (1982) conducted impact tests on beam by using drop weight impact testing machine and obtained good correlation with their theoretical study. The use of beam vibration theory in conjunction with Hertz's contact law led to an integral equation for the contact force.

Other popular impact testing method, the modified Charpy test setup (Banthia et al., 1994), was used mainly to study tensile impact of cementitious composites. It consists of two supports on which the tensile specimen was fixed. One of the supports (called 'trolley') moves along the horizontal direction and other support as fixed to the base. The trolley was struck by the swinging pendulum of mass 42.5 kg on the impact points located on either side of the specimen and in the same plane as the specimen. Since one support was fixed, the impact causes tensile loading in the specimen. Under impact the specimen fractured and the trolley travelled towards the shock absorbers. On its

way it passed through two photocell assemblies, which were used to record the velocity of the trolley. The two load cells located on the impact face of the pendulum recorded the contact load. Accelerometers were mounted on the trolley and pendulum to measure their accelerations.

Radomski (1981) used a rotating impact machine to conduct test on fibre reinforced cement concretes. This notable test set-up was also used by Balasubramanian et al., (1996) to investigate the impact resistance of steel fibre reinforced concrete. This machine was mainly used for the investigation of metallic specimens under impact loading. This machine can achieve impact velocity up to 50 m/s. The impact loading was imposed by a tup, which was unbolted by an electromagnet and pushed out from the flywheel of the impact machine when the required velocity of rotation was reached. The specimen holders were instrumented using piezoelectric gauges and a photocell assembly triggered them. An oscilloscope captured all the data and a camera was usually used to record the whole event.

Naaman and Gopalaratnam (1983) used an instrumented Tinuis Olsen Dynatup drop weight tower to achieve required loading velocity to investigate impact properties of steel fibre reinforced concrete in bending.

The only method specified by ACI Committee 544 (1982) is the repeated drop weight test (Balasubramanian et al., 1996, Soroushian et al., 1992, Bayasi et al., 1993) that was originally developed by Schrader (1981). In this method a hardened steel ball was placed on the specimen and a hammer of weight 45 N was dropped on it from a height of 457 mm repeatedly until a visible crack appeared on the specimen.

2.6 Observations arising from literature review

SCS sandwich structures with adhesive bonding are very poor in shear because there is no vertical shear reinforcement to resist shear force. The sandwich structure with angle shear connector is also performed poor shear and separation of face plate occurs in case of impact loading. Headed stud can not provide through connection between the face plates of the sandwich and separation of face plates due accidental impact load can not be controlled. The only disadvantage of Bi-Steel is that the core thickness must not be too thin ($\geq$ 200 mm) to restrict the placement of the Bi-Steel cross connectors. To overcome all these disadvantages of using adhesive, angle connector, headed stud and Bi-Steel connectors in SCS sandwich structures, it is necessary to develop new type of shear connector which can interconnect both top and bottom steel face plates and their uses will not be restricted by the concrete core thickness.

Extensive experimental research on concrete beams, slabs and other composite materials were carried out in past years. However, the performance of the SCS sandwich structures under impact load has not been explored extensively. Very limited literature on impact behaviour of SCS sandwich structures is available. One impact study on SCS sandwich beams with angle shear connector was reported by Sohel et al., (2003). But, the impact performance of SCS sandwich structures (beams and slabs) with other types of shear connector is not available in the literature.

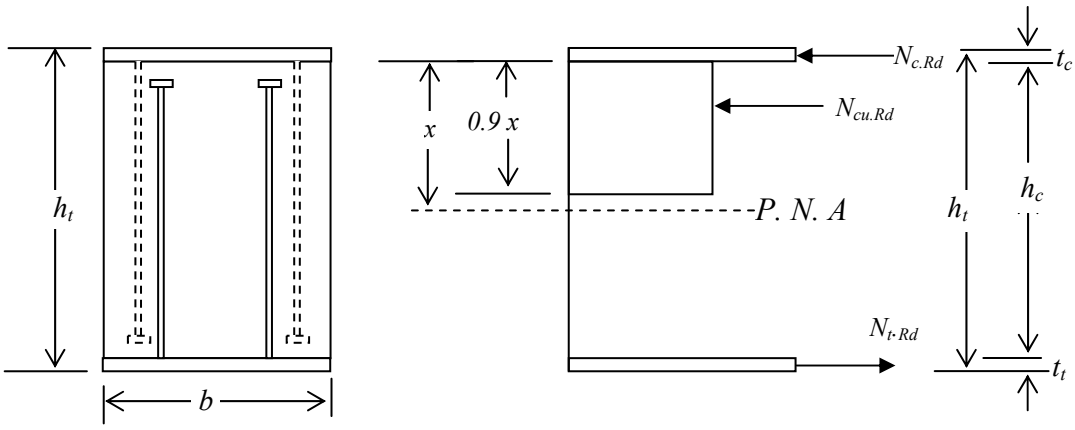

Cross section Stress block

Fig. 2.1 Stresses at fully plastic stage in sandwich beam

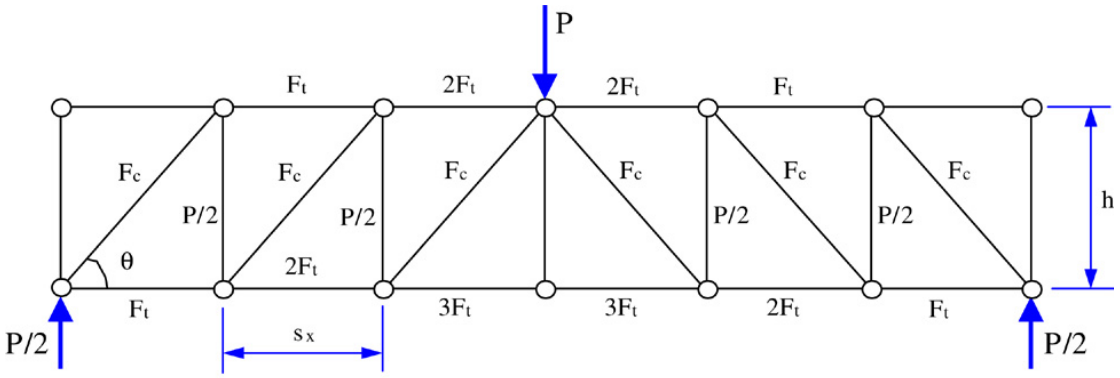

$$F_c = \frac{P}{2\sin\theta} = \frac{P\sqrt{h^2 - s_x^2}}{2h} \qquad F_t = \frac{P}{2\tan\theta} = \frac{P\,s_x}{2h}$$

(a) Truss model for a Bi-Steel beam.

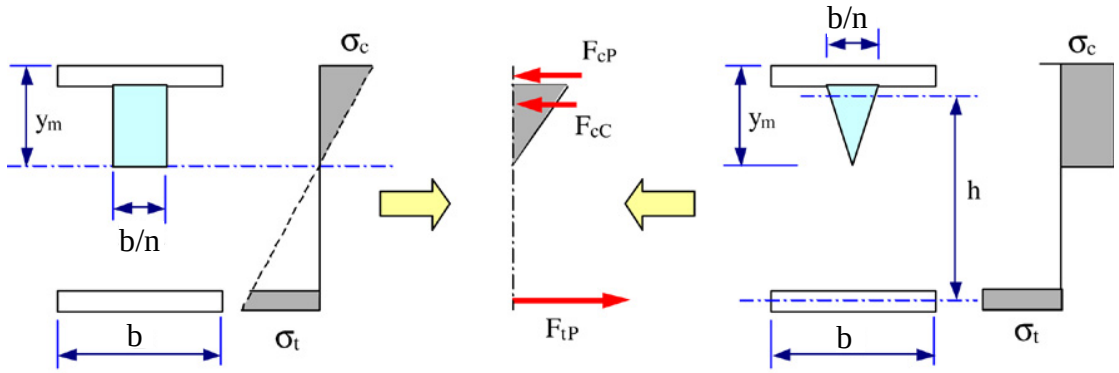

(b) Equivalent steel section (c) Cross section of truss members

Fig. 2.2 Calculation of the depth of truss, *h*. (after Xie et al., 2007)

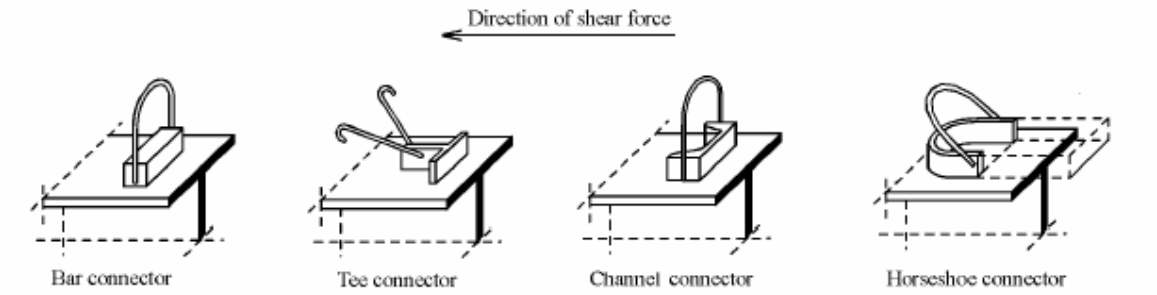

(a) Rigid shear connector with flexible loop (after Slobodan and Dragoljub, 2002)

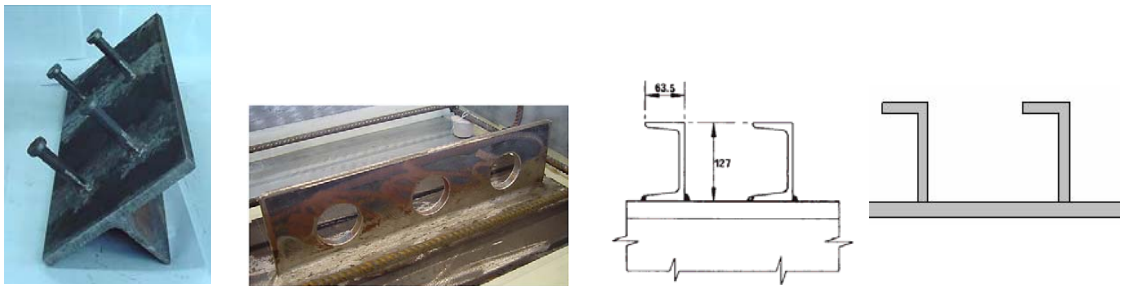

Stud connector Perfobond connector Channel connector Angle connector

(b) Rigid connectors

Fig. 2.3 Different types of shear connector

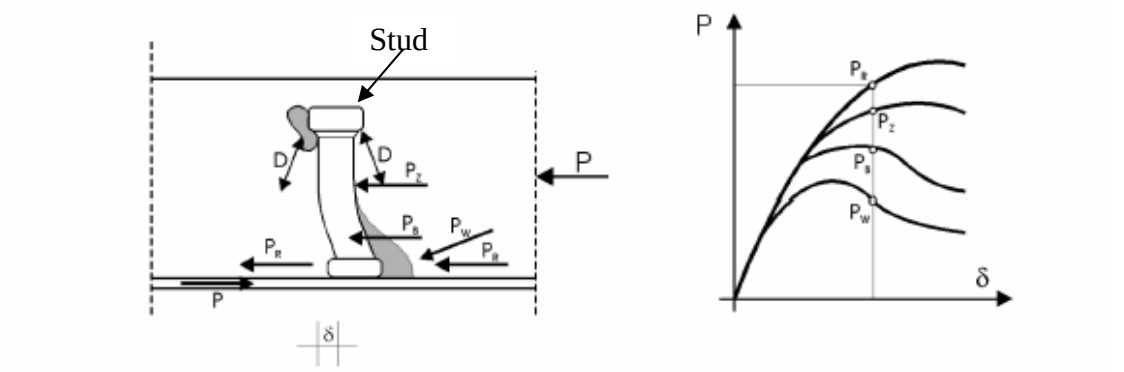

Fig. 2.4 The shearing forces distribution mechanism at headed stud connectors in a composite beam (after Slobodan and Dragoljub, 2002).

Static behaviour of SCS sandwich beams 3

3.1 Introduction

In SCS sandwich structure, steel face plates are connected to the concrete core by shear connectors. Currently, there are two types of mechanical connectors used in SCS sandwich construction. The first type is the conventional headed stud construction in which the studs are welded to the steel plates before concrete is cast. The resistance of the two face plates against tensile separation depends on the pull out strength of the headed studs. The second type is Bi-steel connector in which steel round bar is rotated at high speed and opposite external force is applied to the face plates generating frictional heat that fuse the bar and the plates together (Bowerman et al. 2002). The disadvantage of Bi-Steel system is that the core thickness must longer than 200 mm to restrict the placement of the steel cross connectors (Bowerman et al., 1999). To overcome all these disadvantages of current shear connectors used in SCS sandwich structures, J-hook shear connectors have been developed which are capable of resisting tension and shear, and their uses are not restricted by the concrete core thickness.

This chapter discusses on the novel J-hook shear connector which provides an effective means to prevent tensile separation of the two face plates in the event of impact. J-hook connectors are firstly welded to the face plates using an automatic

welding gun, and they are hooked together by applying a light tension force to the plates before filling the gap between the plates with lightweight concrete (Fig. 3.1). The installation of the J-hook connectors is not restricted by the depth of the sandwich core (≥ 50 mm). This connection technology together with the use of lightweight concrete core would reduce the overall weight of SCS system making it a competitive choice for marine and offshore structures.

Push-out tests have been carried out to evaluate the shear performance of the J-hook connectors in the lightweight and normal weight concrete core. Analytical methods to predict the shear and flexural resistance of SCS sandwich beams with J-hook connectors have been developed. A series of beam tests has been carried out to evaluate the performance of SCS sandwich beams subject to static point load at midspan and the test results have been used to validate the analytical method.

3.2 Development of lightweight sandwich beams

3.2.1 Concept of using J-hook connector in SCS sandwich beams

The bond strength and shear transfer mechanism between the face plates and concrete core are the two most important factors to consider when designing a lightweight sandwich system. In the strut and tie model (Bowerman et al., 2002; Xie et al., 2007; Sun 1998), the bottom steel plate acts as tension member, while the top steel plate and the concrete in compression zone act as compression member. The shear connectors welded to the top and the bottom plates act as vertical tension member, and the inclined compressive force is resisted by the virtual concrete strut as shown in Fig. 3.2. In the impact tests conducted (described in Chapter 5) on sandwich composite beam specimens, large tensile stresses were recorded at the point of impact and the stress

waves travelled to the steel plate and moved towards the supports leading to tensile separation of the face plates. It is therefore necessary to connect both the top and bottom face plates by through connectors to prevent tensile separation of the plates. However, when the sandwich depth is shallow, welding of through connectors between the face plates is not possible and thus a J-hook shear connector is proposed in the present study. The welding of J-hook connectors to steel plates can be done by modified automatic stud welding gun as shown in Fig. 3.1(b). The J-hooks should be placed perpendicular to each other on the top and bottom plates (see Fig. 3.1(a) and 3.2(a)). This type of shear connector is easy to install and is effective in providing restraint against outwards buckling of the compression plate when the sandwich beam is subject to flexural loads.

3.2.2 Lightweight concrete core

Extensive material study was done for choosing the suitable sandwich core material. Following the detailed literature survey of some promising lightweight coarse and fine aggregate are selected. Expanded clay type of lightweight aggregates (coarse and fine) with average particle density of 1000 kg/m^3 were used for the lightweight concrete core. The maximum size of the lightweight aggregate (LWA) was 8 mm. Numerous laboratory trial mixings were done to arrive at the finalized mix design. The design philosophy adopted is similar to that employed for normal weight concrete. Water-to-binder ratio (w/b) was kept low with the use of high range water reducing admixture to achieve desired workability. Supplementary cementitious material such as silica fume was utilized to improve the packing structure and enhance strength development. Both fine and coarse lightweight aggregates were used to get a low unit weight. A mix with

density of approximately 1450 kg/m^3 and strength between 27 MPa to 30 MPa was chosen from these trial designs for use in SCS sandwich beams and slabs.

3.3 Analysis of SCS sandwich beam subject to static load

3.3.1 Flexural resistance of SCS sandwich beam section

There are two methods widely used to analyse the structural response under static load. One is elastic and another is plastic method. Flexural resistance of the SCS sandwich beam also can be analysed using either elastic approach or plastic approach.

3.3.1.1 Elastic approach

Tensile strength of concrete is assumed to be negligible and therefore cracked concrete is ignored in calculating the flexural resistance of a sandwich composite section. The bending stiffness of relatively thin steel plates about their own axes is ignored. It is also assumed that the stresses in the steel plates and concrete in compression are within the elastic range and linearly distributed in the beam section. The closely spaced shear connectors provide lateral restraint to the compression plate preventing the occurrence of local buckling. Considering the above assumptions and from Fig. 3.3(b), the position of the neutral axis, z, can be calculated as

$$z = -n(t_c + t_t) + \left[n^2 \left(t_c + t_t \right)^2 - n\left(t_c^2 - 2t_t h_c - t_t^2 \right) \right]^{1/2} \qquad (3.1)$$

where $n = E_s/E_c$ is the ratio of modulus of elasticity between steel and concrete. The flexural resistance of a sandwich composite section can be determined by taking moments about the line of action of the concrete compressive force by assuming that the normal stress distribution throughout the depth of the concrete core is linear in elastic case (see Fig. 3.3(c)):

$$M = \sigma_c b t_c \left(\frac{z}{3} + \frac{t_c}{2} \right) + \sigma_t b t_t \left(h_c - \frac{z}{3} + \frac{t_t}{2} \right) \tag{3.2}$$

where σ_c, σ_t, b and h_c are the compressive stress at the top plate, tensile stress at the bottom plate, width of the steel plate and distance between the steel plates, respectively. As assumed stress distribution is linear (Fig. 3.3(d)), the compression stress in the top steel plate, σ_c , can be expressed in terms of that in the tension plate, σ_t, as

$$\sigma_c = \sigma_t \frac{z + t_c/2}{h_c - z + t_t/2} \tag{3.3a}$$

if $\sigma_t = \sigma_y$, $\sigma_c = \sigma_y \dfrac{z + t_c/2}{h_c - z + t_t/2}$ (3.3b)

From Eqs. (3.2) and (3.3b), the moment resistance of the sandwich section can be calculated assuming first yield occurs at the tension plate, i.e., $\sigma_t = \sigma_y$,

$$M_y = b t_c \left(\frac{z}{3} + \frac{t_c}{2} \right) \sigma_y \frac{z + t_c/2}{h_c - z + t_t/2} + \sigma_y b t_t \left(h_c - \frac{z}{3} + \frac{t_t}{2} \right) \tag{3.4}$$

In Eq.(3.4), it is assumed that the beam is fully composite. In order to develop full composite action, the maximum longitudinal force generated in the steel face plate, $N_{cs(\max)} = \sigma_y b t_t$, should be resisted by the shear connectors. The number of connectors required depends upon the performance of the individual connectors embedded in the concrete core. This can be obtained from

$$N_{t(\max)} = n_s P_R \tag{3.5}$$

where n_s is the number of shear connectors between the points of zero and maximum moment for full composite, and P_R is the shear resistance of the welded shear connector within concrete. When the number of shear connector is less than the required number of shear connector for full composite, the beam is partially composite

and the moment resistance will be reduced correspondingly (Fang et al., 2000; Wright et al., 1991). The maximum tensile force in the bottom plate will therefore be equal to

$$N_{t(\max)} = n_p P_R \tag{3.6}$$

where n_p is the number of shear connectors between the points of zero and maximum moment for partial composite beam. The maximum stress at the bottom plate can be calculated as

$$\sigma_t = n_p P_R / (bt_t) \tag{3.7}$$

By substituting Eq. (3.7) into Eq. (3.3a) and substituting the resulting equation into Eq. (3.2), the moment resistance for a partially composite sandwich beam can be calculated as

$$M = n_p P_R \left[\left(\frac{t_c}{t_t} \right) \left(\frac{z + t_c/2}{h_c - z + t_t/2} \right) \left(\frac{z}{3} + \frac{t_c}{2} \right) + \left(h_c - \frac{z}{3} + \frac{t_t}{2} \right) \right] \tag{3.8}$$

3.3.1.2 Plastic approach

The plastic moment resistance of a fully composite SCS sandwich section can be determined by assuming a rectangular plastic stress block of depth x_c for the concrete (Fig. 3.4). The concrete beneath the neutral axis (NA) is assumed to be cracked. The forces in the steel plates depend on the material yield strength and shear strength of the connectors in resisting interfacial shear stresses in between the steel plate and the concrete core. It is also assumed that there is no local buckling in the compression steel plate.

The compressive force in concrete (N_{cu}) is given by (Eurocode 4, 2004)

$$N_{cu} = \frac{0.85 f_c}{\gamma_c} b x_c \tag{3.9}$$

where b, f_c and γ_c are the beam width, concrete cylinder strength and partial safety factor for concrete respectively. The plastic neutral axis position can be obtained by equating the compressive force to the tensile force in the section

$$N_{cs} + N_{cu} = N_t \tag{3.10}$$

Putting $N_{ca} = \sigma_y b t_c$, $N_t = \sigma_y b t_t$ and N_{cu} from Eq. (3.9) in Eq. (3.10), the depth of concrete stress block x_c is given by

$$x_c = 1.176\gamma_c\sigma_y(t_t - t_c)/f_c \tag{3.11}$$

where γ_c =1.5 is used as recommended by BS EN 1992-1-1:2004 (Eurocode 2, 2004) for design purposes.

By taking moments about the centre of the compression steel plate, the plastic moment of resistance of the sandwich section is

$$M_{pl} = \sigma_y b t_t \left(h_c + \frac{t_c}{2} + \frac{t_t}{2} \right) - \frac{0.85 f_c b x_c}{\gamma_c} \left(0.5 x_c + \frac{t_c}{2} \right) \tag{3.12}$$

When the steel plates are of equal thickness and strength, the SCS sandwich beams can be treated as an under-reinforced concrete beam. Since an under reinforced beam fails in a ductile manner, the SCS sandwich beam deflected extensively and usually developed extensive and wide cracks in the final loading stages (McKinley and Boswell, 2002; Bowerman et al., 2002). After yielding of tensile steel plate, the cracking of the concrete will continue to rise towards the compression steel plate. In this case, the strain at the bottom plate is very large compared to top steel plate (Fig. 3.5). The moment capacity of the beam is reached when the neutral axis moves near to the lower surface of the compression steel plate (i.e. $x_c \approx 0$) and the tension steel plate is fully yielded.

Therefore, in case of $t_c = t_t = t$, the plastic moment of resistance of the sandwich section is found from Eqs. (3.11) and (3.12)

$$M_{ult} = \sigma_y bt\left(h_c + t\right) \tag{3.13}$$

Eq. (3.13) did not consider tensile fracture of bottom plate when the tensile strain in the steel exceeds the ultimate limit.

If the longitudinal tensile force (N_t) and compressive force (N_{cs}) in the steel plates are controlled by the shear connector capacity, then the SCS beam is termed as partially composite beam and the Eq. (3.10) becomes as following

$$N_{cs} + 0.85 f_c b x_c / \gamma_c = N_t \tag{3.14}$$

or $$x_c = 1.176\gamma_c \ (N_t - N_{cs}) / f_c b \tag{3.15}$$

As the number of shear connectors reduced, the moment resistance of the partially composite beam is also reduced correspondingly. By taking moment about the centre of the compression steel plate, the plastic moment of resistance of the partially composite beam section is determined as

$$M_{pl} = N_t\left(h_c + \frac{t_c}{2} + \frac{t_t}{2}\right) - \frac{0.85 f_c b x_c}{\gamma_c}\left(0.5x_c + \frac{t_c}{2}\right) \tag{3.16}$$

in which, $N_t = n_p P_R$.

Normally, the number of welded J-hook connectors in the top and bottom plates is equal. If the two face plates are of the same thickness and strength, the value of 'x_c' should be taken as zero. Letting t_c=t_t=t and $N_t = n_p P_R$, Eq. (3.16) can be simplified as

$$M_{pl} = n_p P_R\left(h_c + t\right) \tag{3.17}$$

3.3.2 Shear resistance of SCS sandwich beam section

The applied shear force can lead to failure in one of two modes. The first is longitudinal shear, i.e. the failure of the shear connectors to transfer the longitudinal forces (interfacial forces) from the steel plate into the concrete. This shear capacity of the connector may be determined by direct push-out tests. The second mode is transverse shear failure in which the J-hooks connectors may tension in tension as they act as shear stirrups. Similar to reinforced concrete, the transverse shear resistance of a sandwich section consists of the contribution from the concrete core and the J-hook connectors:

$$V = V_c + V_s \tag{3.18}$$

where V_c is the shear resistance of the concrete core obtained as Eurocode 2 (2004):

$$V_c = \left[C_c k_c \eta_1 \left(100 \rho_1 f_{ck}\right)^{1/3} \right] b h_c \tag{3.19}$$

where $k_c = 1 + \sqrt{200/h_c} \le 2.0$ with h_c in mm; $\rho_1 = t_t / h_c \not> 0.02$; $C_c = 0.18/\gamma_c$ for normal weight concrete and $C_c = 0.15/\gamma_c$ for LWC; $\eta_1 = 0.4 + 0.6\rho/2200 \le 1.0$ in which ρ is the density of the concrete (kg/m^3).

If fibres are added into the concrete core, the shear resistance of the concrete may be calculated as (Majdzadeh et al. 2006)

$$V_c = \left[C_c k_c \eta_1 \left(100 \rho_1 f_{ck}\right)^{1/3} + k_f \tau_{f,FRC} \right] b h_c \tag{3.20}$$

where $k_f = 0.216$ for steel fibre (hook end), limited to a maximum of 1% volume fraction; $k_f = 0.290$ for synthetic fibres; and $\tau_{f,RFC} = \tau_{FRC} - \tau_{plain}$ in which τ_{FRC} and τ_{plain} are the shear strength of FRC and plain concrete, respectively, as determined by direct shear test. In this study $\tau_{f,RFC} = \tau_{FRC} - \tau_{plain} = 4.23 V_f$ is used conservatively as

suggested by Mirsayah and Banthia (2002) for flat ended fibre with circular cross section in which V_f is fibre volume faction expressed as percentage.

The shear contribution due to presence of J-hook connectors in the beam may be calculated as:

$$V_s = \left(n_0 F_t / S_s\right) h_c \tag{3.21}$$

where F_t is the direct tensile or pull-out capacity of the J-hook connector within the concrete block and its value may be determined through experiment; and n_0 is the number of J-hook connectors in top or bottom plate across the width of the section. Eq. (3.21) can also be used in situation where connector spacing S_s exceeds the depth h_c . A similar recommendation is also given in the Bi-steel and SCS sandwich design guide (Bowerman et al. 1999, Narayanan et al. 1994).

3.3.3 Deflection

The deflection of a SCS sandwich beam consists of flexural and shear components. When the span length to thickness ratio is small, transfer shear deformation is often dominant. The flexural stiffness of sandwich beam is influenced significantly by the bond strength between the steel plates and the concrete core. Roberts et al. (1996) suggested an approximate method to allow for slip by reducing the effective stiffness of the steel plates using a reduction factor. The stiffness reduction factor for the tension steel plates (k_t) and compression steel plate (k_c) are given by

$$k_t = \frac{n_a K}{n_a K + 2bt_t E_s / L} \text{ and } k_c = \frac{n_a K}{n_a K + 2bt_c E_s / L} \tag{3.22}$$

in which n_a is the number of shear connectors provided between maximum moment and zero moment and K is the stiffness of the connectors, determined from the push-out test.

The flexural deflection of a beam at midspan due to point load F acting at the midspan is

$$\Delta_1 = \frac{FL^3}{48D} \tag{3.23}$$

where $D = (EI)_{eqivalent}$ is the flexural rigidity of the composite section. The moment of inertia for a sandwich beam considering cracked section is

$$I_{eq} = \frac{bk_c t_c^{\,3}}{12} + \left(bk_c t_c\right)\left(z + \frac{t_c}{2}\right)^2 + \frac{(b/n)z^3}{3} + \frac{bk_t t_t^{\,3}}{12} + \left(bk_t t_t\right)\left(h_c - z + \frac{t_t}{2}\right)^2 \tag{3.24}$$

and

$$D = E_s\left\{\frac{bk_c t_c^{\,3}}{12} + \left(bk_c t_c\right)\left(z + \frac{t_c}{2}\right)^2 + \frac{(b/n)z^3}{3} + \frac{bk_t t_t^{\,3}}{12} + \left(bk_t t_t\right)\left(h_c - z + \frac{t_t}{2}\right)^2\right\} \tag{3.25}$$

The shear deflection of a sandwich beam with a midspan point load is calculated as (Allen, 1969; Zenkert, 1997)

$$\Delta_2 = \frac{FL}{4S} \tag{3.26}$$

where S is the shear stiffness of the beam given as (Roark and Young, 1976)

$$S = \frac{G_c^{'} h_c b}{\kappa_s} \tag{3.27}$$

in which κ_s is a shear factor and its value for rectangular section is 1.2, and $G_c^{/}$, the effective shear modulus, is given by

$$G_c^{'} = \frac{\phi G_c}{1 + E_c h_c^2 \Big/ \left(6E_s \left(\frac{t_t + t_c}{2} \right) e \right)} \tag{3.28}$$

where $e = h_c + \left(t_c + t_t \right)/2$ is the distance between centroids of top and bottom plates and ϕ =0.95 is the shear modulus reduction factor to account for the effect of cracked concrete (Thevendran et al., 1999; Liang et al., 2005). Combining Eqs. (3.23) and (3.26), the total force-displacement relationship for the centrally loaded sandwich beam can be calculated as:

$$\Delta = \Delta_1 + \Delta_2 = F\left[\frac{L^3}{48D} + \frac{L}{4S} \right] \tag{3.29}$$

3.4 Test programme

3.4.1 Push-out tests on SCS sections

Seven push-out test specimens, as shown in Fig. 3.6(a), were prepared to determine the direct shear load-slip characteristics of the J-hook shear connectors. The aims of the test programme were to examine the strength and stiffness of interconnected J-hook connectors when the concrete was subjected to a shearing action relative to the steel plates. The J-hook connectors (two pairs) were embedded in concrete blocks (200 mm × 200mm × 80 mm), similar to that used to prepare for the test beam specimens (see Fig. 3.6(b)). The bar diameters of the J-hook connectors were 10 mm, 12 mm and 16 mm. The study included the concrete strengths as one of varying parameters. One of the test specimens was prepared with fibre reinforced lightweight concrete. Compression tests were carried out on the 28-day concrete cylinder to determine the cylinder strength f_{ck}, modulus of elasticity E_c and density of concrete as shown in Table 3.1. The arrangements for the push-out tests are shown in Figs. 3.7(a) & (b). The total load 4*P* from a spherical bearing was transmitted to a 70 mm thick loading block (200

mm × 80 mm) to obtain an approximately uniform load over the top surface of the concrete, resulting in a shear force *P* acting on each J-hook/plate interface. The bottom edges of the plates bear upon a rigid platform of the testing machine. The relative slip between steel plate and concrete were measured by two LVT transducers as shown in Fig. 3.7.

3.4.2 SCS beam specimens and test set-up

Twelve SCS beam specimens with core depth 80 mm, span length 1200 mm and width ranging from 200 mm to 300 mm were subjected to static point load applied at mid-length of the beam. The thickness of the face plates for all the specimens was 4 mm. The diameter of the J-hook connectors was either 10 mm or 16 mm.

The sandwich beams were filled with either plain normal concrete (density = 2400 kg/m^3) or light weight aggregate concrete (density = 1400 kg/m^3). The concrete core of some specimens was reinforced with either PVA fibres (Kuralon RF 4000/30 mm) or steel fibres (Dramix® RC-80/30-BP). Material properties for concrete and steel plates obtained from tests are given in Table 3.2. The spacing of J-hook shear connectors was varied from 80 mm to 300 mm to provide partial to full composite action between steel face plate and concrete core. Details of the test beams are presented in Table 3.2.

The test beams were simply supported over a span of 1000 mm and subjected to three-point loading, as shown in Fig. 3.8. Loads were applied to the beams under displacement control mode using a servo controlled Instron hydraulic actuator of capacity 500 kN, applying a downward displacement at a rate of 0.1 mm per minute. The applied load was measured using a calibrated load cell that was placed below the

actuator. The deflections at different positions were measured by linear displacement transducers which can measure maximum displacements ranging from 100 mm to 200 mm. The slip between steel plate and concrete at the beam's end was measured by a displacement transducer. The concrete core was painted white with a limewater mixture to enable the visual observation of the cracks in the concrete.

Prior to the application of any load on the specimen, all transducers and load cell were connected to a computer via data logger that recorded all data during testing. Load cell and transducer readings were monitored at each increment of loading and they were recorded in the computer. The loads versus central beam's deflections were monitored online to trace the progressive failure of the test specimens. Close observation was made to locate the loads associated with first crack and first yielding in the concrete and steel, respectively. The maximum test load and the mode of failure for each specimen were recorded and the progressive cracking in the concrete were marked. After testing, the concrete were removed to observe the deformation pattern of the shear connectors.

3.5 Test results and discussion

3.5.1 Push-out tests

3.5.1.1 Failure loads and failure modes

Table 3.3 shows the maximum loads recorded from the push-out tests, expressed as the failure load per connector which is the maximum test load divided by the number of shear connectors in the specimen. Test results show that the concrete strength significantly affected the shear resistance of J-hook shear connectors. Load-slip curves for the connectors are plotted in Fig. 3.9. Ductile behaviour of J-hook connector was

observed for both normal weight concrete core and lightweight concrete core after the linear part (serviceability state) of load-slip curve. The J-hook connector within lightweight concrete core displays more flexible load-slip characteristics than that with the normal weight concrete core. The significant, non-linear increasing of the deformation is characteristic for the load levels above the serviceability state. This loss of stiffness is caused by the local crushing of the lightweight concrete around the foot of the J-hook connectors and thus by a load distribution from the weld collar to the shank of the J-hooks. This results in flexural and shear deformation of the J-hooks, which quantitatively depends wholly on the elastic bending, or on the modulus of elasticity of the concrete, respectively. At this state the first cracks were observed. Comparison of the load-slip curves for specimens LWFC-10 and LWC-10 in Fig. 3.9(a) shows that the presence of 1% fibres in the lightweight concrete core slightly increases the ductility of the shear connector in the post-peak range.

Failure occurred either by concrete bearing failure or shear failure at the foot of the connector as shown in Figs. 3.10(a) and 3.10(b). The failure of the specimens with lightweight concrete core of compression strength = 31 MPa was governed by concrete bearing failure, whereas connector with normal concrete core (compression strength > 48 MPa) failed by shear yielding of the connector occurring at about 8 to 10 mm slip. No premature weld failure of shear connector was observed indicating the effectiveness of the welding and that the proposed J-hook connectors are as effective as the headed studs in transferring the shear force required for composite action. The stiffness of J-hook connectors (K) can be determined from the load-slip plots. The average elastic stiffness of the J-hook connector with diameter 10 mm and 12 mm is 30,000 N/mm and for 16 mm diameter connector, the stiffness is about 35,000 N/mm.

3.5.1.2 Comparison of test results with theoretical predictions

Eurocode 4 approach (2004) is used to predict the strength of J-hook connectors used in the push-out test specimen in which the characteristic shear resistance of welded stud connectors is taken as the lesser of:

$$P_R = 0.8\sigma_u(\frac{\pi d^2}{4}) \quad (3.30a)$$

and

$$P_R = 0.29\alpha d^2\sqrt{f_{ck}E_{cm}} \quad (3.30b)$$

where, d = diameter of the stud shank; σ_u = specified ultimate tensile strength of the stud but $\not>500$ MPa; f_{ck} = characteristic cylinder strength of concrete; E_{cm} = secant modulus of concrete; $\alpha = 0.2(h_s/d + 1)$ for $3 \leq h_s/d \leq 4$ or $\alpha = 1.0$ for $h_s/d \geq 4$.; h_s = overall height of the stud.

The shear resistances predicted by Eqs. (3.30a) and (3.30b) are compared with the test results as shown in Table 3.3 by assuming $\gamma_v = 1.0$. Eurocode 4 method underestimates the maximum shear resistance of the J-hook connector by about 17.0% for NWC-10 and 16.5% for LWC-10 specimens. For specimens with lightweight concrete, the shear resistance is controlled by bearing failure of concrete and hence Eq. (3.30b) should be used. However, for specimens with normal concrete, the shear resistance of the connector may govern as represented by Eq. (3.30a). It should be noted that both Eqs. (3.30a) and (3.30b) are developed primarily for a headed stud connector. The proposed J-hook connectors are interlocked thus they provide better shear transfer mechanism between the steel plates and the concrete core. The ratio of the strength predicted by Eurocode 4 and test results ranges from 0.82 to 0.99, except for specimen LWFC-10 with lightweight core of 1% fibres added, Eq. (3.30) underestimates the test load by

23%. The fibres in the concrete core enhance the bearing capacity of the J-hook connectors against the concrete by about 10%. The enhancement of concrete strength due to the presence of fibres was not captured by the Eurocode 4 approach.

3.5.2 Beam tests

3.5.2.1 Load-deflection behaviour

The load-deflection curves for the beams are plotted in four groups with different test parameters as shown in Fig. 3.11. All the beams showed almost linear load-displacement response up to 70% of the maximum load and became nonlinear with the gradual widening of the cracks in the concrete core under the increased load. In the post peak stage, most of the beams showed certain degree of ductility. From Fig. 3.11(a), it is observed that beam SCS100 exhibits a gradual reduction of strength after the peak load. This behaviour was also observed in beam SCS80, but the rate of strength reduction in the post-peak range was less significant than that of SCS100. This is because SCS80 has a very high degree of composite action of 2.1 (calculated by Eq. (3.31)), and the failure was due to tension yielding of the bottom plate. Beam SCS100 having the degree of composite action =1.39, is also a full composite beam, but yielding of shear connectors in the post peak range led to higher load reduction. For other specimens, the softening of the load-deflection curve is due to crack formation in the concrete core, slip of the bottom steel plate and deformation of the J-hook connectors. Degree of composite action is calculated by the following equation,

$$\text{Degree of composite} = N_a/N_s \tag{3.31}$$

where N_a is the number of J-hook connector provided and N_s is the number of J-hook connectors required for full composite action.

The presence of fibres in the concrete increases the ductility of the sandwich beam in term of the post-peak load-displacement behaviour as observed for beams SLFCS100(1) and SLFCS200(2) in Fig. 3.11(b) and (c), respectively. In these two cases, fibres helped to prevent sudden failure of the concrete core in particularly at the large deflection range. The beams could deflect up to 60 to 70 mm without significant reduction in load if there were no sudden failure of J-hook connectors. At the large deflection range, the cracks in the concrete core reached the top plate and the interconnected J-hooks provided the main resistance to the applied shear force.

3.5.2.2 Cracking behaviour of concrete core

For the test beams, cracks normally appeared first at the extreme tension fibre of the concrete core at about 50% of the peak loads. At the same time, the interfacial cracks between bottom steel plate and concrete core would appear at the mid-span where the moment is the largest. These interfacial cracks were then propagated horizontally to both left and right directions, and finally reached the end support of the beams. Some flexural cracks would propagate in a diagonal direction due to the combined action of shear and flexure as observed for beams SCS150 and SLCS150.

When the load increased further, more flexural cracks were formed in the concrete core. The flexural cracks initiated at the tension face of the concrete; however, the formation of these flexural cracks had almost no noticeable influence on the load-deflection response up to 70% of the peak load (see Fig. 3.11). Almost all the beams showed extensive shear cracks during the later stage of loading. However, the shear cracking did not cause abrupt failure, indicating that the interconnected J-hooks provided effective force transfer mechanism between the steel and concrete. For beam

SLCS (without shear connector), the first crack in the concrete appeared at the mid span, followed by the formation of new cracks around the first crack as shown in Fig. 3.13(e). The bonding between steel plates and concrete was lost at the early stage of loading as there was no shear connector provided to resist the applied shear force. Fig. 3.12 shows the typical crack formation in the concrete core with number 1 to 6 representing the order of crack formation for specimen SLCS100. The position of the number in the cracks shows the approximate locations of their first appearance. The inclined cracks labelled as 5-6 in Fig. 3.12 are the cracks that appeared next to the flexural ones. For all specimens with LWC core, extensive crushing of concrete below the applied load was observed at the post-peak range of loading.

3.5.2.3 Maximum load and failure mode

The maximum loads and failure modes of the twelve beam specimens are summarised in Table 3.4. Fig. 3.13 illustrates the observed failure modes of the test beams: (a) flexural failure indicated by tensile yielding of the bottom steel plate and vertical cracks in the concrete core as in Fig. 3.13(a), (b) vertical shear failure indicated by diagonal cracks in the concrete core as shown in Fig. 3.13(b), (c) shear connector failure (Fig. 3.13(c)), and (d) shear bond failure due to excessive slip between the steel plate and the concrete core as shown in Fig. 3.13(d).

For beams SCS80, SLCS80, and SCS100, yielding of the bottom steel plates occurred before failure as indicated in Table 3.4. After significant deformation of the beam, high strain value at the bottom steel plate led to J-hook failure; this type of failure is termed as tensile yielding of bottom plate. These beams are extremely ductile and have a higher maximum load than the beams that failed by other modes. The beams could

sustain a very large deflection until the flexural cracks in the concrete core reach the top plate.

For beams SLFCS100(1), SLCS150, SLCS200, SLFCS200(1), and SLFCS200(2), failure was due to J-hook connectors bearing on concrete rather than by yielding of the bottom steel plate. This is expected because the total longitudinal shear transfer capacity of the J-hook connectors was less than the yield strength of the steel plate i.e. these beams were partially composite as indicated in Table 3.4. Failure of SLCS100 is due to unexpected weld toe failure of the J-hook connectors, and hence the maximum load is much lower than the predicted value.

For beams with connector spacing 150 mm and more, diagonal shear cracks were observed just after the peak load. These cracks developed as a continuation of flexural cracks. Shear cracks can be characterised by the formation of diagonal cracks in between the adjacent connectors or between the loading point and the adjacent shear connector. It is recommended for slim depth beam that the spacing of shear connector should be at most equal to the core thickness to prevent concrete shear failure and to develop effective strut-tie action.

Typical loads versus relative slips between concrete core and bottom steel plate at the beam end are plotted in Fig. 3.14. During the initial stages of loading there was no slip in the steel plates and concrete core. Immediately after the flexural cracks appeared in the concrete core, horizontal slip of bottom steel plate occurred. But this was not the primary cause of failure of the beams except SLFCS300(1) and SLCS in which the failure was due to excessive slip between the face plate and the concrete core in view

of the low degree of partial composite. This failure mode is also termed as 'shear-bond' failure. In general, when the J-hook connectors reached the maximum resistance under the applied longitudinal shear, a sudden drop of load was observed. This was followed by significant slip occurring at the post-peak stage of the loading in which the connectors were loaded in shear and tension. As shown in Figs. 3.11 and 3.14 the ultimate load carrying capacity of the specimens with lightweight concrete is lower than that of the specimens with normal concrete. Comparing specimens SCS80 and SLCS80, SCS100 and SLCS100, SCS150 and SLCS150, the maximum load capacity of specimens with a lightweight concrete core is on average 30% lower than those with normal weight concrete core. This is similar to the findings in (Zhao and Grzebieta, 1999, 2002) where the axial loading capacity of lightweight concrete filled tubular columns is about 20% lower than that using the normal weight concrete, and the ultimate moment capacity of lightweight concrete filled tubular beams is about 15% lower than that using the normal weight concrete. As shown in Section 3.5.2.4, the use of fibres in lightweight concrete increases the load carrying capacity by about 25%, which makes the load carrying capacity closer to that using normal weight concrete.

3.5.2.4 Effect of fibres

The effect of fibres on load-deflection behaviour is shown in Fig. 3.11(b) and (c). An increase in volume fraction of fibres provides a higher post cracking stiffness because a better crack-arresting mechanism and higher tension stiffening, thus resulting in a smaller beam deflection at a particular load level (see Fig. 3.11(c)). The comparison between specimens with fibre reinforced concrete and plain concrete core shows an obvious increase of the post peak strength caused by the fibres. Moreover, the comparison of the maximum test loads shows a clear increase in resistance caused by

fibre reinforcement (Table 3.4, Fig. 3.11(b) and (c)). For example, the specimen without fibres (SLCS100) showed a maximum load of 55.2 kN, whereas, specimen (SLFCS100(1)) with 1% of volume fraction of steel fibres gave maximum load of 68.7 kN i.e. the load carrying capacity increases by about 24%. In case of addition 1% PVA fibre (specimens SLCS200 and SLFCS200(1)), the load carrying capacity increases by about 13.8%. This is because the fibres in the concrete increase the tensile as well as the flexural capacity of the concrete and also increases the connectors' (J-hook) bearing capacity as shown in push-out test. However, the maximum load does not differ much between the beams containing 1% and 2% volume fraction of PVA fibres. Addition of more fibres into the concrete would reduce its workability and will lead to compaction problems during casting of a slim depth sandwich beam.

3.5.2.5 Effect of concrete strength

Concrete strength has a direct effect on the strength of the shear connector. As the key idea of the present research is to develop a lightweight sandwich system for structural decking, the investigation focuses mainly on lightweight concrete cores with a compressive strength of at least 25 MPa. For comparison purposes, some beams with normal weight concrete were constructed. The influence of concrete strength on the behaviour of SCS sandwich system is observed in Fig. 3.11(a) and summarised in Table 3.4. For the same shear connector spacing, beams with lightweight concrete (LWC) exhibit lower ultimate load carrying capacity than beams with normal weight concrete (NWC). For example, beam SLCS100 with LWC gave an ultimate load 55.20 kN, whereas, beam with normal concrete (SCS100) showed an ultimate load 86.24 kN. As indicated earlier, the capacity of the shear connector was influenced by the concrete strength, which in turn affected the load carrying capacity of the beams.

3.6 Discussion on analytical predictions

The load carrying capacity and the elastic beam deflection at 2/3 the peak load obtained from the tests are compared with those obtained using the analytical methods described in Section 3.3 by assuming partial safety factor (γ_c) = 1.0. The comparisons of the ultimate loads are given in Table 3.4. Both elastic and plastic theories were used to predict the moment resistance of the composite beams. The plastic moment capacity of the sandwich beam obtained from Section 3.3.1.2 is always higher than that predicted by the elastic approach described in Section 3.3.1.1. Thus only the ratios between the plastic and experimental results are reported in Table 3.4. The experimental shear capacity of the J-hook connectors was used to predict the ultimate load carrying capacity of the beams in this study. In case of lightweight concrete core, 90% of the experimental ultimate shear capacity of J-hook connector was used because in the push-out tests, LWC has high ductility with little increase (about 8%-10%) of load. The transverse (vertical) shear capacity of the beam obtained from Section 3.3.2 is always higher than the experimental maximum shear force which is reported in Table 3.5 indicating that transverse shear failure was not a controlling failure mode.

The predicted ultimate load is generally conservative except for some beams with partial composite i.e. the predicted maximum load of the beam is lower than the experimental results except for beams SLCS100 and SLCS100(1). Beams SCS80, SLCS80, and SCS100 were designed for tension plate failure due to flexure and the ratio of the predicted load (by plastic theory) to the experimental maximum load ranges from 0.75 to 0.87. For other beams with partial composite design, in which the maximum load was governed by the shear connector bearing (against concrete) failure, the ratio was between 0.83 and 0.99, except beam SLCS100 with strength ratio 1.14 because of the premature weld failure of the J-hook connector.

The flexural stiffness of the sandwich beams reduced with the crack formation in the concrete core. The nonlinearity of the load-deflection relationship depends on the extent of cracks in the concrete core and yielding of the steel plate. Thus, the beam central deflection at two-third of the test peak load was used as the basis for comparison between analytical and experimental deflection (Robert et al. 1996; Xie et al. 2007). The calculated deflections are given in Table 3.6 with the corresponding test results. The shear deflection component is relatively small compared to the flexural deflection. The full composite beams (degree of composite ≥ 1) show reasonably close relation between the experimental and predicted deflections. A significant variation between the predicted deflections and test results is observed for partial composite beams with shear connector spacing greater than 150 mm. In case of the beam SLCS200, the analytical solution over-estimates the measured test deflection by 1.37 times. This may be the cause of low value of the stiffness reduction factor (k_t from Eq. (3.22)) used to account for slip between steel plates and concrete core arising from partial composite action. Thus, it is necessary to modify the Eq. (3.22) for low degree of composite beams based on more test results.

3.7 Summary

This chapter introduces a new concept of using J-hook connectors to construct SCS sandwich structures. Special emphasis is placed on the development of lightweight concrete reinforced with steel fibres to enhance the structural ductility and shear resistance against static applied load. The proposed J-hook connectors can be fitted in shallow depth between the steel face plates for the construction of slim deck structure. Push-out tests confirm the superior performance of J-hook connectors in resisting shear force. Eurocode 4 method, which is originally developed for headed stud connectors,

may be used to predict the shear capacity of the connector in lightweight and normal weight concrete core, although the method underestimated the test results by about 10%-15%.

Test on sandwich beams subject to concentrated point load at the mid-length shows that it is necessary to provide adequate shear connectors in order to delay the formation of shear cracks in the concrete core and to ensure ductile failure mode. It is recommended that the spacing of shear connectors should be at most equal to the core thickness to prevent concrete shear failure for sandwich beams with core depth less than 100 mm. When a sufficient number of connector is provided to achieve full composite action in the sandwich beam, the load-deflection response is ductile and failure is controlled by yielding of the bottom steel plate. Lightweight concrete with steel fibre performs better than PVA fibre in SCS beams. Inclusion of 1% hook end steel fibre in the core material significantly increases (24%) the ultimate load-carrying capacity as well as ductility. The formation of cracks in the concrete core is also delayed and reduced.

Analytical solutions have been proposed to calculate the elastic and plastic moment capacity as well as the elastic deflection of SCS sandwich beams under service load. The calculated load carrying capacity is generally conservative (average about 90% of the experimental maximum load) if connector weld failure can be avoided, and thus the proposed analytical solutions can be used for design purposes. In case of lightweight concrete cores, it is recommended that the shear capacity of the J-hook connectors should be reduced by 0.9 to account for the lower bearing strength of the lightweight core.

Table 3.1 Push-out test specimens and specifications for J-hook connectors

Test ref.	d_j (mm)	h_s (mm)	h_c (mm)	Plate width, (mm)	Plate height (mm)	σ_u (MPa)	f_c (MPa)	E_c (GPa)	Concrete density (kg/m^3)
NWC-10	9.9	51.0	80	300	300	405	48.3	32.5	2400
LWC-10	9.9	51.0	80	300	300	405	28.5	12.7	1450
LWFC-10	9.9	51.0	80	300	300	405	28.1	12.6	1460
NWC-16	15.5	55.5	80	300	300	450	65.0	30.0	2400
LWC1-16	15.5	55.5	80	300	300	450	26.4	11.7	1440
LWC2-16	15.5	55.5	80	300	300	450	30.2	17.0	1700
LWC2-12	11.5	52.5	80	300	300	450	30.2	17.0	1700

Notes: NWC=Normal weight concrete; LWC= Lightweight concrete; LWFC= Lightweight concrete with fibre (1% steel fibre); σ_u= ultimate tensile strength of the J-hook bar; d_j = J-hook bar diameter

Table 3.2 Beam test specimens and specifications for static test

Beam ref. *	t_c & t_t (mm)	h_c (mm)	b (mm)	d (mm)	S_x (mm)	Core type	V_f (%)	ρ (kg/m^3)	f_c (MPa)	σ_y (MPa)
SCS80	4.04	80	240	10	80	NWC	-	2350	48.3	275.0
SLCS80	4.04	80	240	10	80	LWC	-	1445	28.5	275.0
SCS100	4.04	80	200	10	100	NWC	-	2350	48.3	275.0
SLCS100	4.04	80	200	10	100	LWC	-	1445	28.5	275.0
SLFCS100(1)	4.04	80	200	10	100	LWC	1 (steel)	1450	28.1	275.0
SCS150	4.04	80	300	10	150	NWC	-	2350	48.3	275.0
SLCS150	4.04	80	300	10	150	LWC	-	1445	28.5	275.0
SLCS200	3.93	80	200	16	200	LWC	-	1445	27.4	275.5
SLFCS200(1)	3.93	80	200	16	200	LWC	1 (PVA)	1450	28.7	275.5
SLFCS200(2)	3.93	80	200	16	200	LWC	2 (PVA)	1450	28.2	275.5
SLFCS300(1)	3.93	80	300	16	300	LWC	1 (PVA)	1450	28.0	275.5
SLCS	3.93	80	200	NIL	NIL	LWC	-	1445	26.0	275.5

b=width of the beam; d=bar diameter; S_s = spacing of shear connector; σ_y= yield strength of steel plate; f_{ck}=cylinder strength of concrete; SLCS = SCS with lightweight concrete core; SLFCS = SCS with fibre reinforced lightweight concrete core; SCS = sandwich specimen with normal weight concrete core.
* For all beams, span length, L=1000 mm

Table 3.3 Push-out test results and theoretical characteristic shear resistance

Test ref.	Shear capacity (kN)		Ratio (EC4/P_{exp})	Failure mode
	P_{exp}	EC4		
NWC-10	31.0	25.5	0.82	**Bar shear failure**, at the top of the welding flush.
LWC-10	20.8	17.4	0.84	**Concrete bearing**, crack the concrete at position of shear connector.
LWFC-10	22.3	17.3	0.77	**Concrete bearing**, crack the concrete at position of shear connector.
NWC-16	68.5	67.9	0.99	**Bar shear failure**, at the top of the welding flush.
LWC1-16	43.9	36.9	0.84	**Concrete bearing**, crack the concrete at position of shear connector.
LWC2-16	46.5	45.7	0.98	**Concrete bearing**, crack the concrete at position of shear connector.
LWC2-12	33.1	27.6	0.83	**Concrete bearing**, crack the concrete at position of shear connector.

EC4 = Eurocode 4.

Table 3.4 Comparison of beam test results with predicted maximum load

Beam ref.	Capacity of steel plate & J-hooks[a] (kN)		Degree of composite (2)/(1)	Predicted load (kN) F_{el} & F_{pl} [b]		Expt., F_{exp} (kN)	$\frac{F_{pl}}{F_{exp}}$	Failure mode
	$F_{tst(\max)}$ (1)	$n_s.P_{\exp}$ or $n_p.P_{\exp}$ (2)		Elastic theory (Eq. 3.4 or 3.8)	Plastic theory (Eq.3.13 or 3.16)			
SCS80	267	558	2.09	84.82	89.63	119.05	0.75	Tensile yielding of bottom plate
SLCS80	267	337	1.26	86.51	89.63	95.56	0.94	Tensile yielding of bottom plate
SCS100	223	310	1.39	70.69	74.69	86.24	0.87	Tensile yielding of bottom plate
SLCS100	223	187	0.84	60.74	62.93	55.20	1.14	Connector shear failure (governed by bearing against the concrete core) / welding failure of J-hook
SLFCS100(1)	223	201	0.91	65.99	67.47	68.70	0.98	Connector shear failure (governed by bearing against the concrete core)
SCS150	333	186	0.56	59.17	62.53	66.67	0.94	J-hook connector shear failure
SLCS150	333	112	0.34	36.44	37.76	45.35	0.83	Connector shear failure (governed by bearing against the concrete core)
SLCS200	217	118	0.54	38.26	39.61	40.10	0.99	Connector shear failure (governed by bearing against the concrete core)
SLFCS200(1)	217	122	0.56	39.40	40.79	45.60	0.89	Connector shear failure (governed by bearing against the concrete core)
SLFCS200(2)	217	122	0.56	39.40	40.79	48.90	0.83	Connector shear failure (governed by bearing against the concrete core)
SLFCS300(1)	325	81	0.25	26.27	27.19	30.26	0.90	Excessive slip (shear-bond failure)
SLCS	217	NIL	NIL	------	-----	13.11	--	Buckling of steel face plate /concrete flexural

[a] For lightweight concrete, $P_{\exp}$ is the 90% of the experimental ultimate load of push-out test

[b] F_{el} is the predicted static force using elastic theory and F_{pl} is the predicted plastic load using plastic approach

Table 3.5 Check for shear capacity of the beam specimens

Beam ref.	F_t (kN)	n_0	V_c (kN) (Eq. (3.18) or (3.20))	V_s, (kN) (Eq. (3.19))	V, (kN) (Eq. (3.17))	V_{exp} (kN)	$\frac{V_{\exp}}{V_c + V_s}$
SCS80	21	3	31.7	63.0	94.7	59.5	0.63
SLCS80	15	3	17.7	45.0	62.7	47.8	0.76
SCS100	21	2	26.4	33.6	60.0	43.1	0.72
SLCS100	16	2	14.8	25.6	40.4	27.6	0.68
SLFCS100	16	2	29.7	25.6	55.3	34.4	0.62
SCS150	21	2	39.6	22.4	62.0	33.3	0.54
SLCS150	16	2	22.2	17.1	39.3	22.7	0.58
SLCS200	26	1	14.6	10.4	25.0	20.1	0.80
SLFCS200(1)	26	1	34.8	10.4	45.2	22.8	0.50
SLFCS200(2)	26	1	54.7	10.4	65.1	24.5	0.38
SLFCS300(1)	26	1	34.9	6.9	41.8	15.1	0.36
SLCS	-	0	14.7	0	14.7	6.6	0.45

F_t = direct tensile or pull-out capacity of the J-hook connector within the concrete block
n_0 = number of J-hook connectors in top or bottom plate across the width of the section

Table 3.6 Comparison of theoretical and experimental deflections at two-third of the maximum beam test load

Beam ref.	Predicted deflection (mm)			Experimental, Δ_{exp} (mm)	$\frac{\Delta_{com}}{\Delta_{exp}}$
	Due to bending	Due to shear	Total, Δ_{com}		
SCS80	3.52	0.15	3.67	3.45	1.06
SLCS80	3.10	0.25	3.35	3.40	0.99
SCS100	3.56	0.13	3.69	4.15	0.89
SLCS100	2.53	0.17	2.70	2.56	1.05
SLFCS100(1)	3.14	0.22	3.36	3.25	1.03
SCS150	2.84	0.07	2.91	2.87	1.01
SLCS150	2.23	0.09	2.32	1.82	1.27
SLCS200	3.01	0.13	3.14	2.29	1.37
SLFCS200(1)	3.42	0.16	3.58	2.81	1.27
SLFCS200(2)	3.67	0.17	3.84	3.18	1.21
SLFCS300(1)	2.46	0.07	2.53	2.40	1.05

(a) (b)

Fig. 3.1 (a) Arrangement of J-hook connectors in SCS sandwich system; (b) welding of J-hook connector.

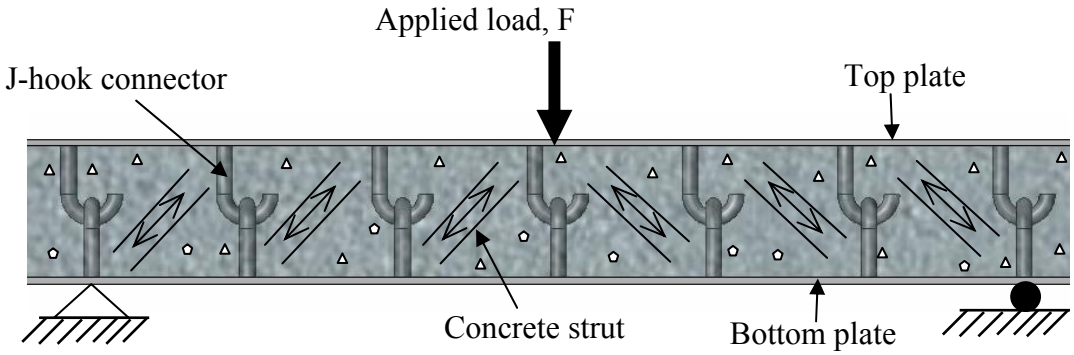

(a)

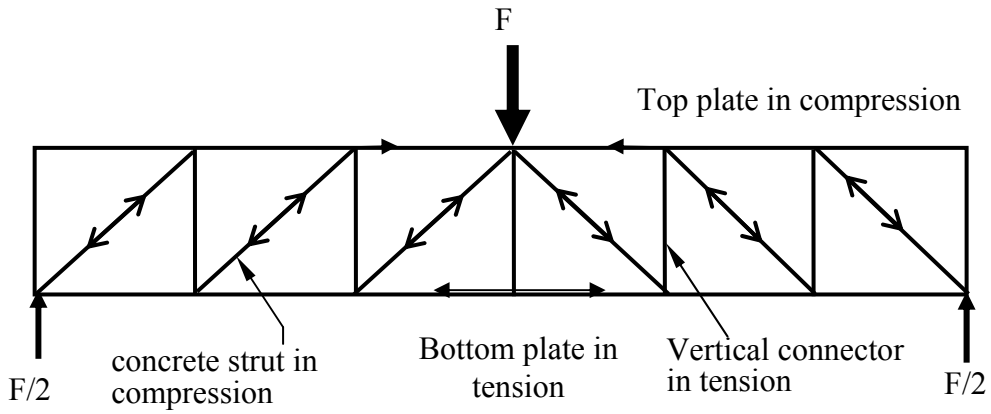

(b)

Fig. 3.2 (a) SCS sandwich beam under concentrated load (b) equivalent strut-and-tie model

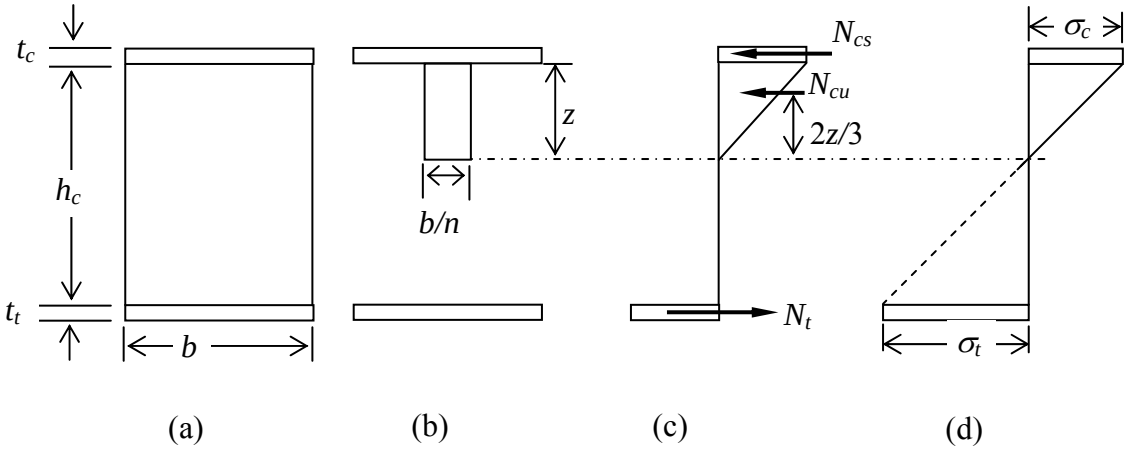

Fig. 3.3 (a) SCS beam section (b) equivalent steel section (c) force distribution in the section; (d) idealized stress distribution.

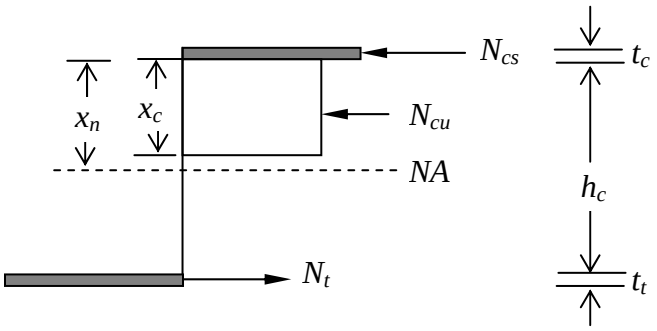

Fig. 3.4 Force distribution in the section at fully plastic stage.

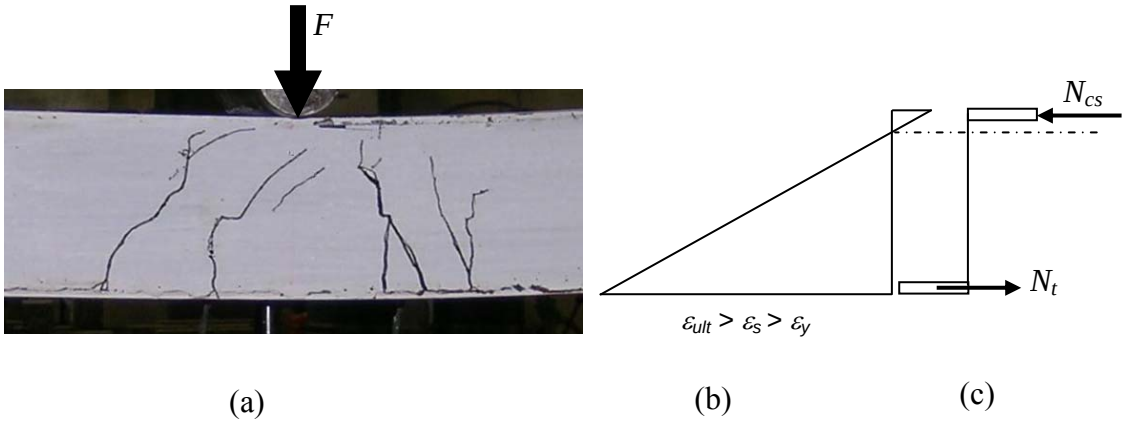

Fig. 3.5 Cracks developed in SCS sandwich test beam at failure: (a) cracking in the concrete core at failure; (b) strain in the section; (c) stress distribution

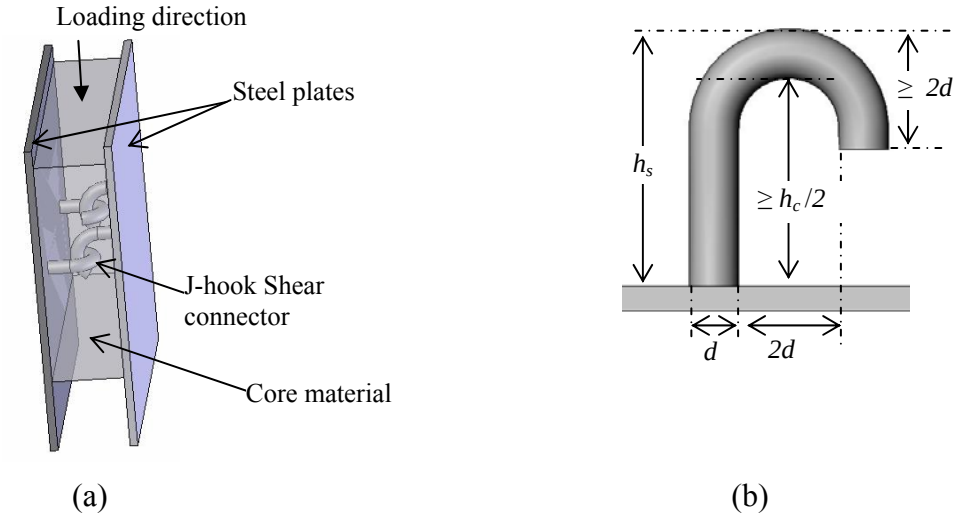

Fig. 3.6 Schematic diagram of (a) push-out test specimen and (b) details of the J-hook connector.

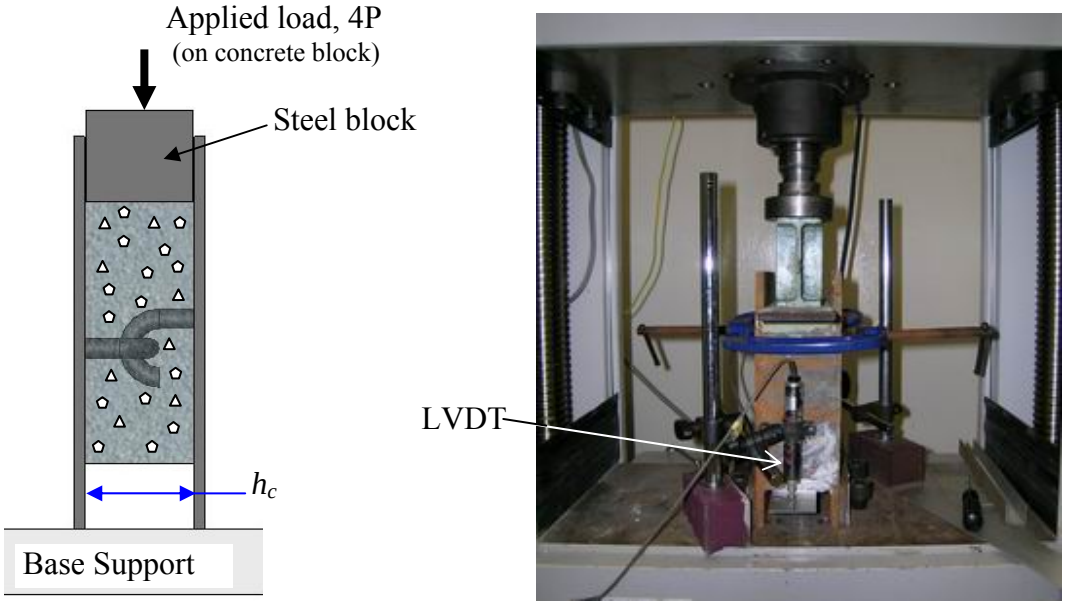

(a) Schematic diagram of test set-up (b) General view of test arrangement

Fig. 3.7 Push-out test arrangement

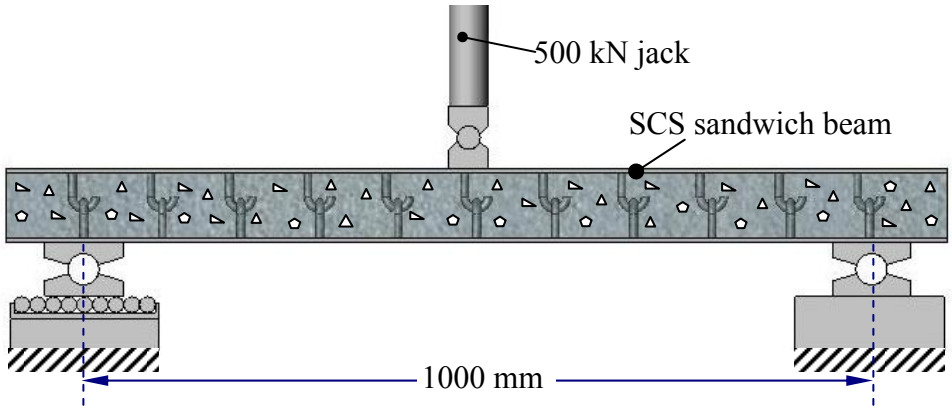

(a) Schematic diagram of the test arrangement.

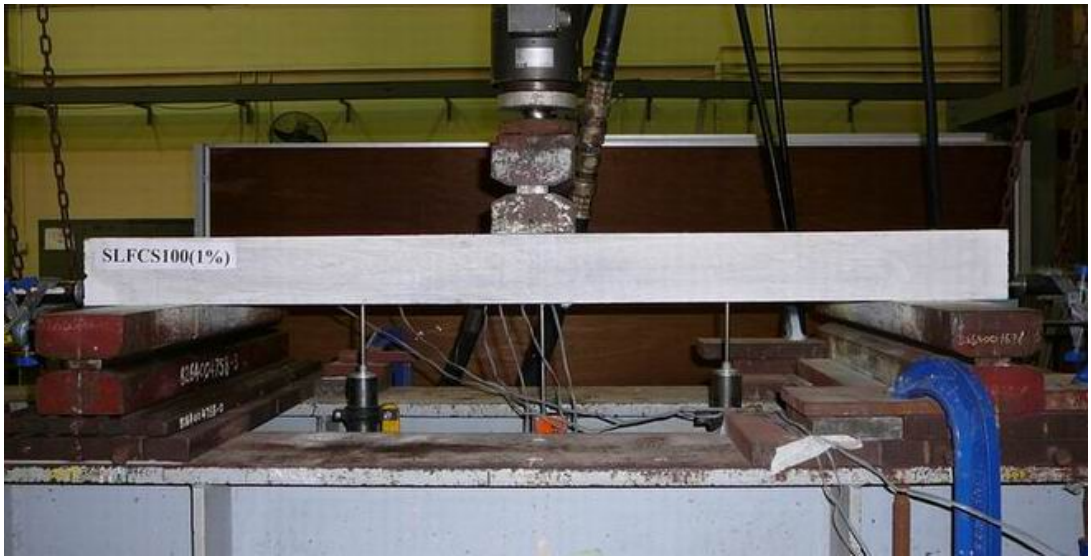

(b) Test set-up for sandwich beam specimen

Fig. 3.8 Test arrangement of SCS sandwich beams.

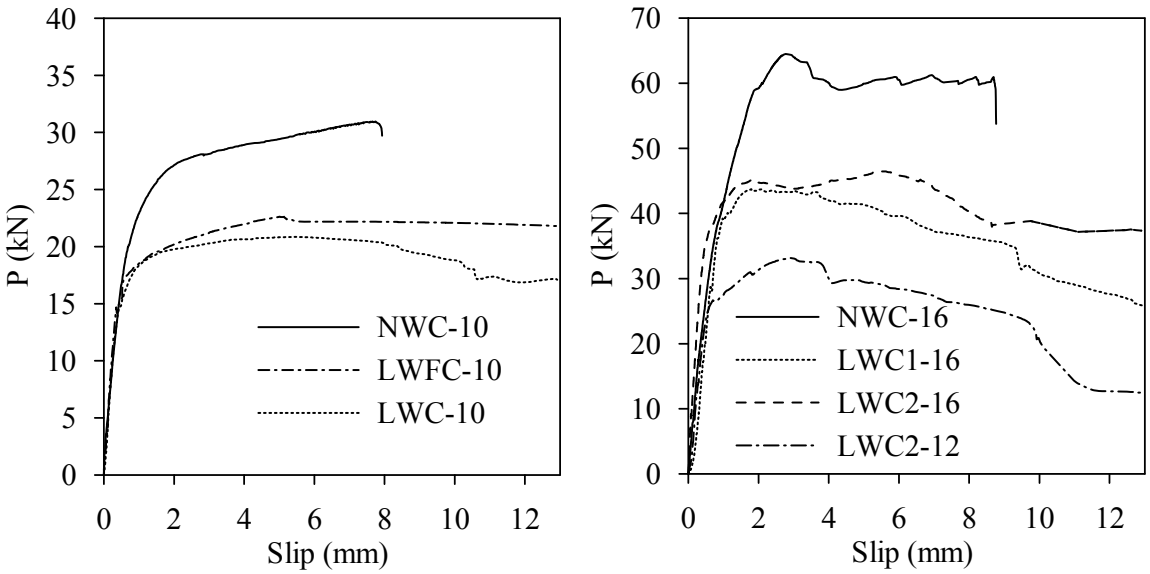

(a) specimen with 10 mm dia. J-hook

(b) Specimen with 12 mm and 16 mm dia. J-hook

Fig. 3.9 Load-slip curves of push-out tests (for each J-hook connector).

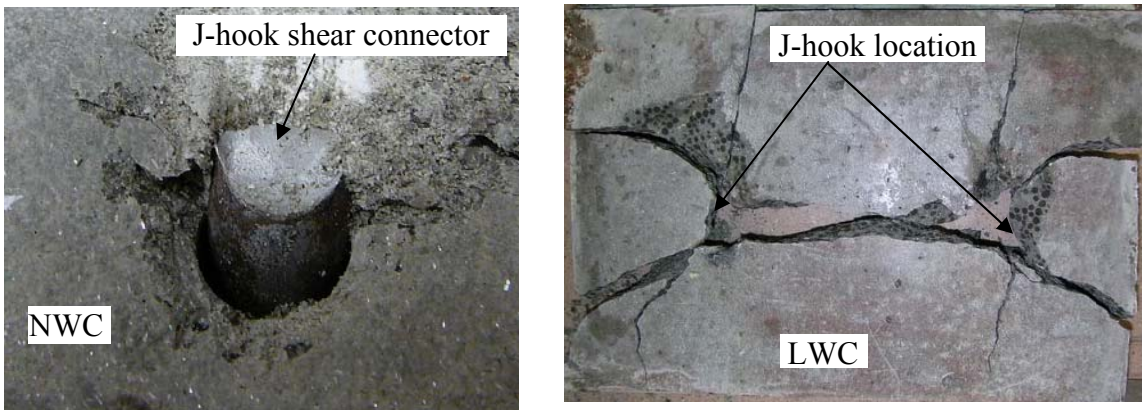

(a) Shearing failure of connector

(b) Concrete bearing failure

Fig. 3.10 Typical failure modes for the J-hook connector embedded in the concrete subjected to direct shear force.

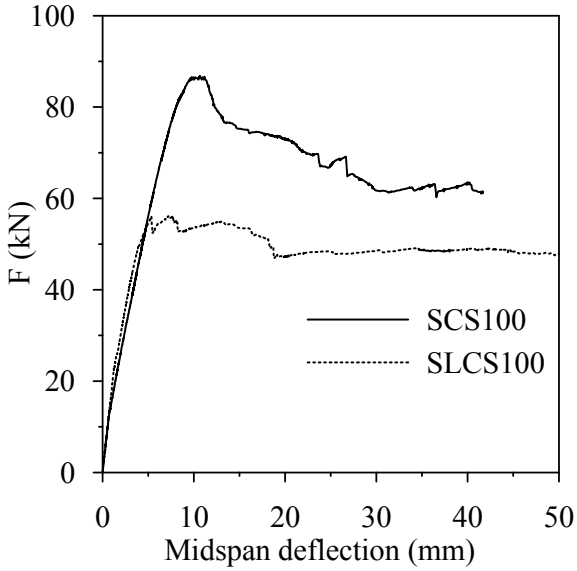

(i) h_c= 100 mm

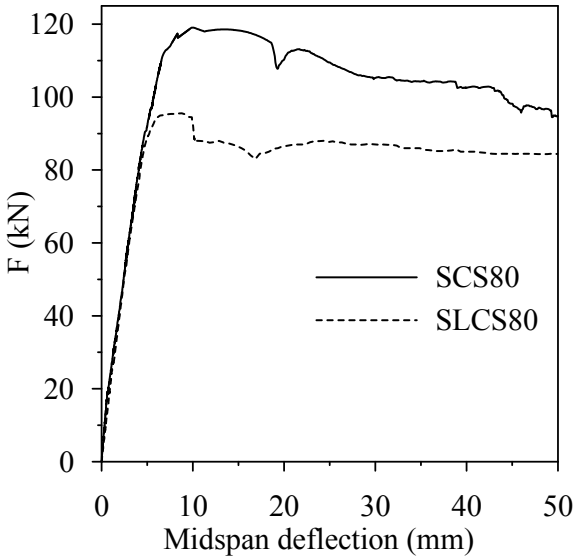

(ii) h_c =80mm

(a) Effect of concrete strength

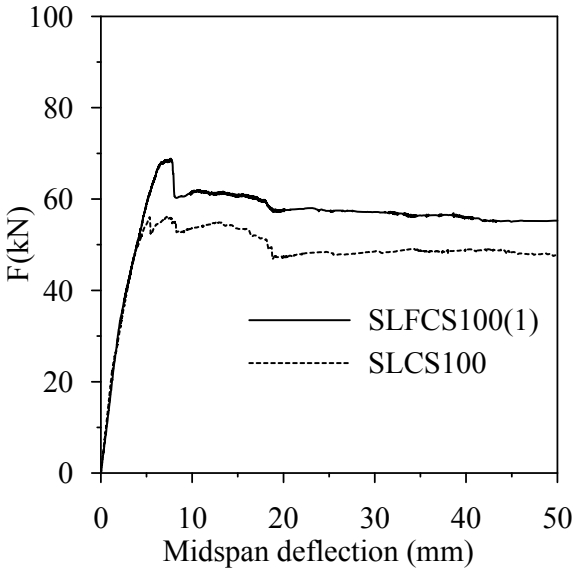

(b) Effect of steel fibre

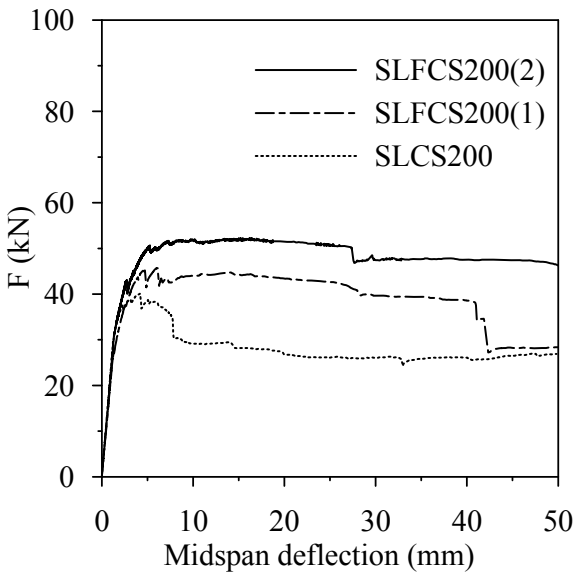

(c) Effect of PVA fibre

Fig. 3.11 Comparison of load-deflection curves of test beams.

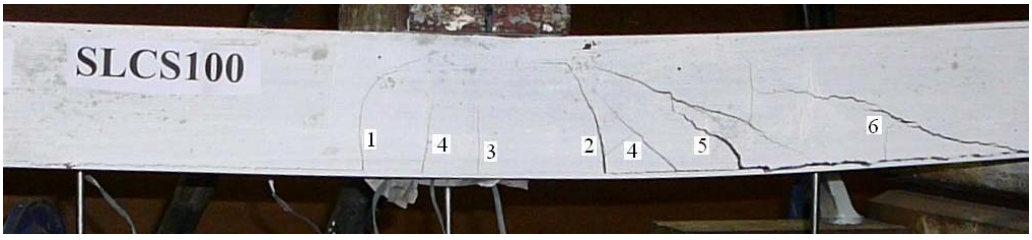

Fig. 3.12. Typical crack pattern and sequence of appearance

(a) Flexural failure

(b) Concrete shear failure

(c) Shear connector failure

(d) Slip at beam end (Beam SLCS300) at the end of test

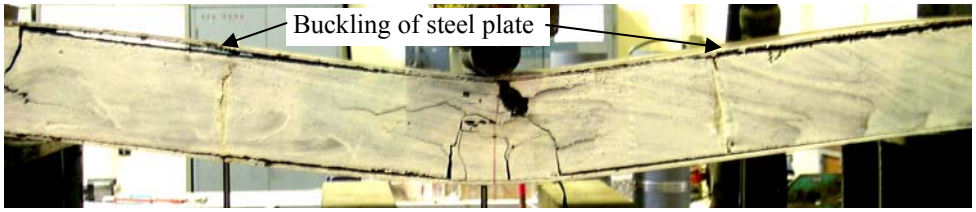

(e) Top plate buckling failure (beam SLCS)

Fig. 3.13 Typical beam failure modes due to static load.

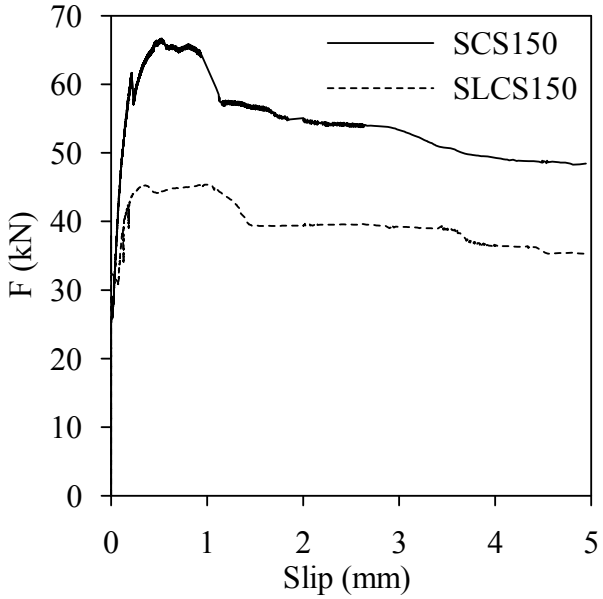

Fig. 3.14 Load versus relative slip between concrete and bottom steel plate at the beam end.

Force-indentation relations for SCS sandwich panels

4

4.1 Introduction

Low velocity impact due to dropping and floating objects or moorings can cause local indentation of the face sheet, permanent compression of the underlying core material, local damage of core and interfacial cracks. These may extend under service loads, possibly causing a catastrophic failure of the sandwich plate. Appropriate modelling of local indentation is important to predict the impact force history and overall response of the sandwich structure impacted by a foreign object. Hertz contact law has been used for evaluation this localized deformation in many analytical solutions. However, this is inappropriate since the indentation of a sandwich panel is dominated by the local deformation of the mechanical properties of core material (Abrate, 1997; Zhou and Strong, 2004; Hoo Fatt and Park, 2001). Generally, for specific shape of projectile, the local indentation depends on the core material and face plate materials. In SCS sandwich panel, core materials are mainly composed of cementitious material which is brittle in nature. However, when confined it shows some elastic-plastic behaviour (Lahlou et al., 1999). This behaviour needs to be considered to model the local indentation of SCS sandwich panel. This chapter addresses the force-indentation relation of SCS sandwich panel. The core is assumed to behave as elastic-plastic because it is virtually confined by

the two steel plates and the surrounding concrete.

4.2 Impact between projectile and SCS sandwich panel

Fig. 4.1 shows a SCS sandwich panel subjected to an impact at the centre by a hemispherical headed projectile of mass m_s and radius R_i. The initial impact velocity of the projectile is denoted by V_0. The impact causes a local indentation on the sandwich panel δ. As the bearing capacity of the concrete core is lower than the steel face plate under the point of impact, the local indentation can be predicted by modelling the top face plate resting on a deformable elastic-plastic foundation (Hoo Fatt and Park, 2001). For large indentation, membrane action due to deformation of the face plate should be considered when calculating the contact force of the sandwich structures under impact (Olsson and McManus, 1996). If the local indentation goes beyond the elastic strain limit of the steel face plate, then the inelastic behaviour of the plate should be considered. Therefore, the response behaviour due to local indentation can be divided into two categories: (1) elastic indentation up to elastic strain limit of the steel plate, and (2) plastic indentation considering the steel plate is sitting on an elastic-plastic foundation.

4.3 Force-indentation relations

4.3.1 Elastic indentation

An approximate solution for the face-sheet indentation for elastic range is derived using the principle of minimum potential energy. The core of the sandwich panel is assumed to

be rigid-perfectly-plastic since the confined concrete behaviour is elastic-plastic (Lahlou et al. 1999). The indentation is local and pointed effect, and it is dominated by the stretching of the steel face plate. The experimental force-indentation result also indicates that the local deformation in the face plate is dominated by membrane stretching (Turk and Hoo Fatt, 1999).

The strain energy in the steel face plate due to membrane stretching is given by (Timoshenko and Woinowsky-Krieger, 1969)

$$V_1 = \frac{E_s t_s}{1-\nu^2}\int_0^{2\pi}\int_0^a \left(\varepsilon_r^2 + \varepsilon_\theta^2 + 2\nu\varepsilon_r\varepsilon_\theta\right) r\,dr\,d\theta \qquad (4.1)$$

where $\varepsilon_r = du/dr + \frac{1}{2}(dw/dr)^2$ is the radial strain; $\varepsilon_\theta = u/r$ is the circumferential strain; E_s is the modulus of elasticity of steel plate; t_s is the steel thickness; and ν is the poison's ratio. The radial displacement can be approximately expressed as $u(r) = r(a-r)(C_1 + C_2 r)$, where C_1 and C_2 are arbitrary coefficients to be determined. From the experimental results of permanent indentation shape (Fig. 4.2), the deflection profile function can be written as, $w = \delta(1 - r^2/a^2)^4$, where δ is the central deflection at $r = 0$ and a is the radius of deformed zone. The edge conditions, $w = 0$ and $dw/dr = 0$ at $r = a$ are satisfied by the deflection profile equation. Using this deflection expression and minimizing the membrane stretching energy with respect to C_1 and C_2 respectively, yield the expressions for the coefficients are

$$C_1 = 0.596084\,\delta^2/a^3 \text{ and } C_2 = -1.50127\,\delta^2/a^4$$

Thus, the membrane stretching energy is

$$V_1 = \frac{3.5014\pi D_s \delta^4}{a^2 t_s^2} \qquad (4.2)$$

where $D_s = \frac{E_s t_s^3}{12(1-\nu^2)}$ and force on concrete core is written as

$$F_{con} = \frac{2\pi E_c}{h_c}\int_0^a wrdr = \frac{\pi a^2 E_c \delta}{5h_c} \tag{4.3}$$

Therefore, work done by concrete is

$$V_{con} = \int_0^\delta F_{con} d\delta = \frac{\pi a^2 E_c \delta^2}{10h_c} \tag{4.4}$$

where E_c and h_c are the concrete modulus of elasticity and concrete core thickness, respectively. The work done by the contact force is given by

$$U = -\int_0^\delta F\, d\delta \tag{4.5}$$

The total potential energy can therefore be written as:

$$\prod = V_1 + V_{con} + U \tag{4.6}$$

Minimizing the total potential energy with respect to the deflection, δ, i.e. $\partial\prod/\partial\delta = 0$, yields a contact force;

$$F = \frac{1.28526\pi t_s E_s \delta^3}{a^2} + \frac{\pi a^2 \delta E_c}{5h_c} \tag{4.7}$$

Minimizing the load F with respect to the radial damage size a i.e. $\partial F/\partial a$, and substituting a into Eq. (4.7) gives the load-indentation relation,

$$F = \left(1.03E_c t_s E_s/h_c\right)^{1/2}\delta^2 = K_e\delta^2 \tag{4.8}$$

where $K_e = \left(1.03E_c t_s E_s/h_c\right)^{1/2}$ (4.9)

4.3.2 Plastic indentation

When the steel face sheet become plastic, the pressure distribution can be assumed uniform (Stronge, 2000). The load-deflection relationship of a plastic membrane in

which material obeying Tresca's yield criterion is given by

$$F_{faceplate} = \frac{2\pi N_0 \delta}{0.5 + \ln(a/R_c)} \tag{4.10a}$$

or $$F_{faceplate} = \frac{2\pi \sigma_0 t_s \delta}{0.5 + \ln(a/R_c)} \tag{4.10b}$$

where $N_0 (= \sigma_0 t_s)$ is the constant tensile force per unit length, R_c is the contact radius of the projectile to steel plate as shown in Fig. 4.1, a is the radius of deformed zone and σ_0 is the plastic tensile strength of steel plate. Details of the derivation are given in the paper written by Onat and Haythornthwaite (1956).

Permanent deformations are introduced in the core when the indentation exceeds the elastic limit. Beyond this, it is assumed that the stress-strain behaviour in the transverse direction of the confined core is elastic-plastic. Lahlou et al. (1999) showed that the dynamic behaviour of confined concrete is similar to that of an elastic-plastic material.

The contact radius is related to the indentation and radius of the projectile head. Considering the simplification made in this analysis, the radius of the plastic zone of the concrete (R_c) is

$$R_c = \sqrt{2\delta R_i} \tag{4.11}$$

where R_i is the radius of the projectile. Using the idealized plastic behaviour of the confined concrete, the contact force for the concrete core can be written as (Christoforou (1993)) and Abrate (1998)),

$$F_{con} = \pi f_c R_c^2 \quad \text{or} \quad F_{con} = 2\pi f_c \delta R_i \tag{4.12}$$

where f_c is the compressive strength of the concrete core and R_c is the contact radius. Vertical equilibrium of the forces for this plastic phase is given by

$$F_{faceplate} + F_{con} = F \tag{4.13}$$

Substituting $F_{faceplate}$ and F_{con} from Eqs. (4.10b) and (4.12) in Eq. (4.13)

$$\frac{2\pi\sigma_0 t_s \delta}{0.5 + \ln(a/R_c)} + 2\pi f_c R_i \delta = F \tag{4.14}$$

The force-indentation relation for the plastic phase is therefore,

$$F = \left(\frac{2\pi\sigma_0 t_s}{0.5 + \ln(a/R_c)} + 2\pi f_c R_i \right) \delta \tag{4.15}$$

For a stiff core and small indentation (i.e., $\delta \leq t_s$), it can be assumed that $R_c = a$, (as shown in Fig. 4.3(a)) and Eq. (4.14) can be further simplified for $\delta \leq t_s$

$$F = (4\pi t_s \sigma_0 + 2\pi R_i f_c)\delta \tag{4.16}$$

The radius of damaged area 'a' becomes gradually larger than the radius of contact R_c as indentation depth increases. Turk and Hoo Fatt (1999) showed in their analysis that in case of large indentation, contact radius R_c is always smaller than the radius of local damage area a which is shown in Fig. 4.3(b). From the present experimental results of indentation profile, the contact radius R_c is approximately 40% of a (the radius of local deformed area) for the indentation depth of 7 mm to 16 mm.

Therefore Eq. (4.15) becomes,

$$F = \left(1.412\pi t_s \sigma_0\right)\delta + 2\pi f_c R_i \delta \tag{4.17}$$

or $$F = \left(1.412\pi t_s \sigma_0 + 2\pi f_c R_i\right)\delta = k_p \delta \tag{4.18}$$

where $$k_p = 1.412\pi t_s \sigma_0 + 2\pi f_c R_i \tag{4.19}$$

is the plastic contact stiffness for large indentation . It should be bear in mind that the

change of the contact stiffness from Eq. (4.16) to Eq. (4.18) is gradual.

In Eq. (4.8), elastic membrane action is considered in which force-deformation relation is not linear (Timoshenko and Woinowsky-Krieger, 1969). On the other hand, in equation (4.18), plastic membrane action is considered in which force-deformation relation is linear (Onat and Haythornthwaite, 1956). For this reason, the force (*F*) is linear with the indentation.

4.3.3 Unloading

For unloading phase, it is assumed that the stress-strain relation of SCS materials will follow the elastic unloading path. Barnhart and Goldsmith (1957) and later Yang and Sun (1982), suggested the following Power law for modelling the unloading phase considering the permanent deformation, δ_r

$$F = F_m \left[\frac{(\delta - \delta_p)}{(\delta_m - \delta_p)} \right]^q \quad , \ \delta_m \geq \delta \geq \delta_{cr} \tag{4.20}$$

or $$\delta = \delta_p + \left(\frac{F}{F_m} \right)^{\frac{1}{q}} (\delta_m - \delta_p) \tag{4.21}$$

where F_m is the maximum contact force just before unloading, δ_m is the indentation corresponding to F_m, δ_p is the permanent indentation during loading and unloading cycle and δ_{cr} is the critical indentation in the sandwich system. Yang and Sun (1982), suggested that $q = 2.5$ provides a good fit to the experimental data.

For $\delta > \delta_p$, with the permanent indentation defined as

$$\delta_p = \delta_m - \delta_{cr} \tag{4.22}$$

According to this model, δ_{cr} can be regarded as the yield point in deformation of the steel face plate for large deflection. From plate analysis, it is found that for large deflection of circular plate, the approximate critical deflection can be found as following (Timoshenko and Woinowsky-Krieger, 1969; §100),

$$\delta_{cr} = \sqrt{\frac{\sigma_0 a^2}{\alpha_r E_f}} \tag{4.23}$$

where α_r is a coefficient.

At the end of elastic indentation and beginning of plastic indentation, the contact zone is small and $a \approx R_c$ and the value of α_r (assuming distributed loaded fixed edge plate) is 0.976. When the contact radius R_c is approximately 40% of a at large indentation depth, the value of α_r (assuming centrally loaded fixed edge plate) is 1.232. In this present study, these two criteria are used to distinguish among the stages of indentation (elastic, initial plastic and final plastic stages).

4.4 Impact force and indentation-time history

Once the force-indentation relation is given, then from Fig.4.1, the indentation of top face plate at impact zone can be written as (assuming there is no global displacement of the panel)

$$\delta(t) = w_p(t) \tag{4.24}$$

where $w_p(t)$ and $\delta(t)$ are the displacements of the projectile and indentation in the sandwich panel at time t respectively.

Denoting the mass of the projectile m_s and impact velocity V_0, the transverse displacement of the colliding projectile with respect to the initial top surface of the object at any time t is given by (Lee, 1940)

$$w_p(t) = V_0 t - \frac{1}{m_s}\int_0^t F(\tau)(t-\tau)d\tau \tag{4.25}$$

If the global displacement of the panel is zero, from Eq.(4.24) and Eq. (4.25), the indentation can be written as

$$\delta(t) = V_0 t - \frac{1}{m_s}\int_0^t F(\tau)(t-\tau)d\tau \tag{4.26}$$

For different loading phases, the load-indentation relation will be different as discussed in section 4.3. For example, in elastic indentation phase, substituting the expression for $\delta(t)$ from Eq.(4.8), Eq. (4.26) becomes

$$\left(\frac{F(t)}{K_e}\right)^{\frac{1}{2}} = V_0 t - \frac{1}{m_s}\int_0^t F(\tau)(t-\tau)d\tau \tag{4.27}$$

This equation cannot be solved in closed form, and hence numerical technique is employed to solve for impact force and displacement history. Eq. (4.27) can be written as following form:

$$\left(\frac{F(t)}{K_e}\right)^{\frac{1}{2}} = V_0 t - \frac{1}{m_s}P(t) \tag{4.28}$$

where $P(t) = \int_0^t F(\tau)(t-\tau)d\tau$ (4.29)

4.5 Numerical procedure

The numerical procedure is applied to solve the Eq. (4.28) for impact force. Several numerical methods are available to solve the dynamic equation (Goldsmith, 1960;

Hughes, 1983; Evans et al. 1991). In the present study, Evans's method has been applied. This numerical method is found to be computationally efficient and give accurate prediction of force and displacement responses. According to this approach, the function $F(t)$ is assumed to be linear over each increment of time Δt. Denoting by F_{j-1} the value of $F(t)$ at time $(j-1)\Delta t$, where j is an integer and by F_j the value at time $j\Delta t$, then the value of $F(t)$ over this interval is represented by

$$F(\tau) = c_j \tau + d_j \qquad (j-1)\Delta t \le \tau \le j\Delta t \tag{4.30}$$

where $c_j = \dfrac{F_j - F_{j-1}}{\Delta t}$ and $d_j = jF_{j-1} - (j-1)F_j$ (4.31)

It follows that

$$\begin{aligned} P(t) &= P(N\Delta t) \\ &= \sum_{j=1}^{N} \int_{(j-i)\Delta t}^{j\Delta t} (c_j \tau + d_j)(N\Delta t - \tau) d\tau \end{aligned} \tag{4.32}$$

The integrals in Eq. (4.32) are analytic and, since at time $t = 0, F_0 = 0$,

$$P(N\Delta t) = (\Delta t)^2 \left(\frac{F_N}{6} + \sum_{j=1}^{N-1} F_j (N - j) \right) \tag{4.33}$$

Hence Eq. (4.28) may be written in the form

$$\left(\frac{F_N}{K_e} \right)^{1/2} = A_N + BF_N \tag{4.34}$$

where F_N is the value of $F(t)$ at time $t = N\Delta t$ and

$$A_N = V_0(N\Delta t) - \frac{1}{m_s}(\Delta t)^2 \sum_{j=1}^{N-1} F_j (N-1) \tag{4.35}$$

$$B = -\frac{(\Delta t)^2}{6m_s} \tag{4.36}$$

Note that B is constant and not varied with time and A_N may be readily calculated since it involves only values F_j up to F_{N-1}. Detailed derivation of this numerical method is

given in the paper written by Evans et al. (1991).

4.6 Strain rate effects on material strength

When a sandwich plate is subjected to a projectile impact load, the yield strength of the steel face plate will be different from static or quasi-static values due to strain rate effects on the steel. Hence it is necessary to evaluate the dynamic strength of the steel plate. The mean uniaxial strain rate $\dot{\varepsilon}_d$ for impact velocity V_0 may be estimated by means of the Perrone and Bhadra (1984) approximation which is further simplified by Shen (1995) as $\dot{\varepsilon}_d = 4w_{pr}V_0 \Big/ \left(3\sqrt{2}R^2\right)$, where R is the radius of a circular plate. The Cowper-Symonds equation has been widely used for strain rates up to about 10^3 s^{-1} (Jones, 1989 and 2008) to estimate the dynamic yield strength, σ_{yd}, of the steel plate from the static yield strength, σ_y, with known $\dot{\varepsilon}_d$:

$$\sigma_{yd} = \sigma_y \left[1 + \left(\dot{\varepsilon}_d \Big/ C_s \right)^{1/p} \right] \tag{4.37}$$

where C_s and p are the material constants. The parameters for mild steel under dynamic loadings are C_s = 40.4 and $p = 5$ as suggested by Cowper and Symonds (Jones, 1989).

Thus, the steel yield strength in proposed formula given in Section 4.5 should be modified to account for the dynamic strain rate effect. In this analysis, the strain rate effect on concrete was not considered, because there is no tool to determine the strain rate in concrete and the strain rate effect on confined concrete at low velocity impact is also unknown.

4.7 Experimental investigation

The experimental investigation focuses on the impact performance of SCS sandwich structures subjected to low-velocity impact. In this experimental programme, the thickness of the steel plates and properties of the core materials are considered.

4.7.1 Test specimens

To investigate local impact behaviour, ten specimens were prepared. Three types of concrete were used, namely Normal Concrete (NC), foam concrete (FC) and lightweight concrete (LWC). Some specimens contained concrete with PVA fibre (Kuralon RF 4000/30mm PVA fibres). All sandwich panels for local impact test were 300 mm square in size with a core thickness of either 60 mm or 80 mm (Fig. 4.4(a)). Thickness of the steel face plates varies from 4 mm to 8 mm. This series covers the local impact testing of sandwich panel containing plain concrete, foam concrete and lightweight concrete. The detailed test program to investigate the local impact behaviour is given in Table 4.1.

4.7.2 Test set-up

An instrumented drop weight impact machine, similar to that described by Ong et al. (1999), are used for impact testing. The entire impact test frame and set-up are shown in Figs. 4.5 and 4.6. A steel frame was designed and fabricated for supporting the specimen under test conditions (Fig. 4.4(b)). The frame was made by welding four 100×50×10 mm parallel flange channels, each of length 404 mm, together to a base plate as shown in Fig. 4.5(b). The test specimens were accommodated in the central square

void of the frame. A 100 mm diameter opening is provided in the centre of the base plate. The thickness of both base plate and cover plate is 15 mm. This entire frame was bolted to the heavy base frame of the test rig. Due to the stiff configuration of the frame, minimum bending was expected when the specimen was loaded centrally. The mode that absorbs most of the energy from the impact would therefore be the local punching failure mode. A central impact was achieved by means of a guide rail which was fabricated using aluminium angles. The projectile (Fig. 4.6(b)) is allowed to slide freely up and down through a guide which is supported by a self-supporting steel frame. The projectile can be raised up to a maximum height of 4.0 meter by a hand winch through a high-tension steel wire. The projectile was dropped from a desired height, guided by the aluminium guide rail, onto the test specimen to generate an impact load on the specimen. Grease was applied to reduce the friction along the guides and to ensure a controlled and smooth fall. In this study, the projectile mass was 58 kg and dropped from a height of 3.78 meter, which produced impact velocity of 8.12 m/sec. The tip of the projectile was hemispherical with a diameter of 90 mm. To achieve desired impact force, a projectile tup was specially designed which is shown in Fig. 4.6(b). The whole set-up was instrumented with the help of dynamic load cells, strain gauges and a laser-diode system. The load cells specification was PCB 206C. More descriptions of the laser-diode system with schematic figures are given in Chapter 5.

The test specimen was mounted and positioned on its supports. All sensors were connected to a 16-channel oscilloscope to capture the data. Then the projectile was

slowly raised to the desired height and hand winch was clamped. After another round of checking of the instrumentation, the clamp of hand winch was quickly removed to allow the projectile to fall freely onto the centre of the specimen. The oscilloscope was triggered by the signal from the top photodiode. All data were recorded at 5 μs intervals (i.e., sampling rate of 2×10^5 per second). Recorded data were stored in an internal hard disk drive and transfer to a personal computer after the test for further analysis. Full view of the experimental set-up is shown in Fig. 4.6.

4.8 Impact test results and discussion

4.8.1 Impact damage

After each impact test, the damage level was evaluated based on the indentation depth, average dent diameter, and crack propagation in the core. In all the cases of SCS sandwich panels, regardless of the composition of the cementitious core material, the steel plates were dented by the projectile impact (Fig. 4.7). Nevertheless the properties of the core material varied, middle plates (core) cracked due to the impact and these cracks propagated radially from the centre (Fig. 4.8). In the case of plain concretes (foam, lightweight and normal weight concrete) the cracking was comprehensive (full depth crack) with several pieces of the core material separating entirely from each other along with numerous fragments (Fig. 4.8). In case of foam concrete, the middle plate pulverized below the point of impact between the two steel plates. On the other hand, for normal weight and lightweight concrete the pulverization was less. In case of fibre reinforced concrete (SFFCS or SLFCS) the fibres held the pieces of core material

together after cracking (Fig. 4.8(c) to (f)). This middle core could therefore be lifted out in one piece after the impact though deep radial cracks were formed. Dent was formed at the point of impact on the top surface of the middle plate, similarly the dent that was formed on the steel plates in all the tests.

4.8.2 Denting in the sandwich panel

Dent depth on the top steel plate of each test specimen was measured after impact. A LVDT transducer was used to measure the permanent dent depth at interval points of half-centimetre apart along a diameter on the circular area of exposure to impact (see Fig. 4.7). The process was repeated thrice to obtain an average dent profile. The typical dent profiles for some sandwich specimens are plotted in Figs. 4.9 and 4.10 and dent depths at centres for all specimens are given in Table 4.2. The dent profiles were generally parabolic in shape. The indentation diameter was varied from 140 to 160 mm, whereas the projectile head diameter is only 90 mm.

The depth of the dent reduced significantly with increase of the compressive strength of the core materials. In sandwich panel (SFCS6-60-6) with foam concrete (16 MPa) a dent of 13.2 mm was observed while in the sandwich panel (SCS6-60-6) with concrete core of 69 MPa a dent of 4.3 mm was noted (Fig. 4.9). Uses of fibre in core material exhibits lower dent depth compared to other core which do not contain fibre (Fig. 4.10). Inclusion of 1% volume fraction of fibre in the lightweight concrete core, dent depth decrease 6.3% which can be calculated from Table 4.2 in case of panels SLCS4-80-4 and

SLFCS4-80-4(1). The dent depth reduced significantly with an increase in steel face plate thickness. In sandwich panel SFCS4-60-4 with 4 mm face plate, a dent depth is 15.0 mm was observed while in the sandwich panel SFCS6-60-6 with 6 mm face plate, a dent depth was 13.2 mm (Table 4.2). The reason may be related to the effect of local bending and membrane action of the facesheet, which is directly related to the facesheet thickness.

Thus it can be concluded that for sandwich panel, the dent depth was a function of the compressive strength of the core material and the face plate thickness. As these two parameters increased in value, the dent depth decreased. Fibre in the concrete core also helped to reduce the dent depth because fibre improves the damage resistance of the concrete.

4.8.3 Impact force-time history

Figs. 4.11 to 4.13 show the impact force-time histories recorded by the load cells near the hammer tip from the test specimens. Upon impact, the SCS sandwich panel experienced a sudden increase in impact force which rises to the maximum value. There are two phases, one is loading and another is unloading phase. The time to reach peak impact force was very short because of the hard contacts between the steel projectile and the steel plate. The peak loads may be influenced by various parameters. However, in the present study, the nose shape of the projectile, core thickness, the boundary conditions and impact velocity were kept the same and hence, the peak load was affected mainly by

the face plate thickness and type of concrete core used in the specimen. Core strength had important effects on the loading response of the sandwich panels. The impact test indicated that the maximum contact force generally increased with increasing core strength as indicated in Fig. 4.11 and Table 4.2. This can generally be explained by a stiffness argument since the soft core material can be deformed more easily under the projectile and less resistance imparted to the projectile. Thus less impact force is generated at the impact event. Use of fibre in the core material also had little effect on the impact force history which can be seen in Fig. 4.12 where the impact force slightly increased by adding 1% volume fraction of PVA fibre in the concrete core.

Impact forces of the sandwich specimens were affected by the steel face plate thickness as the impact forces increased with the increasing of steel face plate thickness for the same impact velocity. This is shown in Fig. 4.13 and Table 4.2. The peak impact force was increased about 11.3 % when the steel face plate thickness changed from 4 mm to 6 mm (Table 4.2). This increase was 15.5% when thickness of the steel face plate changed from 6 mm to 8 mm. This can be attributed to the increase in bending and membrane stiffness when the steel face plate thickness increased.

4.9 Comparison of analytical results with experimental results

A comparison of the experimental values of impact force history and permanent displacement with analytical solution was made. Analytically, the impact force history and indentation history for the local impact on SCS sandwich were obtained using the

analytical methods described in sections 4.3 to 4.6. On the other hand, experimentally the impact force history and the permanent dent depth were obtained for each test. Comparisons between experimental and analytical results for indentation and impact force history are shown in Figs. 4.14 and 4.15. The analytical permanent indentation is lower than experimental indentation for all specimens with foam concrete core. On the other hand, these are higher than experimental indentation for specimens with lightweight and normal weight concrete core (Table 4.3 and Fig. 4.14). This may be the cause of inaccurate prediction of elastic recovery of the steel plate. The impact force-time history obtained by the analytical analysis looks similar to the force history obtained by experiment. There is a first peak at around 0.3 ms in analytical impact force-time history due to change from elastic stage to plastic stage during impact. The error of analytical method in predicting the maximum impact force is within 8%. The little differences are due to idealization of the material properties for analytical solutions. For simplicity, only the concrete compressive strength and modulus of elasticity are considered in the analytical formula. However, the fibre reinforced concrete may have different behaviour from plain concrete under impact. With all of these limitations, the accuracy of the computational impact force history and residual dent depth by analytical model is within reasonable limits. Therefore, the proposed force-indentation relations based on the steel face plate bending and membrane stiffness, and the elastic-plastic behaviour of concrete core can be used to predict the impact response of the SCS sandwich structures during impact.

4.10 Summary

This chapter is concerned with the localized behaviour of SCS panels under low velocity impact. This has been done by both analytical and experimental studies. The dynamic local indentation on SCS sandwich panel has been modelled considering the face plate bending followed by membrane action and deformation of the core as an elastic-plastic material. Impact force history of the sandwich panel can be predicted accurately using the proposed analytical solution. The comparison of results shows that the experimental results agreed well with the analytical results of impact force history as well as indentation.

The experimental investigation shows that the plain concrete cores may crack at the event of impact. Using 1% to 2% fibre in concrete core reduces the cracks significantly and ensures that the core remained as a single piece after the impact. There is no significant difference in permanent indentation depth between using of 1% and 2% fibre in the lightweight concrete core. Moreover, it is very difficult to achieve sufficient compact concrete during the casting of concrete with 2% fibre. Thus, use of 1% fibre is sufficient to reduce the local impact damage for SCS sandwich structures and recommended for the nest series of studies. Considering quality control during casting, strength and impact resistance, lightweight aggregate concrete will used for SCS sandwich beams and slabs.

Table 4.1 Test specimens and specification for local impact

Sl. No.	Test ref. no.	h_c (mm)	t_s (mm)	Core material	ρ (kg/m^3)	f_c (MPa)	E_c (GPa)	σ_y (MPa)
1	SFCS4-60-4	60	4	Foam concrete	1200	16.0	5.5	285.1
2	SFCS6-60-6	60	6	Foam concrete	1200	16.0	5.5	304.2
3	SFCS8-60-8	60	8	Foam concrete	1200	16.0	5.5	314.8
4	SFFCS4-60-4(1)	60	4	Foam concrete with 1 % fibre	1200	16.3	5.6	285.1
5	SFFCS4-60-4(2)	60	4	Foam concrete with 2 % fibre	1200	16.9	5.6	285.1
6	SFFCS4-60-4(3)	60	4	Foam concrete with 3 % fibre	1200	17.9	5.6	285.1
7	SLCS4-80-4	80	4	LWA concrete	1440	28.5	11.5	275.5
8	SLFCS4-80-4(1)	80	4	LWA concrete with 1% fibre	1440	28.9	11.9	275.5
9	SLFCS4-80-4(2)	80	4	LWA concrete with 2% fibre	1440	29.5	11.9	275.5
10	SCS6-60-6	60	6	Normal weight concrete	2350	69.0	31	304.2
11	SCS8-60-8	60	8	Normal weight concrete	2350	69.0	31	314.8

* SFCS = steel-foam concrete-steel; SFFCS=Steel -fibre foam concrete-steel; SLCS= Steel lightweight aggregate concrete steel; SLFCS= Steel-lightweight aggregate concrete with fibre-steel; LWA = Light weight aggregate concrete; ρ = density of concrete; E_c = Concrete modulus of elasticity; σ_y = yield strength of steel; h_c = core thickness

Table 4.2 Results of local impact test

Sl. No.	Test ref. no.	Dent depth (mm)	a (mm)	Impact force (kN)	Damage description
1	SFCS4-60-4	15.0	80	203	Core broke into pieces
2	SFCS6-60-6	13.2	80	226	Core broke into pieces
3	SFCS8-60-8	9.2	80	261	Core broke into pieces
4	SFFCS4-60-4(1)	14.2	80	212	Crack in the core were visible
5	SFFCS4-60-4(2)	14.0	75	213	Crack in the core were visible
6	SFFCS4-60-4(3)	14.0	75	216	Crack in the core were visible
7	SLCS4-80-4	11.2	75	263	Core broke into pieces
8	SLFCS4-80-4(1)	10.5	75	264	Crack in the core were visible
9	SLFCS4-80-4(2)	9.6	75	267	Crack in the core were visible
10	SCS6-60-6	4.3	75	364	Core broke into pieces
11	SCS8-60-8	3.0	70	438	Core broke into pieces

a = radius of the deformed zone.

Table 4.3 Comparison between experimental results and analytical results of maximum impact force and permanent deformation (indentation) of different SCS sandwiches.

Test ref. no.	Core material	$\dot{\varepsilon}_d$ (s^{-1})	Max. impact force (kN)		Permanent indentation (mm)	
			Exp.	Analy.	Exp.	Analy.
SFCS4-60-4	Foam concrete	4.49	203	213	15.0	14.0
SFCS6-60-6	Foam concrete	3.95	226	246	13.2	10.2
SFCS8-60-8	Foam concrete	3.74	261	269	9.2	9.0
SFFCS4-60-4(1)	Foam concrete with 1% fibre	4.25	212	215	14.2	13.8
SLCS4-80-4	LWA concrete	3.81	263	242	11.2	12.0
SLFCS4-80-4(1)	LWA concrete with 1% fibre	3.57	264	253	10.5	11.5
SLFCS4-80-4(2)	LWA concrete with 2% fibre	3.27	267	254	9.6	11.3
SCS6-60-6	Normal weight concrete	1.46	364	352	4.3	6.9
SCS8-60-8	Normal weight concrete	1.17	438	452	3.0	5.0

$\dot{\varepsilon}_d$ = dynamic strain rate; Eep. = experimental results; Analy. = Analytical results

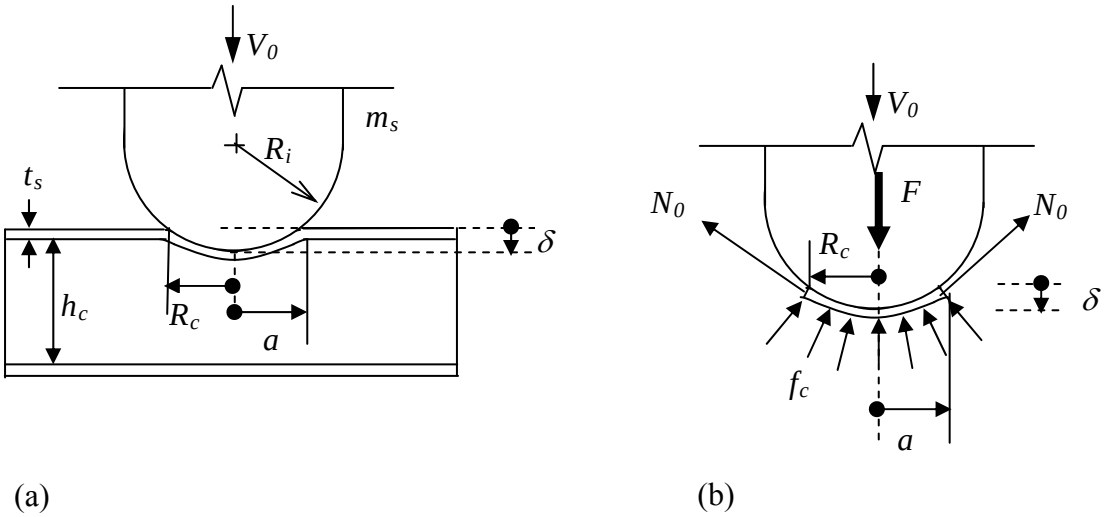

(a) (b)

Fig. 4.1 (a) Indentation on the face plate cause by a spherical-headed indentor and (b) forces acting on the deformed face plate.

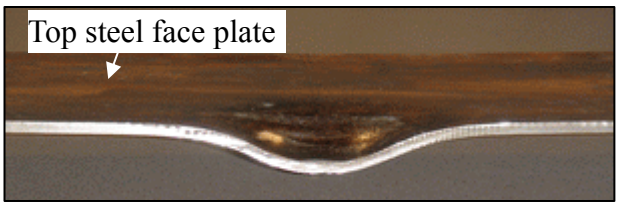

(a)

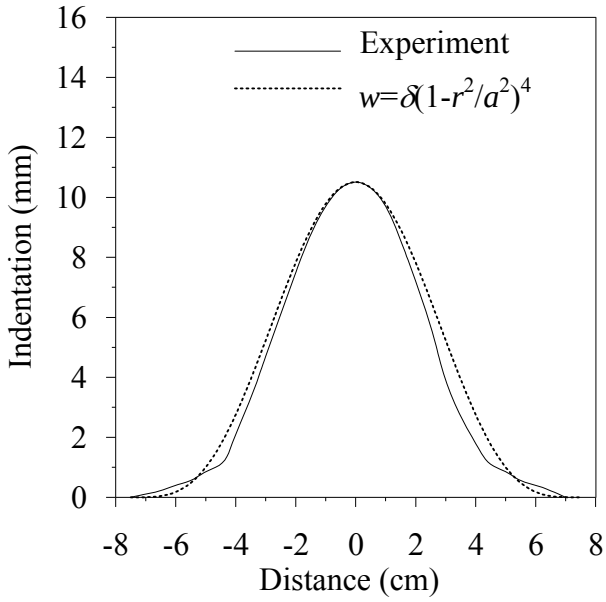

(b)

Fig.4.2 (a) Experimental indentation profile in SCS sandwich panel and (b) Profile equation.

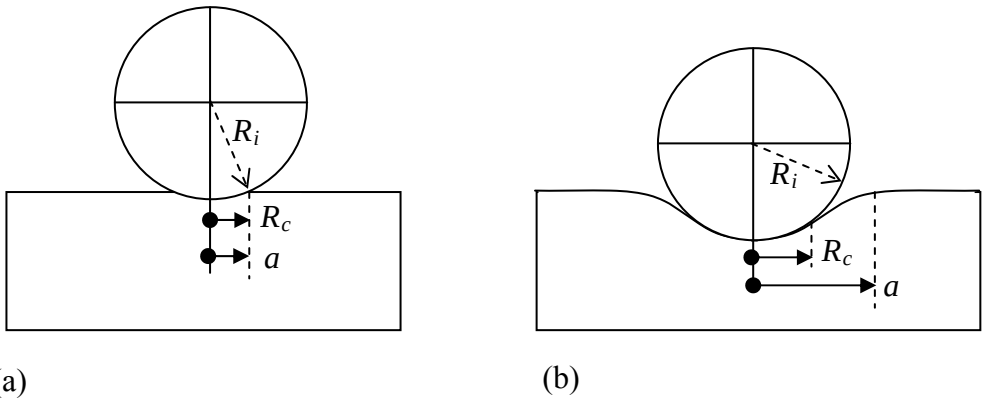

Fig. 4.3 Local indentation shape by spherical-headed indentor: (a) small indentation and (b) large indentation.

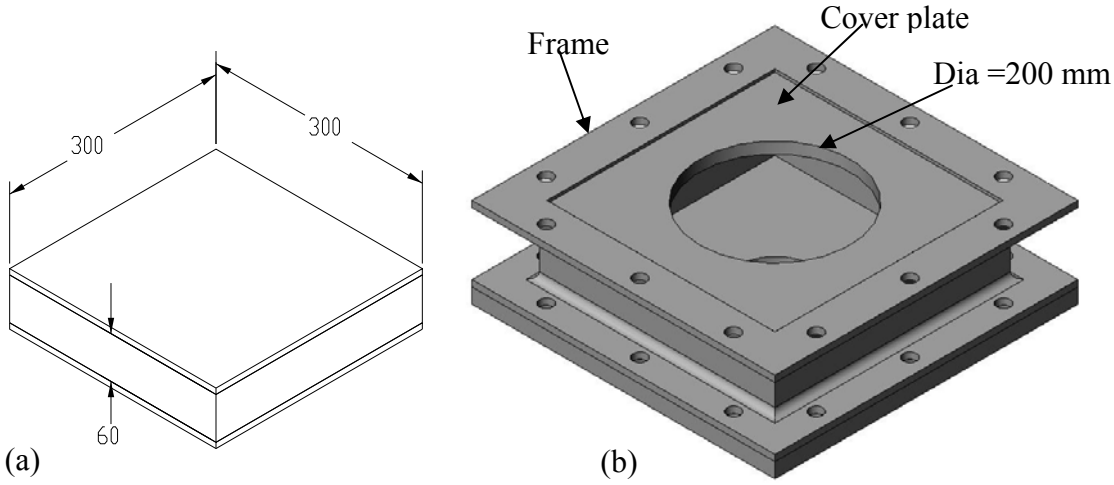

Fig. 4.4 Schematic diagram: (a) specimen and (b) frame to hold the specimen.

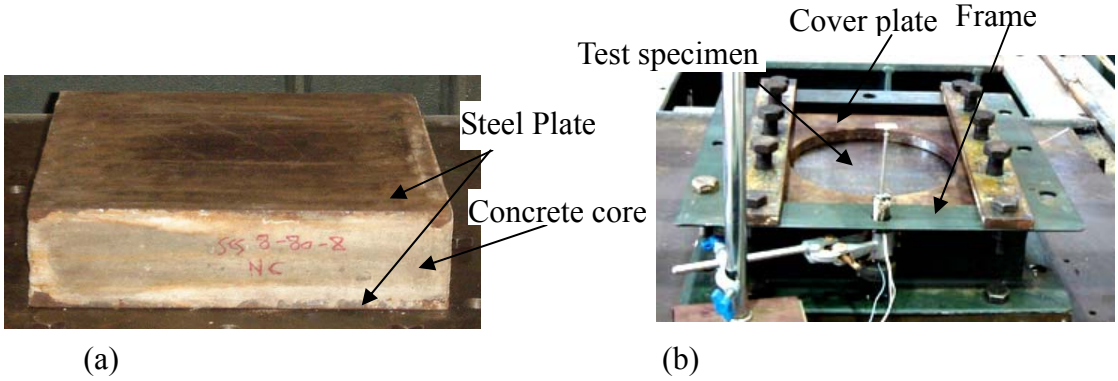

Fig. 4.5 (a) Specimen for the investigation of local impact behaviour and (b) picture of the frame holding the specimen during impact.

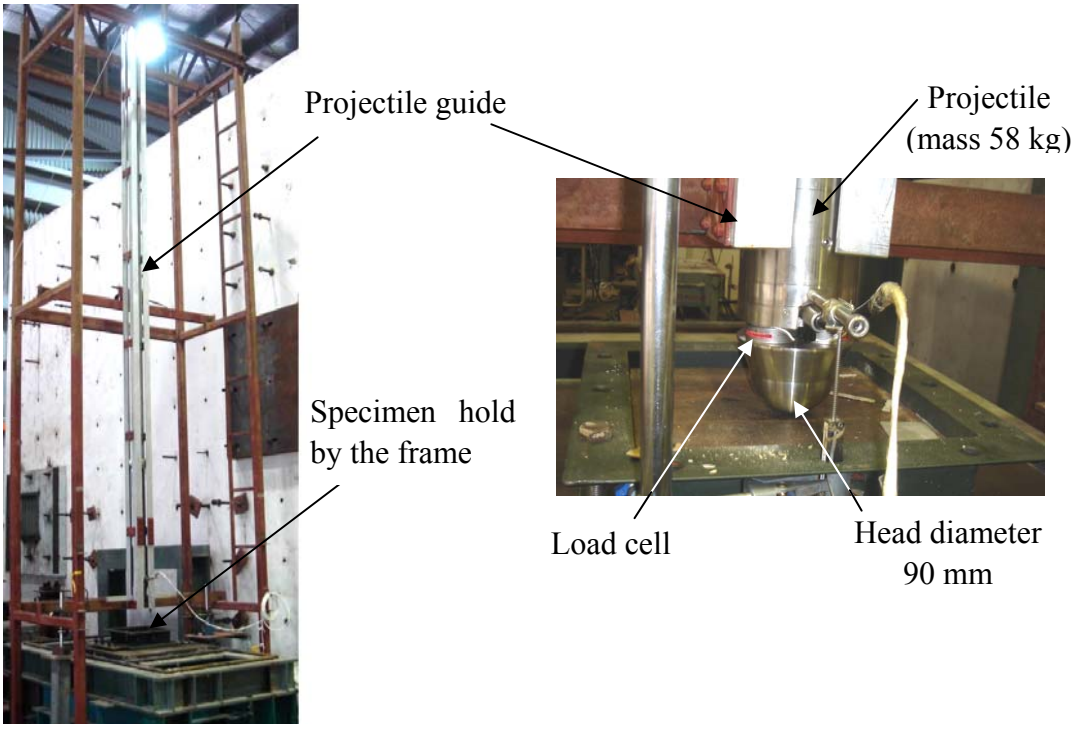

Fig. 4.6 (a) Experimental set-up for impact on SCS sandwiches (b) Projectile into the guide

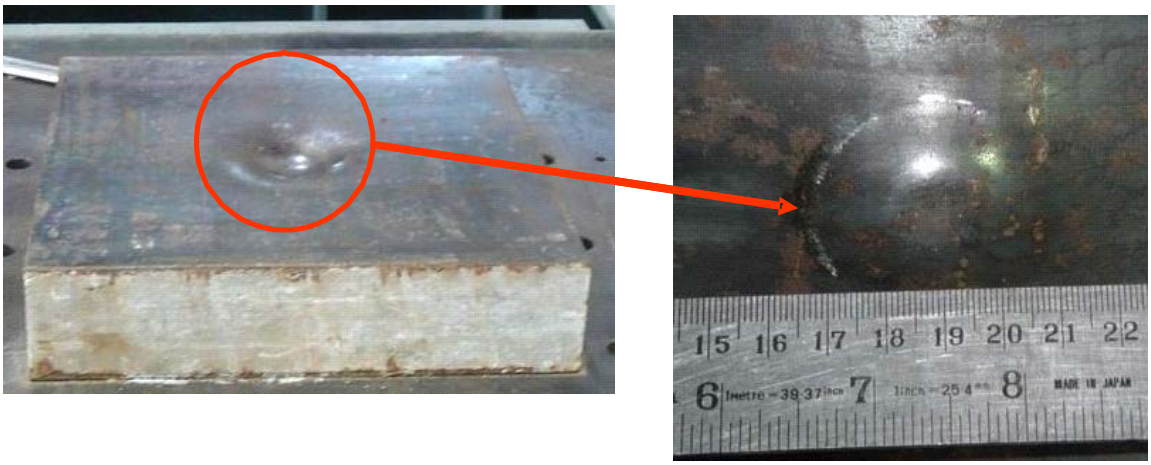

Fig. 4.7 Local impact damage (indentation) of SCS sandwich panel due to projectile impact.

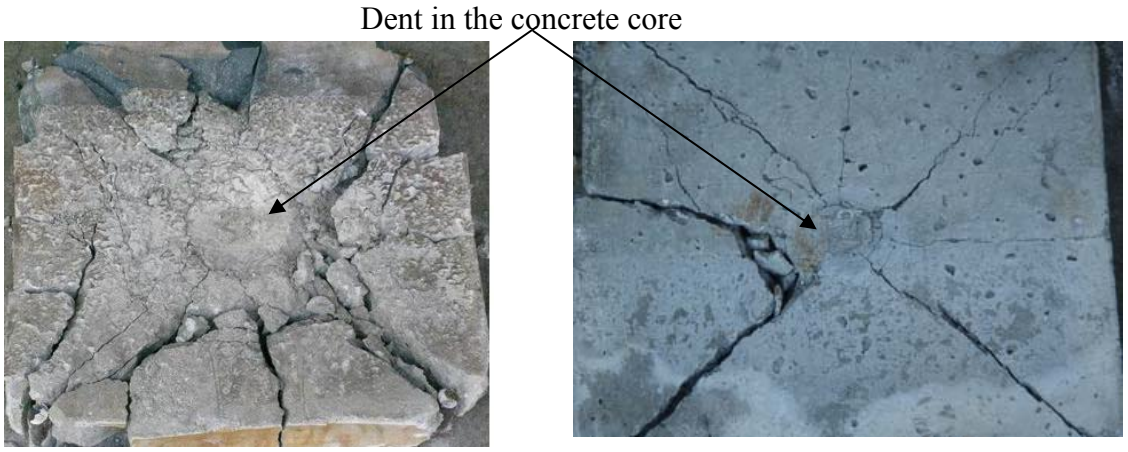

(a) Foam concrete without fibre, SFC S4-60-4

(b) Normal weight concrete, SCS6-60-6

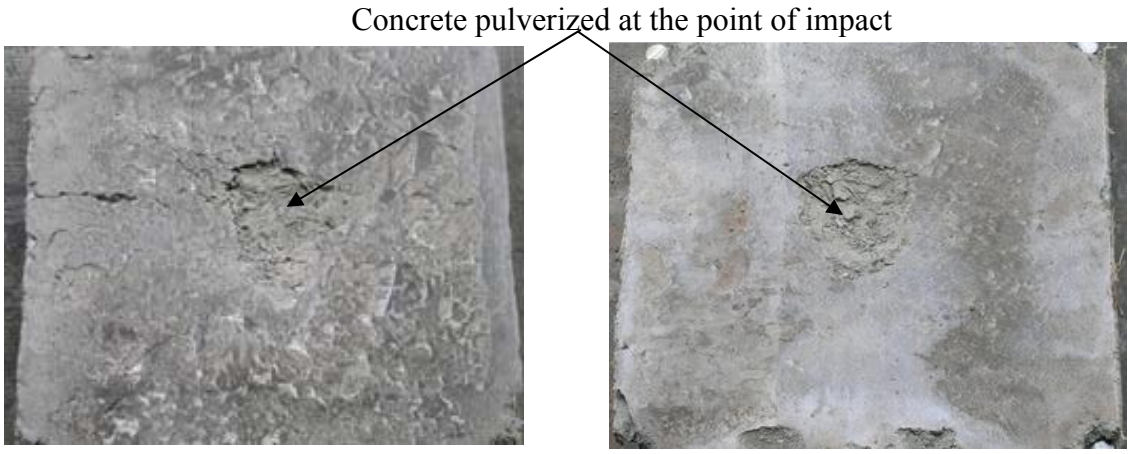

(c) Foam concrete with 2% PVA fibre, SFFCS4-60-4 (2)

(d) Foam concrete with 3% PVA fibre, SFFCS4-60-4(3)

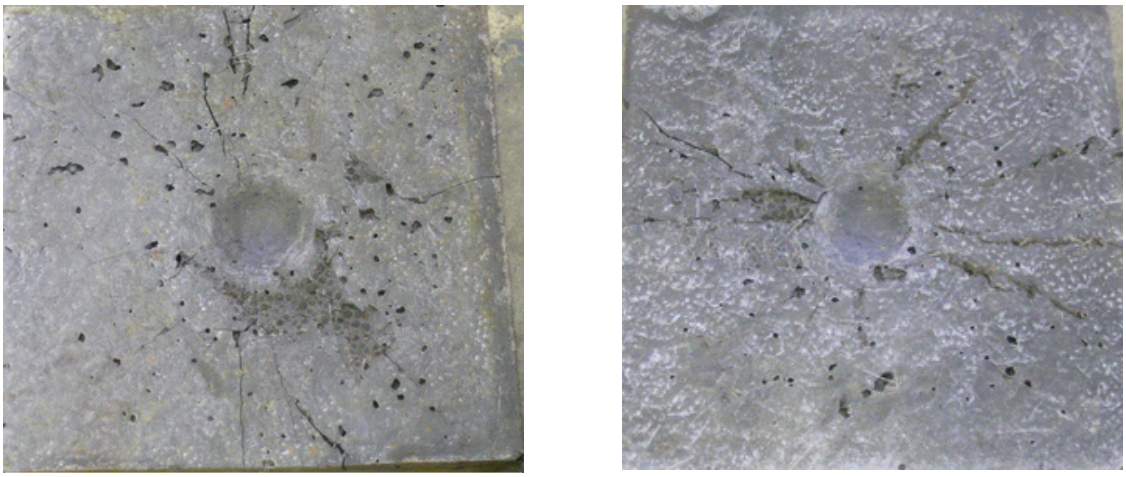

(e) Lightweight concrete with 1% PVA fibre, SLFCS4-80-4 (1)

(f) Lightweight concrete with 2% PVA fibre, SLFCS4-80-4 (2%)

Fig. 4.8 Local impact damage in the concrete core due to projectile impact

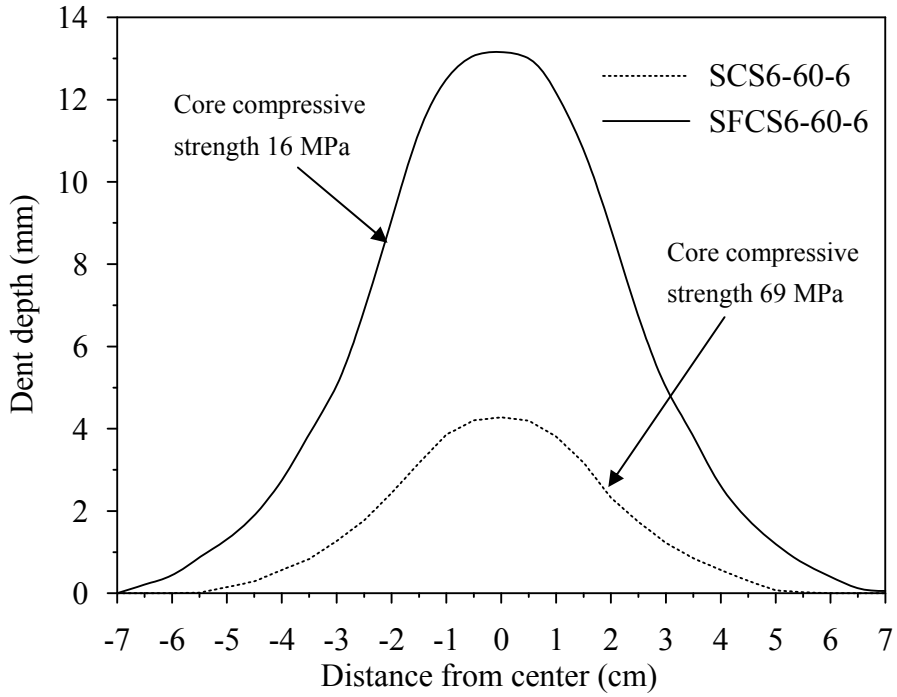

Fig. 4.9 Effect of core compressive strength on the permanent dent profile of face plate of SCS sandwich (6 mm thick face plate).

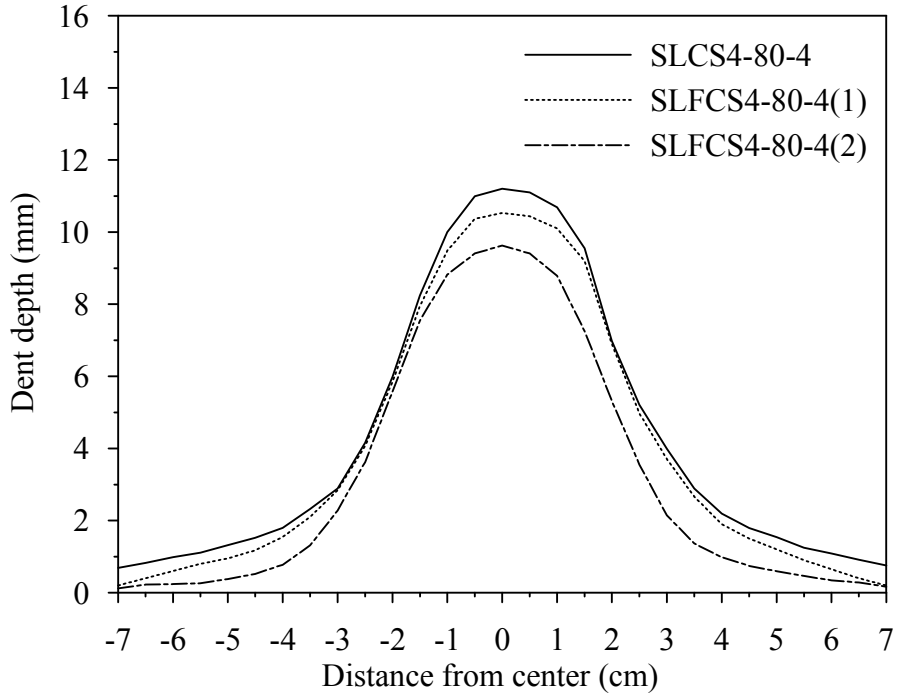

Fig. 4.10 Effect of fibre on the permanent dent profile of face plate of SCS sandwich (face plate thickness=4 mm; core =light weight concrete).

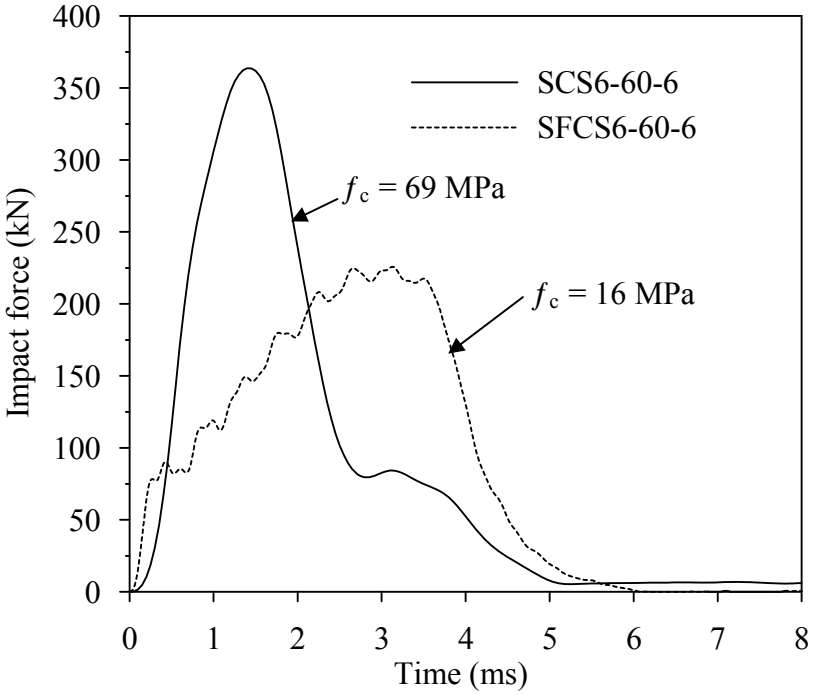

Fig. 4.11 Effect of core compressive strength on the impact force history of SCS sandwich (6 mm thick face plate).

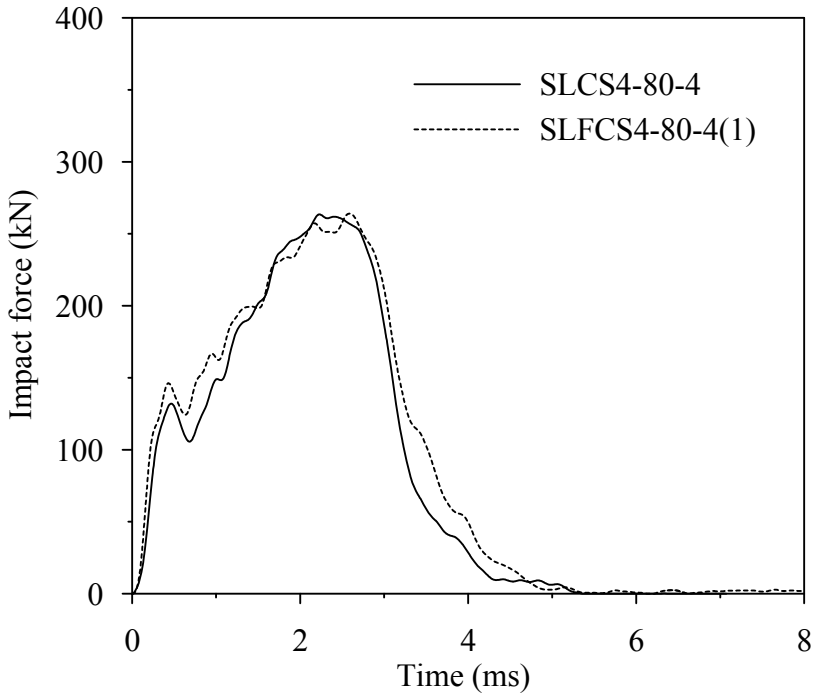

Fig. 4.12 Effect of fibre (PVA) on the impact force history of SCS sandwich (4 mm thick face plate).

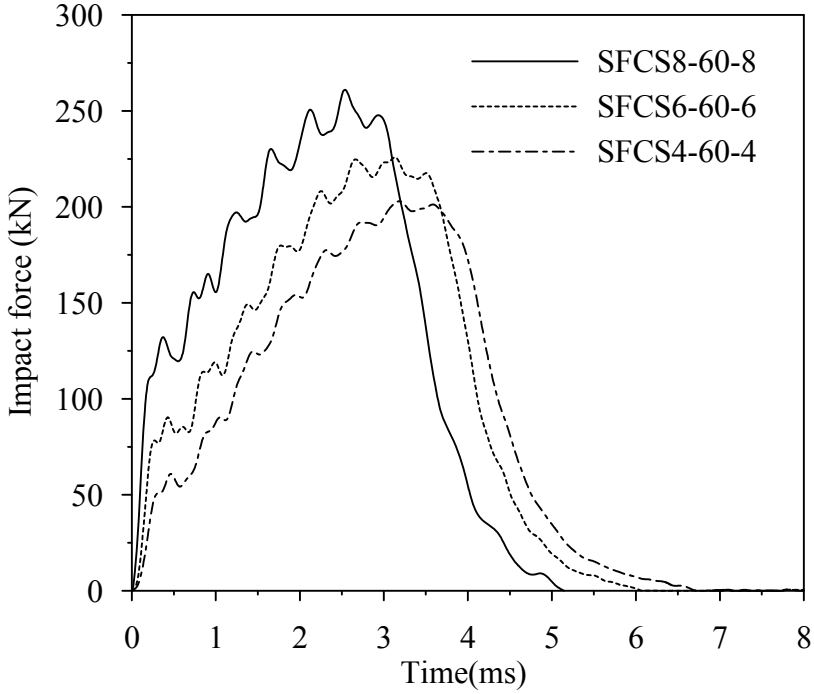

Fig. 4.13 Effect of face plate thickness on the impact force history of SCS sandwich (f_c=16 MPa).

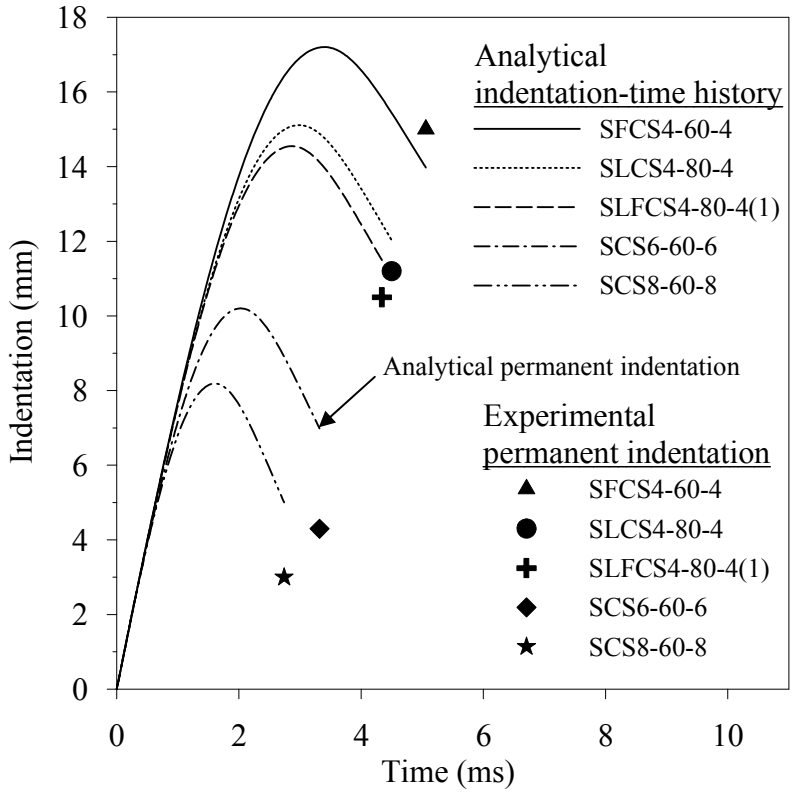

Fig. 4.14 Comparison between analytical indentations (end point of each curve is the analytical permanent indentation) and experimental permanent indentations of the SCS sandwiches with different plate thicknesses and different core strengths.

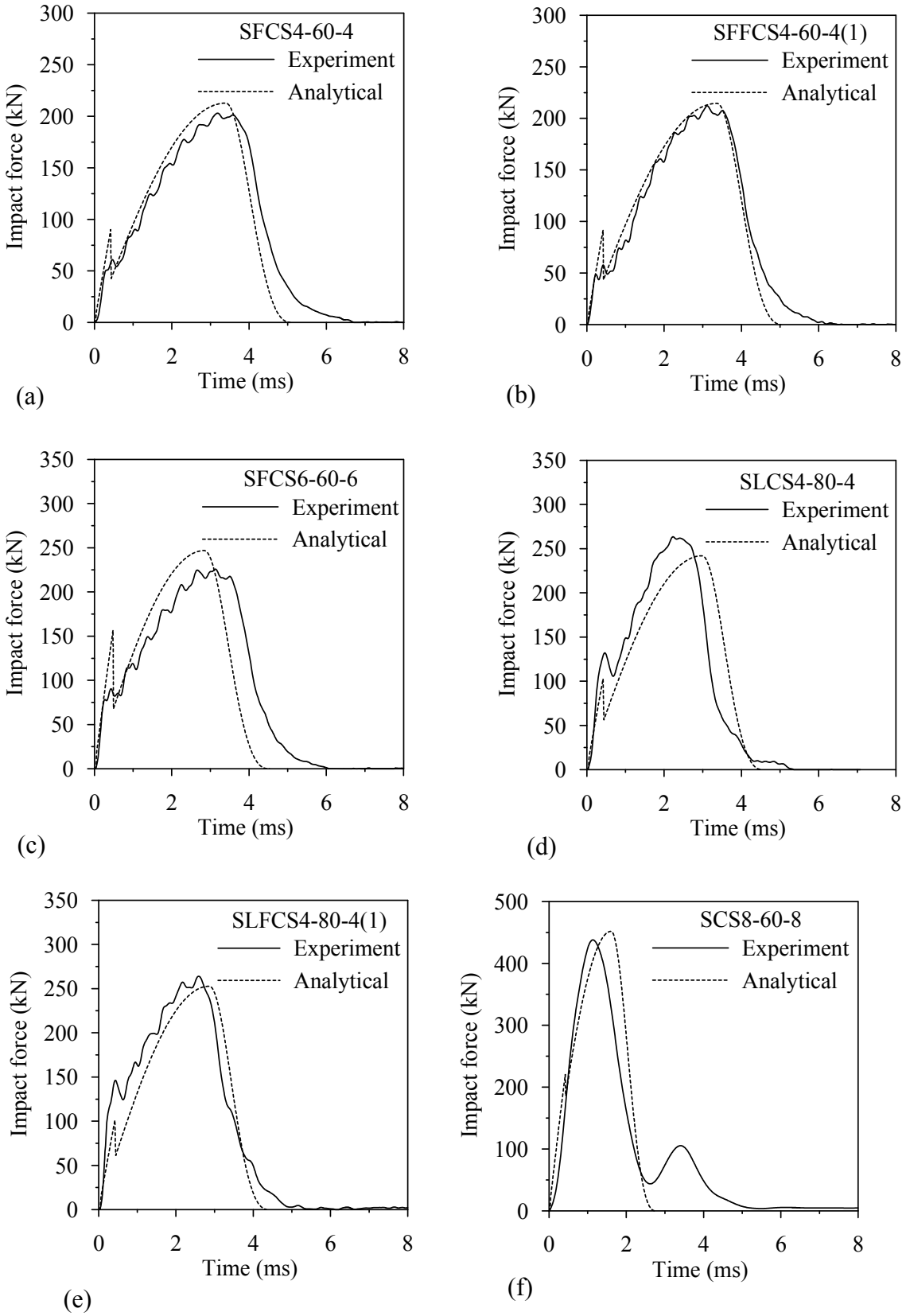

Fig. 4.15 Comparison of impact forces between experimental and analytical: (a)SFCS4-60-4, (b) SFFCS4-60-4(1), (c) SFCS6-60-6, (d) SLCS4-80-4, (e)SLFCS4-80-4(1) and (f) SCS8-60-8.

Response of SCS sandwich beams to impact loading

5

5.1 Introduction

Although SCS sandwich structures have satisfactory performance under static and quasi-static load, they have limited applications. Core is usually brittle because of the concrete and do not have good damage tolerance to impact compared to ductile materials. This is a concern in the applications where the SCS sandwich structures are subjected to impact, such as offshore platform, ship hull and bridge deck structures. Impact from the environment during service, such as dropping of crane, container and floating objects, are threats to the performance of SCS sandwich structures.

Unlike metallic materials, concrete core do not undergo plastic deformation during impact. During impact, metallic structures absorb the impact energy through plastic deformation. Plastic deformation does not significantly reduce the load-carrying capability of the metallic structures, although deformation is permanent. On the other hand, concrete core usually cannot effectively absorb impact energy while maintaining their load-carrying capacity. It is well reported that concrete structures dissipate impact energy through the cracking and crushing. By inclusion of fibre in the concrete, substantial increase in impact strength and energy absorption can be achieved over those plain concrete (Swamy and Jojagha, 1982).

This chapter investigates the impact behaviour of SCS sandwich beam with J-hook shear connectors and lightweight concrete core. In order to understand the mechanism of impact resistance of the sandwich beam, impact tests on beams have been done and failure analysis has been performed. This concrete core is assumed to behave as elastic-plastic because under the point of impact, the core is confined by the two steel plates and the surrounding concrete. Force-indentation relations for SCS sandwich section derived in Chapter 4 are incorporated in the global elastic forced vibration dynamic model of the beam to determine the global response of the SCS sandwich beam.

5.2 Structural behaviour of sandwich beams under impact

The key concept of development of J-hook connector was discussed elaborately in Chapter 3. The bonding and shear transfers between the face plates and the concrete core are important concerns in the design of sandwich structures against impact loads. The behaviour of steel-concrete steel sandwich beam can be simulated using a strut and tie model as discussed in Chapter 3. In this model the shear connectors welded to top and bottom plate is the vertical tension member. During impact, high tensile force is developed in the shear connector due to the localized kinetic impact force pushing the bottom steel plate outward from the core. If the two face plates are not inter-connected by mechanical connectors, then tensile separation will occur during impact (Sohel et al. 2003). Therefore, connecting both top and bottom plates is necessary to prevent separation of steel plates hence maintain the integrity of the sandwich structures. For this reason, the J-hook shear connector was proposed as shown in Fig. 3.1, in consideration of the shallow depth of the SCS sandwich structure.

5.3 Impact test on SCS sandwich beams

5.3.1 SCS sandwich beam specimens

To investigate the impact performance of a SCS sandwich system with J-hook shear connectors, ten SCS sandwich beam specimens were prepared and tested by a drop weight impact machine. All beam specimens, having core depth=80 mm, span length = 1100 mm, and width ranging from 200 mm to 300 mm, were subjected to impact load at the mid-span of the beam. The nominal thickness of the face plates was 4 mm. The J-hook connectors were fabricated from round steel bar of diameter 10 mm or 16 mm. The welding of J-hook connectors to the steel plates was same as described in Chapter 3 (section 3.2.1). The spacing of J-hook connectors was varied from 100 mm to 300 mm. For comparison purposes, one of the beam specimens was fabricated with a conventional threaded stud connector so that the influence of the type of connector on the overall performance of the SCS sandwich beams can be evaluated.

Ordinary Portland cement and an expanded clay type of lightweight aggregate (LWA) (coarse and fine) with average particle density of 1000 kg/m^3 were used to produce the lightweight concrete for the sandwich beams. The maximum size of the LWA was 8 mm. The concrete core was reinforced with either PVA (Kuralon RF 4000/30 mm) or steel fibres (Dramixr RC-80/30-BP) and their performance was compared with the specimens containing a non-reinforced lightweight concrete core. The detailed beam dimensions, strength of the concrete core and face plates and fibre volume content used are given in Table 5.1.

5.3.2 Experimental procedure

The impact resistance of the SCS sandwich beam was determined by an instrumented drop-weight impact test machine as shown in Fig 5.1 which was used for local impact

test on SCS sandwich panels in Chapter 4 (section 4.7.2). The impact was achieved by dropping a 64 kg cylindrical projectile with a hemispheric head of 90 mm diameter from a height of 4 m within the aluminium guide. The projectile had a length of 770 mm and a diameter of 120 mm. When the projectile reached the SCS beam, its speed was approximately 8.14 m/s. The same projectile was used for all the impact tests described in this chapter. Periodic checks on the tup indicated that negligible permanent deformation had occurred as a result of repeated use.

5.3.3 Test set-up

The test set-up and the drop weight impact machine are shown in Figs. 5.1(a) & 5.1(b). The SCS sandwich beams of 1100 mm × 88 mm (length × depth) were simply supported over a span of 900 mm by steel supports welded to the base support frame of the test rig. A linear potentiometer (Fig. 5.1(d)) was placed at the mid-span of the beam to measure vertical deflection. Strain gauges were also attached to the bottom steel plate at mid-span. A photodiode system, comprising of two photodiodes and two laser sources, was used to trigger the data acquisition system. This laser system was set very near to the beam top surface. The diodes and laser sources were positioned such that the lasers pass through the centre line of the hammer. When the falling hammer intercepted the top laser, the data acquisition system was triggered. The falling hammer then blocked the second laser and the impact velocity can be obtained from these two signals as the distance between the two lasers was measured before the impact. When the hammer rebounded, the diodes also registered a signal and hence, the rebound velocity can also be calculated. Quartz force rings (three force rings on the same plane) of total capacity 1050 kN were attached to the projectile as a load cell (Fig. 5.1(c)) in order to measure the impact forces when it struck the specimen. The

force rings were positioned close to the projectile tip to improve the accuracy of readings. A 16-channel digital oscilloscope with an adjusted scan rate of 0.2 MHz per channel was used for data acquisition. A pre-trigger interval was also specified so that data prior to impact was acquired. All data were recorded at 5 μs intervals (i.e., sampling rate of 2×10^5 per second). Potentiometer signal was directly captured by the oscilloscope. The load cell signal was captured via amplifier as voltage, whereas, the strain gauges signals were captured through strain gauge bridge head directly as micro strain. Recorded data were stored in an internal hard disk drive and transfer to a personal computer after the test for further analysis. The test procedure was similar as described in Chapter 4 (section 4.7.2).

A high-speed camera (1000 frames/sec) also was used to record the impact event and to observe the central deformation and the progressive crack formation in the concrete core. The pictures captured by the high speed camera can be used to determine the beam deflection during the impact, in additional to the measured deflection values obtained from the linear potentiometers.

During the impact test, any measurement of displacement, strain or force using electronic signals would be accompanied by random electrical noises of very high frequencies. Filtering is necessary to remove these unwanted noise frequencies. The recorded signals were digitally filtered using a low-pass second-order Butterworth filtering software. A filtering frequency of 5 kHz cut-off was found to be the most optimum to avoid unwanted noise without affecting the signal.

5.4 Test results and discussion

5.4.1 Damage analysis of sandwich beams under impact load

The damage caused by impact load on various sandwich beam specimens is shown in Fig. 5.2. The beams did not fail completely under the applied impact load. Beam specimens with J-hook connectors did not show separation or buckling of the steel face plates (Figs. 5.2(a)), whereas the beam with overlapping stud shear connectors (SLCS100S) experienced tensile separation of the face plates leading to local buckling of the top face plates and large displacement after impact, (see Fig. 5.2(b)).

A series of photos were captured by high speed camera at various time steps as shown in Fig 5.3. It was observed that flexural cracking initiated from the bottom surface of the concrete core below the point of impact and propagated upwards to the top steel plate. Subsequently, similar cracks occurred between the mid-point and the supported end of the beam. This progressive crack formation indicates that high flexural stress was generated by the impact force and travelled from the impact point to the supports. Apart from these flexural cracks, many other random cracks developed in the concrete core and they were not similar to the flexural cracks, i.e. most of the cracks generated by impact were different from those developed in the static point load test. In case of plain concrete beams (SLCS100 and SLCS200), flexural cracks developed first, and then shear (diagonal) cracks appeared. The concrete below the point of impact was crushed when it was not reinforced by fibres (Fig. 5.2(a(ii))). Comparing the crack patterns of the concrete in the beams, plain concrete core broke into pieces after impact. On the other hand, the fibre reinforced concrete cores experienced fewer cracks and maintained its structural integrity without breaking into pieces (Fig. 5.2(a(iii))). As the volume fraction of fibre was increased from 1% to 2%, the number

of cracks and the spread of damage zone were found to decrease reflecting lesser global damage. This is because the fibres bridged the cracks in the concrete and prevented spalling of the concrete. Hence, the energy input required to initiate cracks and to produce failure in the fibre reinforced concrete core is greater than that of the plain concrete core.

When the projectile struck the beam, very high stresses developed in the vicinity of impact point. This stress caused local indentation on the steel plate and crushed the concrete core below the impact point. As the stress wave travels from impact point towards the supports, the top steel plate tends to deflect outwards. Due to travelled stress wave, high shear and local bending in the beam occur. For this reason (shear and buckling action), plates tend to separate from the concrete. Since the top and bottom J-hook connectors are interlocked, the plates could not be pulled-out from the concrete even cracking of concrete was present surrounding the J-hook connectors. The J-hook connectors are found to be effective to prevent the buckling and the separation of the face plates.

5.4.2 Displacement and strain-time history

Upon impact, the beam experienced a sudden downward momentum at the load point. The beam bounced back as soon as the impact load disappeared as shown in Fig. 5.4. The beam deflection-time histories were obtained using a linear potentiometer at the centre of the beams (see Fig. 5.1(d)). These results were verified with deflection-time histories obtained from the analysis of picture frames captured by the high-speed camera. The measured values of maximum and residual deflection are presented in Table 5.2. The residual deflections at the centre of the beams after impact by a 64-kg

projectile with velocity 8.12 m/s were 16.2 mm, 33.9 mm and 79.4 mm for the beams with shear connector spacing 100 mm (SLFCS100(1)), 200 mm (SLFCS200(1)), 300 mm (SLFCS300(1)), respectively, and the central deflection increased to 90.1 mm for beam without any shear connector (SLFCS). The corresponding maximum deflections for the beams are 27.1 mm, 51.7 mm, 107.4 mm and 120.2 mm respectively. Therefore, sandwich beams with a higher degree of composite action enhances the flexural stiffness and thus smaller beam deflection for the same impact energy.

Specimens with a fibre reinforced concrete core exhibit an improved performance in stiffness and integrity after impact compared to the beam with a plain concrete core (see Fig. 5.4). From Table 5.2, it is evident that the maximum and residual deflection of sandwich beam reduced significantly with the use of fibre reinforced concrete core. For example, beam SLCS100 deflected to a maximum value of 38.7 mm upon impact compared to SLFCS100(1) which deflected up to 27.1 mm. The only difference between these two beams is that SLFCS100(1) contains 1% volume fraction of fibre compared to SLCS100 with no fibre in the concrete. In the event of impact, the kinetic energy of the drop object is absorbed by the sandwich beam leading to global displacement of the beam, local indentation of the steel face plate and crushing of the concrete core. Since additional energy is absorbed by the stretching of the fibres in the concrete core, the overall deflection of the SCS sandwich beams with fibre reinforced core can be reduced accordingly.

Strain gauges were placed at the bottom plate of the sandwich beams to measure the strain-time history during impact and the results are shown in Fig. 5.5. The strain value reached the maximum and reduced to a non-zero value of “residual strain” after the impact. As shown in Fig. 5.5, the maximum strain in the steel face plate during

impact is about 1500×10^{-6}, whereas the elastic strain limit of the steel is about 1800×10^{-6}. If the strain rate effect (Cowper-Symonds, 1957) is considered, the yield strength of the steel plate increases from 275 to 375 MPa and the corresponding yield strain increases from 1800×10^{-6} to 2200×10^{-6} m/m. Therefore, the steel face plate did not yield. The residual strain after impact is due to permanent deformation of the beam arising from the impact causing local damage to the concrete core (crushing and spalling), top face plate indentation, and flexural as well as shear cracks developed in the concrete core. Larger residual strains on the steel plates indicate a higher degree of the damage in the concrete core.

As expected, the maximum strain and residual strain are higher for beams with a plain concrete core (e.g. SLCS100) than beams with fibre reinforced concrete (e.g. SLCS100(1)) as seen in Fig. 5.5. The mean strain rate of the bottom steel plate is about $1.13s^{-1}$. From the deflection-time history curves, the percentages of critical damping were obtained. It is also observed that a rapid vibration attenuation (with between 10% and 20% of critical damping) occurred. The damping varied with the degree of damage in the concrete core.

5.4.3 Impact force-time history

The impact force-time history as recorded using load cells in the projectile is presented in Fig. 5.6. Upon impact, the SCS sandwich beam experienced a sudden increase in impact force which rose to a peak within 1.0 ms. The peak load and the duration to reach the peak depend on the nature of the colliding bodies. In the present study, the peak impact-force time duration is very short because of the hard contact between the steel projectile and the steel face plate. The shape and weight of the projectile, core thickness, and the boundary conditions of the sandwich beam were kept the same for

all the test specimens and hence, the peak load was affected mainly by the natural frequency of the beam which is related to the beam's stiffness, mass and types of concrete core used. The mechanical and geometrical properties of the concrete core have significant influence on the force-displacement response of the sandwich structures.

The force time history can be categorised into two parts: one is up to the initial peak (elastic part) and the other is the long and steady unloading part before reducing to the static value as shown in Fig. 5.6. The repeated rises and falls of the impact force time response are due to sequential cracking of the concrete core during the impact. A drop from the peak force indicates that the maximum section capacity of the SCS beam is reached. For all the SCS sandwich beams, the initial first peak force-time history is fairly similar. Nevertheless, the steady unloading part of the force-time history is different for each beam in terms of the force magnitude and duration. The first sharp peak is due to the initial shock of impact which is produced by the inertial of the beam. This inertial force is similar to the force caused by the rigid body acceleration of the specimen from zero velocity at rest position to the velocity of the projectile. The local indentation at the impact zone occurs mainly during this period. If the projectile energy is higher than the beam elastic energy, plastic deformation of the beam occurs and the velocities at the impact zone of the beam and the projectile are identical up to the maximum deflection of the beam. In this study, the projectile mass (64 kg) is greater than the effective beam mass ($0.5m_b \approx 16.25$ kg). Thus, it is likely that the beam and the projectile will move together after impact. The movement of the beam and projectile was captured by the high speed camera in Fig. 5.3 and it was confirmed that they indeed moved together after impact for all the test specimens.

The magnitudes of the first peak impact forces were very close and ranged from 158 kN to 165 kN (Table 5.2) for beams with the same cross section area, e.g. SLCS100, SLFCS100(1), and SLCS200. For these beams, the concrete core strength, steel face plate thickness, beam mass and the first natural frequencies are almost identical. These parameters are directly related to the impact force. In comparison, beams without shear connector (e.g. SLCS and SLFCS(1)) possessed less elastic stiffness (hence with lower first natural frequency) and showed peak impact force ranging from 120 to 140 kN which was less than the beam specimens with shear connectors.

The impact force results show that the presence of fibres in the concrete core does not have any significant effect on the first peak impact force because addition of fibres does not increase the concrete compressive strength (see Table 5.1) and elastic stiffness as seen in Fig. 5.7. However, the presence of fibres in the concrete core has a significant effect on the post-peak behaviour of the impact force-time history of the beams. Fig. 5.6(a) shows that beam specimen SLFCS100(1) with 1% fibre had a higher post peak force (after first peak of the force-time history) of 60.5 kN than SLCS100 with a plain concrete core of 43.2 kN. The observation is also valid for beams with different spacings of J-hook connectors. The magnitude of the force-time history after the first peak generally increased with the increase of degree of composite action as seen in Table 5.2 and Fig. 5.6. It may be seen that beam SLCS100 showed a higher peak value after the first peak than beam SLCS200, though the diameter of the J-hook connectors in SLCS200 was larger than that in SLCS100. A similar behaviour is also observed by comparing the force time history of beams SLCS and SLCS200. This can generally be explained by stiffness enhancement and maximum static load-carrying capacity, since the beam load-carrying capacity is directly related to the

number of shear connectors which would enhance the degree of composite action between the face plates and the concrete core.

Test observations show that even though the LWA concrete is a brittle material, the use of a J-hook shear connector and fibres in the concrete core enhances its overall performance to absorb the impact energy. This is important in view of safety and structural integrity of sandwich structures with lightweight brittle core.

5.5 Residual flexural strength of beams after impact

Two beam specimens SLCS100 and SLFCS100(1) were tested under static concentrated load at mid-span after they were subjected to impact load to determine their residual strength. The test results are compared with those of similar beams without impact damage. The load-deflection curves for the beams without impact damage and with impact damage are shown in Fig. 5.7. The results showed that there was a reduction in flexural stiffness caused by the cracked concrete due to impact, and the reduction of ultimate flexural strength. The strength reduction was 38% and 20% for SLCS100 and SLFCS100(1), respectively (Table 5.3). The reduction of elastic stiffness (initial slope of the load-deflection curves shown in Fig. 5.7) caused by impact was 80% for SLCS100 and was 62% for beam SLFCS100(1). From Fig. 5.7, it can be seen that load-deflection curves of beams with impact damage are nonlinear from the beginning of the applied load rather than a linear behaviour as observed for beams without initial damage caused by impact. This is a result of the progressive crushing and propagation of the shear cracks within the concrete core as well as J-hook connector deformation during impact. The deflection (y_{du}) at ultimate strength (F_{du}) of impact damaged beam SLCS100 is larger than that of beam SLFCS100(1) (Table

5.3). This indicates that the beam with a plain concrete core experiences more impact damage than that with a fibre reinforced concrete core.

5.6 Analysis of impact between projectile and sandwich beam

Fig. 5.8 shows a SCS sandwich beam subjected to an impact at the centre by a hemispherical headed projectile of mass m_s and radius R_i. The initial impact velocity of the projectile is denoted by V_0. The impact causes a local indentation on the sandwich beam δ and an overall displacement of the beam, w_p. The contact zone between projectile and steel face plate is R_c, while a denotes the length of the deformation zone. The local indentation is confined in a very small area and the length of a is very small compared to the beam width. Thus, the assumptions to model the local indentation in beams are same as discussed in Chapter 4 (section 4.2).

5.6.1 Force-indentation relation

5.6.1.1 Elastic indentation

The elastic indentation models presented in Chapter 4 were shown to be able to give a reasonably good prediction of the impact force and local deformation of SCS sandwich panel subjected to drop weight projectile impact. Thus, the force-indentation relation for SCS sandwich beams, which was derived in Chapter 4, is further applied in this beam dynamic model. The elastic force-indentation relation is as following

$$F = \left(1.03 E_c t_s E_s / h_c\right)^{1/2} \delta^2 = K_e \delta^2 \qquad \text{as given by Eq. (4.8)}$$

or $$\delta = \left(F / K_e\right)^{1/2}$$

where $$K_e = \left(1.03 E_c t_s E_s / h_c\right)^{1/2} \qquad \text{as given by Eq. (4.9)}$$

5.6.1.2 Plastic indentation

As discussed in Chapter 4, it was found that the derived plastic force-indentation relation for the SCS sandwich structures can be used to predict the impact force and local deformation.

It is seen from experiment that impact indentation in the SCS sandwich beam is very small. Thus, for stiff core and small indentation (i.e., $\delta \le t_s$), it can be assumed that $R_c = a$, and the plastic force-indentation relation is as following

$$F = (4\pi t_s \sigma_0 + 2\pi R_i f_c)\delta \qquad \text{as given by Eq. (4.16)}$$

or $$\delta = \frac{F}{(4\pi t_f \sigma_0 + 2\pi R_i f_c)}$$

5.6.1.3 Unloading

The unloading phase is similar as derived in Chapter 4.

$$F = F_m \left[\frac{(\delta - \delta_p)}{(\delta_m - \delta_p)} \right]^q, \quad \delta_m \ge \delta \ge \delta_{cr} \qquad \text{as given by Eq. (4.20)}$$

and $$\delta = \delta_p + \left(\frac{F}{F_m} \right)^{\frac{1}{q}} (\delta_m - \delta_p) \qquad \text{as given by Eq. (4.21)}$$

For $\delta > \delta_p$, the permanent indentation is defined as

$$\delta_p = \delta_m - \delta_{cr} \qquad \text{as given by Eq. (4.22)}$$

According to this model, δ_{cr} can be regarded as the yield point in deformation of the face plate for large deflection. From plate analysis, it is found that for large deflection of circular plate, the approximate critical deflection can be found as (Timoshenko and Woinowsky-Krieger, 1969, §99):

$$\sigma_y = \alpha_r E_s \frac{\delta_{cr}^2}{R_c^2} = \alpha_r E_s \frac{\delta_{cr}^2}{2\delta_m R_i} \tag{5.1}$$

where σ_y is the yield strength of plate and α_r is a coefficient and its value for distributed loaded fixed edge plate is 0.976.

5.6.2 Global response of beam under impact load

5.6.2.1 Elastic response

Before formation of a plastic hinge, the beam response under impact force is elastic. According to Timoshenko (1913), the forced vibrations produced in the elastic beam by the time varying force $F(\tau)$ at the point of contact are expressed in terms of the normal modes of vibration. For the transverse impact at the centre on a pin ended beam of length L, the beam can be considered to be one-dimensional. The symmetrical vibration functions are $\left(\sqrt{2/L}\right)\phi_i$ for $i = 1, 3, 5\cdots$ in which $\phi_i = \sin\left(i\pi x/L\right)$ are the shape functions of free vibration, where x is the coordinate of position along the beam length. The corresponding angular frequencies of the natural modes of vibration are ω_i given by the equation

$$\omega_i^2 = \frac{i^4 \pi^4 D}{L^3 m_b} \tag{5.2}$$

in which D is the flexural rigidity of the beam. The central deflection w due to the forced vibrations is given by (Lee, 1940; Goldsmith, 1960)

$$w\left(\frac{L}{2}, t\right) = \frac{2}{m_b} \sum_{i=1,3..}^{\infty} \frac{1}{\omega_i} \int_0^t F(\tau) \sin\{\omega_i (t-\tau)\} d\tau \tag{5.3}$$

where m_b is the total mass of the beam. It is assumed that the initial velocity of the beam is zero.

Denoting the mass of the projectile m_s and impact velocity V_0, the transverse displacement of the colliding projectile with respect to the initial top surface of the beam is given by (Lee, 1940)

$$w_p(t) = V_0 t - \frac{1}{m_s}\int_0^t F(\tau)(t-\tau)d\tau \tag{5.4}$$

Once the force-indentation relation is given, the relative deformation (indentation) of the top face plate at impact zone can be written as (from Fig. 5.8),

$$\delta(t) = w_p(t) - w\left(\frac{L}{2}, t\right) \tag{5.5a}$$

or, $$\delta(t) = V_0 t - \frac{1}{m_s}\int_0^t F(\tau)(t-\tau)d\tau - \frac{2}{m_b}\sum_{i=1,3..}^{\infty}\frac{1}{\omega_i}\int_0^t F(\tau)\sin\{\omega_i(t-\tau)\}d\tau \tag{5.5b}$$

For different loading phases, the load-indentation relation would be different as discussed in Chapter 4 (section 4.3). For example, in elastic indentation phase, substituting the expression for $\delta(t)$ from Eq. (4.8), Eq. (5.5b) becomes

$$\left(\frac{F}{K_e}\right)^{1/2} = V_0 t - \frac{1}{m_s}\int_0^t (t-\tau)F(\tau)d\tau - \frac{2}{m_b}\sum_{i=1,3..}^{\infty}\frac{1}{\omega_i}\int_0^t F(\tau)\sin\{\omega_i(t-\tau)\}d\tau \tag{5.6}$$

This equation cannot be solved in closed form, and hence a numerical technique is employed to solve for impact force and displacement history.

5.6.2.2 Numerical procedure

The numerical procedure is applied to solve the Eq. (5.6) for impact force. This numerical approach assumes that the force function $F(t)$ is linear over each increment of time Δt. Several numerical methods are available to solve the dynamic equation (Goldsmith, 1960; Hughes, 1983; Evans et al. 1991). In the present study, Evans's method has been applied. This numerical method is found to be computationally

efficient and give an accurate prediction of force and displacement responses. According to this method Eq. (5.6) can be written as

$$\left(\frac{F}{K_e}\right)^{1/2} = A_N + BF_N \tag{5.7}$$

where F_N is the value of $F(t)$ at time $t = N\Delta t$ in which Δt and N are the time step and number of time steps respectively.

$$A_N = V_0(N\Delta t) - \frac{1}{m_s}(\Delta t)^2 \sum_{j=1}^{N-1} F_j(N-1) - \frac{4}{m_b \Delta t} \sum_{i=1,3..}^{\infty} \frac{2}{\omega_i^3} \sin^2\left(\frac{\omega_i \Delta t}{2}\right) \times \sum_{j=1}^{N-1} F_j \ \text{Sin}[\omega_i \Delta t(N-j)] \tag{5.8}$$

$$B = -\frac{(\Delta t)^2}{6m_s} - \frac{1}{m_b} \sum_{i=1,3..}^{\infty} \frac{2}{\omega_i^2}\left(1 - \frac{\sin(\omega_i \Delta t)}{\omega_i \Delta t}\right) \tag{5.9}$$

Note that B is constant and does not vary with time and A_N may be readily calculated since it involves only values F_j up to F_{N-1}. Detailed derivation of this numerical method is given in the paper written by Evan's et al. (1991) and repeated in Chapter 4.

5.6.2.3 Elastic-plastic analysis of beam structures using SDOF

Determination of the inelastic response for beams or other structures having distributed mass is difficult. One possible approach, as suggested by Biggs (1964), is to conduct the usual elastic analysis up to the ultimate elastic deflection and then to assume that an idealized hinge has formed at this point, thus creating a plastic system. The assumed beam resistance function is illustrated in Fig. 5.9.

If the impact energy is large, the sandwich beam will have a large global deflection and the local indentation $w_p(t) - w\left(\frac{L}{2}, t\right) \approx 0$ becomes negligible. For negligible

indentation, the model can be simplified as the single-degree-of-freedom (SDOF) system with initial velocity,

$$(m_e + m_s)\ddot{w} + k_e w = 0 \qquad 0 < w_e \tag{5.10}$$

The plastic response equation can be written as follows

$$(m_e + m_s)\ddot{w} + R_u = 0 \qquad w_e < w < w_m \tag{5.11}$$

$$(m_e + m_s)\ddot{w} + R_u - k_r(w_m - w) = 0 \qquad (w_m - 2w_e) < w < w_m \tag{5.12}$$

where m_e is the effective mass of the beam, R_u is the resistance force at yielding of the beam, w_e is the elastic limit displacement until the load-deflection curve remains linear, i.e. the deflection at maximum resistance R_u, k_r is the unloading stiffness of the beam after the formation of plastic hinge, and w_m is the maximum deflection.

In the plastic phase, the shape function of the beam deflection may be written as $\phi_i = 2x/L$ for $i = 1, 3, 5\cdots$ and $x \le L/2$. Using the assumed shape function for the elastic and the plastic stage, the equivalent beam mass (m_e) is as follows

Elastic stage,

$$m_e = 2\int_0^{L/2} (m_b/L)\phi_i^2 dx = 2\int_0^{L/2} (m_b/L)\left(\sin\left(i\pi x/L\right)\right)^2 dx = \tfrac{1}{2} m_b \tag{5.13a}$$

Plastic stage,

$$m_e = 2\int_0^{L/2} (m_b/L)\phi_i^2 dx \quad = 2\int_0^{L/2} (m_b/L)\left(2x/L\right)^2 dx = \tfrac{1}{3} m_b \tag{5.13b}$$

To solve the dynamic plastic response equations for deflection, a central difference method is adopted which is suitable for explicit dynamic analysis of blast and impact problems (Bathe, 1996; Koh et al., 2003).

$$w_i = \frac{(\Delta t)^2}{M}[-Kw_{i-1} + \frac{2M}{(\Delta t)^2} w_{i-1} - \frac{M}{(\Delta t)^2} w_{i-2}] \quad \text{for} \quad 0 < w_e \tag{5.14}$$

$$w_i = \frac{(\Delta t)^2}{M}\left[-R_u + \frac{2M}{(\Delta t)^2}w_{i-1} - \frac{M}{(\Delta t)^2}w_{i-2}\right] \quad \text{for } w_e < w < w_m \tag{5.15}$$

$$w_i = \frac{(\Delta t)^2}{M}[-R_u + K_r w_m - K_r w_{i-1} + \frac{2M}{(\Delta t)^2}w_{i-1} - \frac{M}{(\Delta t)^2}w_{i-2}] \quad \text{for } (w_m - 2w_e) < w < w_m \tag{5.16}$$

where $m_e + m_s = M$. If damping is considered in post peak region of deflection, then damping term ($C\dot{w}$) should be added in the left side of Eq. (5.12) and the numerical solution of this equation will be as following

$$w_i = \left(\frac{M}{(\Delta t)^2} + \frac{C}{2\Delta t}\right)^{-1}\left[-R_u + K_r w_m - K_r w_{i-1} + \frac{2M}{(\Delta t)^2}w_{i-1} - \left(\frac{M}{(\Delta t)^2} - \frac{C}{2\Delta t}\right)w_{i-2}\right]$$

$$\text{for } (w_m - 2w_e) < w < w_m \tag{5.17}$$

where Δt is the time step. The initial velocity of the system is $\dot{w}_0 = m_s V_0/(m_s + m_e)$.

5.6.3 Strain rate effects on material strength

When the sandwich beam is subjected to a projectile impact load, the yield strength of the sandwich materials will be different from static or quasi-static values due to strain rate effects on the materials. Hence it is necessary to evaluate the dynamic strength of the sandwich materials. The mean uniaxial strain rate $\dot{\varepsilon}_d$ for impact velocity V_0 may be estimated by means of the Perrone and Bhadra's (1984) approximation which is further simplified by Jones (1989) for beam as

$$\dot{\varepsilon}_d = 4w_{pr}V_0\Big/\left(3\sqrt{2}L^2\right) \tag{5.18}$$

where w_{pr} = maximum permanent deflection and L = length of the beam.

As discussed in Chapter 4 (section 4.6), the Cowper-Symonds equation has been used to estimate the dynamic yield strength (σ_{yd}) for the estimated strain rate ($\dot{\varepsilon}_d$). Thus,

the steel strength parameters in proposed formula given in Section 5.6.2 are modified to account for the dynamic strain rate effect. In this analysis, the strain rate effect on concrete was not considered for the same reason as discussed in Chapter 4 (section 4.6).

5.7 Comparison of analytical results with test results

The analytical solutions derived in section 5.6 will be compared with the experimental results in section 5.4. Four cases of study are selected to predict the structural response on the basis of elastic-plastic theory discussed in section 5.6. They correspond to the impact of a hemispherically headed projectile on simply supported SCS sandwich beams.

5.7.1 Impact force-time history

Sandwich beams are designed to resist impact force due to dropping objects. The impact force may cause punching and shear failure of the core. Eq. (5.7) predicts the impact force as a function of the contact stiffnesses (K_e and K_p), projectile impact velocity (V_0), projectile mass (m_s), mass of the beam (m_b) and natural frequency of the beam (ω). The first natural frequency can be computed using Eq. (5.2) given in Section 5.6.2.1. The required parameters to predict the impact response of the sandwich beams can be obtained from Tables 5.1 and 5.4.

The accuracy of theoretical impact force and the displacement history depends on the values of ω_1, R_u, k_r and w_e assumed. In the present study, these parameters are obtained from the static test results as shown in Fig 5.7. The static tests load-displacement curves are obtained from the tests performed in Chapter 3. The computed

solution depends on the time interval chosen for the integration and on the number of modes assumed in the solution. Convergence study shows that solutions with 11 modes are found to be sufficient and the use of higher modes does not improve the accuracy of the results by more than 1% .

In the test set-up, the load cell is mounted on top of the projectile tup as shown in Fig. 5.1(c). Thus the test results need to be modified to allow for the additional mass of the indentor (tup), below the load cell. The additional tup mass below the load cell is 3.92 kg which is about 6% of the projectile mass of 64 kg. The measured impact force should be increased by 6%. Figs. 5.10(a), 5.11(a), 5.12(a), and 5.13(a) show the theoretical and experimental results for beams SLCS100, SLFCS100(1), SLCS200 and SLFCS200(1). The predicted impact force at the first peak is close to the experimental result. Table 5.5 compares the maximum impact forces between experiment and predicted values and the differences range from 5 to 10%.

Comparison of the impact force-time responses of the beams in Figs. 5.10 to 5.13 shows that proposed solution cannot predict the impact force at the post peak region and the impact force reduced to zero after it reaches the peak value. This is due to the limitations of forced vibration theory which is applicable for the elastic range only. In the experimental force-time history, the fluctuations of the impact forces are due to cracks and crushing of the concrete core during the impact; whereas, the present theory can only capture the global energy loss due to local damage at the impact point. Nevertheless, the shapes of the theoretical impact force-time curves up to the peak value agree reasonably well with the test results.

5.7.2 Displacement-time history

Table 5.4 shows the input parameters required to predict the displacement-time history. Figs. 5.10(b), 5.11(b), 5.12(b) and 5.13(b) compare the displacement-time history of the sandwich beam specimens with the predicted response obtained from the proposed numerical procedure. The accuracy of the prediction of beam response depends on the accuracy in predicting the beam plastic resistance, R_u. In the present study R_u is taken from the maximum load capacity of the static test results to evaluate the impact displacement time history.

The rebound stiffness of the beam is not the same as the elastic stiffness if the beam undergoes plastic deformation. The rebound stiffness depends on the extent of damage after impact. In case of lightweight SCS sandwich beams, the rebound stiffness is found to be about 20% to 30% of the elastic stiffness as shown in Fig. 5.7. Thus, the rebound stiffness of 30% of the elastic stiffness is assumed if the permanent deflection is less than span/deflection ratio (i.e. *L/w*) of 14 as recommended by US Dept. of the Army (1990) for the design of doubly reinforced RC beam under dynamic loading. This criterion may be applied to a SCS sandwich beam as its flexural behaviour is similar to the doubly reinforced RC beam. It was observed from the test results in Fig. 5.4 that the displacement did not oscillate much after first rebound and the oscillation died off. To account for this behaviour, damping needs to be considered in the free vibration analysis. The value of the damping factor (or in terms of percentage of critical damping) depends on the degree of damage in the beam. The predicted post peak displacement-time history agrees well with the experimental results as shown in Figs. 5.10(b) and 5.13(b), if 15% to 20% of critical damping is considered for all the beams considered for analysis in this present case.

A SCS sandwich beam may be designed to attain large deflections corresponding to support rotation of about 8 degree (US Dept. of the Army 1990) (i.e. $L/w \leq 14$). To assure the integrity of the beam, an adequate number of J-hook connectors must be provided to permit this high level of ductile behaviour. As suggested by US Dept. of the Army (1990), a limiting deflection $\approx L/53$, or a limiting ductility ratio of 10 (whichever governs) is specified as a reasonable estimate of the absolute magnitude of the beam deformation where safety for personal and equipment is required. It should be bear in mind that the dynamic formulae in Eqs. (5.10) to (5.17) are valid for only elastic-plastic cases.

5.8 Summary

This chapter investigates the impact performance of SCS sandwich beams with ultra-lightweight concrete core of density less than 1450 kg/m^3. J-hook connectors were proposed to provide composite action between the steel face plate and the concrete core. Test results show that J-hook shear connectors are effective in preventing tensile separation of the steel face plates, thus reducing the overall beam deflection and maintaining the structural integrity despite the presence of flexural and shear cracks in the concrete core. Test observation shows that the ultra-lightweight concrete core exhibits brittle behaviour and may crack into many pieces at the impact event. Using 1% to 2% volume fraction of fibre in concrete core could reduce the cracks significantly and enhance the overall integrity of the sandwich beams. Test results also showed that the reduction of flexural strength of the damaged beams after impact is less than 30% if the maximum deflection during impact is less than span/14.

The elastic-plastic force-indentation relationship and dynamic model based on a single-degree-of-freedom system of the sandwich beam has been proposed to predict the impact force-time and displacement-time response. The predicted results are verified against the test results. For given impact velocity and beam configuration, the central deflection-time and force-time history of SCS sandwich beams can be determined with reasonable accuracy using the proposed dynamic models.

Table 5.1 Beam specimens and specifications for impact test

Sl. No.	Beam Reference	t_c (mm)	t_b (mm)	h_c (mm)	b (mm)	d (mm)	S_x (mm)	*Length* (mm)	Fibre by vol.	σ_y (MPa)	f_c (MPa)
1	SLCS100	4.04	4.04	80	200	10	100	1100	-	275.0	28.5
2	SLFCS100(1)	4.04	4.04	80	200	10	100	1100	1%(steel)	275.0	28.1
3	SLCS150	4.04	4.04	80	300	10	150	1100	-	275.0	28.5
4	SLCS200	3.93	3.93	80	200	16	200	1100	-	275.5	27.4
5	SLFCS200(1)	3.93	3.93	80	200	16	200	1100	1%(PVA)	275.5	28.7
6	SLFCS200(2)	3.93	3.93	80	200	16	200	1100	2%(PVA)	275.5	28.2
7	SLFCS300(1)	3.93	3.93	80	200	16	300	1100	1%(PVA)	275.5	28.0
8	SLCS100S	4.04	4.04	80	200	10	100	1100	-	275.0	28.0
9	SLFCS(1)	3.93	3.93	80	200	NIL	NIL	1100	1%(PVA)	275.5	28.7
10	SLCS	3.93	3.93	80	200	NIL	NIL	1100	-	275.5	26.0

t_c and t_b = top and bottom steel face plate thicknesses respectively ;b=width of the beam; d = diameter of the connector; S_x = spacing of shear connector; *Length*= total length of the beam; f_y= yield strength of steel plate; f_c=cylinder strength of concrete; SLCS = sandwich beam with lightweight concrete core ; SLFCS = sandwich beam with fibre reinforced concrete core.

Table 5.2 Results of the impact tests

Beam reference	Maximum impact force at first peak (kN)	Maximum force in plastic part (kN)	Impact duration (ms)	Maximum central displacement (mm)	Permanent displacement (mm)
SLCS100	162	43.4	22.2	38.7	24.2
SLFCS100(1)	163	60.5	15.2	27.1	16.2
SLCS150	198	41.0	18.5	51.3	37.2
SLCS200	161	20.5	40.1	73.3	43.8
SLFCS200(1)	158	34.2	32.5	51.7	33.9
SLFCS200(2)	165	36.4	31.8	51.6	31.7
SLFCS300(1)	161	20.7	35.8	107.4	79.4
SLCS100S	163	14.2	50.6	78.3	52.9
SLFCS(1)	140	15.9	62.1	120.2	90.1
SLCS	93	11.9	68.2	171.1	119.7

Table 5.3 Strength comparison between beams with and without impact damage

Beam reference	Undamaged beam				Impact damaged beam					
	F_{ult} (kN)	y_u (mm)	F at y_{max} (kN)	K (N/m) $\times 10^6$	F_{imp} (kN)	y_{max} (mm)	y_{res} (mm)	F_{du} (kN)	y_{du} (mm)	K_d (N/m) $\times 10^6$
SLCS100	56.1	5.4	48.7	16.3	162	38.7	24.2	41.1	50.9	3.3
SLFCS100(1)	68.7	7.4	59.5	16.4	163	27.1	16.2	56.4	17.3	6.2

F_{ult} = ultimate strength; y_u=deflection at F_{ult}; F_{imp} = maximum impact force; y_{max} = maximum deflection during impact; y_{res} = residual deflection after impact; F_{du} = static ultimate strength of impact damaged beam; y_{du}= defection at F_{du}; and K_d and K are the initial slopes of the load-deflection curves of impact damaged beams and undamaged beams respectively.

Table 5.4 Required input parameters for the prediction of beam impact response

Beam reference	ω_1	R_u (kN)	K^* (kN/mm)	K_r^{**} (kN/mm)	m_b (kg)	m_s (kg)	V_0 (m/s)
SLCS100	1103	55.1	16.3	3.3	32.5	64	8.41
SLFCS100(1)	1103	68.2	16.4	6.2	32.5	64	8.21
SLCS200	1114	41.1	20.2	0.6	32.5	64	8.12
SLFCS200(1)	1142	43.5	21.5	1.4	32.5	64	8.12

$^*K$= elastic stiffness; $^{**}K_r$=rebound stiffness, ω_1=is the first angular frequency of the beam.

Table 5.5 Comparison of the test and predicted impact forces and displacements

Beam reference	Maximum impact force			Maximum displacement (mm)			Residual displacement (mm)		
	Exp. (kN)	Pre. (kN)	Exp./ Pre.	Exp. (mm)	Pre. (mm)	Exp./ Pre.	Exp. (mm)	Pre. (mm)	Exp./ Pre.
SLCS100	162	172.9	0.94	38.7	40.2	0.96	24.2	26.3	0.92
SLFCS100(1)	163	170.8	0.95	27.1	27.2	0.99	16.2	17.0	0.95
SLCS200	161	172.0	0.94	73.3	73.6	0.99	43.8	43.5	1.00
SLFCS200(1)	158	173.9	0.91	51.7	52.5	0.98	33.9	32.6	1.04

Exp.=Experiment; Pre.=Prediction.

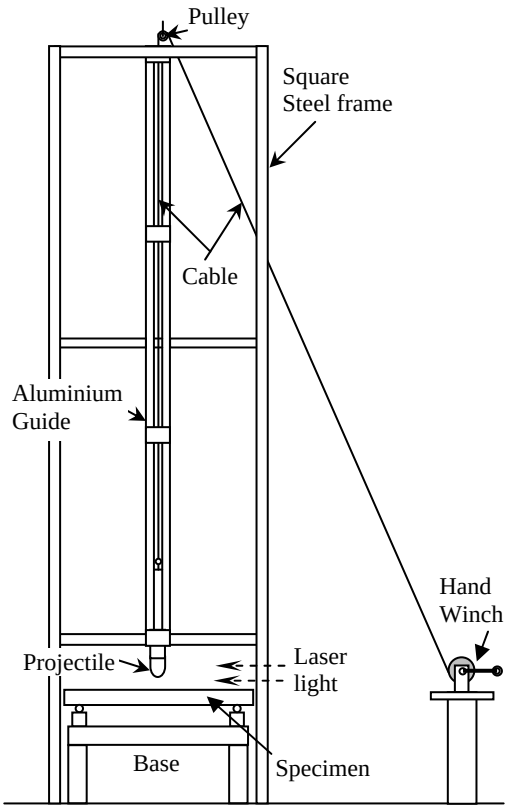

(a) Schematic view

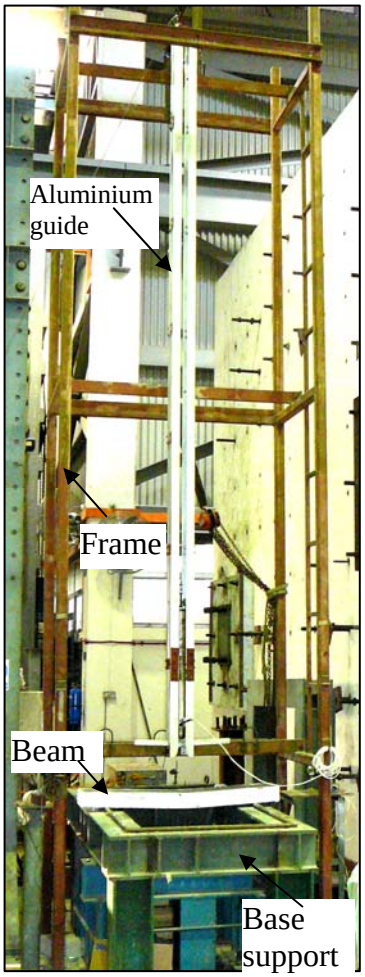

(b) Picture of actual test set-up

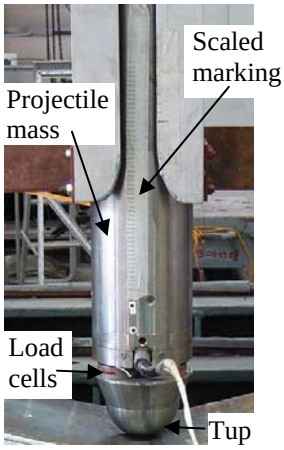

(c) Projectile details

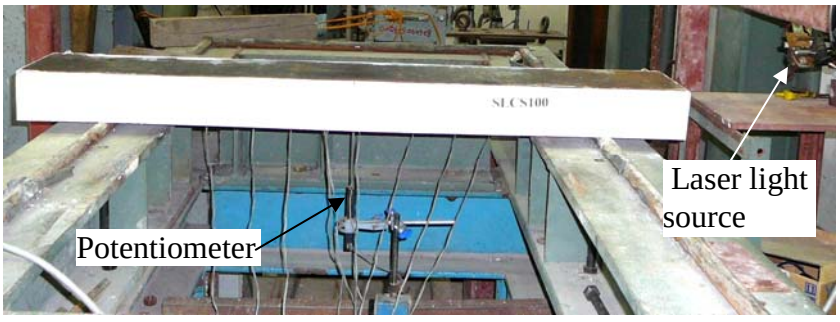

(d) Potentiometer set at the midspan of the beam

Fig. 5.1 Test set-up for impact on SCS sandwich beams.

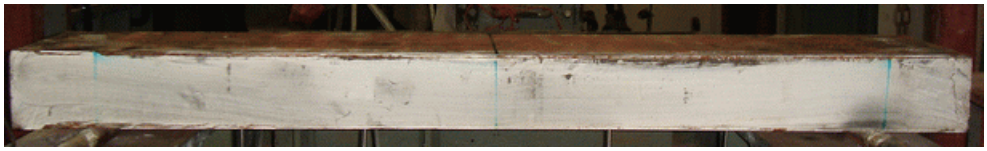

(i) SCS sandwich beam (before impact)

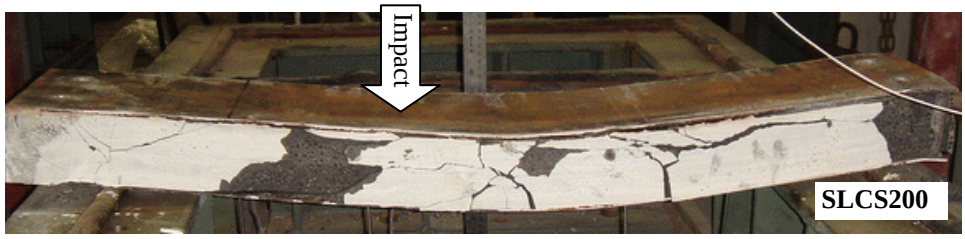

(ii)After impact (plain concrete core)

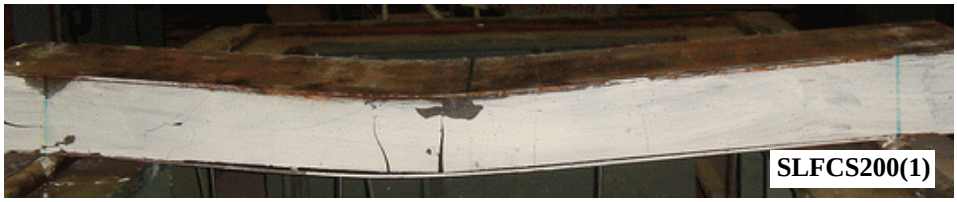

(iii) After impact (fibre reinforced concrete core)

(a) Beam with J-hook connectors

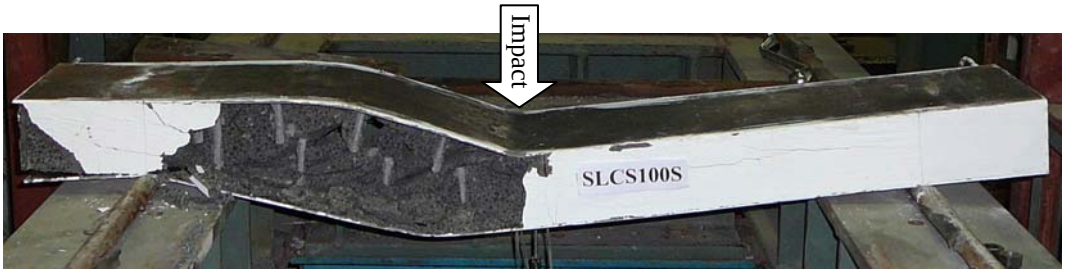

(b) Beam with threaded stud shear connectors

Fig. 5.2 Damage in the SCS sandwich beams after impact

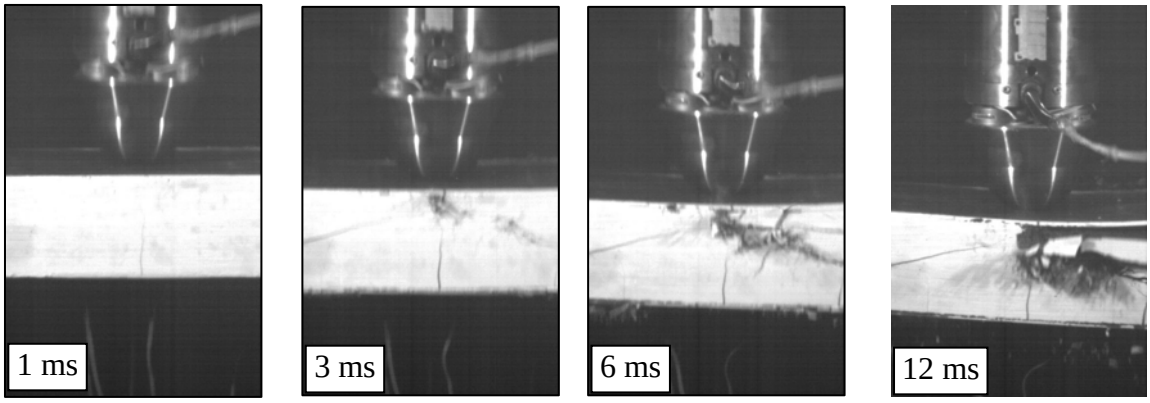

(a) SLCS100

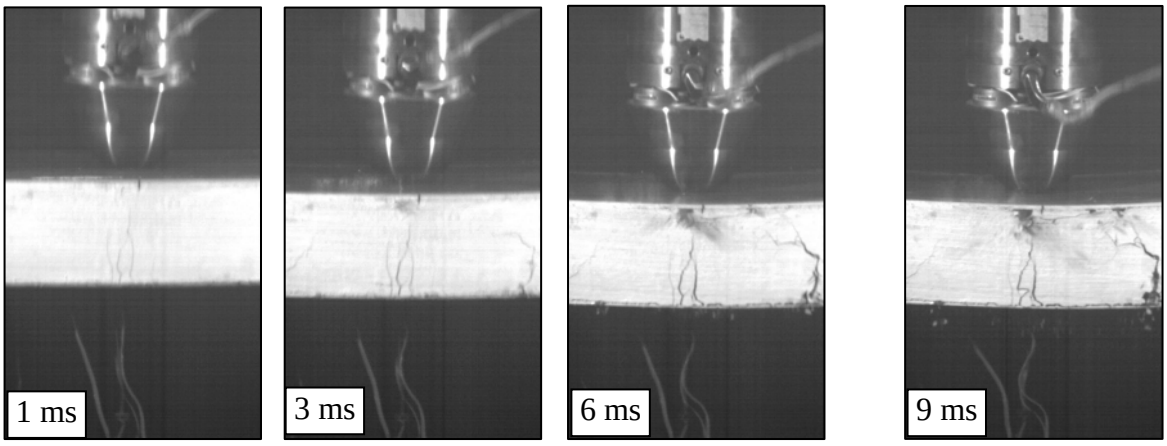

(b) SLFCS100(1)

Fig 5.3 Photos captured by high speed camera at different time intervals at the impact event: (a) SLCS100 and (b) SLFCS100(1).

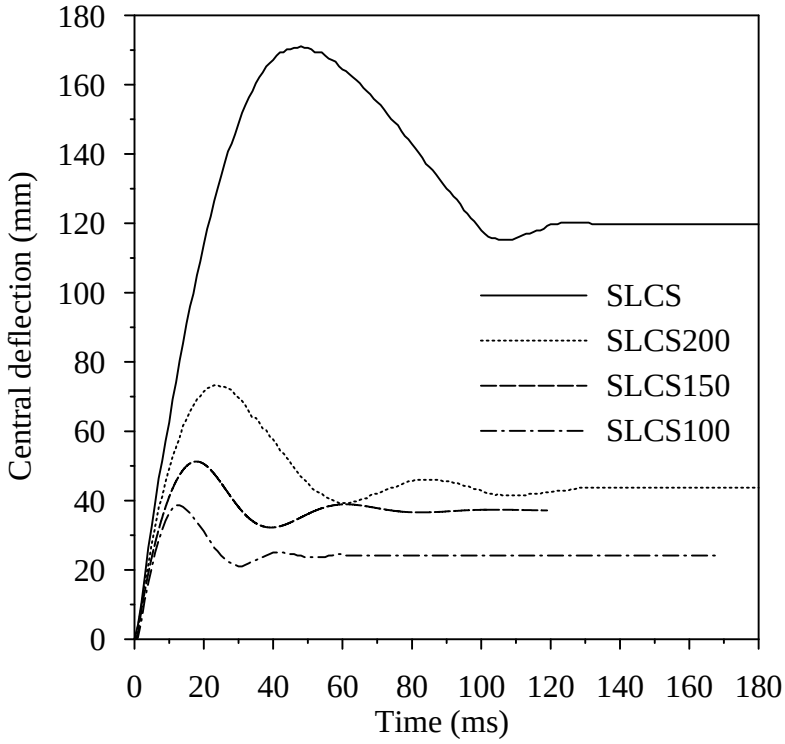

(a) Beams with plain LWC

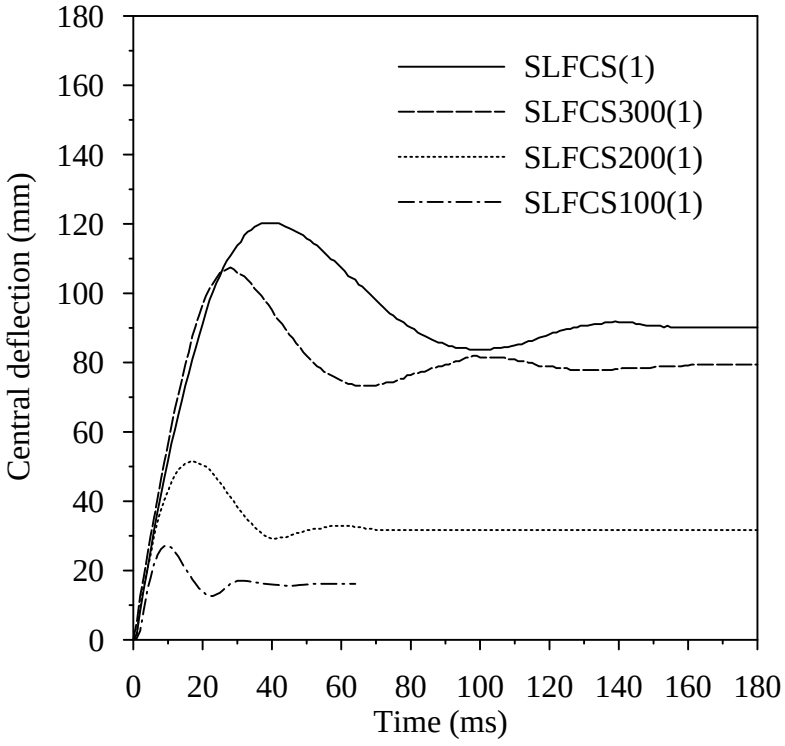

(b) Beams with fibre reinforced concrete core

Fig. 5.4 Mid-span deflections of the SCS sandwich beams under impact load.

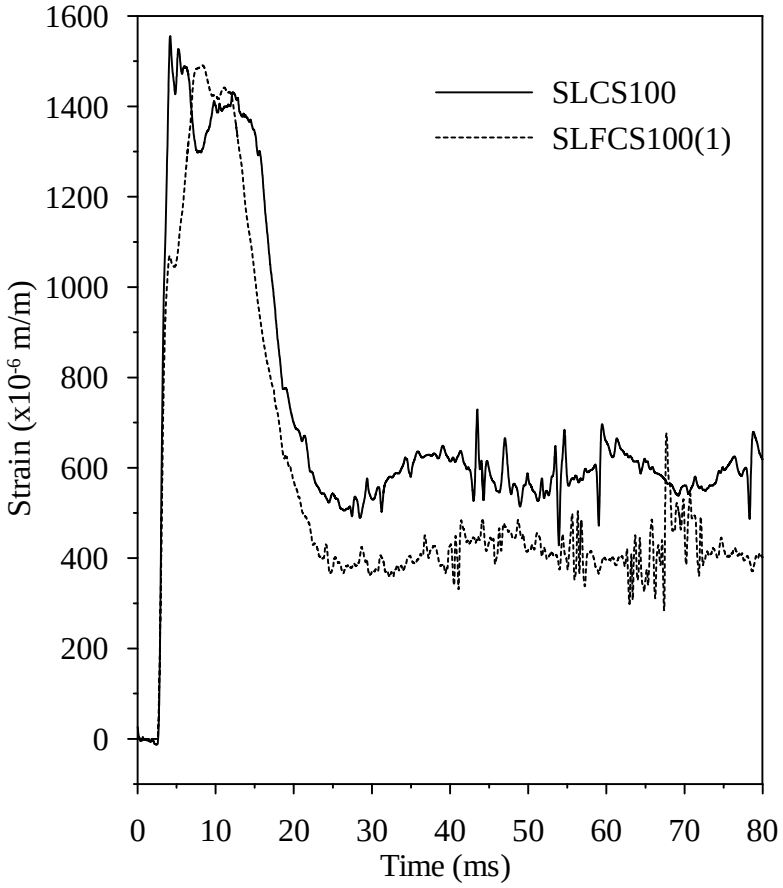

Fig. 5.5 Strain (longitudinal)-time history of bottom steel plate at mid-span.

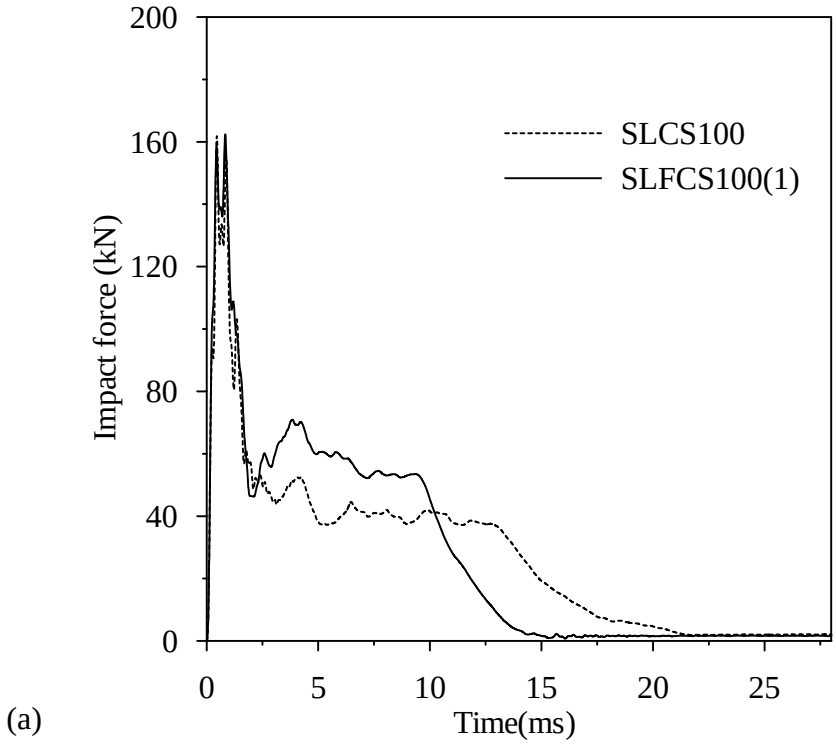

(a)

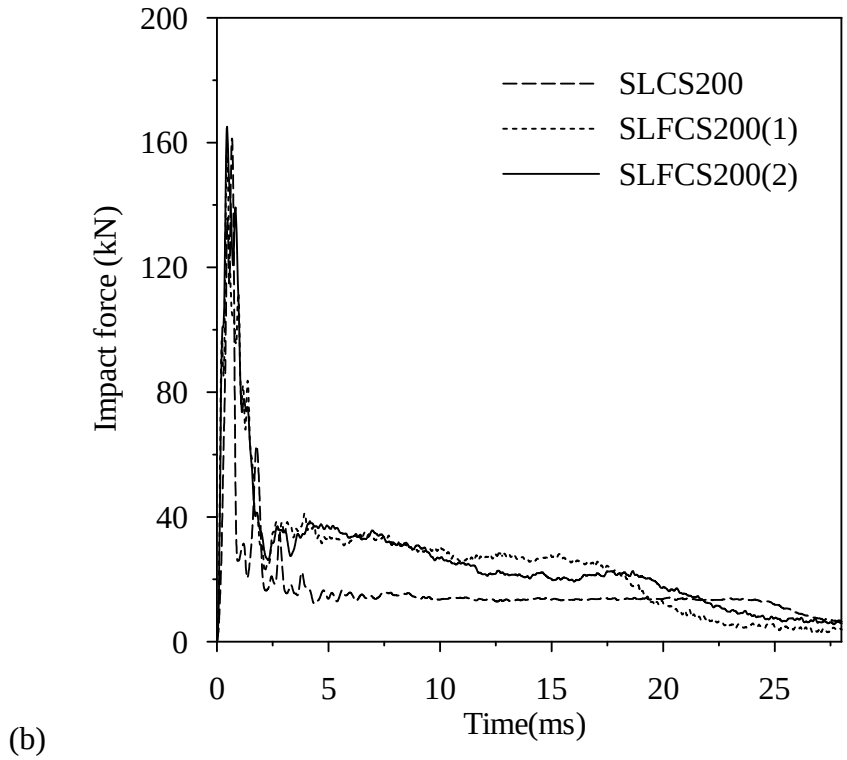

(b)

Fig. 5.6 Impact force histories of the SCS sandwich beams.

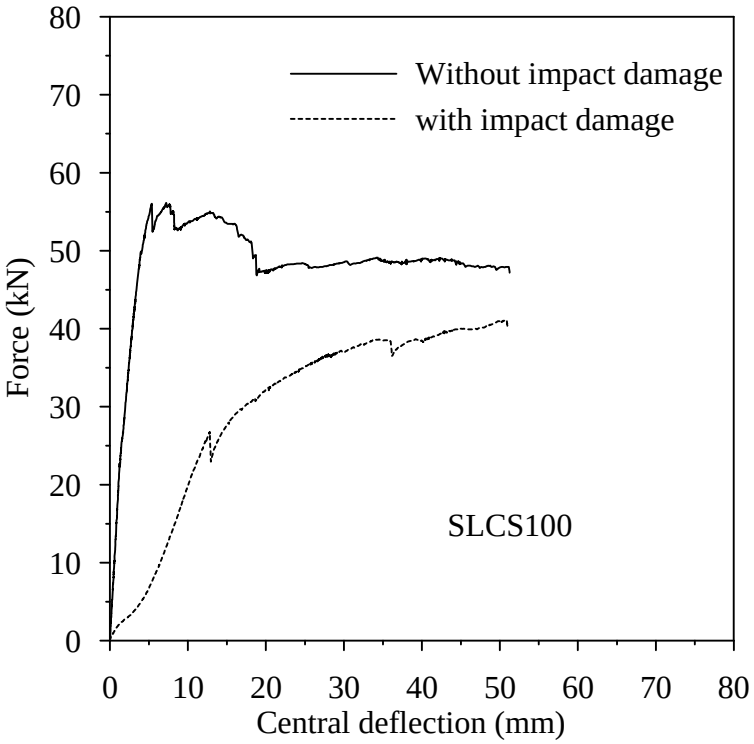

(a)

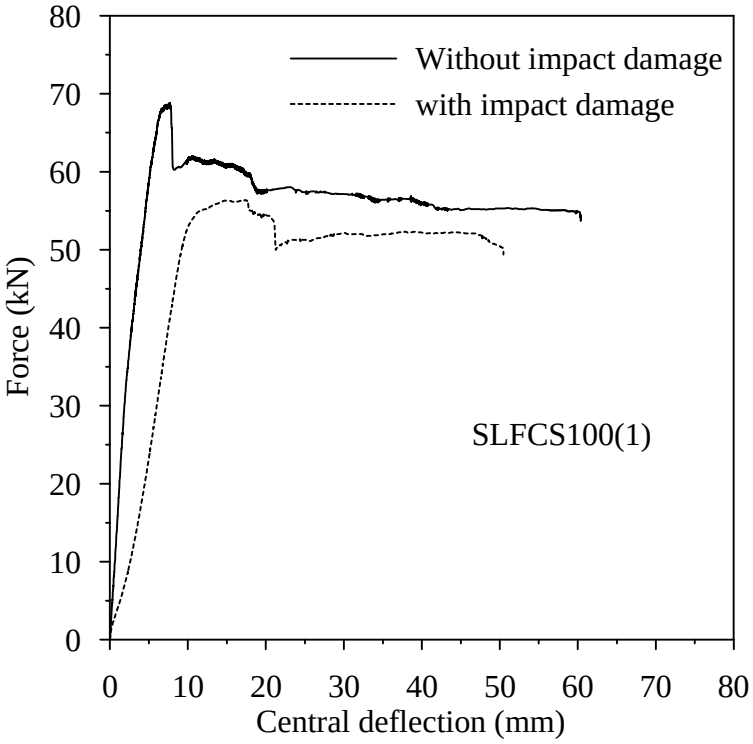

(b)

Fig. 5.7 Comparison of static load-displacement behaviour of beams with and without impact damage (a) SLCS100; and (b) SLFCS100(1).

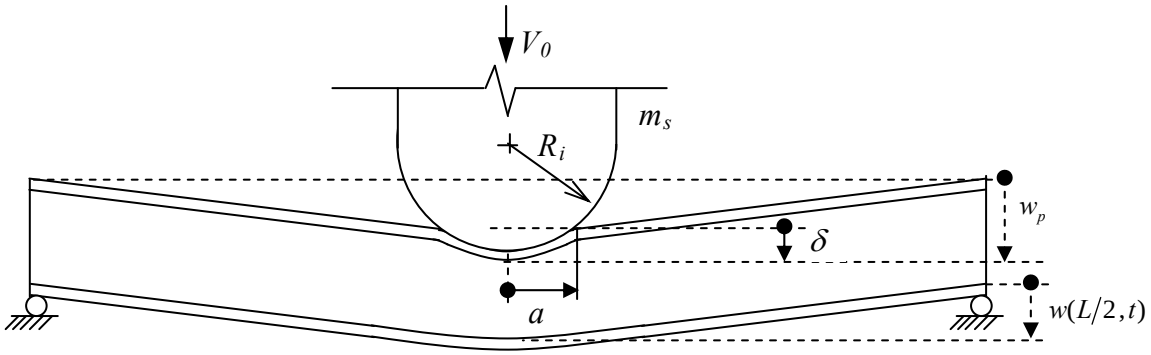

Fig. 5.8 Beam deformation caused by an impact due to a hemispherical headed projectile.

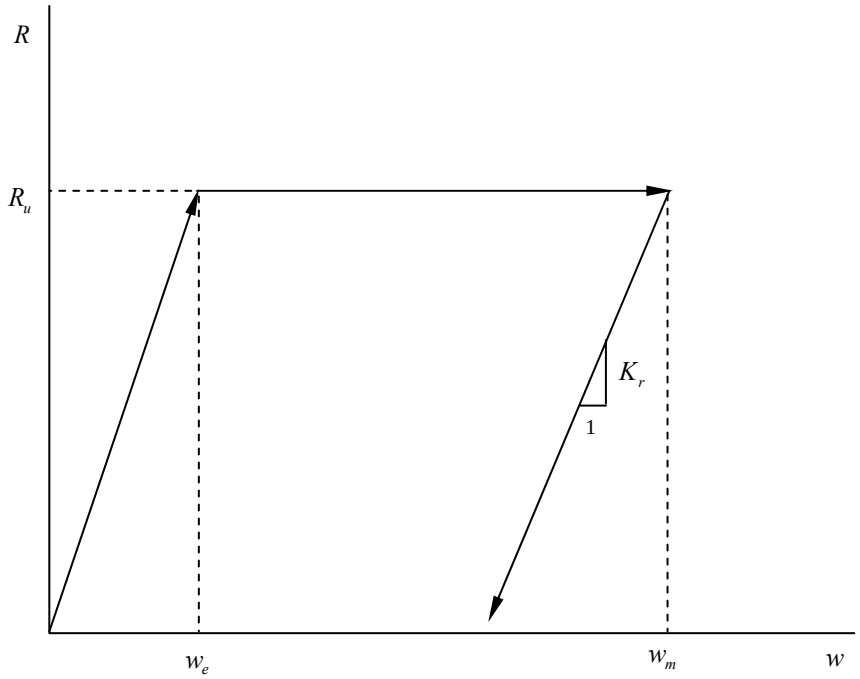

Fig. 5.9 Idealized force displacement curve of a beam (Resistance function of a beam)

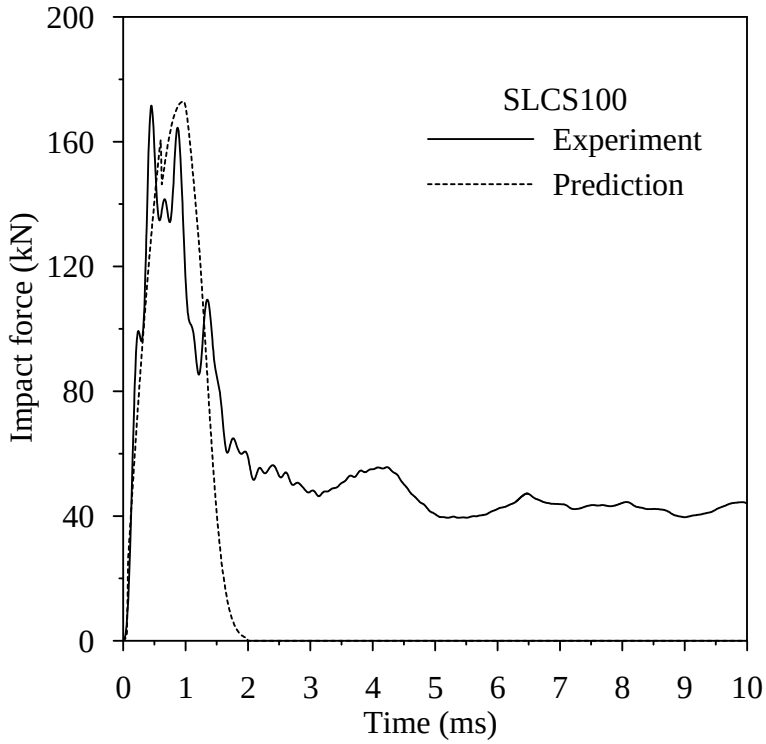

(a) Impact force-time history

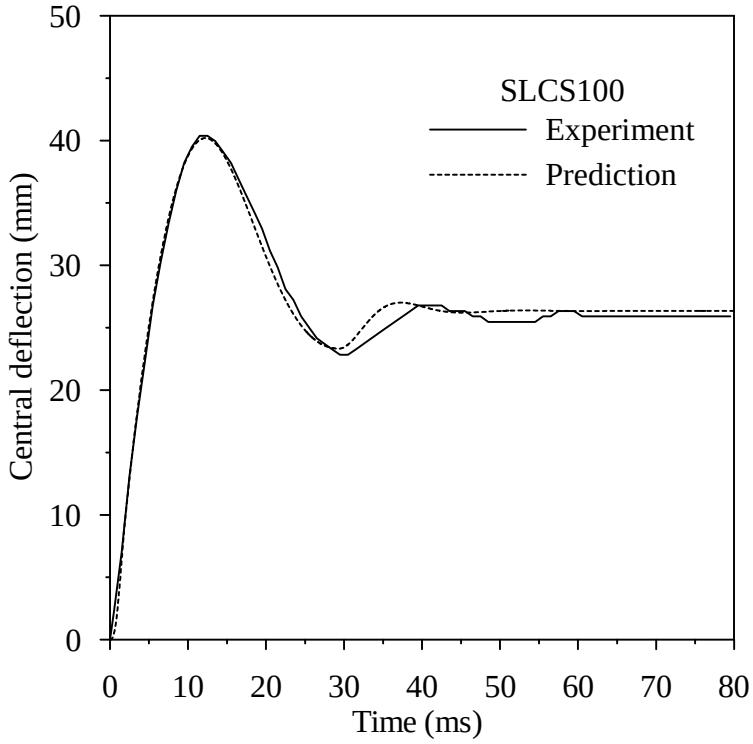

(b) Central deflection-time history

Fig. 5.10 Comparison of predicted results with experiment for beam SLCS100

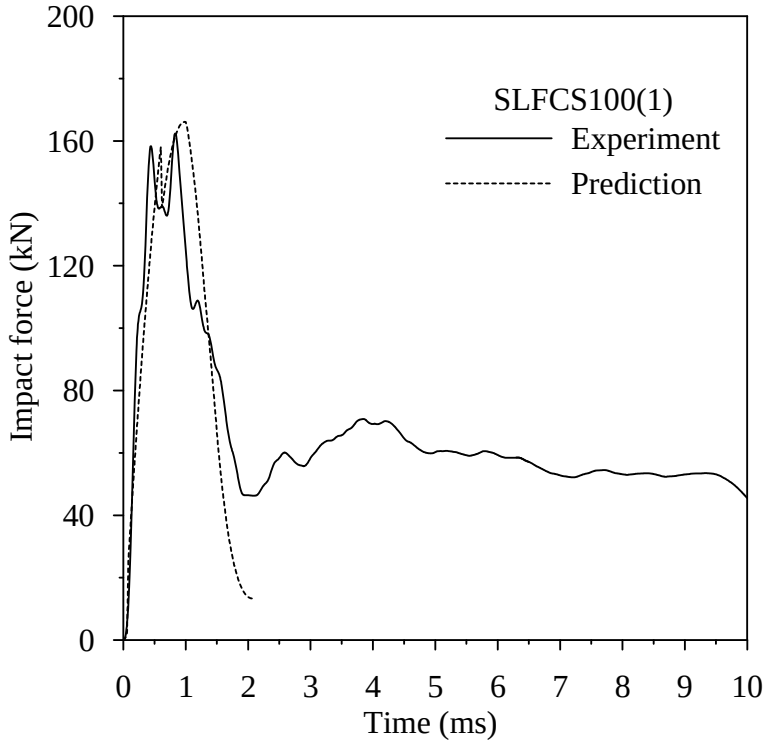

(a) Impact force-time history

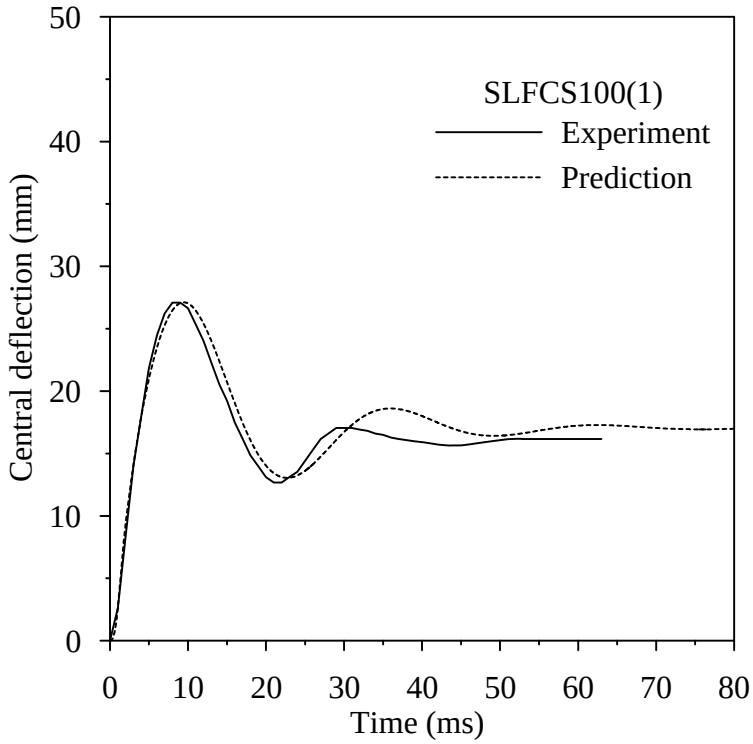

(b) Central deflection-time history

Fig. 5.11 Comparison of predicted results with experiment for beam SLFCS100(1)

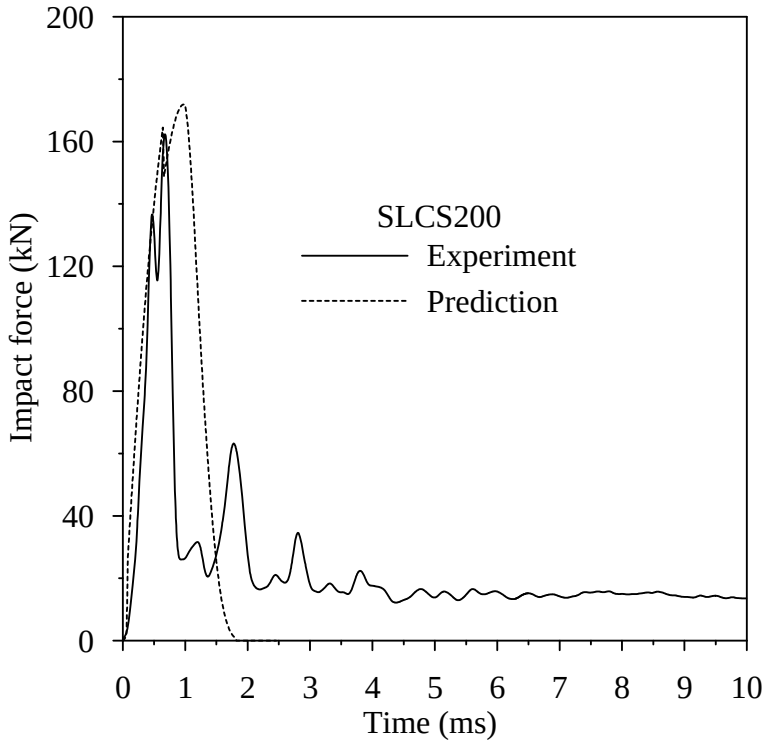

(a) Impact force-time history

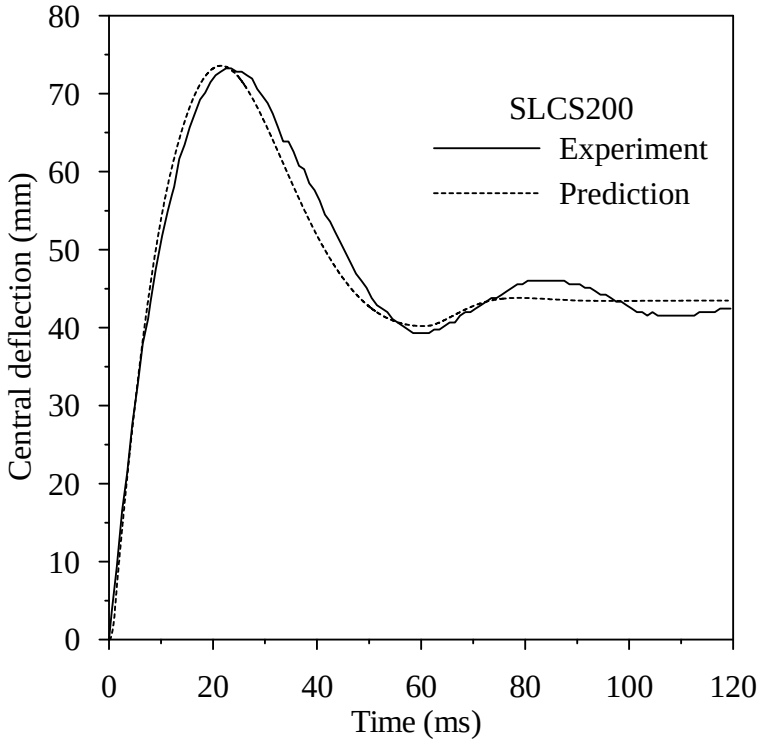

(b) Central deflection-time history

Fig. 5.12 Comparison of predicted results with experiment for beam SLCS200

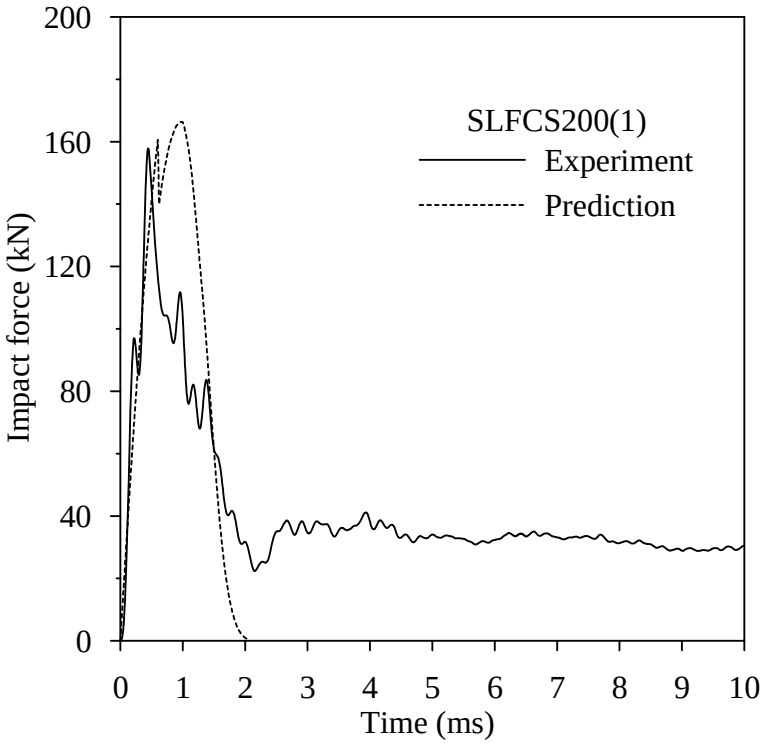

(a) Impact force-time history

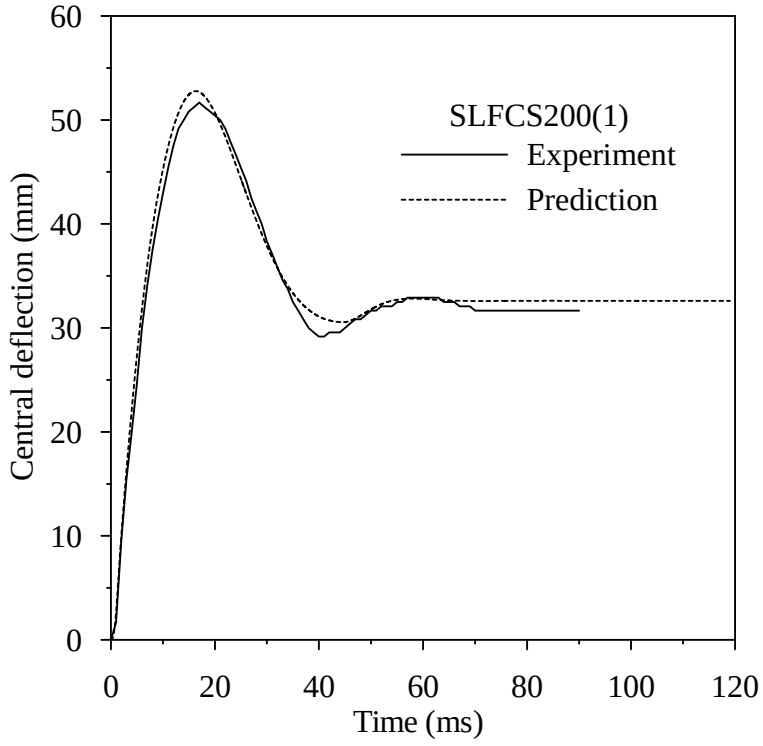

(b) Central deflection-time history

Fig. 5.13 Comparison of predicted results with experiment for beam SLFCS200(1)

Response of SCS sandwich slabs to impact loading

6

6.1 Introduction

In chapters 3 and 5, the development of J-hook connectors and their performance in sandwich beams has been discussed elaborately. The primary modes of failure in the beams were yield, slip in tension plate and tension or pull out failure of the shear connectors. Sandwich slab is different from that of beams, as it resists lateral load by flexural bending in two directions (Shanmugam et al. 2002). Moreover, most of the previous studies in literature also have been focused on the static performance of SCS sandwich beams (Oduyemi and Wright 1989; Narayanan et al., 1994; Xie et al., 2007; McKinley and Boswell, 2002). Crawford et al. (2006), Corbett et al. (1993) and Santos (2003) carried out test on small SCS sandwich panels without shear connectors subject to blast, bullet penetration and punching by low velocity projectile, respectively. These SCS sandwich panels were found to have enhanced performance when compared with stiffened steel plates or fibre reinforced concrete slabs. However, global performance of full scale SCS sandwich slabs under impact force has not been studied extensively.

The objective of this chapter is to fill the gaps by studying the dynamic behaviour of SCS sandwich slabs (Fig. 6.1) caused by a projectile. The force-indentation relations derived in Chapter 4 are incorporated in the global elastic forced vibration dynamic model of the slab to determine the global response behaviour. Using these force-

indentation relations, simplified punching model is developed and energy balance model is adopted to analyse the global dynamic response of SCS sandwich slabs.

6.2 Impact test on SCS sandwich slabs

6.2.1 Test program

To investigate the local and global impact behaviour, drop weight impact test were conducted on SCS sandwich slab specimens of different core thicknesses (80 and 100 mm) as well as different steel face plate thicknesses (4, 6 and 8 mm). Other parameters were investigated including J-hook shear connectors and steel fibre with lightweight concrete ($1400 \leq$ density ≤ 1450 kg/m^3) which is much lighter than normal concrete (2400 kg/m^3). The test program summarized in Table 6.1 is divided into two parts: (a) studying the impact resistance of SCS sandwich slabs with light weight concretes, namely LWC and LWFC, and (b) evaluating the performance of SCS sandwich slabs consisting of normal weight concrete core with different thicknesses of steel face plate and compared with SCS sandwich slabs containing LWC core.

6.2.2 Preparation of test specimens

A total number of eight SCS sandwich slabs measuring 1200×1200 mm^2 (width × length) was prepared for impact test. All the panels were fabricated with J-hook shear connectors. The diameter of J-hook connectors was 10 mm for five specimens and others contained 12 mm diameter connectors. The spacing of the connectors in both directions was 100 mm for all specimens. Plain lightweight concrete (LC) (density = 1440 kg/m^3) was used for one specimen. Lightweight concrete (density = 1445 kg/m^3) with 1% volume fraction of fibres (Dramix® RC-80/30-BP) were used as core material for three specimens. Ordinary Portland cement and expanded clay type of lightweight

aggregate (LWA) (coarse and fine) with average particle density of 1000 kg/m^3 were used to produce the lightweight concrete. The maximum size of the LWA was 8 mm. The remaining four specimens were casted with normal weight concrete (NWC) or normal weight concrete with fibres (NWFC). The details of the test specimens are given in Table 6.1.

The J-hook connectors may be welded to the steel plates by manual arc welding. However, this process was rather slow and costly and did not produce consistent quality welding. Manual arc welding also produced high heat which caused distortion of the steel plate. To overcome this problem, the welding of J-hook connectors to the steel plate was done by modified automatic stud welding gun (discussed in Chapter 3) as shown in Fig. 6.2(a). With this modified welding gun, the welding of the J-hook connector was as fast as headed stud welding.

A steel frame was fabricated to hold the sandwich slab vertically and the pre-fabricated sandwich slab skeleton was inserted into the frame before casting of concrete. Three sides of the slab were closed by wooden planks which were attached to the steel frame to prevent outflow of the concrete during casting, leaving only the top side of the panel open. Concrete was poured into the empty panel through the open top side as shown in Fig. 6.2(b).

6.3 Test set-up

Impact tests were conducted on the SCS sandwich slabs by an instrumented drop-weight impact test machine as shown in Fig. 6.3. A 7.5-meter tall steel frame was constructed and firmly bolted on the concrete base to increase the rigidity of the entire

system. A central impact in the vertical direction was achieved by means of smooth rollers so that the projectile can slide freely along the guide rails. Grease was applied on the rollers and guide rails to reduce friction and to ensure a smooth fall of the projectile. The impact can be achieved by dropping a 1255 kg projectile with varying (flat, hemispherical or conical) head of 90 to 200 mm diameter from a height of 5.5 m within the guide rail. The projectile can be dropped from a different height to achieve a different impact velocity. A mechanical hoisting system (winch) which is controlled by hydraulic system was used to raise the projectile to the required height. In this study, the drop height of 3 meters and the projectile mass of 1246 kg were used. The tip of the projectile was hemispherical with a diameter of 90 mm. When the projectile reached the specimen, its speed was approximately 95% of its free fall velocity. Five percent loss of free fall velocity was due to friction in hoisting winch and friction between the rollers and the guide rails. The same projectile was used for all the impact tests described in this chapter. Periodic checks on the tup indicated that negligible permanent deformation had occurred as a result of repeated use. The SCS sandwich slab of 1200×1200 mm^2 (width × length) was simply supported on a base frame over a span of 1000 mm. The base frame was firmly bolted to the concrete floor to achieve a rigid base support. The set-up of the impact test is shown in Fig. 6.4.

For this experiment, both the projectile and the specimens were instrumented in order to capture the damage and response of the specimens as well as for comparison with finite element simulation results obtained from a parallel study. Quartz force rings (three force rings on the same plane) of total capacity 1050 kN were attached to the projectile as a load cell in order to measure the impact forces as described in Chapter 5 (section 5.3.3). Four linear potentiometers were attached to the bottom surface of the

slab at the centre, and 100 mm, 200 mm and 300 mm away from the centre of the slab respectively. They were used to determine the deflection of the slab during impact. Strain gauges and rosettes were mounted to bottom surface of the SCS sandwich slab to capture strain time history during impact. The data from strain gauges is useful for calibration of finite element model. A 16-channel digital oscilloscope with an adjusted scan rate of 0.2 MHz per channel was used for data acquisition. A photodiode and laser system was used to trigger the data acquisition system. The detail description of this system is given in Chapter 5 (section 5.3.3). A high speed camera which is capable of capturing 1000 frames per second was used to observe the slab deformation and projectile movement during impact. The pictures obtained from the high speed camera were used to measure the projectile penetration depth to the sandwich slabs during impact event.

The test specimen was mounted and positioned on its supports. All sensors were connected to a 16-channel oscilloscope to capture the data. Then the projectile was slowly raised to the desired height by the motorized winch. After another round of checking of the instrumentation, the winch clamp was removed to allow the projectile to fall freely onto the centre of the specimen. The oscilloscope was triggered by the signal from the top photodiode. All data were recorded at 5 μs intervals (i.e., sampling rate of 2×10^5 per second). Recorded data were stored in an internal hard disk drive and transfer to a personal computer after the test for further analysis. The filtering of unwanted high frequency noises was performed as described in Chapter 5 (section 5.3.3).

6.4 Results and discussion

A total of eight SCS sandwich slabs of rectangular size, as indicated in Table 6.1, were subjected to impact by a hemispherical-tipped projectile. The responses of the SCS sandwich slabs in terms of damage, force-time history, central displacement-time history of bottom plate, and deformation profiles are presented. The test results are summarized in the Table 6.2 and 6.3.

6.4.1 Damage analysis of SCS sandwich slabs

The damage characteristics were almost similar for all the SCS sandwich slabs with major deformation occurred at the impact point. For Specimen SCS4-80, the projectile penetrated the top plate and the concrete slab with the formation of a circular hole at the impact point as shown in Fig. 6.5. This is because the 4 mm top plate is too thin to resist the impact force. When the plate thickness increased to 6 mm, the projectile could not penetrate the slabs (Fig. 6.6(a)) for the same impact energy. However, strains at impact point of the top steel plates almost reached or exceed their ultimate strain limit due to local indentation for every slab except SCFS8-100(12). This can be checked by using following equation for strain of the plate in radial direction given by Wang et al. (2000).

$$\varepsilon \approx 0.5\left(\frac{\delta}{a}\right)^{0.5} \tag{6.1}$$

where a is the radius of indentation zone in the top steel face plate (shown in Fig. 6.5(a)) and δ is the depth of the local indentation. Using Eq. (6.1), the strain of the top steel face plates were calculated using the indentation measured after test and compared with the fracture strains (ε_{ult}) obtained from coupon test given in Table 6.3. From this table, it can be seen that strain of the top steel face plates for slabs SLFCS6-

80, SLFCS6-100 and SCFS6-100(12) just exits the ultimate strain limit and experienced partial fracture which is characterized by a circumferential tearing in the steel skin under the projectile as shown in Fig. 6.7. This behaviour can be explained as the projectile caused local indentation leading to membrane stretching in the top steel face plate and subsequently face plate fracture, which was evidenced by the circumferential tearing of the top steel face plate. The diameter of the fractured area was between 75 mm to 80 mm while the projectile head diameter was 90 mm and indentation diameter ranged from 160 mm to 300 mm. Tables 6.2 and 6.3 summarised the test results and identified the failure modes and damages observed after the impact for all test specimens. The penetration resistance of the SCS sandwich slab depends on the top plate thickness, core thickness, core strength, and the capacity of the J-hook connectors.

A series of photographs were captured by high speed camera at various time steps and sample pictures are shown in Fig. 6.8. When the projectile struck the slab, very high compressive stresses were developed at the point of impact. This stress caused local indentation and crushing of the concrete core below the impact point. The impact stress waves travelled from the impact point to the supports and induced cracks in the concrete core. The slab gained momentum as the projectile travelled downward causing large displacements which further induced more damage due to the formation of flexural cracks in the concrete core. The bottom steel plate experience impact pressure due to large local indentation and tends to move downward and separate from concrete core which is shown in Fig 6.9. This separation of the bottom plate was prevented by the J-hook connectors which were connected to the steel face plates at both. The J-hook connectors were found to be effective to prevent the buckling of top

steel face plate which was in compression due to flexural bending. No noticeable slip between the steel face plates and concrete core was observed after the impact. This indicates that the J-hook connectors also effective in providing shear resistance as well as preventing tensile separation of face plates due to impact.

The concrete core was crushed and cracked under the point of impact and the cracks were extended to the edge of the slab, which were visible at the four sides of the slab. Comparing the crack patterns in the concrete core at the four sides of the slabs for Specimens SLCS6-80 and SLFCS6-80 in Figs. 6.6(a) and 6.6(b), it was observed that the plain concrete core for SLCS6-80 was broken into pieces while the fibre reinforced concrete core of SLFCS6-80 developed less cracks and remained relatively intact after impact. This shows that the fibres were effective in controlling crack propagation and provided bridging between cracks to prevent spalling of the concrete core.

6.4.2 Local indentation due to impact

The dent on the top steel face plate of each test specimen was measured after impact. A transducer was used to measure the permanent local indentation of top steel face plate for all the specimens. Measurement was taken at every point half centimetre apart in the longitudinal and transverse directions with respect to the centre of the impact. The final deformation profile was taken as an average of the measurements on these two directions. The top plate deformation profiles for the specimens are plotted in Fig. 6.10. The same procedure was applied to measure the bottom plate deformation profiles which are shown in Fig. 6.11. The depth of the deformation reduced with the increase of the compressive strength of core material. For SLFCS6-100(12) with LWC core of compressive strength f_c =28.5 MPa, a deformation of 57.6 mm at the centre of

the top plate with respect to the edge was recorded; whereas for SCFS6-100(12) with concrete strength f_c =59 MPa, a deformation of 47.2 mm was recorded as shown in Tables 6.2 and 6.3. Specimens with fibre reinforced concrete core exhibited smaller local indentation depth as compared to the ones without fibre in the core (see Fig. 6.10). The indentation depth also reduced significantly with the increase of steel face plate thickness. For example, in SCS sandwich slab with 6 mm face plate, a dent depth 47.2 mm was observed whereas for sandwich slab with 8 mm face plate, a dent depth 28.9 mm was measured (Table 6.3). This is because the penetration resistance and flexural stiffness of the face plate are directly related to its thickness, as well as the ability of thicker plate to distribute the impact load to a larger contact area on the concrete core.

The diameter of local indentation ranged from 160 to 250 mm for sandwich slabs with LWC core except for SLCS6-80 in which indentation diameter was approximately 340 mm as shown in Fig. 6.10(b). From photos taken after the test (Fig. 6.5) and the deformation profile plot in Fig. 6.10(a), it was observed that for SCS4-80 with normal weight concrete core and 4 mm steel face plates, the local indentation was very high (93.7 mm) but the global displacement of the slab is small. Similar deformation pattern was also observed in Fig 6.10(a) for the slabs with normal weight fibre reinforced concrete core and with 12 mm diameter J-hook connectors (SCFS8-100(12) and SCFS6-100(12)). For the slabs with normal weight concrete, the indention was more localized and the diameter of indentation area was about 200 mm. For thin steel face plate (4 mm), most of the damage occurred at the impact point (Figs. 6.5(a), 6.10(a) and 6.11(a)) and thus most of the impact energy was absorbed through local punching of the slab rather than global plastic deformation. In these cases, the flexural stiffness

and load carrying capacity of the slabs were relatively higher than the punching stiffness and punching capacity. Thus, the impact energy was absorbed through deformation due to local punching. It can therefore, be concluded that the local indentation of SCS sandwich slab depends on the steel face plate thickness, compressive and tensile strength of the interconnect J-hook connectors as illustrated in Fig. 6.9. Increasing the plate thickness and enhancing the concrete strength and stiffness will reduce the local indentation.

The permanent deformation of bottom steel face plates is shown in Fig. 6.11. The shape of the deformation profiles of the slabs with LWC is similar to that of the top steel face plate. However, the plastic deformation zone in the bottom face plate was wider than that of the top face plate, because the impact stress was spread through the thickness of the slab. Consequently, the bottom face plate experienced impact punching force over a larger area than that of the top face plate as illustrated in Fig. 6.9. When the bottom face plate was subjected to the impact stress, the J-hook connectors on the bottom face plate provided tensile restraints to prevent it from being push-out from the concrete core. Thus, connecting the top and bottom face plates by through connectors, such as the proposed J-hook connectors, is important to prevent such local failure. Moreover, if the top face plate is failed by punching, the bottom face plate can absorb the rest of the impact energy until it is punched through. This is possible only with the present of tensile connectors.

6.4.3 Displacement-time history

Upon impact, the slab experienced a sudden displacement at the load point. The displacement time history at the centre point of the bottom steel face plate was

measured by using linear potentiometer which was attached by screw at the centre of the bottom face plate. Displacement time histories for the sandwich specimens are presented in Fig. 6.12. It can be seen from the figures that a portion of the elastic displacement was recovered as soon as the impact force reduced to zero. The experimentally recorded maximum deflections (w_{max}) and residual deflections are given in Table 6.2 for all the slabs. Comparing SCFS6-100(12) with SCFS8-100(12)) of face plate thickness = 6mm and 8mm, respectively in Fig. 6.12(b) shows that the overall displacement decreases by 31% with the steel face plate thickness increases by 33%. This is because of the increase in flexural resistance and punching stiffness of the slab when the face plate thickness increases. Increase in concrete core thickness reduces the maximum deflection of the slab as core thickness contributed to the flexural rigidity and load carrying capacity. As expected, the inclusion of fibres in concrete core reduced the impact deformation. The test results given in Table 6.2 show that addition of 1% steel fibres in the concrete core reduces the maximum central deflection by 10 %. It is also noted that the deflection profile of Specimens SLCS6-80, SLFCS6-80 with lightweight concrete core, as shown in Fig. 6.13, was almost linear (measuring from the edge to central) instead of half-sinusoidal as expected in the case of elastic response. This indicates that plastic yield line had already formed and considerable plastic deformation had contributed to the total displacement.

The recorded residual deflections (i.e. permanent deformations of bottom plate) at centre of the slabs were 34.01 mm and 29.74 mm for SLFCS6-100(12) and SCFCS8-100(12), respectively. This reflects that the increase in plate thickness reduces the degree of damage experienced by the slab. Specimens with fibres reinforced core showed improved performance in terms of stiffness and structural integrity under

impact. From Table 6.2, it is evident that the maximum and residual deflections can be significantly reduced by adding 1% steel fibre into the concrete core.

6.4.4 Impact force-time history

It is necessary to measure the impact force which is responsible for the punching failure of the slab. The measured impact force-time history is plotted in Fig. 6.14. At the beginning of impact, there was a sharp increase in impact force due to the elastic contact between projectile and sandwich until the load suddenly decreased with the occurrence of a local punching-shear failure within the concrete core around the impact area. After core punching failure, the SCS sandwich slabs were still able to sustain impact force due to the presence of steel face plates. The post punching (concrete punching) behaviour was dependent on thickness of the steel face plates and J–hook connectors' capacity. Most of the local indentation occurred when the contact zone of sandwich slab became plastic.

The peak impact force may be influenced by various parameters. However, in this study, the nose shape of the projectile, core thickness and boundary conditions were kept the same for all the specimens and hence, the peak impact force was affected mainly by the drop height of the projectile, the steel face plate thickness and type of concrete core used. The test results shown in Fig. 6.14(e) indicate that the maximum contact force generally increases with higher core strength. This is because of the enhancement of the local and slab stiffness of the slab due to the increase of core thickness. Use of 1% volume fraction of fibres in concrete has little effect on the impact force time history as shown in Fig. 6.14(a). This is because the concrete compressive strength did not increase significantly by the addition of steel fibres.

The impact force response for the sandwich specimens was affected by the steel face plate thickness. Increase in plate thickness increases the impact force as shown from the test results plotted in Fig. 6.14(d). The peak impact force increased by about 25% when the steel face plate thickness increased from 6 mm to 8 mm (Table 6.2). This can be attributed to the increase in contact stiffness, and increase in global bending and membrane resistance of the slab as the face plate thickness increases.

6.5 Analysis of impact between projectile and SCS sandwich slab

Fig. 6.15 shows a SCS sandwich slab subjected to an impact at the centre by a hemispherical headed projectile of mass m_s and radius R_i. The initial impact velocity of the projectile is denoted by V_0. The impact causes a local indentation on the sandwich slab δ and an overall displacement of the slab, w_p. The contact zone between projectile and steel face plate is R_c, while a denotes the length of deformation zone. The assumptions to model the local indentation are same as discussed in Chapter 4 (section 4.2).

6.5.1 Force-indentation relations for SCS sandwich slab

6.5.1.1 Elastic indentation

Indentation is local and pointed effect, and it is dominated by the stretching of the steel face plate. The force-indentation curves in the available literature also indicate that the local indentations of the face plates are dominated by membrane stretching of the skins (Turk and Hoo Fatt, 1999).

From the experimental results of permanent indentation profile (Fig. 6.16), the deflection profile function can be approximated as $w = \delta(1 - r^2/a^2)^4$ for large

deflection (assuming $w > t_s$). Formulation and minimizing the total potential energy using the above deformation field was done in chapter 4 and will not be repeated here. The following force-deformation is taken from chapter 4:

$$F = \left(1.03 E_c t_s E_s / h_c\right)^{1/2} \delta^2 = K_e \delta^2 \qquad \text{as given by Eq. (4.8)}$$

and $K_e = \left(1.03 E_c t_s E_s / h_c\right)^{1/2}$ as given by Eq. (4.9)

where E_c and E_s are the modulus of elasticity of concrete and steel respectively, t_s and h_c are the steel face plate and core thickness respectively.

6.5.1.2 Plastic indentation

When the steel face plate becomes plastic and the contact radius is equal to radius of indented area (Fig. 6.17(a)), the force- indentation relation for plastic contact zone was derived in chapter 4 using Onat and Haythornthwaite (1956) expression for plastic deformation of steel face plate. The following force-plastic deformation is taken from chapter 4:

$$F = (2\pi t_s \sigma_0 / [0.5 + \ln(a/R_c)])\delta + 2\pi R_i f_c \delta \qquad \text{as given by Eq. (4.14)}$$

If R_c=a, $F = (4\pi t_s \sigma_0 + 2\pi R_i f_c)\delta$ as given by Eq. (4.16)

where σ_0 is the plastic strength of steel plate, f_c is the compressive strength of the concrete core.

Turk and Hoo Fatt (1999) showed in their analysis that in case of large indentation, contact radius R_c is always smaller than the deformed zone radius a which is shown in Fig. 6.17(b). From the indentation profiles obtained from tests, it was observed that for large indentation in SCS sandwich slab, the contact radius R_c is approximately 40% of a (the radius of local deformed area). For larger indentation depth, the

concrete reaction force is concentrated under the projectile only and it is assumed that this reaction is equal to the tensile capacity of the J-hook connectors nearby the impact point as shown in Fig. 6.9. Therefore, for large local indentation, Eq. (4.15) becomes,

$$F = \left(1.412\pi t_s \sigma_0\right)\delta + n_{ah}F_t \tag{6.2}$$

where n_{ah} is the number of J-hook connector attached to the bottom plate within the diameter of $a+h_c$ as shown in Fig. 6.9 and F_t is tensile capacity of the J-hook connectors within concrete block.

6.5.1.3 Unloading

For unloading phase, it is assumed that the stress-strain relation of SCS materials will follow the elastic unloading path. The same procedure described in chapter 4 section 4.3.3 is applied for SCS slab impact.

6.5.2 Global slab response under impact load

6.5.2.1 Elastic analysis

According to Timoshenko (1913), the displacement $w(x,t)$ depends on the vibrational response of the specimen to the impact force $F(x,t)$. The well known forced vibration for a simple slab is given as follows

$$D\nabla^4 w + \rho\frac{\partial^2 w}{\partial t^2} = F(x,y,t) \tag{6.3}$$

where D and ρ are the flexural rigidity of the slab, mass of unit area respectively. For a transverse impact on the slab, the loading function is specialized to a point contact force $F(t)$. A solution for $w(x,y,t)$ is usually sought as an expansion in the normal modes of free vibration (Goldsmith, 1960). For the central transverse impact in the

rectangular plate with side lengths A and B, simply supported along all edges, the solution of Eq. (6.3) for central (x_0, y_0) displacement is (Goldsmith, 1960)

$$w(x_0, y_0, t) = \frac{4}{\rho AB} \sum_{i=1,3..}^{\infty} \sum_{j=1,3..}^{\infty} \frac{\left(\sin\frac{i\pi}{2}\sin\frac{j\pi}{2}\right)^2}{\omega_{ij}} \int_0^t F(\bar{t})\sin\{\omega_{ij}(t-\bar{t})\}d\bar{t} \qquad (6.4)$$

where frequency of vibration, $\omega_{ij}^2 = \frac{D}{\rho}\left[\left(\frac{i\pi}{A}\right)^2 + \left(\frac{j\pi}{B}\right)^2\right]^2$ (6.5)

For square slab Eqs. (6.4) and (6.5) become

$$w(x_0, y_0, t) = \frac{4}{m_p} \sum_{i=1,3..}^{\infty} \sum_{j=1,3..}^{\infty} \frac{\left(\sin\frac{i\pi}{2}\sin\frac{j\pi}{2}\right)^2}{\omega_{ij}} \int_0^t F(\bar{t})\sin\{\omega_{ij}(t-\bar{t})\}d\bar{t} \qquad (6.6)$$

and $\omega_{ij}^2 = \frac{D}{\rho}\left[\left(\frac{i\pi}{A}\right)^2 + \left(\frac{j\pi}{A}\right)^2\right]^2$ (6.7)

where m_p is the mass of the slab. It is assumed that the initial velocity of the slab is zero. The transverse displacement of the colliding projectile relative to the initial top surface of the structure (w_p), may be expressed as

$$w_p(t) = V_0 t - \frac{1}{m_s}\int_0^t d\tau \int_0^\tau F(\bar{t})d\bar{t} \qquad (6.8)$$

where V_0 and m_s are the impact velocity and the mass of the projectile respectively. The deformation (indentation) of top face plate at impact zone can be written as

$$\delta(t) = w_p(t) - w(x_0, y_0, t)$$

or $\delta(t) = V_0 t - \frac{1}{m_s}\int_0^t d\tau \int_0^\tau F(\bar{\tau})d\bar{\tau} - \frac{4}{m_p} \sum_{i=1,3..}^{\infty} \sum_{j=1,3..}^{\infty} \frac{\left(\sin\frac{i\pi}{2}\sin\frac{j\pi}{2}\right)^2}{\omega_{ij}} \int_0^t F(\bar{\tau})\sin\{\omega_{ij}(t-\bar{\tau})\}d\bar{\tau}$ (6.9)

For different loading phases, the force-indentation relation will be different as discussed earlier. In elastic indentation phase (putting δ value from Eq. (4.8)), the above equation becomes

$$\left(\frac{F}{K_e}\right)^{\frac{1}{2}} = V_0 t - \frac{1}{m_s}\int_0^t d\tau \int_0^\tau F(\bar{\tau})d\bar{\tau} - \frac{4}{m_p}\sum_{i=1,3..}^{\infty}\sum_{j=1,3..}^{\infty}\frac{\left(\sin\frac{i\pi}{2}\sin\frac{j\pi}{2}\right)^2}{\omega_{ij}}\int_0^t F(\bar{\tau})\sin\{\omega_{ij}(t-\bar{\tau})\}d\bar{\tau} \tag{6.10}$$

Closed form solution of Eq. (6.10) is not available; therefore following numerical procedure proposed by Evans et al. (1991) is applied to solve Eq. (6.10) for force and displacement time history. This numerical method is found to be computationally efficient and gives accurate prediction of force and displacement responses. The force function $F(t)$ is assumed linear over each increment of time Δt. Details of this procedure are given in the paper written by Evans et al. (1991). According to this procedure Eq. (6.10) can be written as

$$\left(\frac{F_N}{K_e}\right)^{1/2} = A_N + BF_N \tag{6.11}$$

where F_N is the value of $F(t)$ at time $t = N\Delta t$ in which Δt and N are the time step and number of time step respectively.

$$A_N = V_0(N\Delta t) - \frac{1}{m_s}(\Delta t)^2\sum_{k=1}^{N-1}F_k(N-1) - \frac{16}{m_p\Delta t}\sum_{i=1,3..}^{\infty}\sum_{j=1,3..}^{\infty}\frac{\left(\sin\frac{i\pi}{2}\sin\frac{j\pi}{2}\right)^2}{\omega_{ij}^3}\sin^2\left(\frac{\omega_i\Delta t}{2}\right)$$
$$\times\sum_{k=1}^{N-1}F_k\ \mathrm{Sin}[\omega_{ij}\Delta t(N-k)] \tag{6.12}$$

$$B = -\frac{(\Delta t)^2}{6m_s} - \frac{4}{m_p}\sum_{i=1,3..}^{\infty}\sum_{j=1,3..}^{\infty}\frac{\left(\sin\frac{i\pi}{2}\sin\frac{j\pi}{2}\right)^2}{\omega_{ij}^2}\times\left(1-\frac{\sin(\omega_{ij}\Delta t)}{\omega_{ij}\Delta t}\right) \tag{6.13}$$

Note that B is constant and does not vary with time and A_N may be readily calculated since it involves only values F_j up to F_{N-1}.

6.5.2.2 Plastic analysis

Determination of inelastic response of structures having distributed mass is extremely difficult. One possible approach, suggested by Biggs (1964), is to conduct the usual elastic analysis up to the ultimate elastic capacity and then to assume that an idealized hinge has formed at this point, thus creating a new plastic system.

The response equitation can be written as following

$$m_e\ddot{w} + F_p = F(t) \qquad w_e < w < w_m \tag{6.14}$$

$$m_e\ddot{w} + F_p - k_r(w_m - w) = F(t) \quad (w_m\text{-}2w_e) < w < w_m \tag{6.15}$$

where w is the global deflection of the sandwich slab; w_e is the elastic deflection; w_m is the maximum deflection; F_p is the resistance force at yielding of the slab; k_r is the rebound stiffness of the slab; and m_e is the effective mass of slab which is 17% of the total slab mass in plastic range (Biggs, 1964; US Dept. of the Army, 1990; Morison, 2006). In the present study, a simple yet effective explicit method known as the central difference method is chosen which is suitable for explicit dynamic analysis of short duration problems (e.g. blast, impact) (Koh C.G. et al., 2003; Bathe, 1996). The details are given in chapter 5. A simple program for every time step was written in Matlab instead of hand calculation to get the force and deflection time history.

6.5.3 Energy balance model

In this section, the energy method is used to predict the maximum slab displacement (both elastic and inelastic) and determine the impact force, which are essential for serviceability deflection check and ultimate strength design of sandwich slabs, respectively.

In the energy balance model, the kinetic energy of the impacting mass will be converted into strain and fracture energy due to flexural, shear and local indentation of the slab, plastic yielding of steel plate and crushing and cracking of the concrete core. The energy losses from material damping, surface friction, and higher modes of vibration are assumed to be negligible and therefore they are not considered in the energy equations.

Fig. 6.18 and Fig 6.19 show the plastic mechanism and deformation of the SCS sandwich slab subjected to a concentrated load at the centre of the slab. The maximum plastic resistance F_p of the sandwich slab can be determined using plastic yield-line method. From virtual work priciple, the flexural capacity was evaluated using the following equation presented by Rankin and Long (1987)

$$F_p = 8m_{pl}\left(\frac{L_s}{L-c} - 0.172\right) \tag{6.16}$$

where c is the side length of the loading area, L_s is the dimension of the slab specimen; L is the span between the supports; m_{pl} is the plastic moment capacity per unit length along the yield line and can be determined as following,

$$m_{pl} = \frac{1}{8} n_t (P_R)\left(h_c + t\right)/l \tag{6.17}$$

in which $l = L_s/(2\cos\theta)$. Detail description of determination of m_{pl} is given in Appendix A.

After yielding with increasing deflection, the load carrying capacity of the composite sandwich slab is dominated by the membrane stretching of the steel face plates due to

large deflection. Fig. 6.18(b) shows an idealized force-deflection curve of a SCS sandwich slab.

The impact energy absorbed by the slab in flexural response can be expressed as

$$E_{impact} = E_e + E_p + E_m + E_{local} \tag{6.18}$$

where $E_{impact} = \frac{1}{2} m_s V_0^2$ is the kinetic energy due to an impacting mass of weight m_s at an impact velocity, V_0. $E_e = \frac{1}{2} F_p W_w^2$, $E_p = F_p \left(W_p - W_e \right)$ and $E_m = \frac{1}{2}(F_p + F)(W - W_p)$ are the maximum elastic strain energy (recoverable), the plastic work (irrecoverable) when the system reaches the plastic deflection w_p and the energy absorbed by both bending and membrane stretching of the slab. Some of the impact energy is also absorbed by local damage E_{local}, due to local indentation of face plate and core crushing. Using the force-indentation relation for large indentation from Eq. (6.2), the energy absorbed in the contact region due to local indentation can be defined as

$$E_{local} = \int_0^{\delta} F d\delta = \int_0^{\delta_m} \left(K\delta + F_{con} \right) d\delta = \frac{1}{2} K \delta_m^2 + F_{con} \delta_m \tag{6.19}$$

where $F = K\delta + F_{con}$ from Eq.(6.2) in which $K = 1.412 \pi t_f \sigma_0$ and $F_{con} = n_{ah} F_t$

Using force-indentation relation equation, the maximum local indentation (δ_m) can be expressed in terms of the resistance force (F) of the slab for applied impact. i.e.

$$F = K\delta_m + F_{con} \quad \text{or} \quad \delta_m = \frac{F - F_{con}}{K} \tag{6.20}$$

Putting the expression for δ_m to Eq. (6.19), the local energy absorption is

$$E_{local} = \left(F^2 - F_{con}^2 \right) / 2K \tag{6.21}$$

Thus, the energy balance equation (Eq. (6.18)) can be written as,

$$\frac{1}{2} m_s V_0^2 = \frac{1}{2} F_p w_e^2 + F_p (w_p - w_e) + \frac{1}{2}(F_p + F)(w - w_p) + \left(F^2 - F_{con}^2 \right) / 2K \tag{6.22}$$

When the impact energy delivered is small, i.e., $E_{impact} < E_e + E_{local}$, the deflection occurs within the elastic range ($w < w_e$) and the slab can survive the impact without global damage.

For moderate levels of impact energy $E_e + E_{local} < E_{impact} < E_e + E_p + E_{local}$, plastic deformation is induced but the maximum displacement is within the range of w_e and w_p. The SCS sandwich slabs can still withstand the impact with some local damage and global plastic deformation. The magnitude of maximum plastic deformation depends on how much plastic work is needed to dissipate the impact energy.

When the impact energy is large, i.e., $E_{impact} > E_e + E_p + E_{\mathrm{m}} + E_{local}$, the slab is unable to dissipate the total impact energy, resulting in collapse. US Dept. of the Army (1990) recommends that SCS sandwich slabs may be designed to attain large deflections corresponding to support rotation of about 8 degrees which corresponds to a span to deflection ratio of $L/w \leq 14$ for general cases. To ensure structural integrity of the slab, adequate number of J-hook connectors must be provided to permit ductile deformation and redistribution of forces in the mechanical connectors. However, when safety for personal and equipment is required, a limiting deflection ratio of $L/W \leq 53$ or a limiting ductility ratio of 10, whichever governs, is specified as a reasonable estimate of the absolute magnitude of the slab deformation as suggested by US Dept. of the Army (1990).

The SCS sandwich slab may be designed to behave in a ductile manner to allow large global deformation with higher flexural capacity, but the local punching resistance of

the slab must be checked. If the punching resistance is lower than the flexural capacity F_{m}, local punching failure may occur before reaching the ultimate global resistance of the slab.

6.5.4 Punching resistance

The punching resistance (V_p) of composite sandwich slab may be obtained by summing the shear resistance provided by the concrete core and steel face plates, and the contribution from the shear connectors as:

$$V_p = V_c + V_s \tag{6.23}$$

where V_c is the resistance of the concrete core and V_s is the resistance of the steel face plate and shear connectors. But concrete core failed in punching earlier than reaching ultimate fracture capacity of the steel face plate (Shukry and Goode, 1990; Solomon et al. 1976) and J-hook connectors. Because steel face plate exhibit long ductile behaviour leading to deep indentation at the impact point before reaching its fracture capacity. For this reason, to calculate the ultimate punching capacity of the SCS sandwich slabs, concrete contribution is ignored. Thus, the top steel plate punching resistance for hemispherical headed projectile can be written in combination of face plate capacity (Eqs. 4.10b)) and J-hook connectors tensile capacity as following

$$V_p = F_{faceplate} + n_{ah}F_t = \frac{2\pi N_0 \delta}{0.5 + \ln(a/R_c)} + n_{ah}F_t \tag{6.24}$$

where F_t is the tensile capacity of each J-hook connector obtained from direct tensile test of interconnected J-hooks within a concrete block as show in Fig. 6.20.

By knowing the fracture strain limit, indentation depth δ at fracture can be measured by Eq. (6.1). In this present study, the radius of local deformation zone (a) is

approximately 100 mm and the contact radius (R_c) is approximately 40 mm. Therefore, the Eq. (6.24) will be as following

$$V_p = (1.412\pi t_s \sigma_0)\delta + n_{ah} F_t \tag{6.25}$$

At the event of fracture, the stress in the steel plate should be ultimate strength. After top plate fracture, the bottom face plate will resist rest of the impact energy.

6.6 Comparison of analytical results with test results

The results obtained from the analytical model described in Section 6.5.2 to section 6.5.4 are compared with the experimental results in terms of impact force, central displacement and punching resistance of the slab. The strain rate effect (described in Chapter 4) on the steel strength is considered to evaluate the contact parameters (force-indentation relations).

Eq. (6.10) predicts the impact force as a simple function of the contact stiffness, impact velocity (V_0), mass of the projectile (m_s), mass of the slab (m_p), and natural angular frequency (ω_1) of the slab. The accuracy of theoretical impact force and the displacement history depends on the values of ω_1, F_p, K_r and w_e calculated or assumed. In the present study, these parameters are taken from static test results as shown in Fig. 6.18 and static test results are given in Appendix A. Eq. (6.10) requires numerical techniques to solve for impact force and displacement. These are discussed in the section 6.5.2.1, and it is observed that the computed solution depends on the fineness of the time interval chosen for the integration and, more critically, on the number of modes assumed in the solution. Convergence study shows that solutions

with 17 modes are found to be sufficient and the use of higher modes does not improve the accuracy of the results by more than 1% (Evans et al., 1991).

Two cases of study are selected to predict the structural response on the basis of elastic and plastic theories discussed in sections 6.5.2. Figs. 6.21 and 6.22 depicted the force-time history and projectile displacement history respectively for two SCS sandwich slabs of SLCS6-80 and SLFCS8-100(12). The results were compared with the test data. The analytical models are able to predict the impact response reasonably well. The variation may be the cause of experimental limitation to capture impact force as well as the idealization of the contact parameters. In the analytical models, the change of slab response from elastic to plastic is sudden but in test the change from elastic to fully plastic is in gradual manner. Similarly the force-indentation relation also changes gradually in the test. These parameters have influence on the accuracy of the predicted force-time history and displacement history. It is found that the variation of maximum impact force between experiment and theory is about 5 % to 10 % for these two specimens. It is difficult to use this model for those specimens which experienced top plate fracture at impact point. For this reason, only two specimens which did not experience any fracture at the impact point are considered.

Table 6.4 shows the input data (F_p, w_e, w_p, and F at 60 mm deflection are obtained from static tests) required for the model to predict the response behaviour of sandwich slab subjected to a given impact energy. Table 6.5 compares the predicted results with the test results in terms of the maximum slab displacement and the contact force between the projectile and the slab and they show reasonably good agreement. However, the energy method underestimates the maximum impact force by 8% to 20%

when compared to the test results except slab SCFS8-100(12) which shows a difference of 24%. This is because the input parameters were based on load-displacement relationship obtained from static tests and thus material strain rate effect was not considered in the material model. The predicted maximum deflection is close to the experimental central deflection and the difference is within 11% for all slabs except slab SCS4-100. This slab experienced full fracture of the top plate during impact which influenced the central deflection.

Table 6.6 compares the impact forces from test measurements with the punching resistance of the slabs obtained from Eqs. (6.23) to (6.25). The face plate fracture resistance is close to the maximum test impact force. From Table 6.3, it can be seen that the estimated strain is near to the failure strain of the face plate for all specimens except slabs SCS4-80 and SCS4-100. In these two specimens the top plate fully fractured and experienced very large local deformation. The punching capacity is considered to be reached when the top face plate fractures. It has been observed that the impact forces were higher than the punching capacity for those slabs which experienced face plate fracture. For SLCS6-80, SLFCS6-100(12), and SCFS8-100(12), the maximum impact force is lower than the value of the punching capacity and no fracture of top plate was observed. Therefore, the proposed punching model can be used to estimate the punching capacity of SCS sandwich slab in practice.

6.7 Summary

Impact tests have been carried out to confirm the structural behaviour of SCS sandwich slabs in flexure and punching failure. Test results show that J-hook shear connectors are effective in preventing separation of the steel face plates, thus reducing the overall

slab deflection and maintaining the structural integrity despite the presence of flexural and shear cracks in the concrete core. The impact response of slab with LWC core is similar to slab with normal weight concrete. However, sandwich slab with LWC core absorbs most of the impact energy by global plastic deformation compared to sandwich slab with NC core. If the loading area is small, depth of local indentation may be very large, which may be leading to punching failure of the slab before reaching ultimate flexural capacity of the slab. Addition of 1% steel fibres in the concrete core showed significant beneficial effects in terms of less global deflection and less cracking and spalling of the core material due to impact. SCS sandwich slabs with J-hook connectors and fibre-reinforced concrete core also enhance the contact stiffness and can absorb high impact energy before punch through.

Using the proposed force-indentation relations, an energy balance method was developed to analyze the global behaviour, especially the energy absorption capacity of SCS sandwich slabs. Using this approach, maximum force and central deformation of the slab during impact can be determined with reasonable accuracy for a given impact energy and slab configuration. The punching model was proposed to calculate the ultimate punching capacity of the sandwich slab. In this punching model, steel face plate thickness and the J-hook connector tensile capacity are the controlling parameters to enhance the punching capacity of the SCS sandwich slab. The forced-vibration dynamic equations can be used for impact analysis in elastic range.

Table 6.1 SCS sandwich specimens and specifications for impact test

Sl. No	Specimen No.	t_s (mm)	d_j (mm)	h_c (mm)	Concrete type	f_c (MPa)	σ_y (MPa)
1	SCS4-80	4	10	80	NC	57.2	275.5
2	SCS4-100	4	10	100	NC	57.2	275.5
3	SLCS6-80	6	10	80	LC	27.0	315.0
4	SLFCS6-80	6	10	80	LFC	28.5	315.0
5	SLFCS6-100	6	10	100	LFC	28.5	315.0
6	SLFCS6-100(12)	6	12	100	LFC	28.5	315.0
7	SCFS6-100(12)	6	12	100	NCF	59.0	315.0
8	SCFS8-100(12)	8	12	100	NCF	59.0	355.0

d_j= diameter of J-hook connector; NC = Normal weight concrete; LC = Lightweight concrete; NCF = Normal weight concrete with fibre; LFC = Lightweight concrete with fibre; t_s=steel face plate thickness, h_c= core thickness; S = spacing of J-hook connector; f_c = concrete cylinder strength; σ_y = yield strength of steel plate

Table 6.2 Results of impact test on SCS sandwich slabs

Specimen No.	V_0 (m/s)	F_{impact} (kN)	$w_{\max}$ (mm)	w_{res} (mm)	y_{res} (mm)	Max. projectile displacement (mm)
SCS4-80	7.40	545	---	79.4	92.6	98.9
SCS4-100	6.67	563	51.2	45.6	70.4	72.7
SLCS6-80	7.42	568	71.3	55.1	75.2	101.6
SLFCS6-80	7.36	657	64.4	43.1	74.5	90.1
SLFCS6-100	7.43	681	57.9	38.6	66.7	81.9
SLFCS6-100(12)	7.42	694	52.0	35.2	57.6	72.4
SCFS6-100(12)	7.42	899	50.8	34.0	47.2	54.8
SCFS8-100(12)	7.42	1182	35.3	29.7	36.9	45.6

V_0= impact velocity; $w_{\max}$ =maximum deflection during impact; w_{res} = residual deflection; y_{res} =residual displacement at the centre of the top steel plate with respect to edge; F_{impact} = maximum impact force.

Table 6.3 Damage description of the SCS sandwich slabs

Specimen No.	y_{res}	δ (mm)	a (mm)	ε (Eq. 6.1)	ε_{ult}	Damages observations
SCS4-80	92.6	91.9	90	0.51	0.34	Punch through failure of top and bottom plates
SCS4-100	70.4	66.2	80	0.45	0.34	Circumferential tear in the top face plate
SLCS6-80	75.2	56.5	170	0.29	0.33	No crack (the radius of indentation is very large)
SLFCS6-80	74.5	51.7	100	0.36	0.33	Circumferential tear in the top face plate (50% of $2\pi R_c$)
SLFCS6-100	66.7	46.5	100	0.34	0.33	Circumferential tear in the top face plate (40% of $2\pi R_c$)
SLFCS6-100(12)	57.6	45.1	125	0.30	0.33	No crack (the radius of indentation is very large)
SCFS6-100(12)	47.2	47.2	90	0.36	0.33	Circumferential tear in the top face plate (60% of $2\pi R_c$)
SCFS8-100(12)	36.9	29.7	100	0.27	0.34	No crack

δ = depth of local indentation; ε_{ult}= fracture strain of the steel face plate (from coupon test); a = radius of the indentation zone; $2R_c$=contact diameter (75 to 80 mm).

Table 6.4 Input parameters for the energy balance model

Specimen No.	F_p (kN)	w_e (mm)	w_p (mm)	F_{con} (kN)	K_e (kN/mm)	m_s (kg)	F (kN) At 60 mm deflection
SCS4-100*	517.9	6.4	25	363.6	80.7	1246	273.0
SLCS6-80	252.1	4.1	25	171.8	61.5	1246	465.5
SLFCS6-80	302.4	5.5	25	181.3	54.7	1246	529.3
SLFCS6-100	363.9	6.0	25	181.3	60.4	1246	600.1
SLFCS6-100(12)	453.8	7.0	25	181.3	64.8	1246	611.2
SCFS8-100(12)**	891.7	8.5	25	376.1	104.8	1246	863.9

* there is an punching failure both in concrete and steel plate due to concentrated load in static test.
**There is an unloading after reaching plastic capacity (F_p) and after 23 mm deflection the load was increasing due to membrane action.

Table 6.5 Comparison between experimental measurements and related results obtained from the energy balance model.

Specimen No.	Experiment			Energy method	
	V_0 (m/s)	w_{max} (mm)	F_{max} (kN)	w_{max} (mm)	F_{max} (kN)
SCS4-100*	6.67	51.2	563	40.1	518
SLCS6-80	7.42	71.3	568	70.0	515
SLFCS6-80	7.36	64.4	657	57.0	512
SLFCS6-100	7.43	57.9	681	53.0	513
SLFCS6-100(12)	7.42	52.0	694	51.9	556
SCFS8-100(12)	7.42	35.3	1182	37.2	891

* Complete fracture of top plate influenced the central deformation; w_{max} = maximum central displacement; F_{max}= maximum impact force

Table 6.6 Check for steel plate punching capacity of the slab specimens

Specimen No.	F_t (kN)	n_{ah}	ε_{ult}	δ_{pun} (mm)	σ_{ult} (MPa)	V_p (kN)	F_{impact} (kN)	$\frac{F_{impact}}{V_p}$
SCS4-80	22	5	0.34	46.3	413	449	545	1.21
SCS4-100	22	5	0.34	46.3	413	449	563	1.25
SLCS6-80	16	5	0.33	43.6	450	602	568	0.94
SLFCS6-80	18	5	0.33	43.6	450	612	657	1.07
SLFCS6-100	18	5	0.33	43.6	450	612	681	1.11
SLFCS6-100(12)	25	5	0.33	43.6	450	697	694	0.99
SCFS6-100(12)	40	5	0.33	43.6	450	723	899	1.25
SCFS8-100(12)	40	5	0.34	46.3	590	1184	1182	0.99

σ_{ult}= ultimate tensile capacity of the steel face plate; δ_{pun} = indentation depth before plate fracture. F_t = direct tensile capacity of interconnected J-hook connectors within concrete block, V_p = ultimate punching resistance of the SC S sandwich

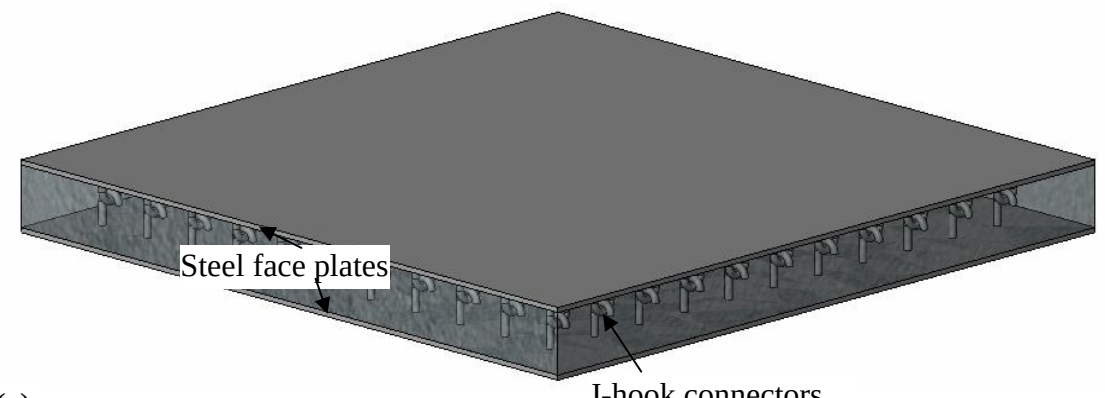

(a)

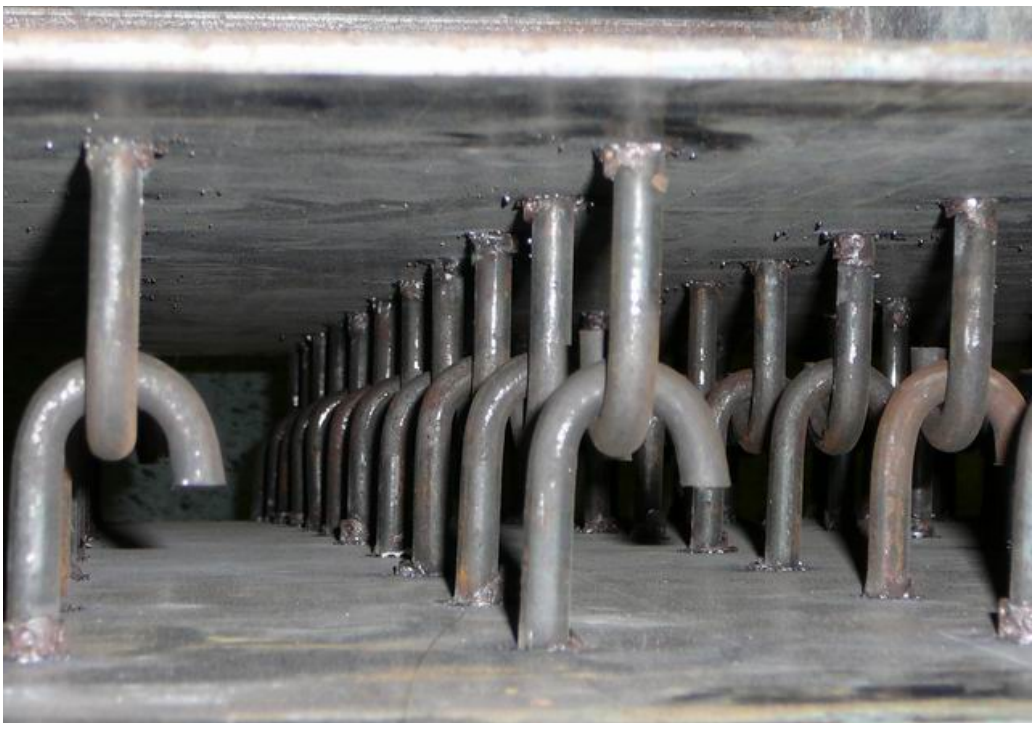

(b)

Fig. 6.1 Sandwich slab with J-hook connectors: (a) schematic and (b) close-up view

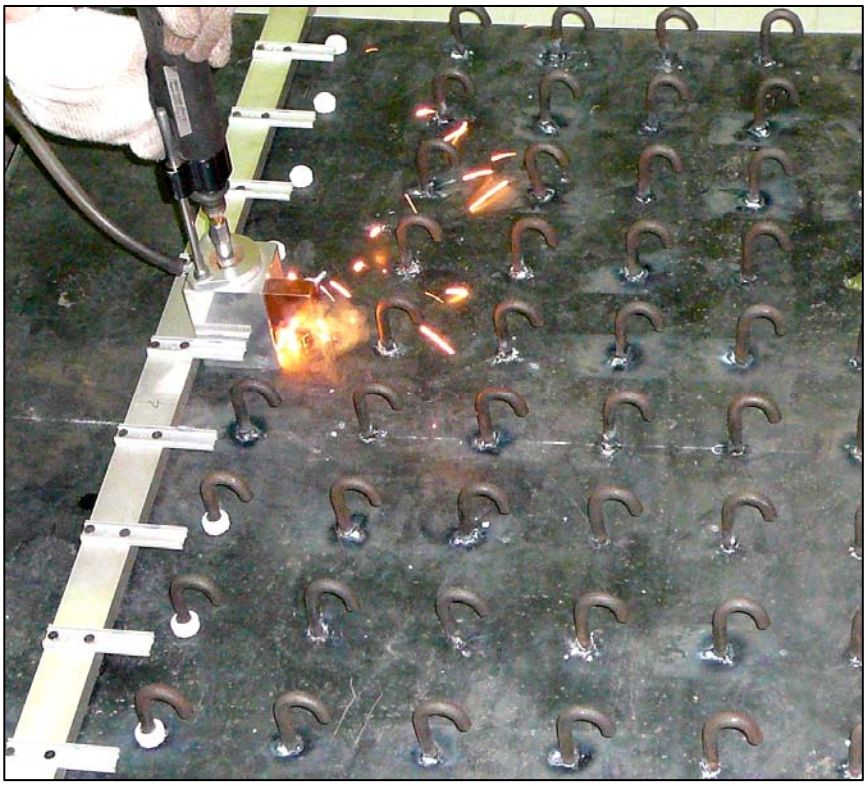

(a)

(b)

Fig. 6.2 (a) Welding of J-hook connectors by modified welding gun and (b) concrete casting.

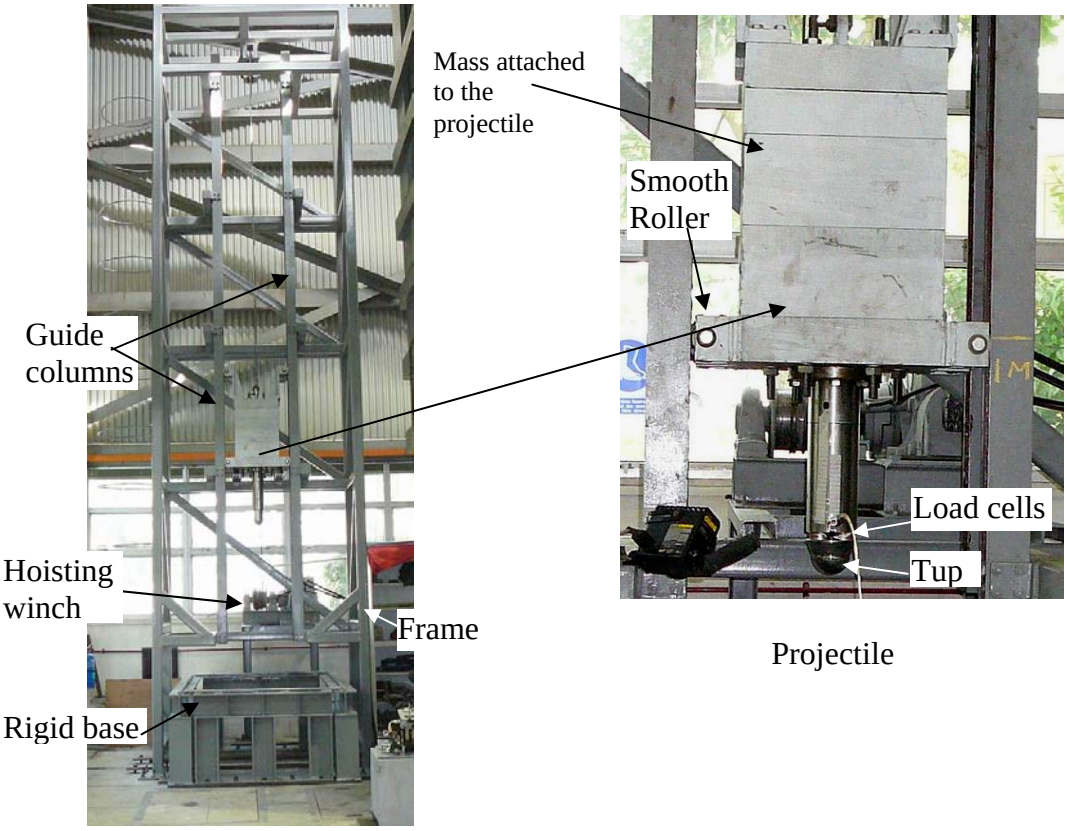

Fig. 6.3 Drop weight impact test machine

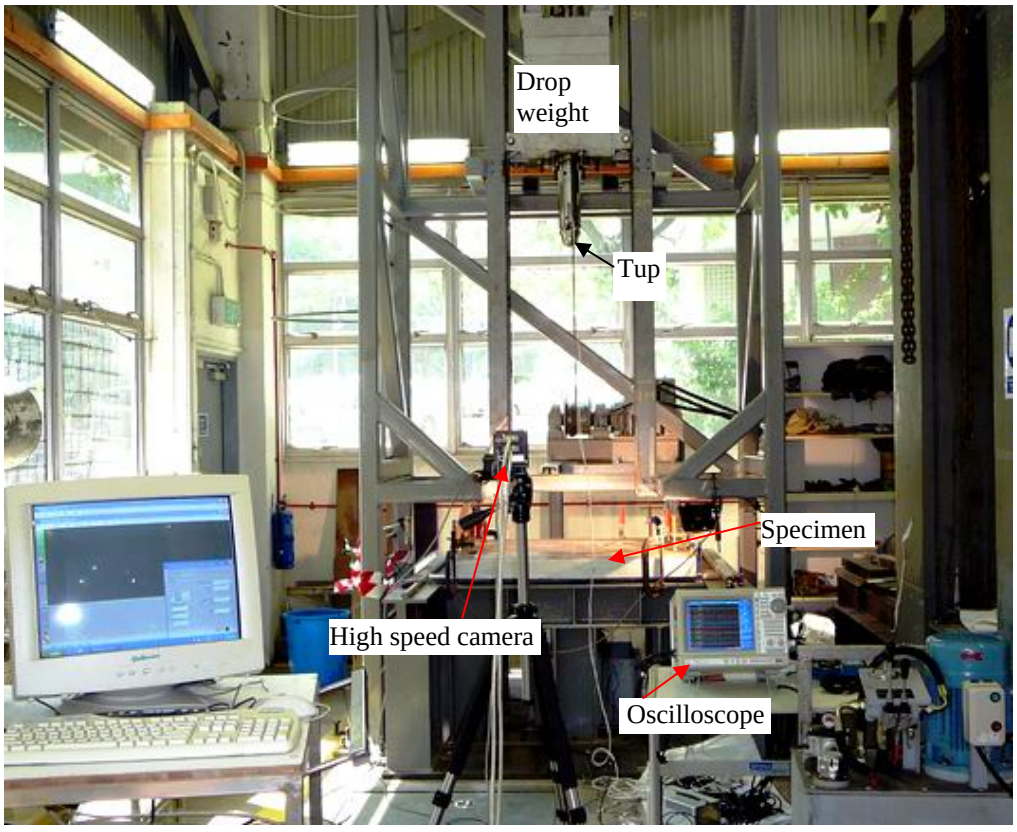

Fig. 6.4 Test set-up for impact on SCS sandwich slabs.

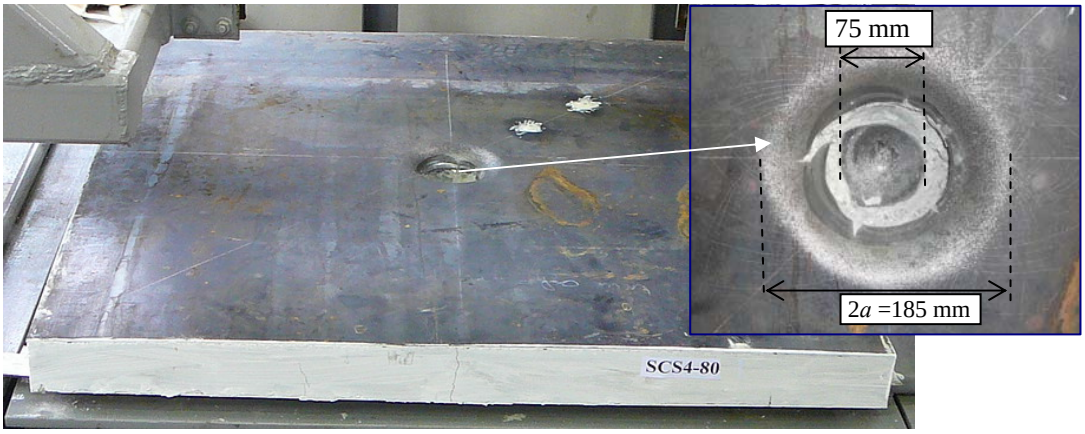

(a) Top plate indentation

(b) Fracture point of bottom plate

Fig. 6.5 Punching failure through top and bottom plates due to impact (SCS4-80)

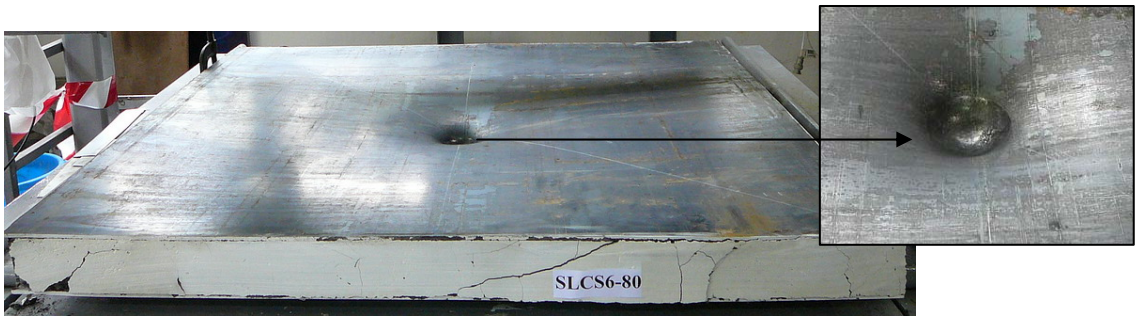

(a)

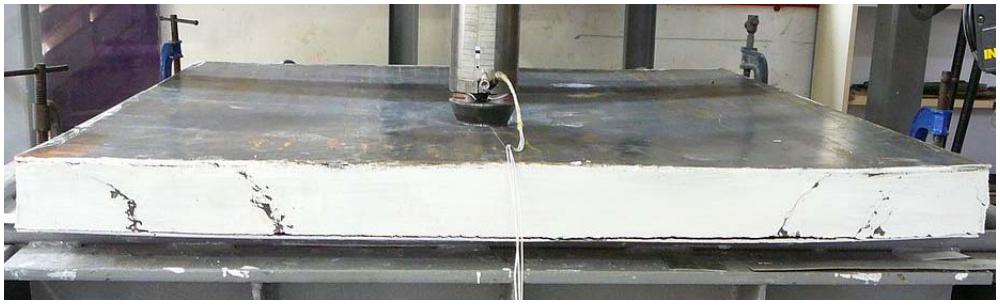

(b)

Fig. 6.6 Impact damage in sandwich slabs (a) SLCS6-80, concrete cracking and spalling at the edges of the slab (b) SLFCS6-80, concrete cracking but no spalling.

Fig. 6.7 Local indentation on the top steel face plates

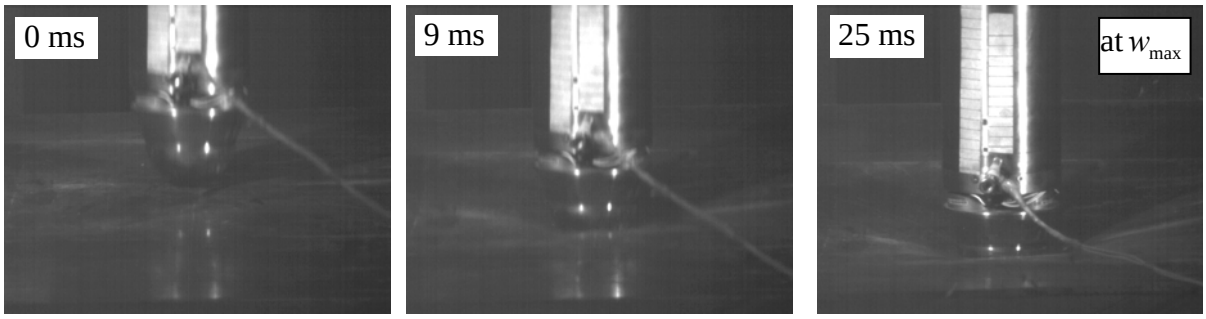

(a) SLCS6-80

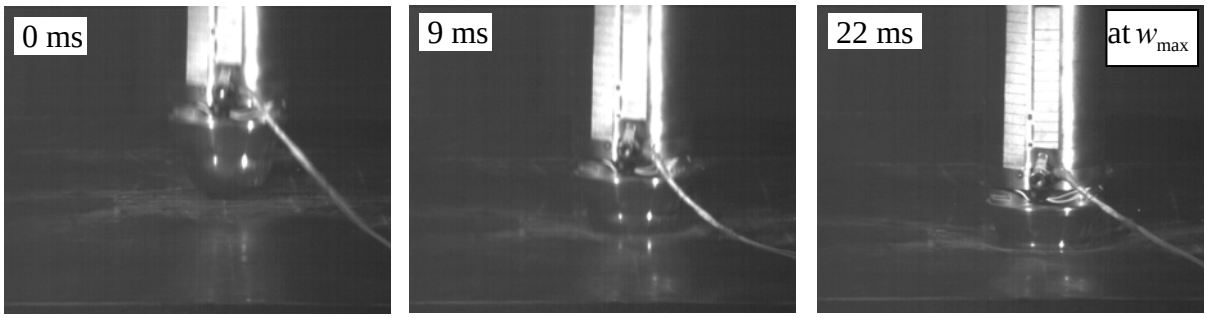

(b) SLFCS6-100

Fig. 6.8 Pictures from high speed camera for different time at the event of impact; w_{max} is the maximum deflection.

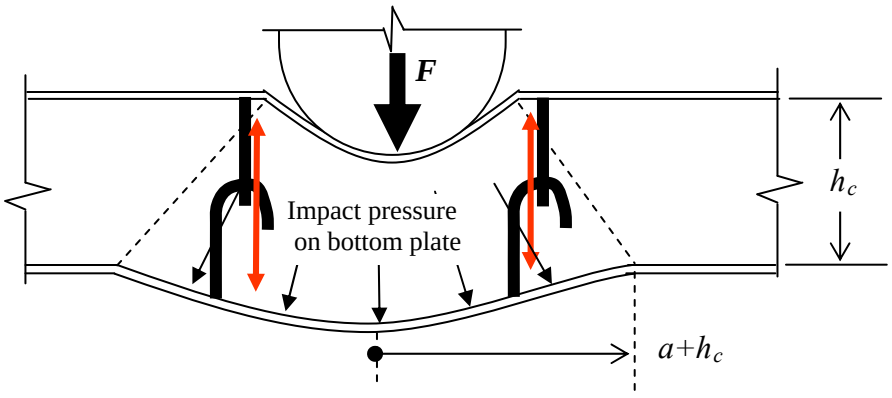

Fig. 6.9 Sketch of deformed shape of the impact point of a SCS slab.

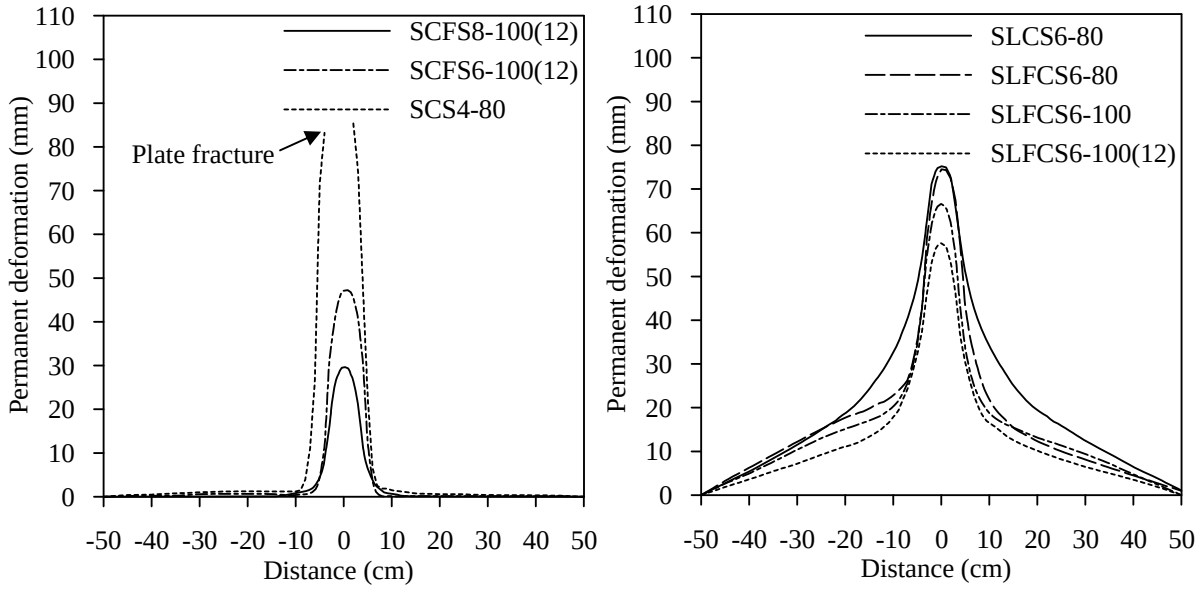

(a) Slabs with normal weight concrete core (b) Slabs with LW concrete core

Fig. 6.10 Top plate deformation profile after impact.

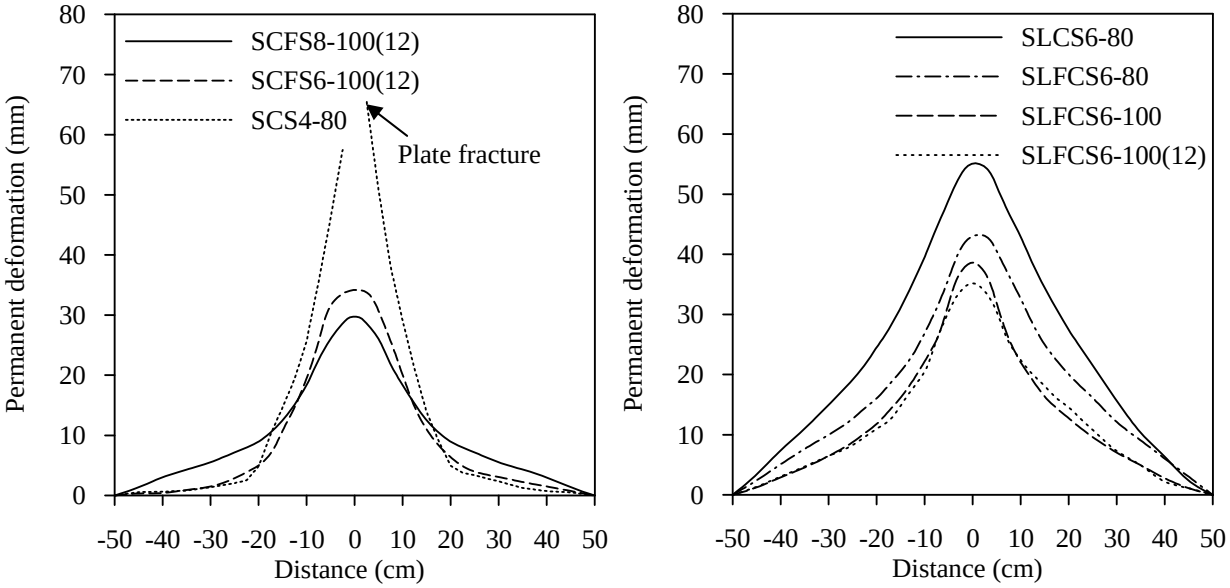

(a) Slabs with normal weight concrete core (b) Slabs with LW concrete core

Fig. 6.11 Bottom surface permanent deformation profile after impact.

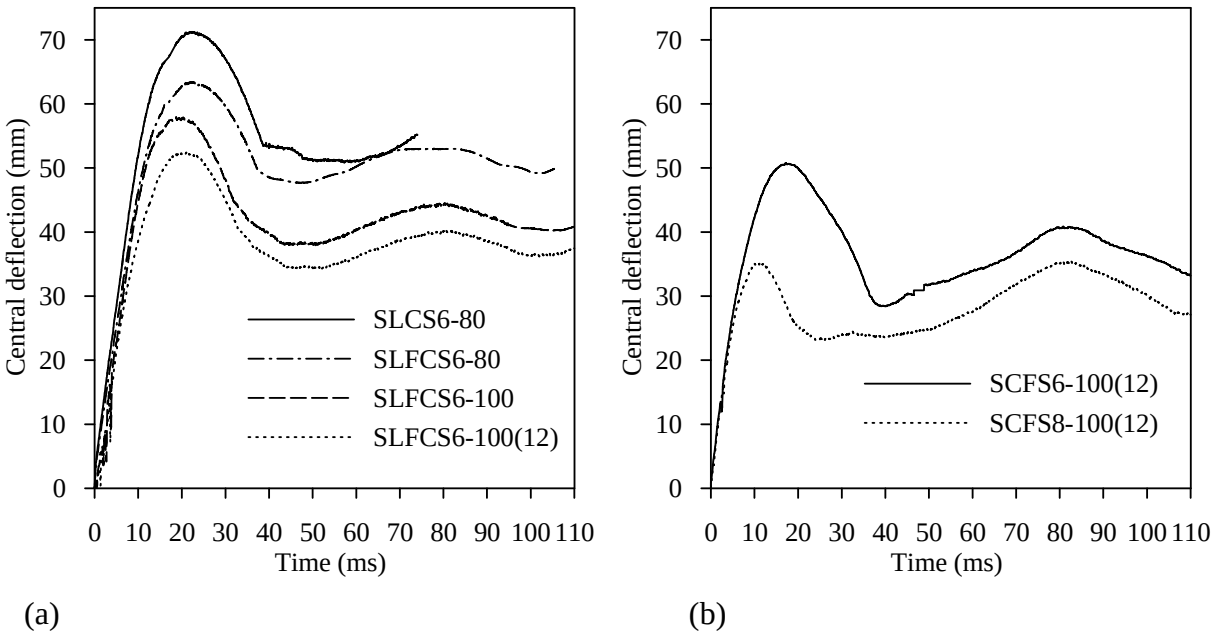

Fig. 6.12 Comparison of central deflection-time histories of the sandwich slabs

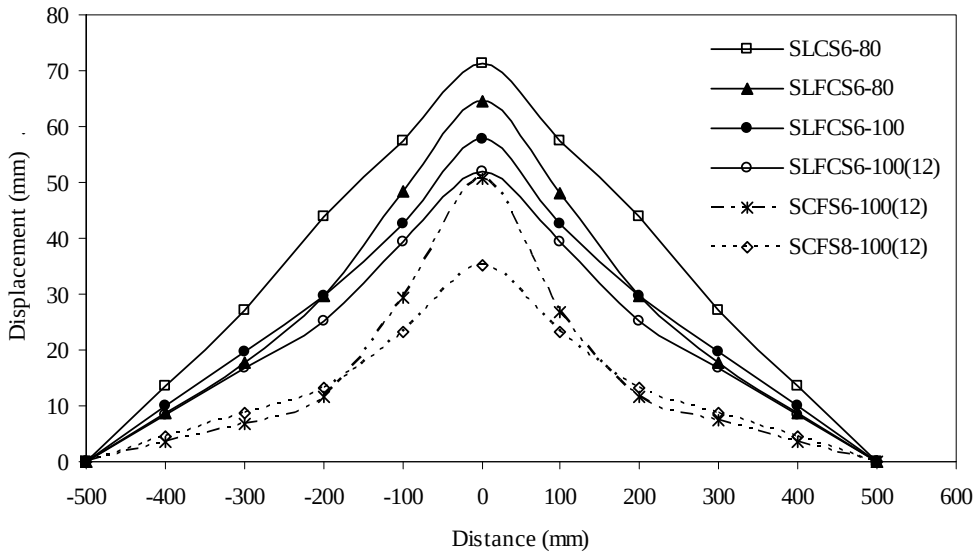

Fig. 6.13 Bottom plate profile at maximum deflection during impact captured by potentiometer.

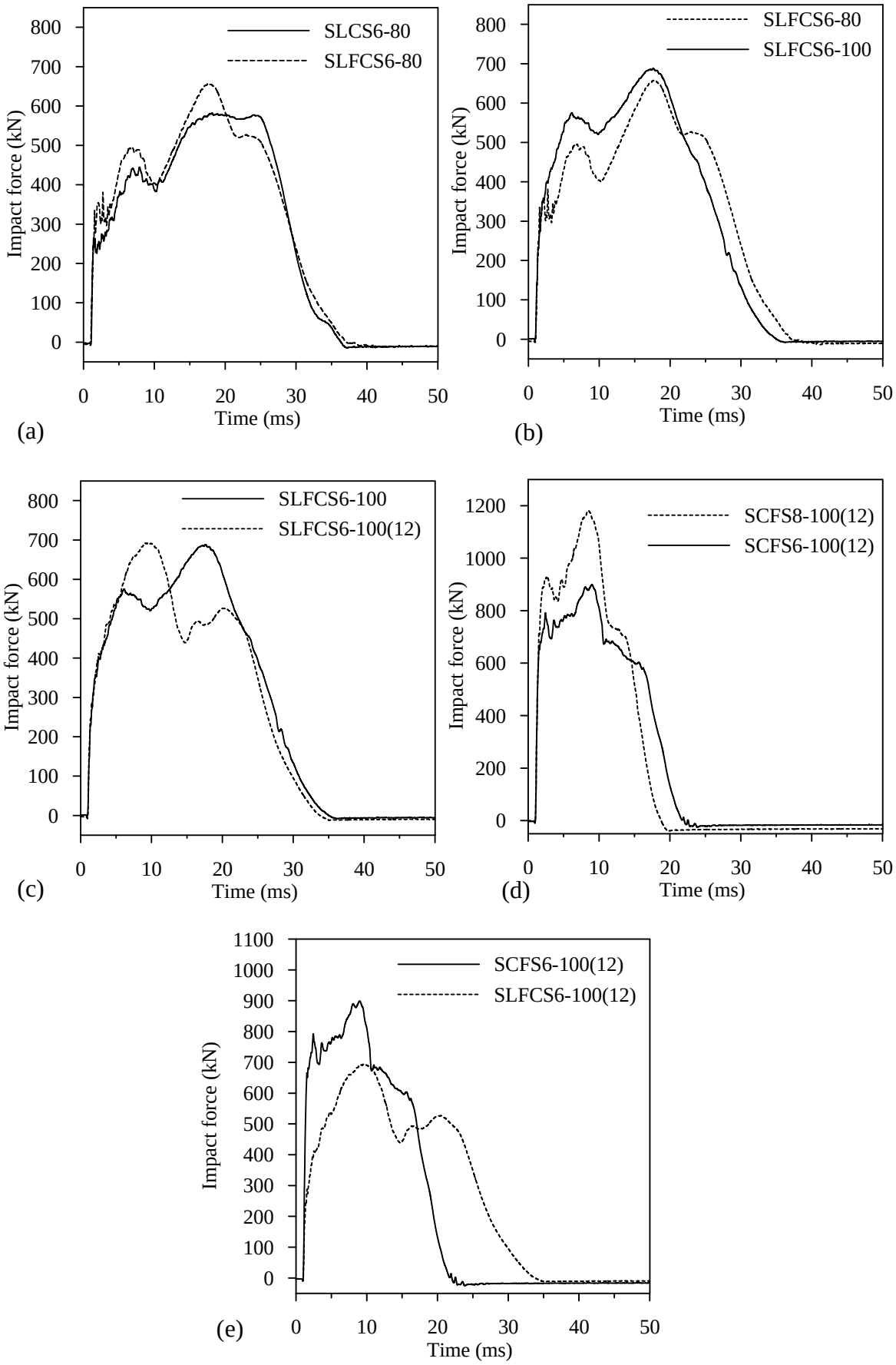

Fig. 6.14 Comparison of impact force-time histories for various sandwich slabs.

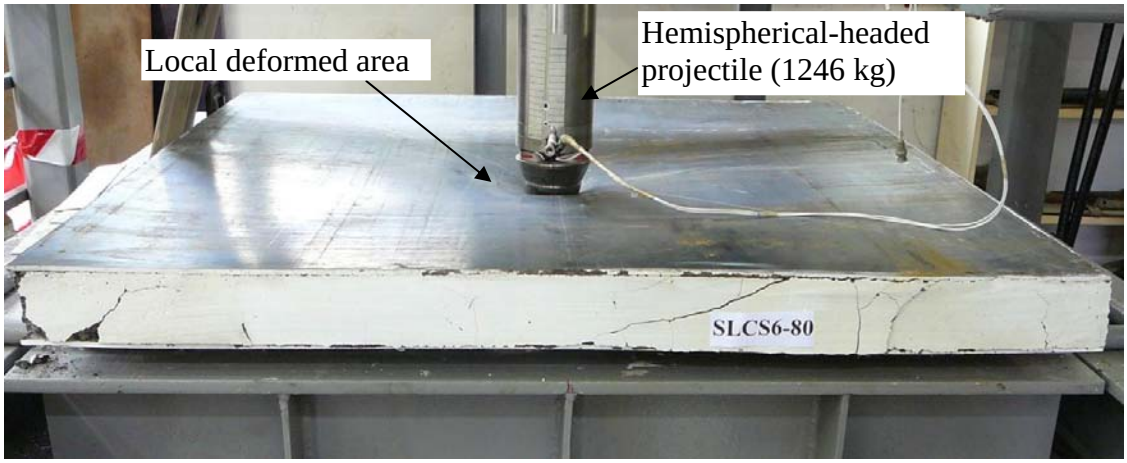

(a)

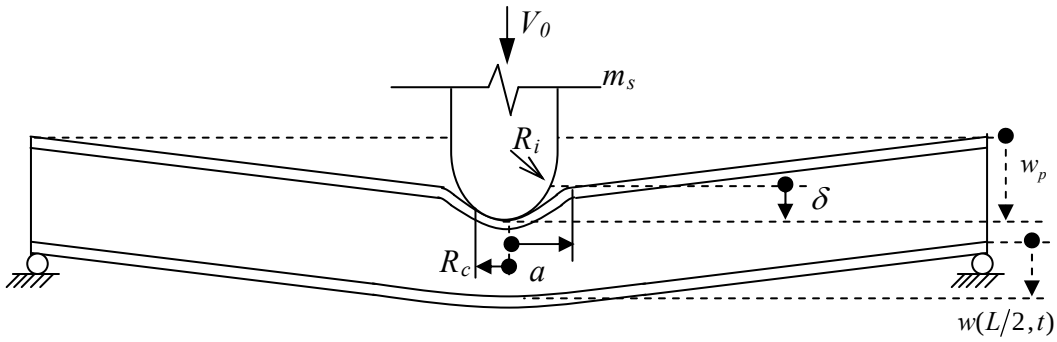

(b)

Fig. 6.15 (a) Deformation of sandwich slab caused by a hemispherical-headed projectile impact and (b) schematic diagram of the slab deformation.

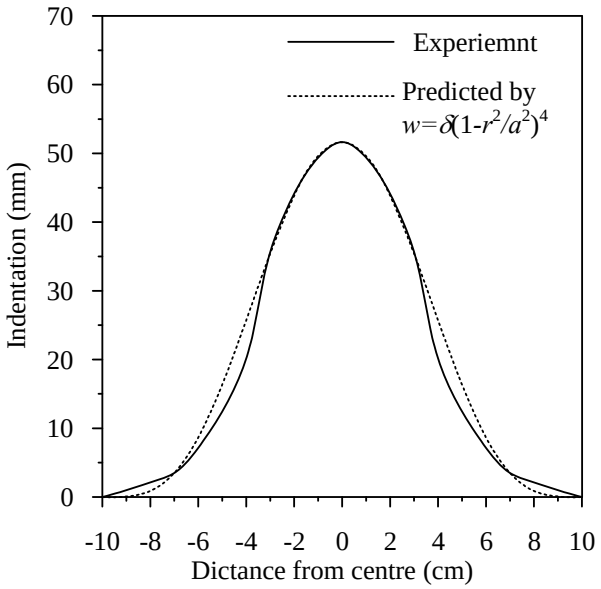

Fig. 6.16 Local indentation profile in SCS sandwich slab due to hemispherical-headed projectile impact

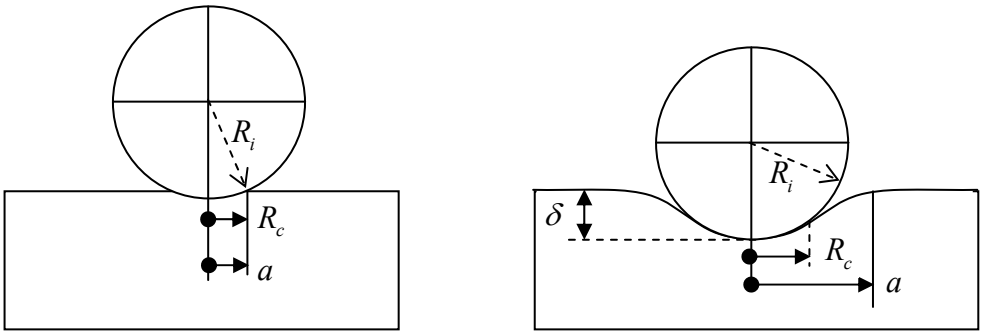

(a) Small indentation (b) Large indentation

Fig. 6.17 Local indentation shape by spherical-headed indentor.

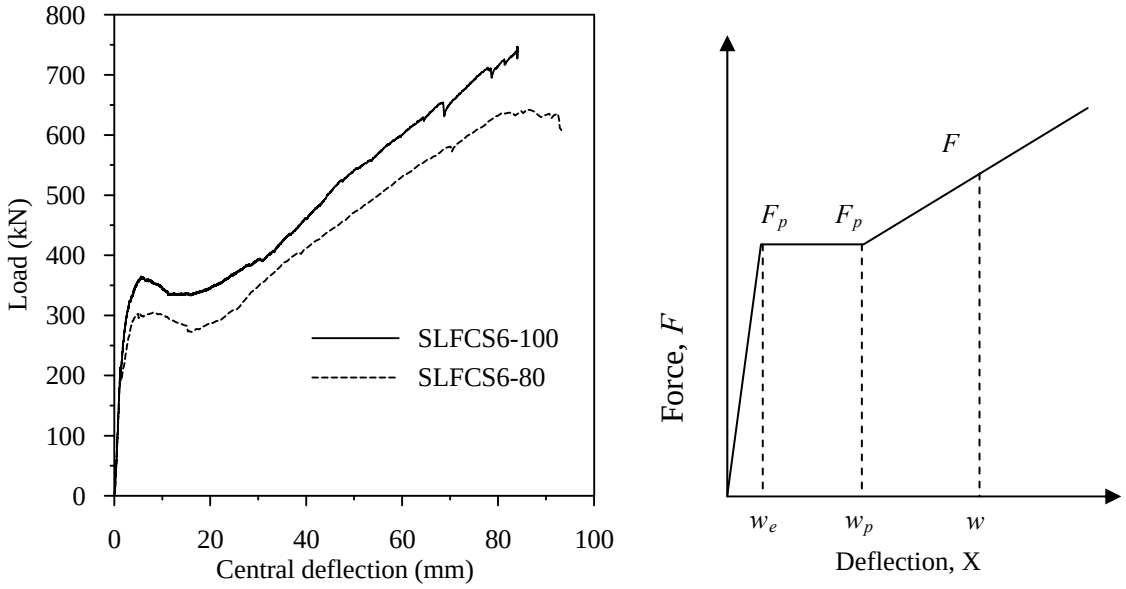

(a) Experimental load-displacement curve (b) Idealized load-displacement curve

Fig. 6.18 Load-displacement relationship of simply supported SCS sandwich slabs subjected to static point load at centre.

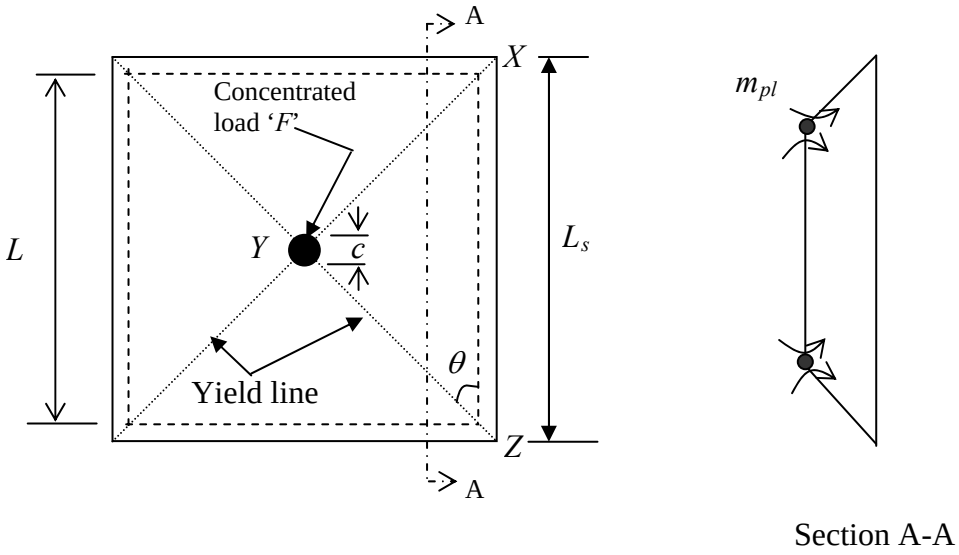

Fig. 6.19 Formation of yield-line mechanism of sandwich slab subjected to concentrated mid-point load

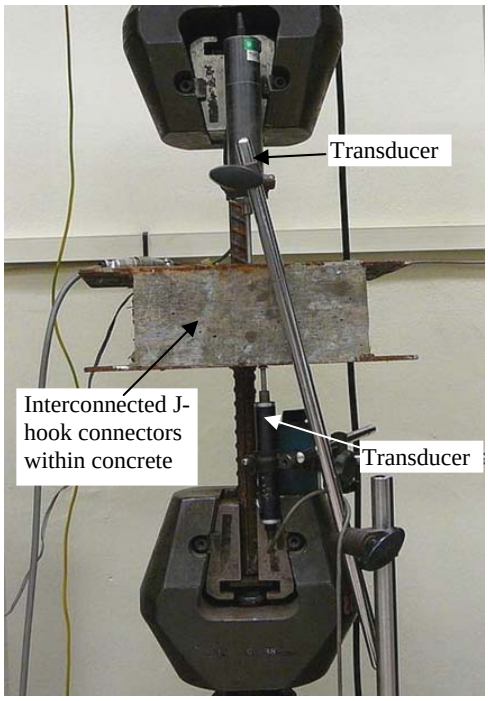

Fig. 6.20 Direct tensile test on J-hook connectors within concrete.

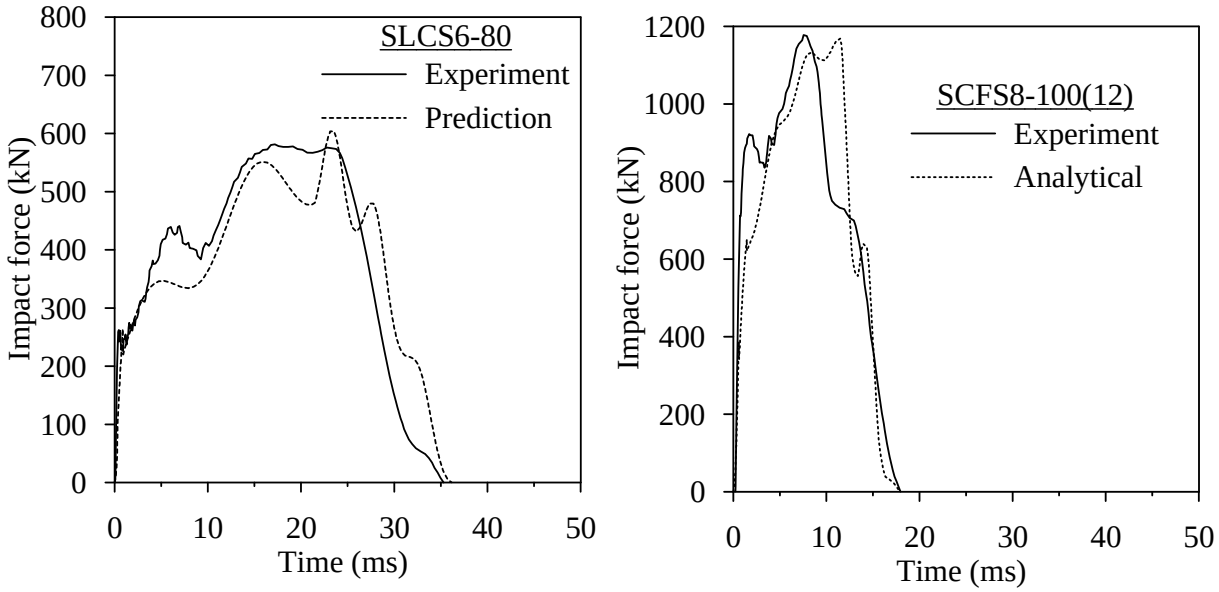

(a) SLCS6-80 (b) SLFCS6-80

Fig. 6.21 Comparison of impact forces between experimental results and predicted results.

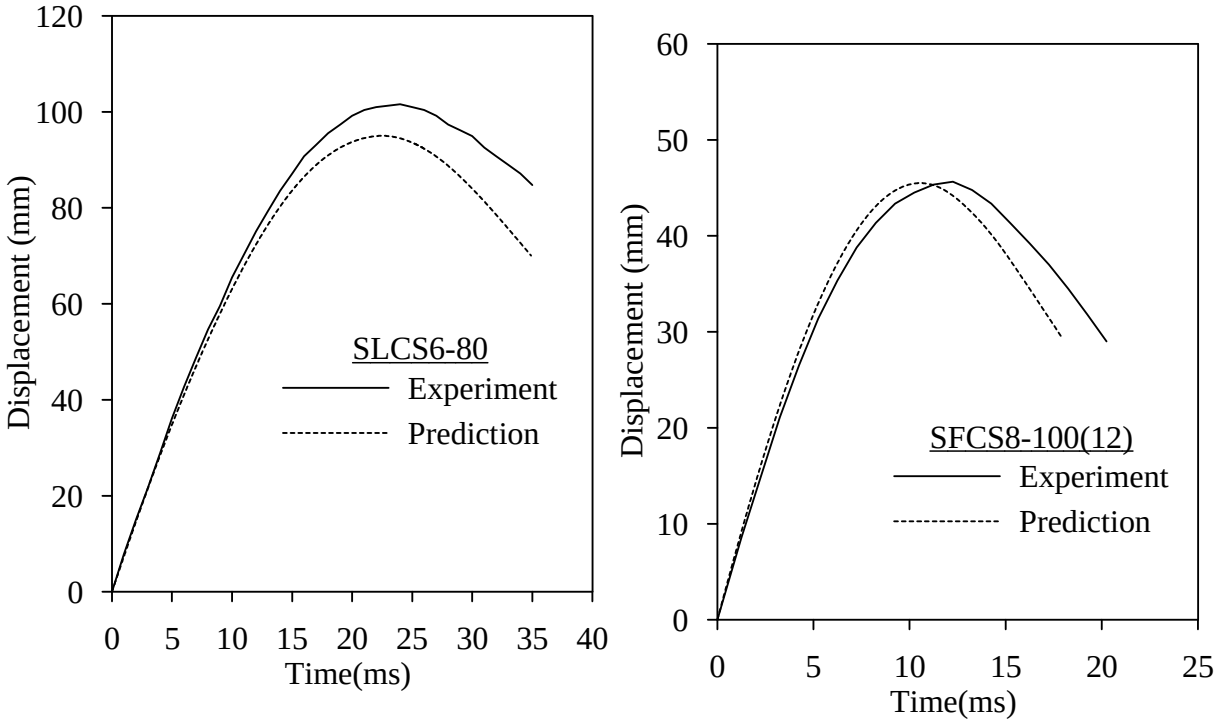

(a) SLCS6-80 (b) SFCS8-100(12)

Fig. 6.22 Comparison of projectile displacements between experimental results and predicted results.

7 Finite element analysis

7.1 Introduction

In Chapters 4, 5 and 6, the effectiveness of SCS sandwich beams and slabs in resisting low velocity impact was investigated through a series of experimental tests which are limited and costly. Moreover, experimental investigations are usually lacking in capturing the inside behaviour of the material at the time of impact loading. Theoretical analysis of structures subjected to impact loading usually involves simplified assumptions and complex analytical procedure. Therefore numerical models such as FEM may be used, but their accuracy needs to be established by comparing the results with those from experimental study. Whirley and Engelmann (1992), Williams (1994), Malvar et al. (1997), Thabet and Haldane (2001) and Esper (2004) used finite elemnt method to investigate the response of structures under impact and blast loading.

The existing literature shows little work done on finite element modelling of SCS sandwich structures. Foundoukos and Chapman (2008) modelled Bi-Steel beams in two-dimensional space ignoring the stress variation in the third direction. Shanmugam et al. (2002) modelled the SCS sandwich slabs using spring analogy. In this spring analogy, headed shear studs were assumed as two spring acting in series. However, in case of interconnected J-hook shear connectors, tensile behaviour is non-linear and the

connecting point of both J-hooks experienced rotation due to opposite movement of the top and bottom plates. Thus the spring analogy is not applicable for J-hook connectors.

In this chapter, three-dimensional (3D) finite element (FE) models of SCS sandwich beams and slabs subjected to low velocity impact were developed to complement the experimental program. The LS-DYNA explicit nonlinear Finite Element (FE) code (Hallquist, 2006) was utilized in this research to simulate the impact response of the aforementioned SCS sandwich composites structures and the FE results are reported and discussed in the following sections. Discrete beam element is used to model the interconnected joint behaviour of J-hook connectors in the SCS sandwich structures. This allows a rapid generation of three-dimensional sandwich structures for the explicit analysis within LS-DYNA. To save time, limited specimens were selected from each group which covers specimens with both normal weight and lightweight concrete. Specimens with fibre reinforced lightweight concrete also modelled.

7.2 Simplified model of J-Hook Connectors

To model the actual geometry of the J-hook connectors (see Fig. 7.1(a)), fine solid mesh of irregular shapes is inevitable as shown in Fig. 7.1(b). Such irregular mesh often leads to numerical instabilities particularly for contact problem and is associated with long computational hour that can considerably reduce the efficiency of FE analysis. Hence, a simplified FE model of J-hook connectors is proposed for SCS sandwich beams and slabs.

Each pair of J-hook connectors shown in Fig. 7.1 may be modelled using two straight solid round bars connected by a discrete beam element with a finite initial length (e.g. ≤ 0.05 mm) as shown in Fig. 7.2. Shear and flexural deformations of the connectors were simulated by the solid bars whereas the discrete beam was used to emulate only the tensile elongation (straighten of hook bend) between top and bottom connectors. The discrete beam has up to 6 degrees-of-freedom. In the model the discrete beam element is free to rotate and the r-axis is adjusted to lie along the line between the two beam nodal points (node1 to node2) as shown in Fig 7.2(b). Thus the beam element behaviour is similar to hinge where only axial force is active. The only disadvantage of this model is that it does not consider the eccentricity of J-hook connectors which are aligned eccentrically as shown in Fig 7.1(b). This may have very little effect on the global behaviour of the slab.

Tensile tests on a pair of 10 mm diameter J-hook connectors embedded in normal weight concrete (SCS), lightweight concrete (SLCS) and fibre reinforced lightweight concrete (SLFCS(1)) as shown in Fig 6.20 (Chapter 6) were conducted to determine the tensile load-displacement relationship of the discrete beam, taking into consideration the effect of surrounding concrete material. The tensile test results are plotted in Fig. 7.3. It is shown in the figure that inclusion of 1 % steel fibres helped to delay the straightening of J-hook connectors under tension.

7.3 Material models

7.3.1 Concrete core material

Material model 72 Release III (MAT 72R3 - Concrete Damage Model) in LSDYNA was utilized for the normal weight and lightweight concrete core in SCS sandwich beams and slabs, and the material properties are given in Table 7.1. To date, very limited triaxial and hydrostatic tests have been conducted on lightweight concrete material. Since triaxial test data is not available for the lightweight concrete considered in the present study, the material behaviour under high confinement was defined based on the data for normal concrete (Chen, 1994) where ($p/f_c^{'}$, $\Delta\sigma_m/f_c^{'}$) = (4.92, 6.03). $f_c^{'}$ is the uniaxial compressive strength, p is the pressure and $\Delta\sigma_m$ is the deviatoric stress limit for the maximum failure surface (Malvar et al., 1997). This approximation may overestimate the strength of the lightweight concrete material at high confinement level (Hanson, 1963). In MAT 72R3, the volumetric response is defined by Equation of State 8 (EOS8 - Tabulated Compaction), which relates pressure (p) to volumetric strain in the loading (compression) phase as

$$p = C(\varepsilon_v) \tag{7.1}$$

Unloading follows the slope that corresponds to the bulk modulus. The volumetric strain, ε_v, is given by the natural logarithm of the relative volume, ln(V/V_0) and C are coefficients which are tabulated against ln(V/V_0). Here, V_0 is the initial volume. The values of C and ln(V/V_0) were generated by using the automated generation option in MAT 72R3 based on uniaxial strain tests on concrete.

The model uses three independent fixed surfaces to define the plastic behaviour of concrete. The surfaces, which define three important regions of concrete behaviour, can be seen easily if one plots the stress-strain response from an unconfined uniaxial compression test (see Fig. 7.4). The material response is considered linear up until point 1, or first yield. After yielding, a hardening plasticity response occurs until point 2, or maximum strength, is reached. After reaching a maximum strength, softening occurs until a residual strength, which is based on the amount of confinement, is obtained. The three surfaces are defined by the following equations:

$$\Delta\sigma_y = a_{0y} + \frac{p}{a_{1y} + a_{2y}p} \qquad \text{(yield failure surface)} \qquad (7.2)$$

$$\Delta\sigma_m = a_0 + \frac{p}{a_1 + a_2 p} \qquad \text{(maximum failure surface)} \qquad (7.3)$$

$$\Delta\sigma_r = \frac{p}{a_{1f} + a_{2f}p} \qquad \text{(residual failure surface)} \qquad (7.4)$$

where a_{0y}, a_{1y}, a_{2y}, a_0, a_1,a_2, a_{1f}, and a_{2f} are all user-defined parameters which change the shape of the failure surface.

The current failure surface is calculated from the three fixed surfaces using a simple linear interpolation technique:

1. if the current state lies between the yield surface and the maximum surface, the failure surface is calculated using

$$\Delta\sigma_f = \eta(\Delta\sigma_m - \Delta\sigma_y) + \Delta\sigma_y \qquad (7.5)$$

2. if, on the other hand, the current state is located between the maximum surface and the residual surface, the failure surface is defined by

$$\Delta\sigma_f = \eta(\Delta\sigma_m - \Delta\sigma_r) + \Delta\sigma_r \qquad (7.6)$$

where η varies between 0 and 1, and depends on the accumulated effective plastic strain parameter λ. The η value is 0 when $\lambda = 0$, 1 at some value $\lambda = \lambda_m$, and again 0 at some larger value of λ. Therefore, if $\lambda \le \lambda_m$, the current failure surface is calculated using Eq.(7.5), and if $\lambda \ge \lambda_m$, the current failure surface is calculated using Eq.(7.6). In essence, the (η, λ) values define where the current failure surface is in relation to the three fixed surfaces for different values of plastic strain. The current value of the plastic strain parameter λ (also called damage parameter) is defined using the following relationships:

$$\lambda = \int_0^{\bar{\varepsilon}^p} \frac{d\bar{\varepsilon}^p}{\dot{r}_f \left(1 + p/\dot{r}_f f_t\right)^{b_1}} \qquad \text{for } p \ge 0 \quad \text{(compression)} \qquad (7.7)$$

$$\lambda = \int_0^{\bar{\varepsilon}^p} \frac{d\bar{\varepsilon}^p}{\dot{r}_f \left(1 + P/\dot{r}_f f_t\right)^{b_2}} + b_3 f_d k_d \left(\varepsilon_v - \varepsilon_v^{yield}\right) \quad \text{for } p \le 0 \quad \text{(tension)} \qquad (7.8)$$

where $\dot{r}_f$ is the strain enhancement factor; f_t is the strength in uniaxial tension; $d\bar{\varepsilon}^p$ is the effective plastic strain increment expressed as $d\bar{\varepsilon}^p = \sqrt{(2/3) d\varepsilon_{ij}^p d\varepsilon_{ij}^p}$ in which ε_{ij}^p is the plastic strain tensor (strain after yielding); k_d is the internal scalar multiplier; ε_v and ε_v^{yield} are the volumetric strain and volumetric strain at yield respectively; and f_d is a factor expressed as

$$f_d = \begin{cases} 1 - \dfrac{\left|\sqrt{3J_2}/p\right|}{0.1} & \text{for } 0 \le \left|\sqrt{3J_2}/p\right| < 0.1 \\ 0 & \text{for } \left|\sqrt{3J_2}/p\right| > 0.1 \end{cases} \qquad (7.9)$$

where $J_2 = \left(s_1^2 + s_2^2 + s_3^2\right)/2$ in which s_i is the deviatoric stress tensor.

In MAT 72R3, the stress-strain relationship is governed by the damage parameter (λ)-strain (ε) function together with the damage scaling exponents, b_1 for the unconfined

uniaxial stress-strain curve in compression and b_2 for the hardening and softening of the unconfined uniaxial tensile stress-strain curve (Malvar et al., 1997). The values of b_1 and b_2 are determined through curve-fitting of the experimental uni-axial unconfined compression and tension stress-strain curves respectively. The process for the curve fitting described elsewhere (Malvar et al.,1997; Noble et al., 2005; Lee, 2006; Vincent, 2008). Similar to the parameters b_1 and b_2, parameter b_3 can be determined through curve fitting using the results obtained from hydrostatic tri-axial tensile test. In absence of these test data, parameter b_3 is assumed to be 1.15 (Malvar et al., 1997). The input stress-strain relationship for lightweight concrete is shown in Fig. 7.6.

7.3.2 Projectile and steel bars support model

Since the stress time history of the projectile is required for the calculation of the impact force, material model 3 (MAT 3 - Plastic Kinematic) in LSDYNA was specified for the projectile. MAT 3 was also applied for the steel bar supports. Kinematic, isotropic, or a combination of kinematic and isotropic hardening may be specified by varying hardening parameter β' between 0 and 1. For β' equal to 0 and 1, respectively, kinematic and isotropic hardening are obtained as shown in Fig. 7.5.

7.3.3 Steel face plates and shank of J-hook connector model

The Piecewise Linear Plasticity material model (MAT24) in LS-DYNA was utilized in this study to model the stress-strain relationships of the steel plates and shank of J-hook connectors as plotted in Figs. 7.6 (a) and (b).

7.4 Strain rate effect

Material under short-duration dynamic loading deforms rapidly and the material response can be significantly influenced by the strain-rate effect as compared to slower quasi-static loading case. Due to strain-rate effect, a material undergoes continuously varying strength as well as energy-absorbing and dissipating properties. Thus, it is important to incorporate the strain-rate effect into the FE model so that realistic time-dependent behaviours of the material can be simulated under impact loading.

The enhancement of material strength due to strain-rate effect was taken into consideration in the FE material models in the form of Dynamic Increase Factor (DIF), which is defined as the ratio of dynamic test value to quasi-static test value. The compression-DIF-strain-rate relationship of the ultra-lightweight concrete material was based on the Comite Euro-International du Beton (CEB) code (CEB, 1993) and is given as

$$\mathrm{DIF}_{\text{concrete (compression)}} \begin{cases} (\dot{\varepsilon}_d / \dot{\varepsilon}_s)^{1.026\alpha_s} \text{ for } \dot{\varepsilon}_d \le 30\mathrm{s}^{-1} & \text{with} \quad \alpha_s = 1/(5+9f'_c/10\,\mathrm{MPa}) \\ \gamma_s (\dot{\varepsilon}_d / \dot{\varepsilon}_s)^{1/3} \text{ for } \dot{\varepsilon}_d > 30\mathrm{s}^{-1} & \text{with} \quad \log\gamma_s = 6.156\alpha_s - 2 \end{cases} \tag{7.10}$$

where $\dot{\varepsilon}_d$ is the dynamic strain-rate and $\dot{\varepsilon}_s$ is the static strain-rate. The modified CEB model proposed by Malvar and Ross (1998) was applied as the tension-DIF-strain-rate relationship of the ultra-lightweight concrete material. The relationship is given as

$$\mathrm{DIF}_{\text{concrete (tension)}} \begin{cases} (\dot{\varepsilon}_d / \dot{\varepsilon}_s)^{\delta} \text{ for } \dot{\varepsilon}_d \le 1\,\mathrm{s}^{-1} & \text{with} \quad \delta = 1/(1+8f'_c/10\,\mathrm{MPa}) \\ \beta (\dot{\varepsilon}_d / \dot{\varepsilon}_s)^{1/3} \text{ for } \dot{\varepsilon}_d > 1\,\mathrm{s}^{-1} & \text{with} \quad \log\beta = 6\delta - 2 \end{cases} \tag{7.11}$$

The DIF-strain-rate relationship for the yield strength of steel was specified using the Cowper and Symonds model (Hallquist, 2006) and is defined as

$$\text{DIF}_{\text{steel (yield strength)}} = 1 + \left(\frac{\dot{\varepsilon}_d}{C_s} \right)^{\frac{1}{p}} \tag{7.12}$$

where C_s (unit of 1/s) and p are the Cowper-Symonds strain-rate parameters. The values of C_s and p were determined by equating Eq. (7.12) with the DIF-strain-rate relationship proposed by Malvar (1998), which is given in Eq. (7.13). A non-linear curve-fitting function was used to solve for C_s and p.

$$\text{DIF}_{\text{steel (yield strength)}} = \left(\frac{\dot{\varepsilon}_d}{\dot{\varepsilon}_s} \right)^{\chi} \text{ where } \chi = 0.074\text{-}0.040 \left(\frac{\sigma_y}{414 \text{ MPa}} \right) \tag{7.13}$$

By equating Eq. (7.12) and Eq. (7.13), a non-linear curve-fitting function was adopted to determine the values of C_s and p. For steel material with yield strength, σ_y , of 300 MPa, the C_s and p values were found to be 255.4 and 7.59, respectively, whereas for σ_y = 275 MPa, the C_s and p values were obtained as 151.7 and 7.52, respectively.

7.5 Contact model- Lagrangian formulation

In the Lagrangian formulation, the projectile interacts with the top steel face plate, and the steel face plates interact with the concrete core through “master-slave" contact interfaces, which were defined by using the automatic surface to surface contact option in LS-DYNA. The penalty method is utilized to compute the contact forces between the slave body and master body, which results from impenetrability assumption. At every time step, each slave node is checked for penetration into the master surfaces. When penetration of slave node into master surface is detected, fictitious spring is introduced to apply an interface force between the slave node and its contact point to push the node out from the master surface. When two deformable surfaces are in contact, the master

surface is generally the stiffer body or the surface with coarser mesh if the two surfaces have comparable stiffness. The parameters of the automatic surface to surface contact option are listed in Table 7.2. The static and dynamic frictional coefficients assumed between the steel concrete contact surfaces were 0.57 and 0.45 respectively (Rabbat and Russell, 1985).

7.6 FE simulation of 300mm×300mm SCS sandwich for local impact

Small SCS sandwich panels subjected to impact for local response were tested in the first series of the experimental investigation. Three types of concrete materials were investigated; namely LWC, normal weight concrete and LWC with 1 % PVA fibres. Four different configurations of SCS sandwich slabs were simulated in this FE study as listed in Table 7.3.

7.6.1 FE model

The FE model of the 300 mm x 300 mm SCS sandwich panel and steel projectile is shown in Fig. 7.7. The concrete core, projectile and support plates were meshed using 8-node solid elements and 8-node thick-shell elements were applied for the top and bottom steel plates. The steel side plates were modelled using Belytschko-Tsay shell elements. The element size of the core layer and simplified shear connectors were approximately 9.0 mm^3 and 4.5 mm^3, respectively. Due to symmetry, only half of the SCS slab, projectile and support were considered in the FE analysis to reduce the computation time.

The experimentally-recorded striking velocity of 8.12 m/s was applied as initial velocity of the projectile, which was positioned right on top of the sandwich panel in the FE model. The contact interfaces among the projectile, steel face plates, support and sandwich panel were defined by using the surface to surface contact option in LS-DYNA.

7.6.2 Boundary conditions

In the test setup, the 300 mm x 300 mm SCS panel was held in position by a top steel plate support with 200 mm (diameter) opening and a bottom steel plate support with 100 mm (diameter) opening as shown in Fig. 7.8(a). This boundary condition was modelled by restricting the translation of the highlighted nodes of the top and bottom steel supports shown in Fig. 7.8(b).

7.7 FE model of SCS sandwich beams subjected to impact

In the second series of impact test, SCS sandwich beams were subjected to impact, two types of shear connectors were investigated; namely J-hook shear connector and threaded stud shear connectors. Five SCS sandwich beams of different configurations were simulated in this FE study as listed in Table 7.4. Lightweight concrete was used as a core material for these beams.

7.7.1 FE model

Due to symmetry, half of the SCS sandwich beam with round bar shear connectors, steel

projectile and steel bars support were modeled as shown in Fig. 7.9. The projectile, shear connectors, concrete core of the beam and steel bar supports were meshed with 8-node solid elements and 8-node thick-shell elements were used for the top and bottom steel face plates. Automatic surface to surface contact option was used to model the contact interfaces. The coincident nodes between the elements of top steel face plate and top J-hook shear connectors were merged in the FE model to simulate a perfect weld condition and likewise for the coincident nodes of the bottom steel face plate and bottom J-hook shear connectors. The material models discussed in sections 7.3 are used for these SCS sandwich beams.

The velocity of projectile was recorded in the impact test (Chapter 5) by using a laser-diode system positioned at 80 mm (average distance) away from the impact face of the sandwich beam. The projectile has a hemispherical head of 90 mm diameter. In the FE model, the tip of the projectile was placed right above the top steel plate (see Fig. 7.9). Thus, the initial striking velocity of projectile is the sum of the velocity recorded by the laser system and velocity due to gravity acceleration of projectile for the 80 mm distance (from the laser light to the slab). The striking velocity is

$$V_0 = \sqrt{V_{laser}^2 + 2gS_{laser-slab}} \tag{7.14}$$

where V_0 is the striking velocity; V_{laser} is the recorded velocity by laser system; g is the gravity acceleration and $S_{laser\text{-}slab}$ is the distance from laser light to slab top. Using Eq. (7.14), the striking velocity of the projectile for the beam FE simulation was 8.12 m/sec.

7.7.2 Boundary conditions

In accordance to the test setup mentioned earlier, nodes along the bars support were restricted from translation and rotation in the FE model as shown in Fig. 7.10. One round bar was put on the steel face plate to prevent uplift the beam and support condition was pin connected. The top support bar can rotate to its central axis as shown in Fig. 7.10(a).

7.8 FE model of 1.2 m×1.2 m SCS sandwich slabs subject to impact

The 1.2 m × 1.2 m SCS sandwich slab was laid-flat on four steel bars of 30 mm diameter, which were welded to a rigid rectangular mounting frame bolted to strong floor as described in Chapter 6. The centres of the steel bars support were positioned at 100 mm away from the four edges of the SCS slab, giving a support-to-support distance of 1000 mm. SCS sandwich slab with both normal weight and lightweight concrete core materials were tested in this series of impact test. Five sandwich slabs of different configurations were considered in the present study, namely (i) SCS4-80, (ii) SCS4-100, (iii) SLCS6-80, (iv) SLFCS6-80, and (v) SLFCS6-100.

The first two slabs in the above list were fitted with 10 mm diameter J-hook connectors with normal weight concrete whereas lightweight concrete and 10 mm diameter J-hook connectors were used in the fourth slab. The connectors were spaced at 100 mm in both directions. Detail properties of the slabs are given Table 7.5.

7.8.1 FE model

Due to symmetry, a quarter of the 1200 mm x 1200 mm SCS slab with round bar shear connectors, steel projectile and steel bars support were modeled as shown in Fig. 7.11. The projectile, shear connectors, concrete core of the slab and steel bar supports were meshed with 8-node solid elements and 8-node thick-shell elements were used for the top and bottom steel face plates. Automatic surface to surface contact option was used to model the contact interfaces. The coincident nodes between the elements of top steel face plate and top J-hook shear connectors were merged in the FE model to simulate a perfect weld condition and likewise for the coincident nodes of the bottom steel face plate and bottom J-hook shear connectors. The J-hook connectors are designed for taking shear and tensile force. As the top and bottom J-hook connectors were not welded together, they will separate when being subjected to compression force along the J-hook connectors. A pair of J-hook connectors located right below the projectile was replaced by concrete because they were under compression during impact. Replacement of this pair of connectors was required in the simplified FE model in order to avoid a much stiffer response of the sandwich panel due to top connector hitting the bottom connector in this highly compressive zone during impact. The material modeling discussed in section 7.3 was used for these SCS sandwich slabs.

The velocity of projectile was recorded in the impact test (Chapter 6) by using a laser-diode system positioned at 70 mm (average distance) away from the impact face of the sandwich slab. The projectile has a hemispherical head of 90 mm diameter. In the

FE model, the tup of the projectile was placed right above the top steel plate (see Fig. 7.11). Thus, the initial striking velocity of projectile is the sum of experimentally recorded velocity plus velocity due to gravity acceleration of projectile for the 70 mm distance (using Eq. (7.14)). The calculated initial striking velocities of projectile for the slab FE simulations are given in Table 7.5.

7.8.2 Boundary conditions

In accordance to the test setup mentioned earlier, nodes along the bottom of the steel bars support were restricted from translation and rotation in the FE model as shown in Fig. 7.12.

7.9 Results and discussion

Comparison of the ultimate displacement-time history, local indentation and impact force-time history obtained from the finite element analyses with those obtained experimentally provides a means to verify the accuracy of the proposed finite element models. Analytical results were also compared with FEM results.

7.9.1 Force-indentation for local impact specimens

The FE predicted indentation depth and diameter of indentation size of top steel face plates of the sandwich panels are compared to impact test results in Fig. 7.13. It can be seen from the comparison that the FE models are capable of predicting the local damage of the SCS slabs with reasonable accuracy. Table 7.6 also shows the close agreement of the local indentation between FEM and test results. The extent of yielding in the top and

bottom steel plates of the SCS slabs were determined by plotting the effective plastic strain contour and is shown by the shaded area in Fig. 7.14. The size of the yielded area reached the maximum when the projectile rebounded at time, t = 0.0022 s for the SLCS4-80-4 slab. It can be seen from the figure that the yielded area of slab SCS6-60-6 is smaller than those of slab SLCS 4-80-4 and increasing of plate thickness and concrete strength helped to reduce the local damage as well as improve the impact resistance of the composite system. For the slab SCS6-60-6, the yielded area is significantly smaller than SLCS4-80-4 and the projectile rebounded earlier at time, t = 0.0018 s.

In the experimental program, the impact-force time history of the projectile was recorded by a dynamic load cells located at 85 mm above the tip of the projectile-head as shown in Fig. 7.7. The FE model predicted impact-force time history was thus obtained by calculating the average z-stress (parallel to impact direction) of the projectile at the same location of the load cell and is plotted together with impact test results in Fig. 7.15. It can be seen from the figures that the FE model predicted impact force-time history is in good agreement with the load cell data. Comparison among FE results, corresponding test results and analytical results are given in Table 7.6. The devotion of impact forces predicted by FEM from test results is within 7%.

7.9.2 Impact on SCS sandwich beams

For global response, the midspan deflection time histories of the SCS sandwich beams were recorded in the experimental study which was described in Chapter 5. Midspan

deflection history obtained from the finite element analyses for specimens SLCS100, SLFCS100 and SLCS200 are presented along with the corresponding experimental curves in Fig. 7.16. From these figures, reasonably good agreement between the FE predicted deflection-time history and the corresponding experimental test results was observed. However, the FE post-peak curves show some deviation from the experimental curves. This may be attributed to the concrete damage properties in the FE model which was obtained by the LS-DYNA software due to lacking of triaxial test results of the concrete.

The finite element, experimental and analytical maximum impact forces and deflection are summarized in Table 7.7. In all cases, the maximum impact force predicted by finite element modeling agrees closely with the corresponding experimental values. It can be observed that the finite element method overestimates the maximum deflection compared with the experimental results in some cases and underestimate in other cases. The agreement between the analysis and experiment is generally close with the mean value of the ratio between the analytical and experimental results being 1.03. The maximum deviation is 13% as in the case of the specimen SCLC200. In view of the approximations involved in the analysis the prediction by the finite element modeling can be considered accurate enough for design purposes.

Contours of the effective strain obtained from the LS-DYNA analysis for two typical specimens SLCS100 and SLCS100S are also shown in Fig. 7.17 in which the stain

contour is shown for concrete core. Fig. 7.17(a) shows the cracking pattern for beam SLCS100 observed during the impact tests and compared to the FE model. The FE predicted damage trend was similar to the experiment, but the extent of damage was not same as experiment, which can be visualized from the Fig. 7.17. The cracking pattern in the FE model is symmetric about the centre, but in experiment, one side experienced higher damage due to imperfection in the specimens. The cracking contours in the FE model were obtained by plotting the maximum tensile principal strain contours of concrete elements, and setting as a lower limit the cracking strain for concrete in tension. Therefore, any highlighted elements represent elements that have cracked. The cracking pattern predicted by the FE model is similar to the test cracking pattern. The uncertainties associated with concrete tensile behaviour may be the reason for occasional differences in crack positions.

7.9.3 Impact on SCS sandwich slabs

7.9.3.1 Permanent deformation of bottom steel face plate

The FE simulated permanent deformation of top and bottom steel plates of the SCS4-80, SCS4-100, and SLCS 6-80 sandwich slabs are compared to impact test results in Fig. 7.18 and 7.19, respectively. For the slabs SCS4-80 and SCS4-100, the top steel face plates experienced fracture (Fig. 7.20). For this reason only for SLCS6-100 slab the top steel face plate permanent deformation is given. It can be seen from the comparison that the FE predictions of permanent deformation of bottom steel plates agree reasonably well with impact test data for all slabs. The FE simulated permanent deformation of top

steel plates are in reasonably good agreement with impact test results except for the localized damage located directly below the point of impact. The area under the tip of projectile was subjected to high confinement stresses during impact. Consequently, the overestimation of material strength of the ultra-lightweight concrete core at high confinement level is likely to be one of the reasons that caused the underestimation of the localized deformation. Moreover, erosion of failed concrete material due to crushing and excessive cracking under the impact point was not accounted for in the FE simulations. This possibly led to the underestimation as well. Furthermore, it may be important to model the actual geometry of the J-hook connectors in this high stress zone under the impact point in order to correctly simulate the interactions between the connectors and concrete core so that the localized deformation can be captured properly. Despite the simplification of J-hook connectors in the FE model and lack of triaxial test data for the characterization of the lightweight concrete material, the simplified FE model presented in this thesis appeared to be capable of describing the permanent deformation of the sandwich slabs with satisfactory accuracy.

7.9.3.2 Central displacement time-history of sandwich slabs

The FE predicted central displacement time-histories of the SCS4-100, SLCS6-80 and SLFCS6-80 sandwich slabs are compared to impact test results in Fig. 7.21. From the comparison, it was found that the FE model is able to produce reasonably close predictions of the pre-peak central displacement time-histories of the sandwich slabs. In the impact test described in Chapter 6, the central displacement time-history was

recorded by using spring potentiometer attached to the centre of the bottom steel plate. The threaded head of the potentiometer was fastened to a nut glued onto the plate. There was a spring with the moving shank of the potentiometer and the spring kept the head of the potentiometer touching to the slab in addition to nut. In the post-impact observations, it was found that the nut was detached from the slab during impact due to impact shock. There may have some possibility to delay when the touching head of the potentiometer bounced back to the slab by the spring action. This could possibly cause a time delay between the response of potentiometer and the actual response of the slab during unloading, which explains the difference between the FE simulation results and impact test data for the unloading part of the displacement time-history curves (see Fig. 7.21). Results of FE model for other specimens are given in Table 7.8. This table compares the FE results with test results and the results obtained by energy balance method (section 6.5.3). The maximum central deflections from FE models agree well with the test results.

7.9.3.3 Response of J-hook connectors

As expected, all J-hook connectors were under tension during impact except for the connectors located directly below the projectile as seen from the deformed shape of the SLCS6-80 sandwich slab at the time of maximum displacement (see Fig. 7.22). It was observed in the figure that the tensile elongation between top and bottom connectors were small, and hence, the connectors were effective in resisting the separation of steel plates and maintaining the integrity of the sandwich slabs under impact loading.

7.10 Summary

Simplified three-dimensional FE models of SCS sandwich composite beams and slabs with novel J-hook shear connectors are presented in this chapter. The FE model was applied to simulate a 1.2 ton drop-weight impact at 7.5 m/s on SCS sandwich slabs and to simulate a 64 kg drop-weight impact at 8.12 m/s on SCS sandwich beams. Despite using a simplified model for the J-hook connectors and lack of triaxial test data for the characterization of the ultra-lightweight concrete material, it has been demonstrated that the simplified FE model is capable of describing the permanent deformation and central displacement time-history of the sandwich slabs and beams with reasonable accuracy. From the FE simulations, it has been observed that the J-hook connectors are effective in resisting the separation of steel plates and maintaining the integrity of the sandwich slabs and beams under the drop-weight impact. The FE model for local impact on small SCS panel gives reasonable good agreement to the test data. Thus this FE model can be used to verify the analytical force-indentation relations for SCS sandwich structures. These FE model can be used to do parametric studies for different span lengths to observe different failure modes and the influence of core strength and thickness.

Table 7.1 Properties of concrete used in SCS sandwiches

Concrete type	Density (kg/m^3)	f_c (MPa)	f_t (MPa)	E_c (GPa)	ν
Normal weight concrete*	2350	69.0	3.28	31	0.19
Normal weight concrete**	2350	57.2	3.01	31	0.19
Normal weight concrete with 1% volume fraction of steel fibre	2400	59.0	4.67	31	0.19
Lightweight concrete	1430	27.4	0.89	11.5	0.23
Lightweight concrete with 1% volume fraction of steel fibre	1450	28.0	1.73	11.5	0.23

f_c= cylinder compressive strength, f_t = direct tensile strength of concrete, E_c= Young modulus of concrete, ν = poisons ratio of concrete

* Concrete used in sandwich panel for local impact test (300 mm × 300 mm);

** Concrete used in Sandwich slabs (1200 mm × 1200 mm)

Table 7.2 Parameters for automatic surface-to-surface contact

Projectile to top steel face plate contact		Steel face pate to concrete core contact	
Parameters		Parameters	
Slave part	Steel face plate	Slave part	Concrete core
Master part	Steel Projectile	Master part	Steel face plate
Control type	SOFT	Control type	SOFT
Dynamic coefficient of friction	0.30	Dynamic coefficient of friction	0.45
Static coefficient of friction	0.35	Static coefficient of friction	0.57

Table 7.3 Sandwich specimens of 300 mm × 300 mm for FE simulation (local impact)

Panel ref.	t_{steel} (mm)	h_c (mm)	Core material	ρ (kg/m^3)	f_c (MPa)	E_c (GPa)	σ_y (MPa)	E_s (GPa)
SLCS4-80-4	4	80	LWA concrete	1440	28.5	11.5	275.5	195
SLFCS4-80-4(1)	4	80	LWA concrete with 1% fibre	1440	28.9	11.9	275.5	195
SCS6-60-6	6	60	Normal weight concrete	2350	69.0	31	304.2	195
SCS8-60-8	8	60	Normal weight concrete	2350	69.0	31	314.8	200

* SFCS = steel-foam concrete-steel; SFFCS=Steel -fibre foam concrete-steel; SLCS= Steel lightweight aggregate concrete steel; SLFCS= Steel-lightweight aggregate concrete with fibre-steel; LWA = Lightweight aggregate concrete; ρ = density of concrete; E_c= Concrete modulus of elasticity; σ_y= yield strength of steel, E_s = Elastic modulus of steel.

Table 7.4 Beam specimens and specifications for FE analysis

Beam ref.*	t_c (mm)	t_b (mm)	h_c (mm)	b (mm)	d (mm)	S_x (mm)	L (mm)	Fibre by vol.	σ_y (MPa)	f_c (MPa)
SLCS100	4	4	80	200	10	100	1000	-	275.0	28.5
SLFCS100(1)	4	4	80	200	10	100	1000	1%(steel)	275.0	28.1
SLCS200	4	4	80	200	16	200	1000	-	275.5	27.4
SLFCS200(1)	4	4	80	200	16	200	1000	1%(PVA)	275.5	28.7
SLCS100S	4	4	80	200	10	100	1000	-	275.0	28.0

b=width of the beam; d =J-hook bar diameter; S_x = spacing of shear connector; L= span length of the beam; f_y= yield strength of steel plate; f_c=cylinder strength of concrete; SLCS = Steel-lightweight aggregate concrete-steel ; SLFCS = steel-lightweight aggregate concrete with fibre; SCS = Steel-normal concrete-steel

* All beams containing lightweight concrete (either plain or fibre reinforced).

Table 7.5 SCS sandwich slab (1200 mm ×1200 mm) specimens and specifications for FE analysis

Name of the slabs	t_s (mm)	$d_{J\text{-}hook}$ (mm)	h_c (mm)	S (mm)	Concrete type	f_c (N/mm^2)	σ_y (N/mm^2)	V_0 (m/s)
SCS4-80	4	10	80	100	NC	57.2	275.5	7.5
SCS4-100	4	10	100	100	NC	57.2	275.5	6.8
SLCS6-80	6	10	80	100	LWC	27.0	315.0	7.5
SLFCS6-80	6	10	80	100	LWC-F (1%)	28.5	315.0	7.5
SLFCS6-100	6	10	100	100	LWC-F (1%)	28.5	315.0	7.5

NC = Normal weight concrete; LWC = Lightweight concrete; LWC-F(1%) = Lightweight concrete with 1% volume fraction of fibre; t_s=steel face plate thickness, h_c= core thickness; S = spacing of J-hook connector; f_c = concrete cylinder strength; f_y = yield strength of steel plate; V_0 = initial impact velocity (corrected).

Table 7.6 FE results for local impact and comparison with test and analytical results.

Panel ref.	Max. impact force (kN)			Max. residual indentation depth (mm)		
	FEM	Exp.	Analy.	FEM	Exp.	Analy.
SLCS4-80-4	265	263	242	10.1	11.2	12.0
SLFCS4-80-4(1)	268	264	253	8.6	10.5	11.5
SCS6-60-6	398	364	352	4.2	4.3	6.9
SCS8-60-8	468	438	452	3.0	3.0	5.0

Table 7.7 FE results for beam impact and comparison with test and analytical results

Beam ref.	Max. impact force (kN)			Max. deflection (mm)		
	FEM	Exp.	Analy.	FEM	Exp.	Analy.
SLCS100	164	162	172.9	40.6	38.7	40.2
SLFCS100(1)	171	163	170.8	28.9	27.1	27.2
SLCS200	150	161	172.0	77.2	73.3	73.6
SLFCS200(1)	161	158	173.9	46.0	51.7	52.5
SLCS100S	170	163	-----	78.6	78.3	-----

Table 7.8 FE results for slab impact and comparison with test and analytical results.

Slab ref.	Max. impact force (kN)			Max. deflection (mm)		
	FEM	Exp.	Analy.	FEM	Exp.	Analy.
SCS4-80	532	545	----	68.0	--	--
SCS4-100	591	563	518	50.0	51.2	40.1
SLCS6-80	623	568	515	70.9	71.3	70.0
SLFCS6-80	702	657	512	67.2	64.4	57.0
SLFCS6-100	712	681	513	56.0	57.9	53.0

(a) (b)

Fig. 7.1 (a) J-hook connectors in the sandwich slab and (b) FE model of a pair of J-hook connectors

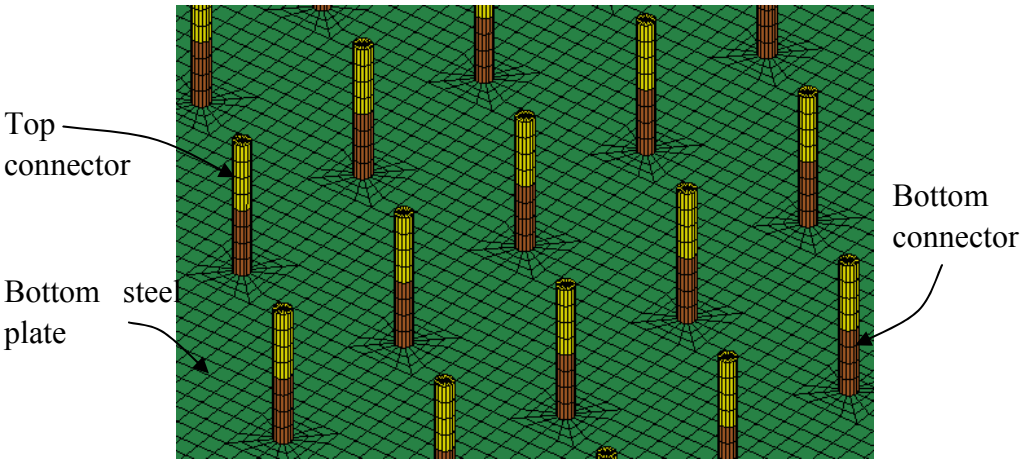

(a)

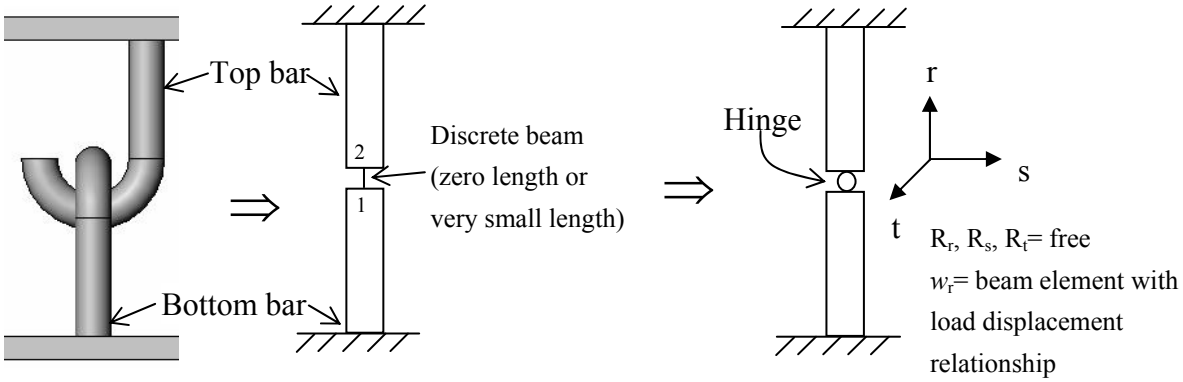

(b)

Fig. 7.2 (a) Simplified straight round bar connectors and (b) details of discrete beam element.

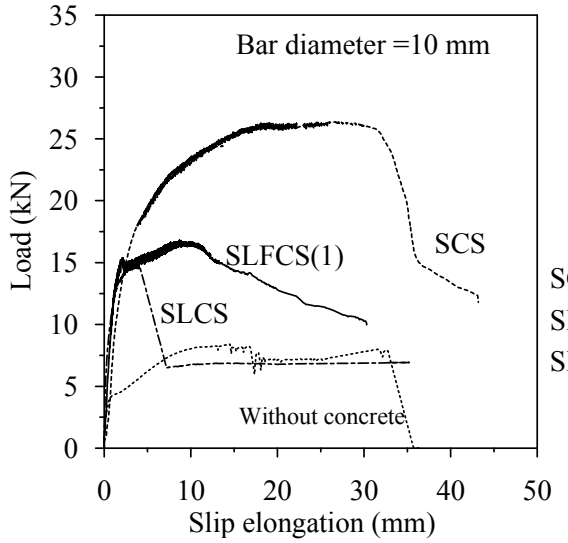

SCS= J-hooks within normal weight concrete
SLCS = J-hooks within lightweight concrete
SLFCS(1)= J-hooks within fibre reinforced concrete (1% steel fibre)

Fig. 7.3 Tensile load-displacement relationships of interconnected J-hook connectors

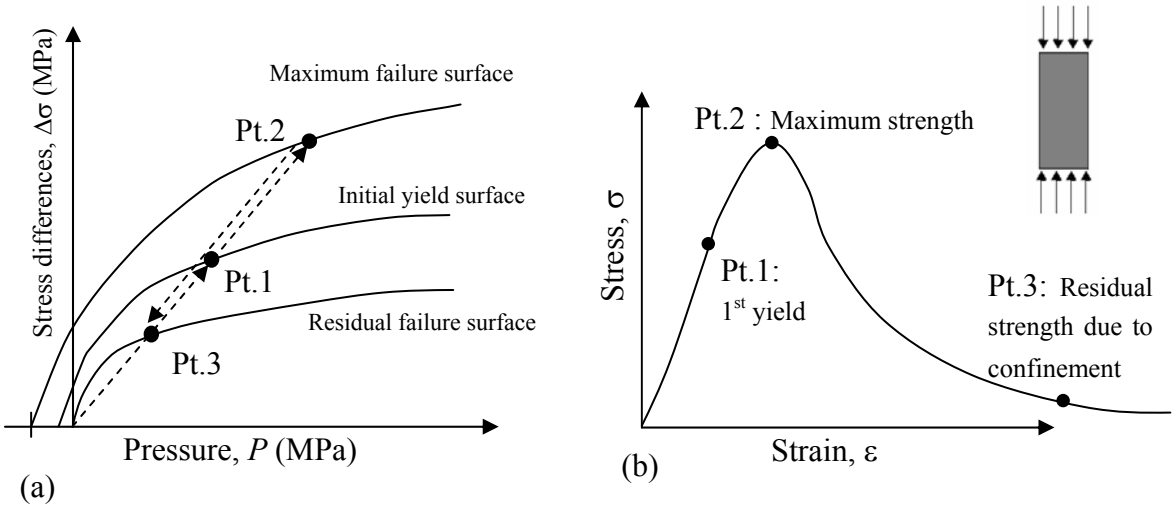

Fig. 7.4 (a) Illustration of concrete failure surfaces and (b) material stress-strain curve.

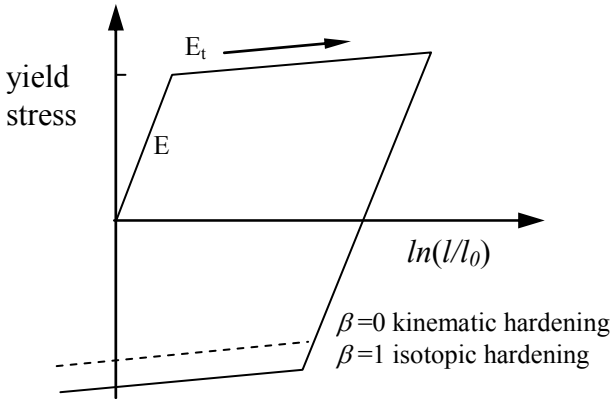

where l_0 and l are undeformed and deformed lengths of uniaxial tension specimen. E_t is the slope of the bilinear stress strain curve

Fig. 7.5 Elastic-plastic behaviour with kinematic and isotropic hardening (after Hallquist, 2007).

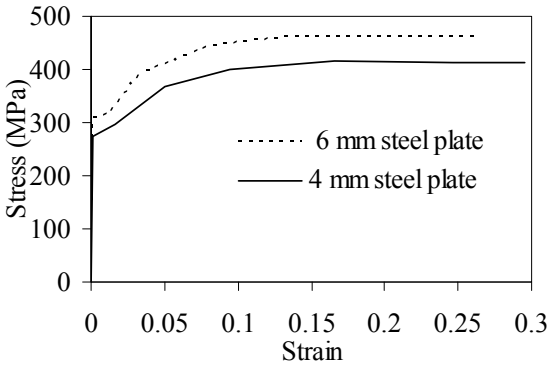

(a) Steel face plate

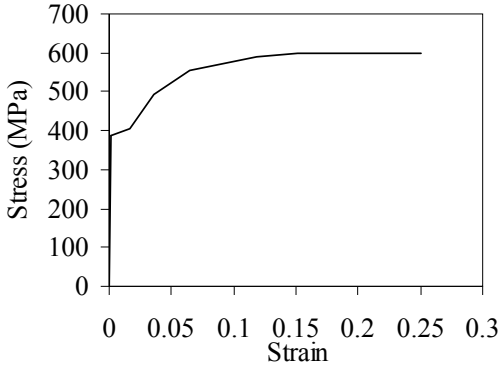

(b) J-hook connectors (10 mm diameter)

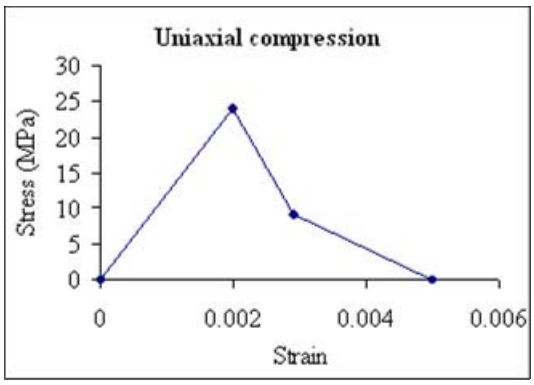

(i)

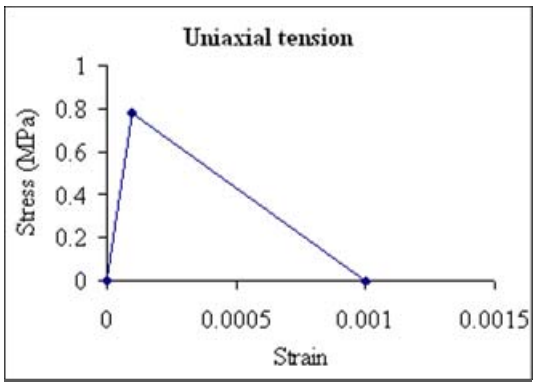

(ii)

(c) Lightweight concrete

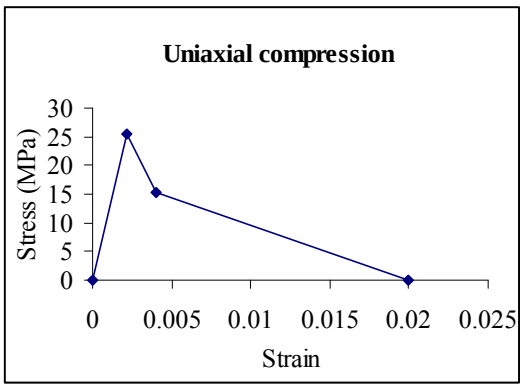

(i)

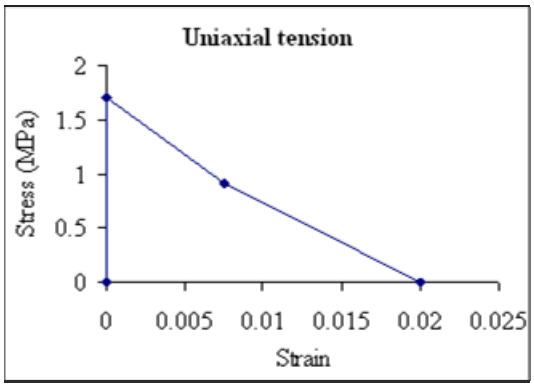

(ii)

(d) Lightweight fibre reinforced concrete (1% hooked end fibres)

Fig.7.6 Stress-strain relationships: (a) steel plates, (b) J-hook connectors, (c) plain lightweight concrete and (d) lightweight fibre reinforced concrete.

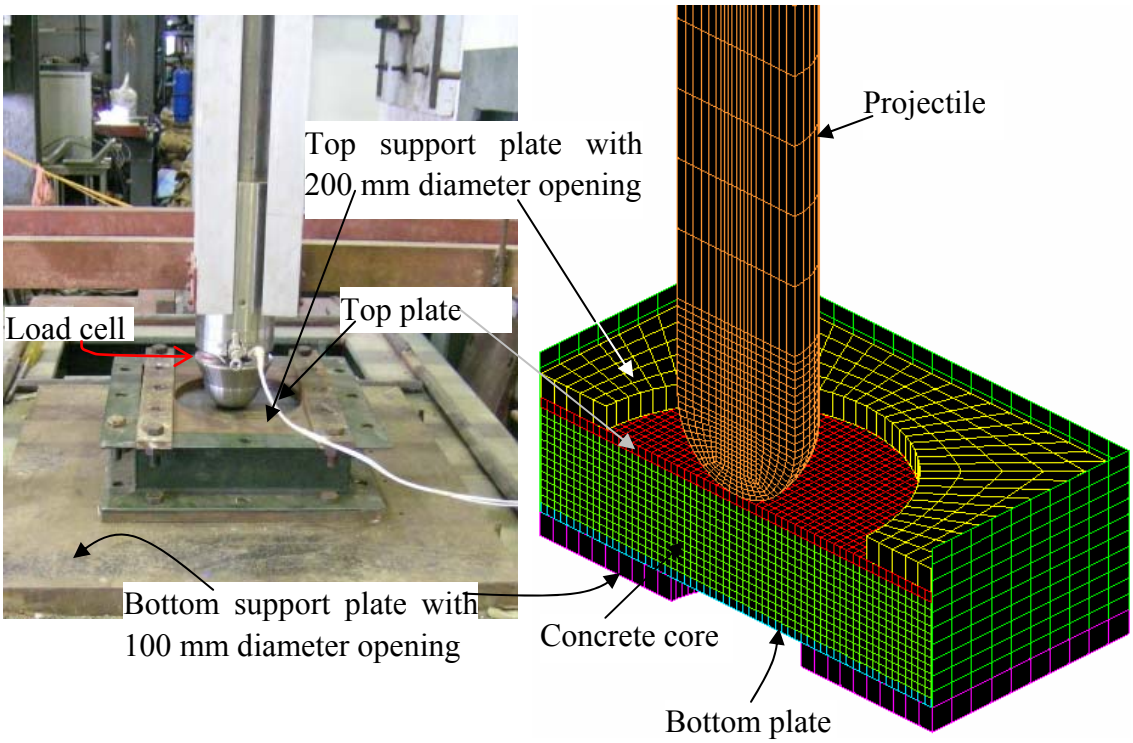

Fig. 7.7 FE model of 300 mm × 300 mm SCS sandwich panel for local impact

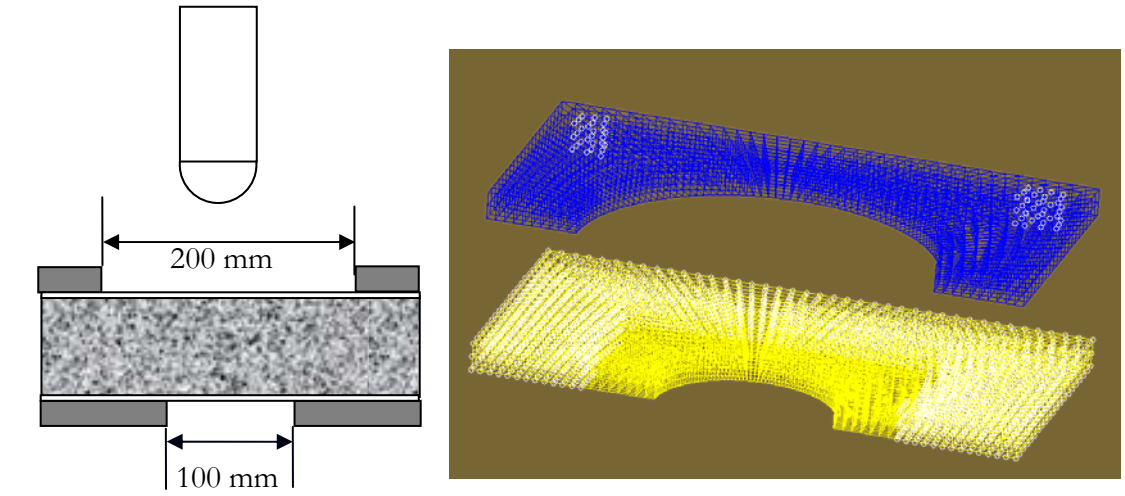

(a) (b)

Fig. 7.8 (a) Schematic diagram of test set-up and (b) nodes of top and bottom steel plate supports that are restricted from vertical translation.

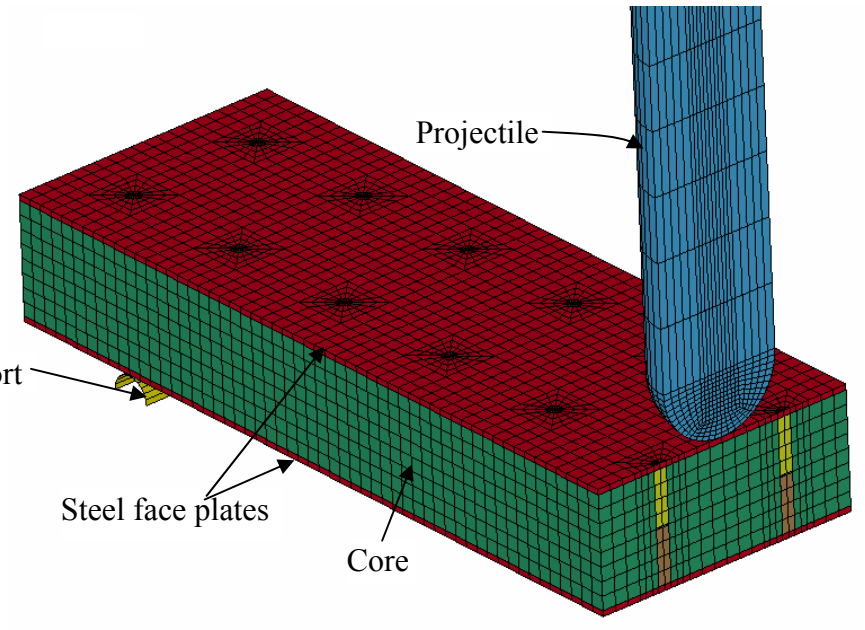

Fig. 7.9 Half model of SCS sandwich beam, projectile and support.

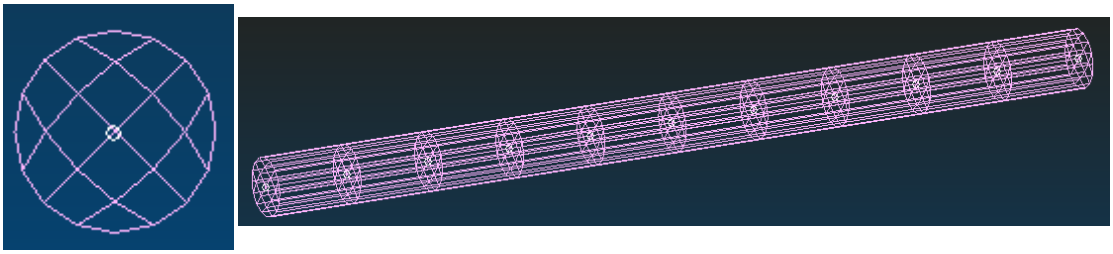

(a)

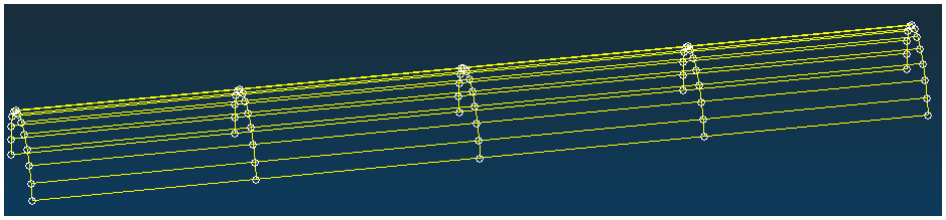

(b)

Fig. 7.10 (a) Top support can rotate only through its axis which is highlighted and (b) fixed boundary condition for the highlighted nodes of steel bars support

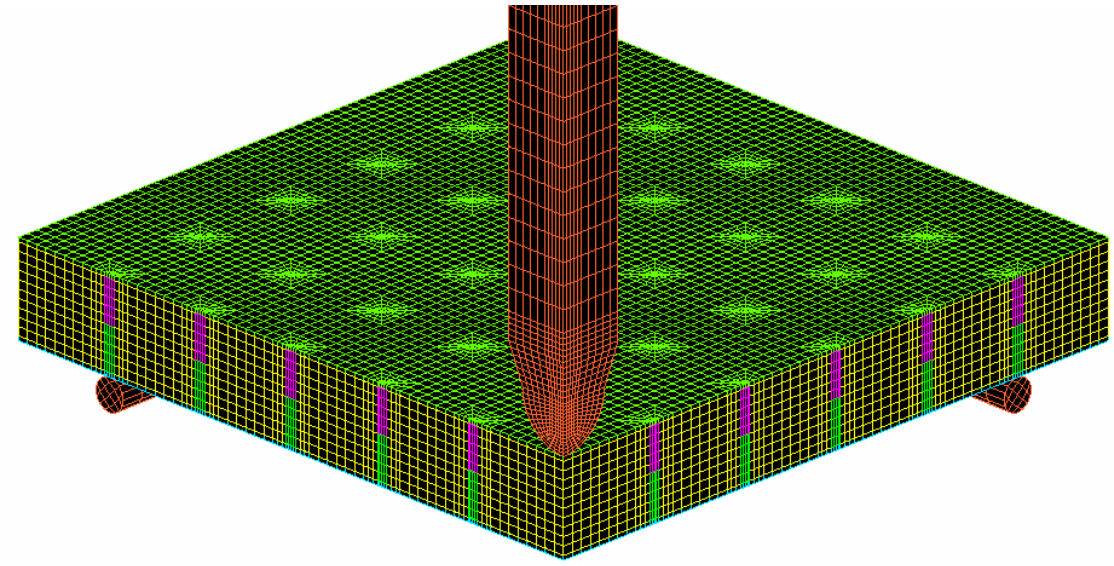

Fig. 7.11 Quarter model of SCS sandwich slab, projectile and support.

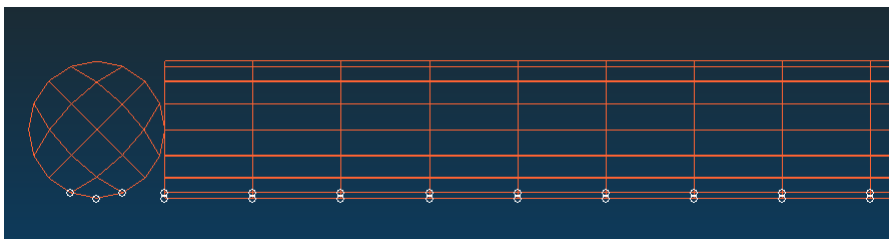

Fig. 7.12 Fixed boundary condition for the highlighted nodes of the bars support.

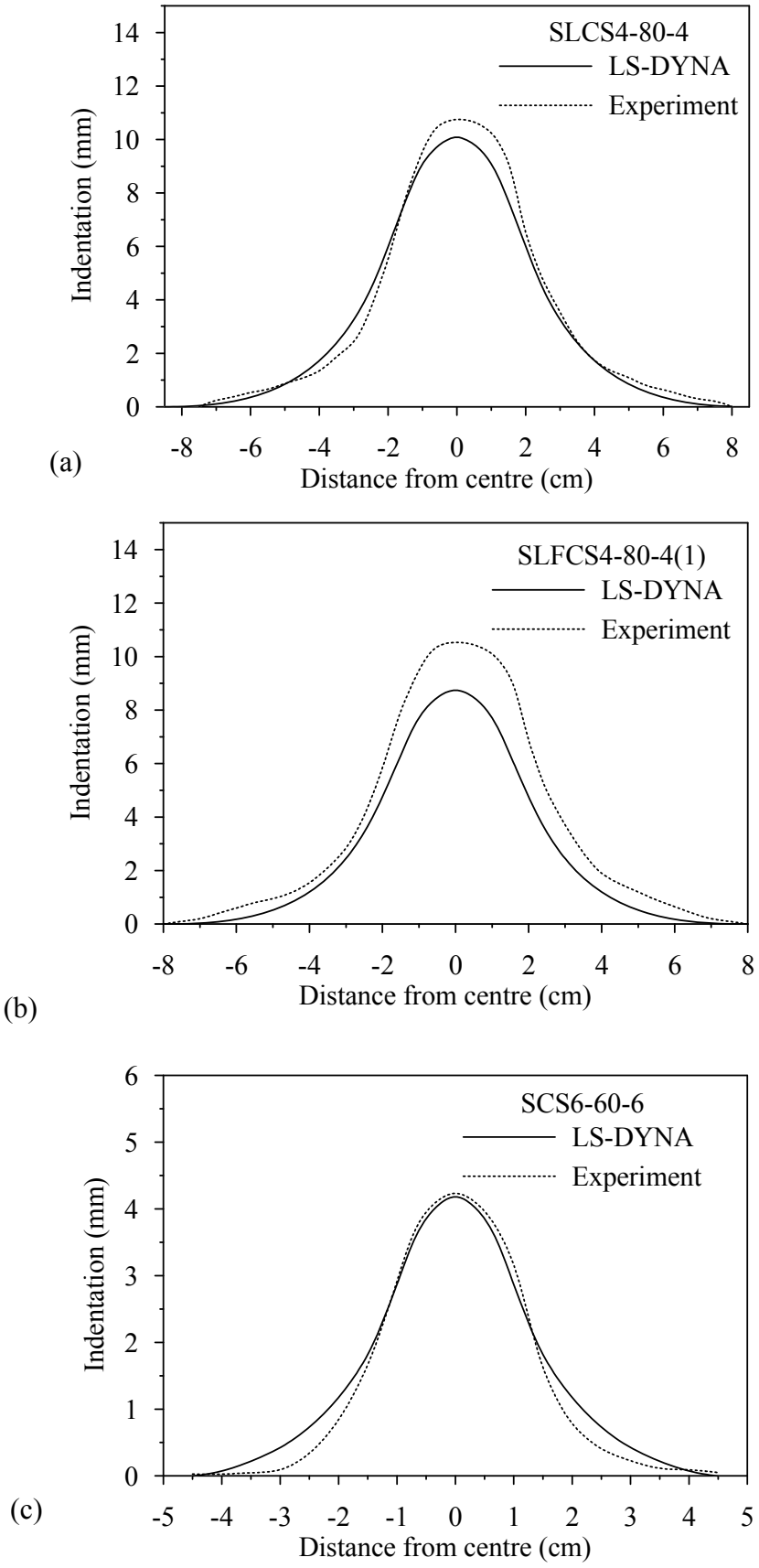

Fig. 7.13 Indentation comparison for local impact specimens: (a) SLCS4-80-4 (b) SLFCS 4-80-4(1) and (c) SCS6-60-6

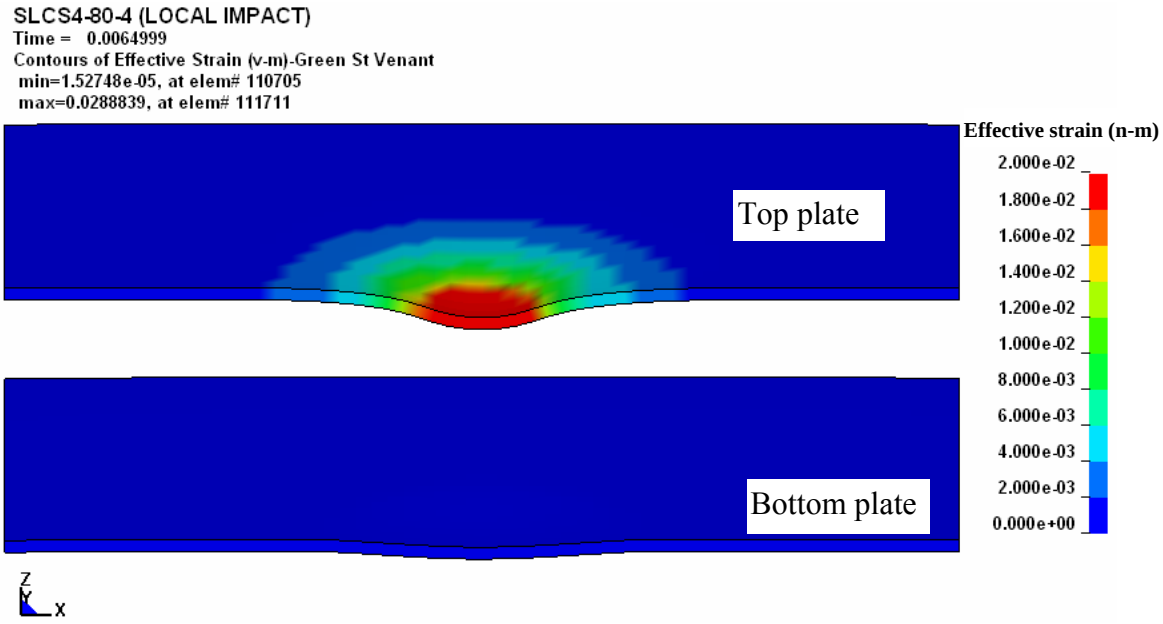

(a) SLCS4-80-4

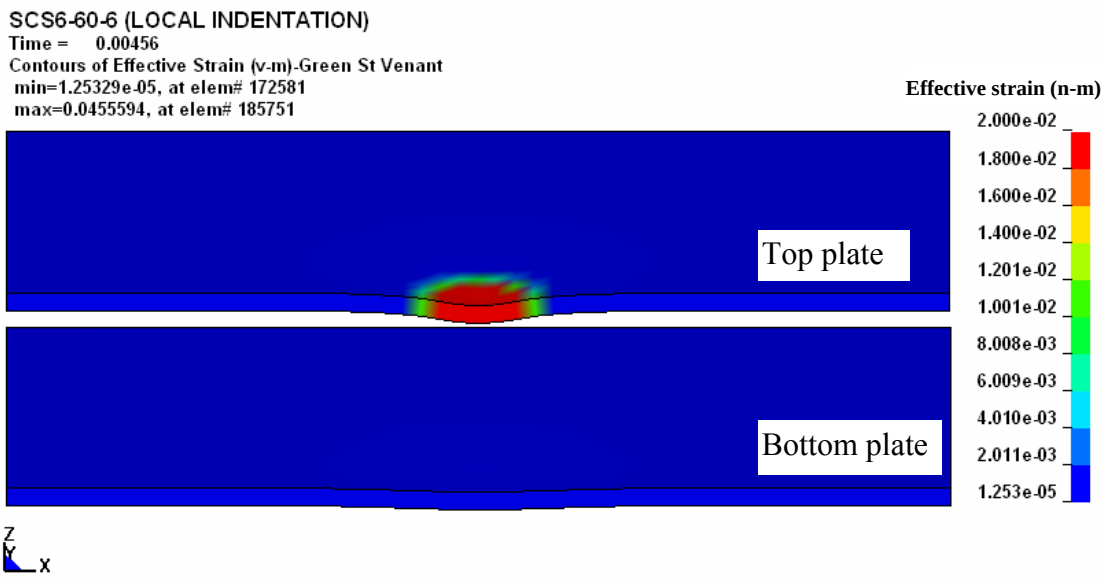

(b) SCS6-60-6

Fig. 7.14 Top plate strain contour for local impact specimens (half model)

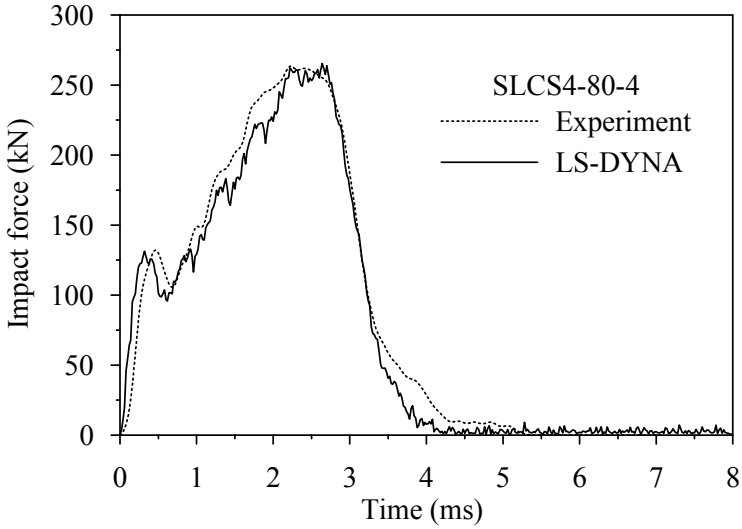

(a) SLCS4-80-4

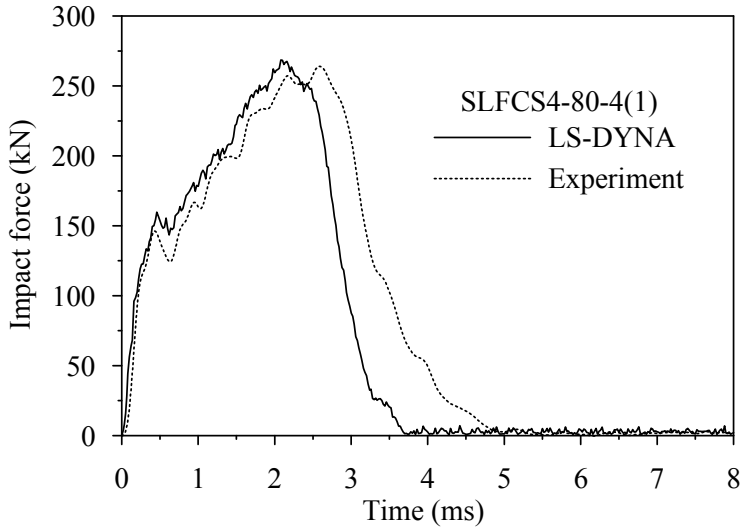

(b) SLFCS4-80-4(1)

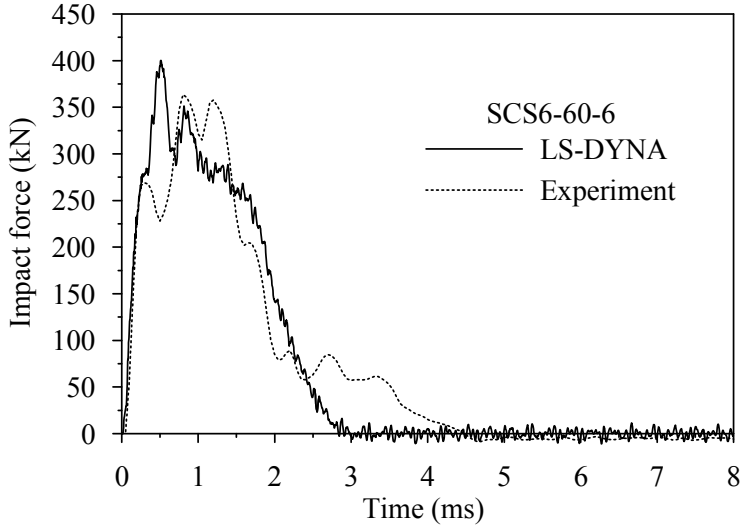

(c) SCS6-60-6

Fig. 7.15 Impact force comparison for local impact specimens.

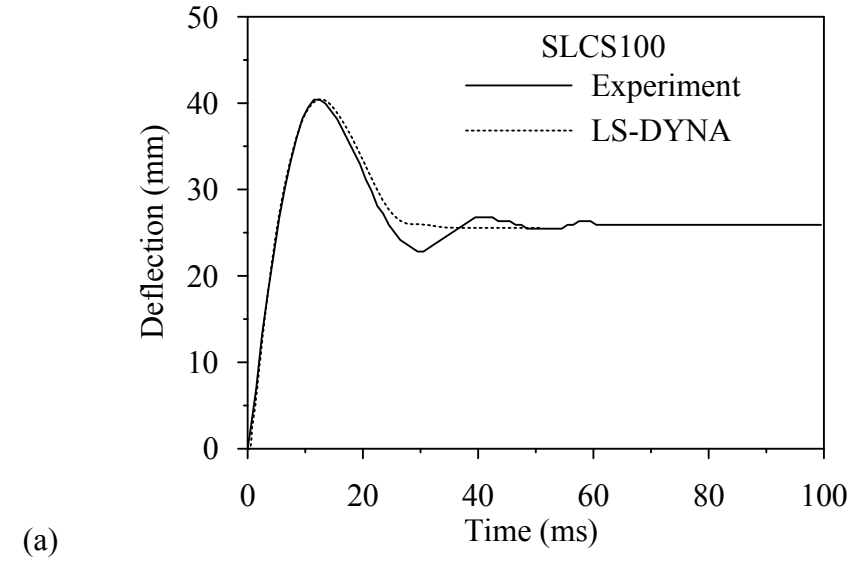

(a)

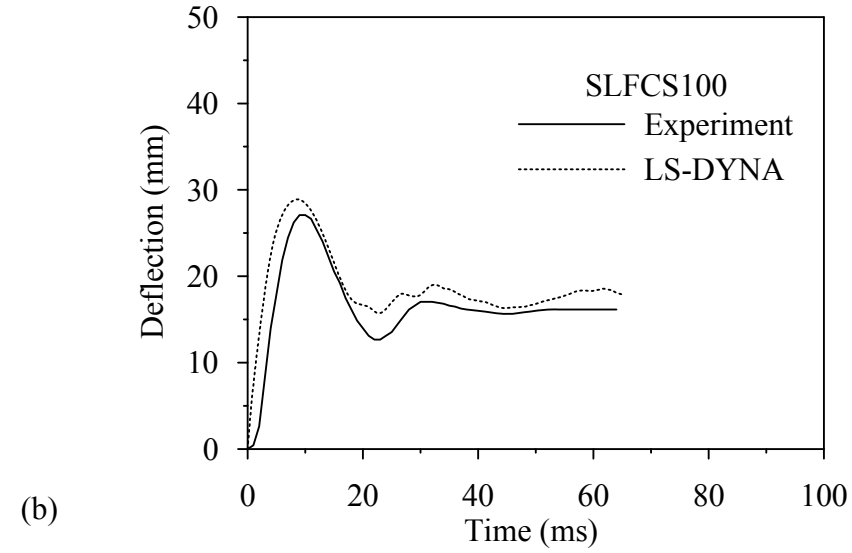

(b)

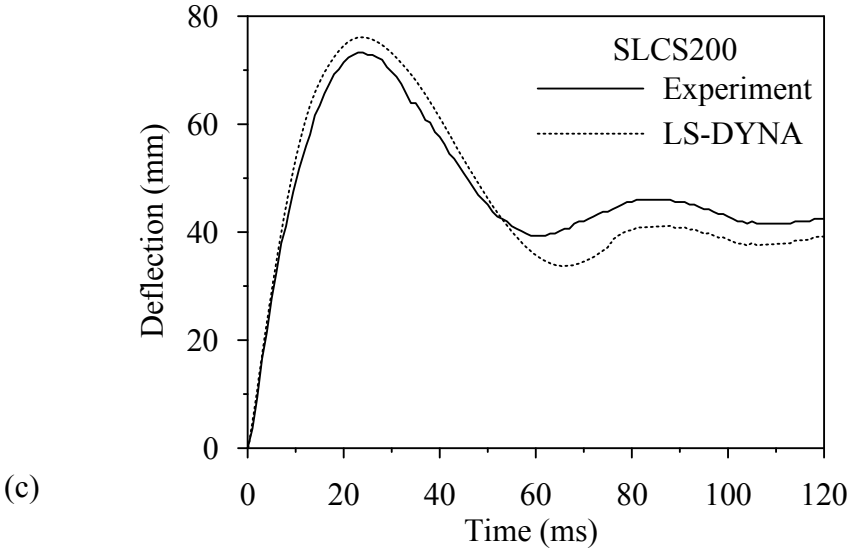

(c)

Fig. 7.16 Midspan deflection obtained in the FE analysis and compared to the experiment: (a) SLCS100 (b) SLFCS100 and (c) SLCS200

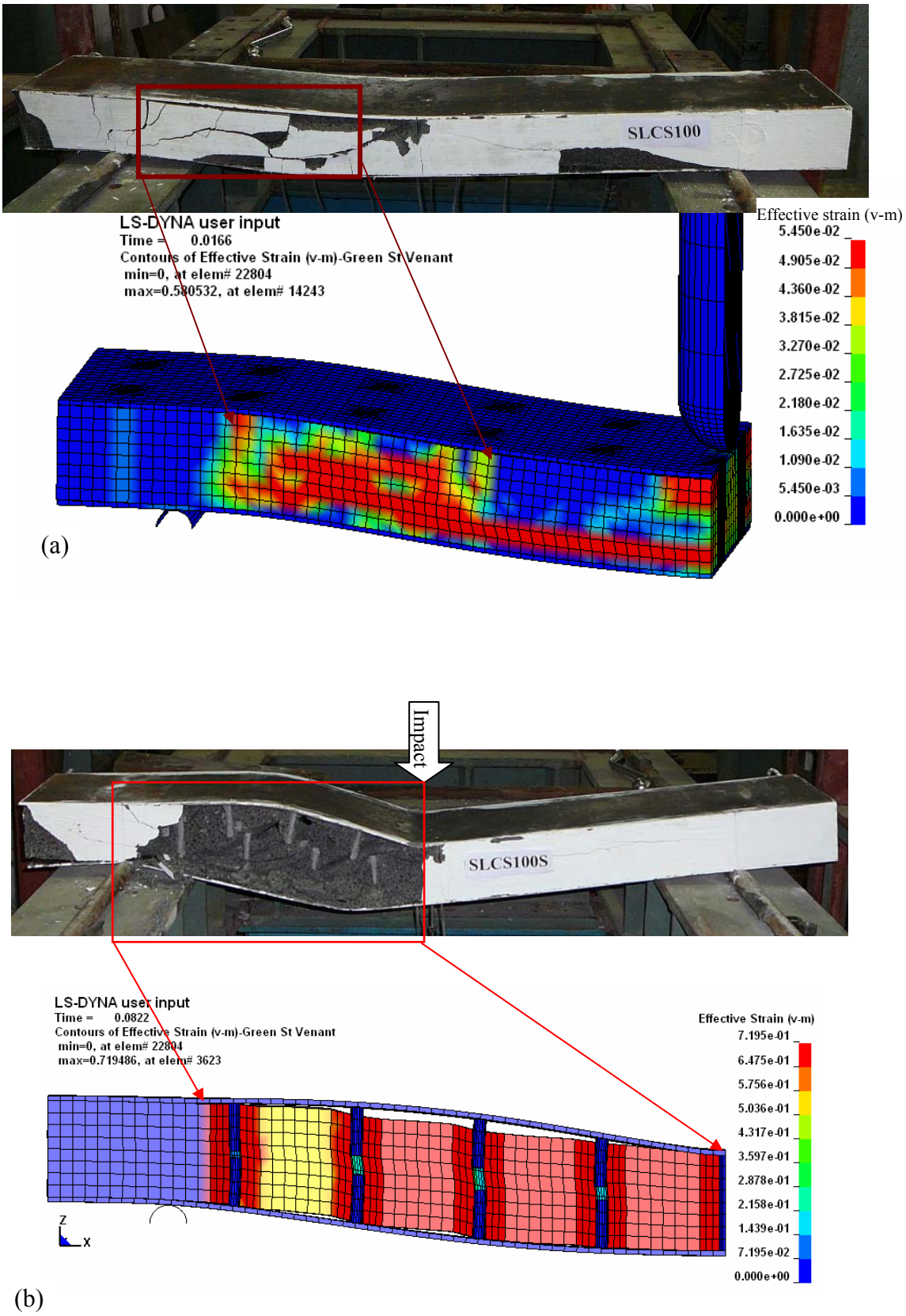

Fig. 7.17 Comparison of FEM damages pattern with test the beams: (a) SLCS100 and (b) SLCS100S (beam with stud)

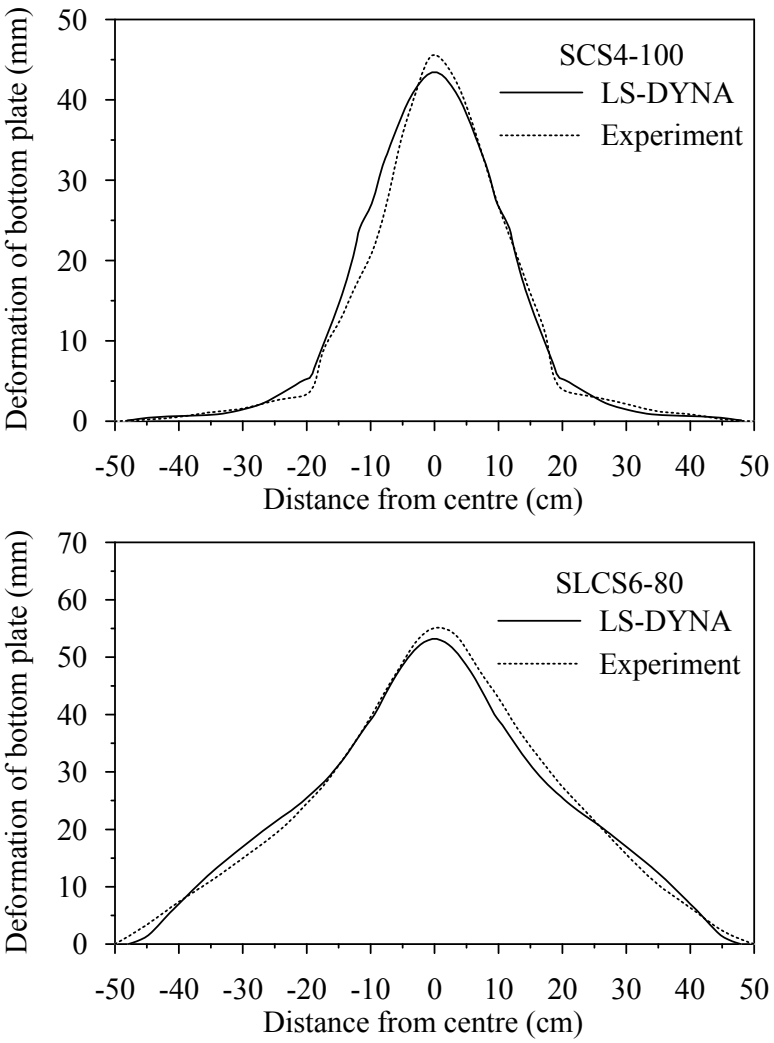

Fig. 7.18 FE simulated permanent deformation of bottom steel plates for sandwich slabs SCS4-100 and SLCS6-80 in comparison to impact test results.

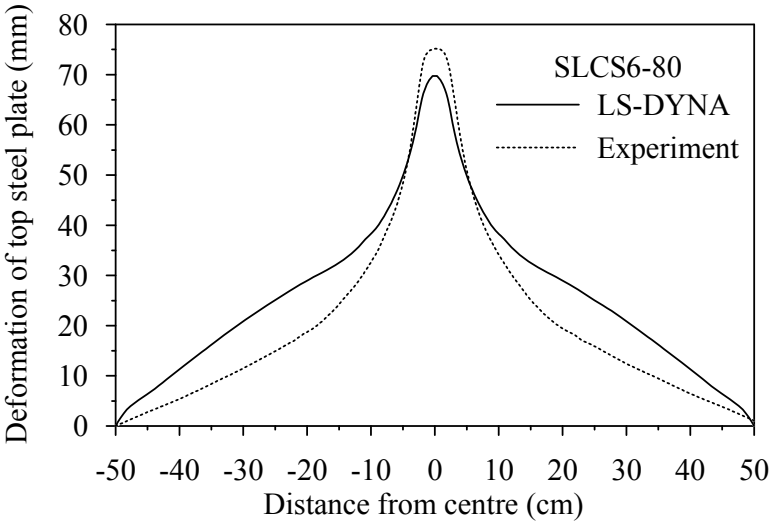

Fig. 7.19 FE simulated permanent deformation of top steel plates for sandwich slab SLCS6-80 in comparison to impact test result.

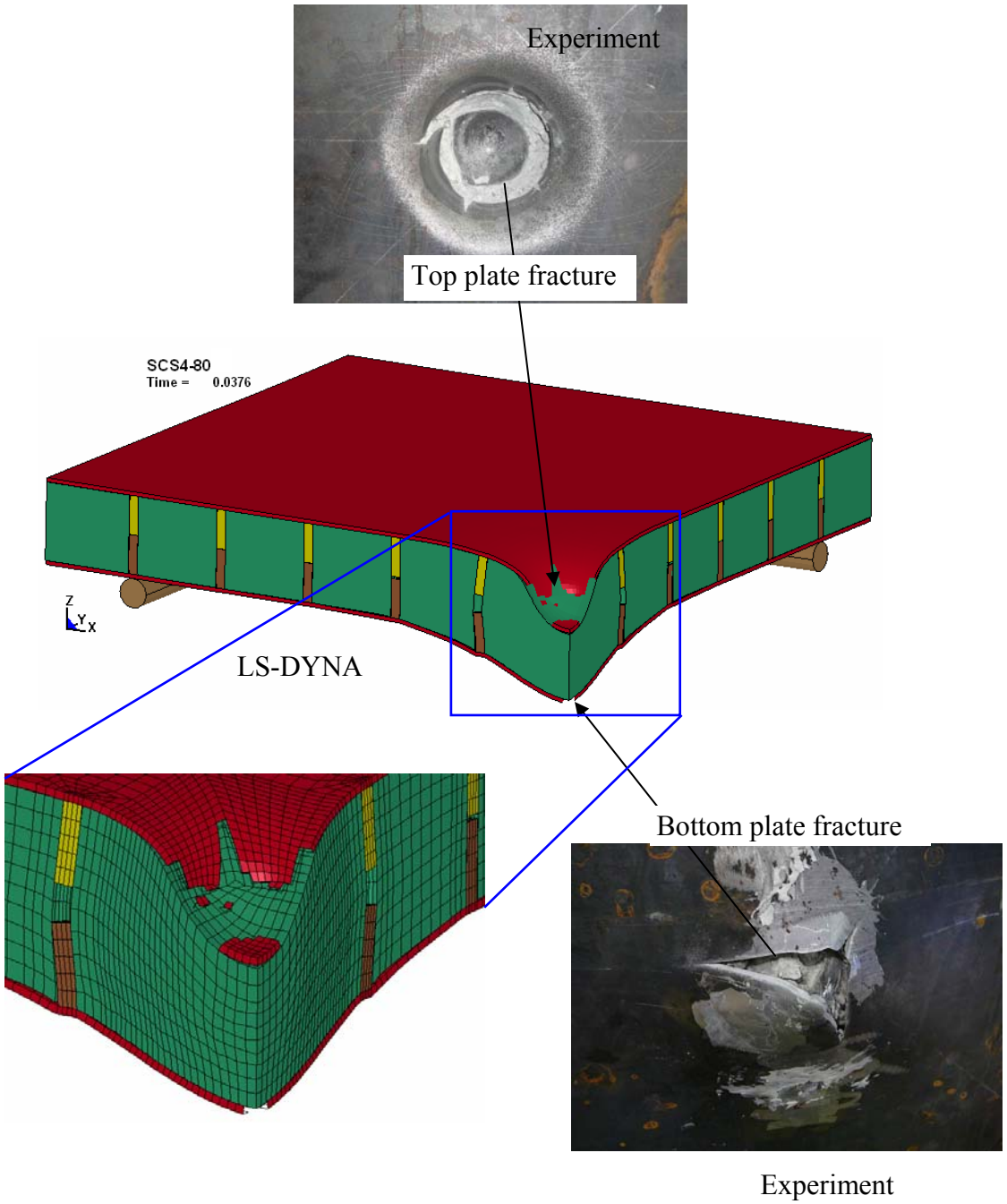

Fig. 7.20 FE simulated the steel face plates fracture for the sandwich slab SCS4-80 in comparison to impact test result.

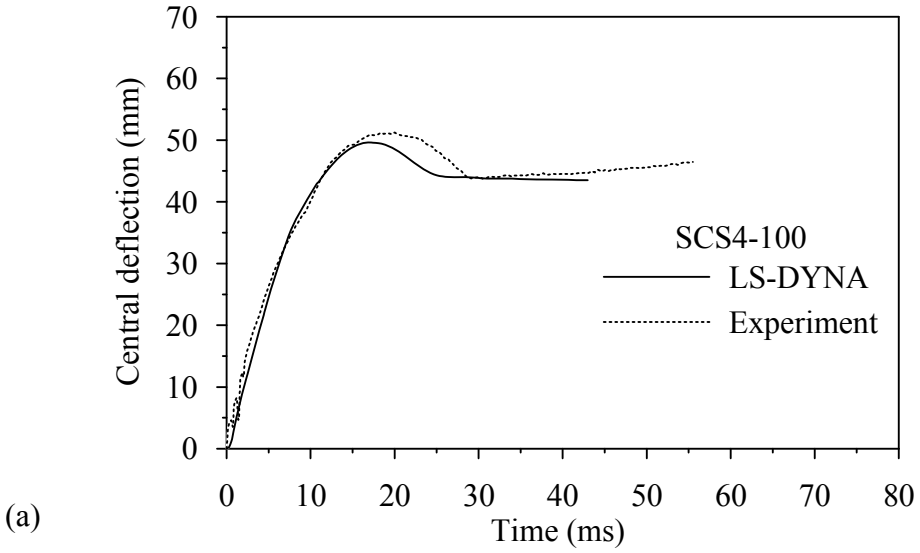

(a)

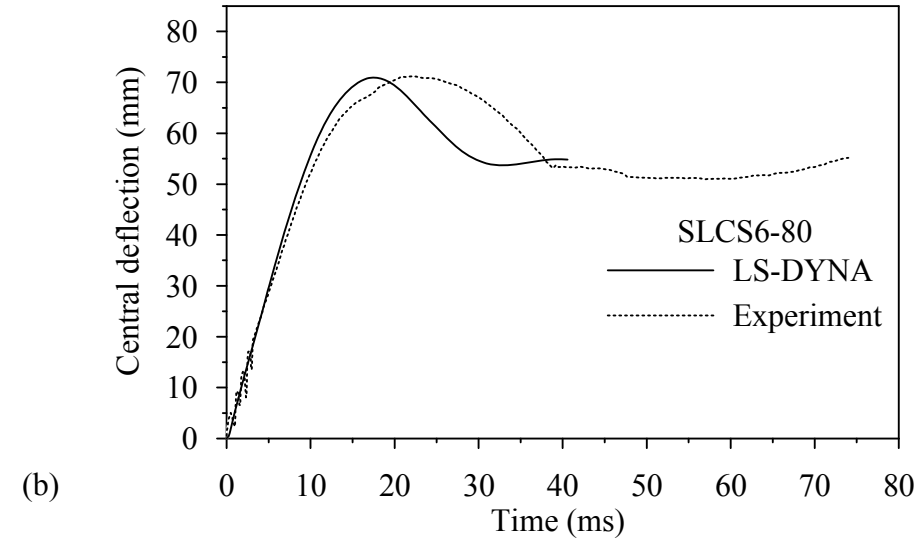

(b)

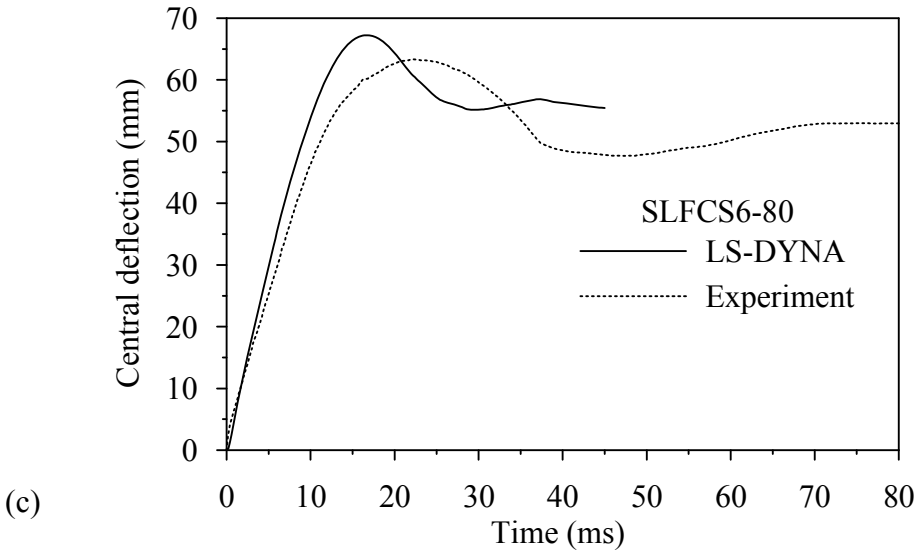

(c)

Fig. 7.21 Central deflection obtained in the FE analysis and compared to the experiment: (a) SCS4-100 (b) SLCS6-80 and (c) SLFCS6-80.

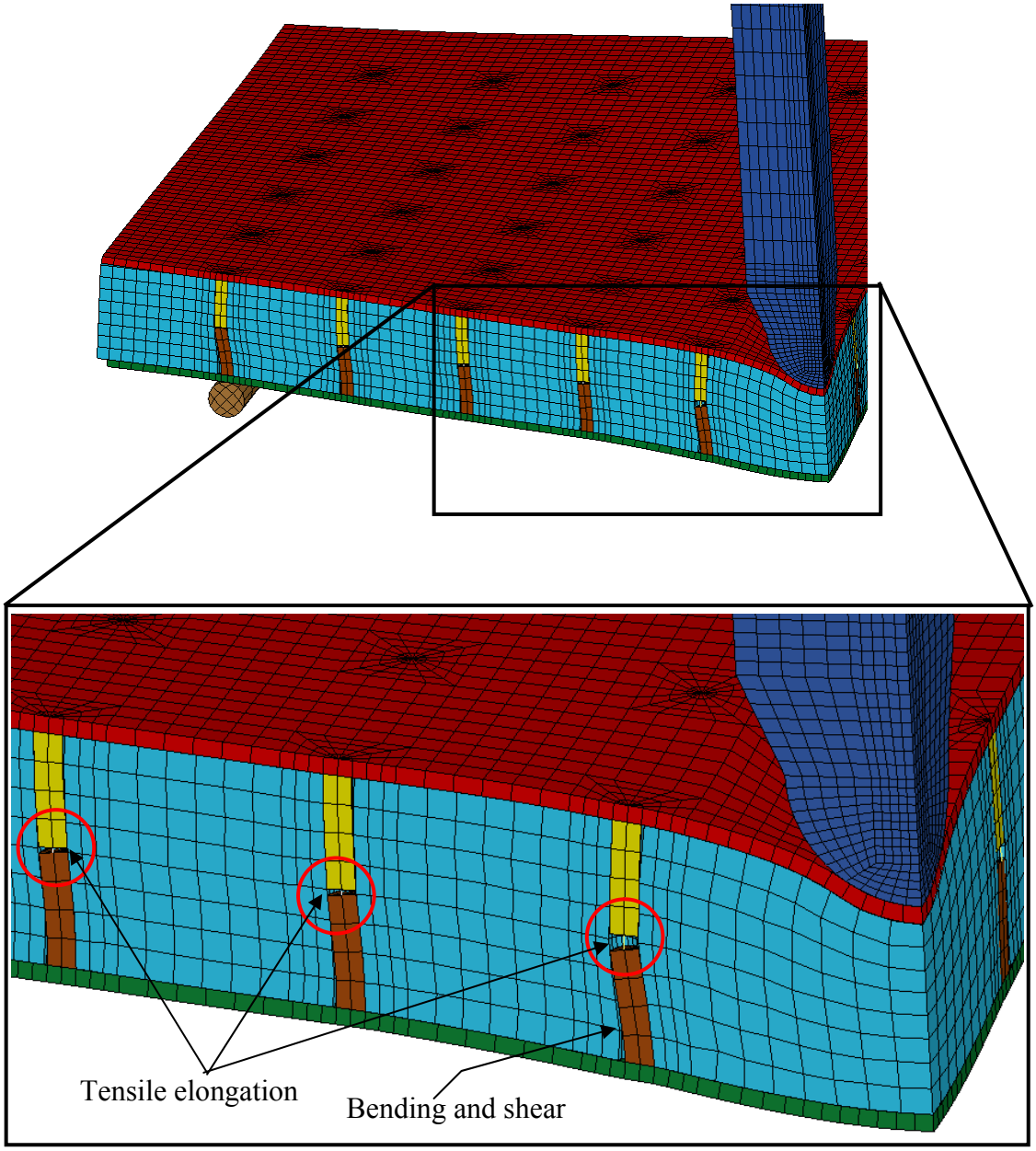

Fig. 7.22 J-hook connectors in sandwich slab SLCS6-80 at the time of maximum slab displacement (quarter model).

Conclusions and recommendations

8

8.1 Review on completed research work

The objective of this research is to study the behaviour of SCS sandwich structures subject to drop weight impact loading and to evaluate the potential of SCS sandwich structures with innovative J-hook connectors as an impact resistant system which can be used in deck-like structures. Instrumented impact (large mass) test facility developed in Structural Engineering Laboratory of NUS was used to carry out tests on SCS sandwich structures. In addition, push-out test and static test on SCS sandwich structures were carried out to evaluate the effectiveness of the new form of SCS sandwich system.

The key concept of development of SCS sandwich structures with J-hook shear connector was the first part of this thesis (Chapter 3). Analysis was carried to determine analytically the flexural resistance of the SCS Sandwich section. Moreover, the analysis included elastic deflection and shear resistance of the SCS sandwich beam. The rigorous investigation was carried out to choose suitable lightweight concrete mix design to produce structural ultra lightweight concrete (($f_c \geq 25$ MPa and density $\leq$ 1500 kg/m^3). Seven push-out test specimens were tested under direct shear force to determine the direct shear load-slip characteristics of the J-hook shear connectors. Twelve SCS sandwich beam specimens with core depth 80 mm, length 1100 mm and

width ranging from 200 mm to 300 mm were tested under static point load applied at mid-span of the beams. The ultimate capacity of the SCS sandwich beams from the tests are used to validate the analytical results.

In the second part of this research (Chapter 4), force-indentation relationships for SCS sandwich panels were derived assuming the elastic-plastic behaviour of confined concrete core. Eleven SCS sandwich panels measuring 300 mm square in size with a core thickness of 60 to 80 mm were tested under impact load. The test set-up was designed such a way that only local effect of impact could be achieved. Steel face plates thickness vary from 4 mm to 8 mm. Dynamic load cells were attached in the projectile head to get the impact force history at the impact event. The permanent indention was measured using linear transducer after the impact event. The test results were used to verify the proposed force-indentation relations.

Dynamic elastic-plastic analysis was carried out to obtain impact response of SCS sandwich beams in the third part of this research (Chapter 5). The force-indentation relations from second part of the research (Chapter 4) were incorporated in the dynamic model of the SCS sandwich beam. A total of 10 beams having core depth (80 mm), total length 1100 mm, and width ranging from 200 mm to 300 mm were tested under impact load at mid-span of the beam. The impact was achieved by dropping a 64 kg cylindrical projectile with a hemispherical head of 90 mm diameter from a height of 4 m, and the impact velocity was about 8.12 m/s. Lightweight concrete (density ≤1450 kg/m^3) was used as a core in all the beam specimens. The experimental investigation focused on the performance of J-hook connectors embedded in lightweight concrete core and the measured impact forces and central displacements were used to validate the theoretical model.

In the fourth part of the research (Chapter 6), impact response of SCS sandwich slab by large mass was investigated. Eight SCS sandwich slabs measuring 1200 mm square in size with a core thickness of 80 mm to 100 mm were tested under large mass impact. J-hook shear connectors were used as shear connectors for all the slab specimens; where both lightweight concrete and normal weight concrete were used as core. The mass of the projectile was 1246 kg and the impact velocity was about 7.43 m/s. The experimental investigation focused on the performance of the SCS sandwich slabs under very large mass impact where local punching is the dominant mode of failure. The force-indentation relations developed in previous chapter were then incorporated in the global elastic-plastic dynamic model for SCS sandwich slab. Simplified energy balance model and punching model were also proposed for design purposes.

In the fifth part of the research (Chapter 7), three-dimensional FE models were applied to simulate the force history, local indentation depth and deformed zone diameter of SCS sandwich panels with dimension same as described in the second part of the research. Three-dimensional FE models were also used to predict the global (displacement time history) and local responses (penetration depth) of the SCS sandwich slabs and beams due to low-velocity drop-weight impact by 1246 kg and 64 kg for slabs and beams respectively. The model dimensions were same as test beams and slabs subjected to low-velocity drop-impact are discussed earlier. Special attention was given to model the J-hook connectors for EF analysis. The FE predictions were compared to the test results in order to verify the FE models.

8.2 Conclusions

Within the scope of the experimental and analytical investigations reported in this thesis on SCS sandwich structures with J-hook connectors, the following major conclusions can be drawn:

i) A new form of SCS sandwich structures comprising a lightweight concrete core sandwiched in between two steel plates which are interconnected by J-hook shear connectors was developed. Specifically, lightweight concrete of weight less than 1450 kg/m^3 and novel J-hook connectors that are capable of resisting tension and shear have been developed for this purpose. The J-hook connectors can be fitted in shallow depth (≥ 50 mm) between the steel face plates for the construction of slim deck structure.

ii) Push-out tests confirm the superior performance of J-hook connectors in resisting shear force. Eurocode 4 method, which is originally developed for headed stud connectors, may be used to predict the shear capacity of the connector in lightweight and normal weight concrete core, although the method underestimated the test results by about 10%-15%.

iii) Test on sandwich beams subject to concentrated point load at the mid-span shows that it is necessary to provide adequate number of shear connectors in order to prevent the formation of shear cracks in the concrete core and to ensure ductile failure mode. It is recommended that the spacing of shear connectors should be at most equal to the core thickness to prevent concrete shear failure for sandwich beams with core depth less than 100 mm. When a sufficient number of connectors is provided to achieve full composite action in the sandwich beam, the

load-deflection response is ductile and failure is controlled by yielding of the bottom steel plate. Inclusion of 1% fibre (steel or PVA) in the core material significantly increases the ultimate load-carrying capacity (24% in case of steel fibre and 14% in case of PVA fibre) as well as increase the ductility.

iv) Analytical solutions have been proposed to calculate the elastic and plastic moment capacity as well as the elastic deflection of SCS sandwich beams under static service load. The calculated load carrying capacity is generally conservative (average about 90% of the experimental maximum load) if connector weld failure can be avoided, and thus the proposed analytical solutions can be used for design purposes. In case of lightweight concrete cores, it is recommended that the shear capacity of the J-hook connectors should be reduced by 0.9 to account for the lower bearing strength of the lightweight core.

v) A new contact law (i.e. force-indentation relationship) for SCS sandwich structures has been derived by considering the face plate local bending followed by membrane action and deformation of the core as an elastic-plastic material. This contact law has been verified with the test results. The local impact test on SCS sandwich shows that use of 1% steel fibre is sufficient to reduce crack significantly in the lightweight concrete core and also reduce indentation depth during impact.

vi) J-hook shear connectors in the sandwich beams are effective in preventing tensile separation of the steel face plates, thus reducing the overall beam deflection and maintaining the structural integrity despite the presence of flexural and shear cracks in the concrete core under impact load. The lightweight concrete core

exhibits brittle behaviour and cracks into many pieces at the impact event. Using 1% volume fraction of fibre in the concrete core could reduce the cracks significantly and enhance the overall integrity of the sandwich beams. The reduction of flexural strength of the damaged beams after impact is less than 30% if the maximum deflection during impact is less than span/14.

vii) Using the developed force-indentation relations, dynamic models based on a single-degree-of-freedom system of the sandwich beam has been proposed to predict the impact force-time history and displacement-time history. The predicted results are verified against the test results. For given impact velocity and beam configuration, the central deflection-time history and force-time history of SCS sandwich beams can be determined with reasonable accuracy using the proposed dynamic models.

viii) Unlike beam specimens, low velocity impact by large mass on SCS sandwich slab is more likely dominated by local punching. The punching mode of failure was observed for all sandwich slabs. For a given impact energy, the top steel plate thickness is more important to resist the punching mode of failure for a large mass impact. The J-hook shear connector performs well to resist the separation and slip failure of the slab. SCS sandwich slabs with J-hook connectors and fibre-reinforced concrete core exhibited higher contact stiffness and they could absorb high impact energy to increase the punching resistance.

ix) Using the force-indentation relation with force vibrational equation of the slab, impact force history can be calculated with reasonable accuracy (maximum error

10%). The impact force history can be used for designing the SCS sandwich slab against punching failure.

x) Punching model for SCS sandwich slab has been proposed where steel plate strength and thickness, and the tensile capacity of J-hook connectors are the controlling parameters that enhance the punching capacity of the SCS sandwich slab. Fibre reinforced concrete core can be used to increase the punching resistance without changing steel face plate thickness and J-hook configuration. If the impact force and the loading area are known, the sandwich slab can be designed accordingly to resist the impact.

xi) Using the proposed force-indentation relations, an energy balance concept was adopted to analyze the global behaviour, especially the energy absorption capacity of SCS sandwich slabs. Using this simplified model, maximum deformation of the slab during impact can be measured. For a given impact energy and slab configuration, the central deflection of the SCS sandwich slab can be determined with reasonable accuracy using this energy balance model.

xii) The yield line method is successful in predicting ultimate flexural static patch load for the SCS sandwich slabs. The section capacity along the yield line depends on the J-hook connectors capacity within the area pertained to the yield line. For large deflection, membrane action of the steel plates should be considered. The J-hook connectors' shearing capacity determines the average membrane stress in the steel face plates. Generating the load-deflection curves for a given sandwich slab (using flexural and membrane analysis), energy

balance model can be used to predict dynamic responses for a given object impact.

xiii) FE analyses for force-indentation relation of SCS sandwiches subjected to low velocity impact showed good agreement with experimental and analytical results. Thus, the proposed force-indentation relations for sandwich structures can be used for dynamic analysis.

xiv) The interconnected part of the interconnected J-hooks was modelled using discrete beam with free of rotation. Despite using a simplified model for the J-hook connectors and lack of triaxial test data for the characterization of the lightweight concrete material, the simplified FE model is capable of describing the permanent deformation and central displacement time-history of the sandwich slabs and beams with reasonable accuracy.

xv) Numerical results show that at the impact event, J-hook experienced tensile force and they are effective in resisting the separation of steel plates and maintaining the integrity of the sandwich slabs and beams under the drop-weight impact.

SCS sandwich structures with J-hook connectors are fully suitable for deck-like structures where low velocity impact by falling object is expected in service life. The static analysis can be used for service load design and the dynamic analysis can be used for expected low velocity impact load design. The proposed punching formula is suitable for punching resistance design of SCS sandwich structures.

8.3 Recommendations for further studies

The following are some ideas for further studies to attain a better insight into the behaviour of SCS sandwich structures:

i) The intention of this research is to propose a sandwich plate system for offshore structure and other deck like structures subjected to static as well as impact loading. Lightweight concrete (density ≈1450 kg/m^3) of strength about 30 MPa has been used in the SCS sandwich structures. Increasing the strength of the ultra lightweight concrete, the structural efficiency of the SCS sandwich may be increased a lot.

ii) To prevent separation of top and bottom steel plates at the event of dynamic force, interconnection between top and bottom steel face plates done by J-hook shear connectors. The effect of different parameters of J-hook connector (e.g. bend diameter and bend length) may be studied to get optimum geometry of the J-hook connector.

iii) The current push-out test set-up is not able to mobilize relative slippage between the steel plates, and hence, the relative displacements and rotations of the attached J-hooks cannot be mobilized. Hence, this gives an upper bound shear resistances of the shear connections. A modified test set-up in which both steel plates can move opposite to each other is suggested as shown in Appendix B (Fig. B.1). Hopefully, this test set-up is able to mobilize relative deformations and rotations between the attached J-hooks in the way similar to those observed in the beam tests (Fig. 3.12(c)).

iv) In this current study, lightweight concrete and normal weight concrete were used as a core material in the SCS sandwich structures. In some application (bridges, onshore decking, and protective structures) where self-weight is not a big issue, high strength and ultra high strength concrete may be used to increase the structural efficiency. The impact response of SCS sandwich structures with high strength and ultra high strength concrete need to be studied.

v) Analytical and numerical modelling of impact events require a knowledge of dynamic material properties, response mechanics, and constitutive relations. Hence material behaviour at different strain rates should be established for different types of concrete (lightweight and normal concretes).

vi) The FE parametric study can be further expanded to evaluate the effect of different parameters (for example diameter of J-hook connector, fibre content in the core, and tensile strength of the J-hook connectors) on the impact response.

vii) The dynamic response of SCS sandwich structures under drop weight impact loading was studied in this research. However, the dynamic response of these structures should be different under impulsive blast loadings. FE analysis may be carried out to understand the response of SCS sandwich structures under blast load. Field explosion test can be carried out to further verify the FE parametric study.

viii) Dynamic response of SCS sandwich structures under extreme cold and hot temperatures is one of the research areas and further study is required. This may be useful to simulate the effect of ice impact if the SCS sandwiches are used in marine and offshore structures in arctic region.

References

Abrate S. Impact on composite structures. Cambridge University Press 1998.

Abrate S. Impact on laminated composite materials. Applied Mechanics Review 1991; 44(4):155-190.

Abrate S. Localized impact on sandwich structures with laminated facings, Applied Mechanics Reviews 1997; 50(2):69-82.

Abrate S. Modeling of impacts on composite structures. Composite Structures 2001;51(2):129–38.

ACI-ASCE COMMITTEE 326. Shear and diagonal tension. Journal of the American Concrete Institute 1962; 59(1):1-30, 59(2):277-334, 59(3):353-396.

Akil Hazizan M, Cantwell WJ. The low velocity impact response of foam-based sandwich structures. Composites Part B: Engineering 2002;33(3):193–204.

Aymerich F, Marcialis P, Meili S, Priolo P. An instrumented drop-weight machine for low velocity impact testing. Proceedings of the Fourth International Conference on Structures Under Shock and Impact IV, July 1996, Udine, Italy. pp. 243-253.

Balasubramanian K, Bharatkumar BH, Gopalakrishnan S, and Prameswaran VS. Impact resistance of steel fibre reinforced concrete. The Indian Concrete Journal 1996;70(5): 257-262.

Bangash, M.Y.H. Impact and explosion analysis and design. Oxford: Blackwell Scientific Publications. 1993.

Banthia NP, Chokri K, Ohama Y, Mindess S. Fiber reinforced cement-based composites under tensile impact. Advanced Cement Based Materials 1994; 1(3):131-141.

Banthia NP, Mindess S, Bentur A. Impact behaviour of concrete beams. Materials and structures 1987; 20 (4): 293-302.

Banthia NP, Mindess S, Bentur A. Pigeon M. Impact testing of concrete using a drop-weight impact machine. Experimental Mechanics 1989: 29(1):63-69.

Barnhart KE, Goldsmith W. Stresses in beams during transverse impact. Journal of Applied Mechanics 1957;24:440-446.

Bathe KJ. Finite element procedures. Upper Saddle River, New Jersey: Prentice-Hall. 1996.

Bayasi Z, Zeng J. Properties of polypropylene fiber reinforced concrete. ACI Materials Journal 1993; 90 (6):605-610.

Bentur A, Mindess S, Banthia NP. The behaviour under impact loading: Experimental procedure. Materials and structures 1986; 19(5):371-378.

Bentur A. and Mindess S. Fibre reinforced cementitous composites. Elsevier Applied Science, UK. 1990.

Bergan PG, Bakken K. Sandwich design: a solution for marine structures? International Conference on Computational methods in Marine Engineering, Marine 2005, 27-29 June 2005, Oslo, Norway.

Bergan PG, Bakken K, Thienel KC. Analysis and design of sandwich structures made of steel and lightweight concrete. Computational Mechanics: solids, structures and coupled problems. Springer, Dordrecht, The Netherlands. pp.147-164.

Biggs JM. Introduction to structural dynamics. New York: McGraw-Hill; 1964. pp. 20-26.

Bowerman H, Coyle N, Chapman JC. An innovative steel/concrete construction system. The Structural Engineer 2002; 80(20):33–38.

Bowerman H, Gough M, King C. Bi-Steel design & construction guide. Scunthorpe: British Steel Ltd; 1999.

Burgan BA, Naji FJ. Steel-Concrete-Steel sandwich construction. Journal of Constructional Steel Research 1998; 46(1-3):219.

CEB. CEB-FIP Model Code 1990. Trowbridge, Wiltshire, UK: Comité Euro-International du Béton, Redwood Books; 1993.

Chen WF. Constitutive Equations for Engineering Materials: Vol. 2 - Plasticity and Modeling. Elsevier, Amsterdam, 1994.

Christoforou AP. On the contact of a spherical indenter and a thin composite laminate. Composite Structures 1993;26(1-2):77-82.

Clubley SK, Moy SSJ, Xiao RY. Shear strength of steel–concrete–steel composite panels. Part I—testing and numerical modelling. Journal of Constructional Steel Research 2003; 59(6): 781–794.

Clubley SK, Moy SSJ, Xiao RY. Shear strength of steel–concrete–steel composite panels. Part II—detailed numerical modelling of performance. Journal of Constructional Steel Research 2003; 59(6):795–808.

Corbett GG, Reid SR. Local loading of simply-supported steel-grout sandwich plates. International Journal of Impact Engineering 1993;13(3):443-461.

Crawford JE, Lan S. Blast barrier design and testing. Proceedings of the 2006 Structures Congress; Brad Cross, John Finke Ed., St. Louis, Missouri, USA; May 18–21, 2006: pp. 26.

Dai XX, Liew JYR. Steel-Concrete-Steel sandwich system for ship hull construction. In: Camotim D *et al.* editors, Proceedings of International Colloquium on Stability and Ductility of Steel Structures, September 2006, Lisbon, Portugal, pp.877-884.

Esper P. Performance of buildings under blast loading and recommended protective measures. In Proc. International Symposium on Network and Center-Based Research For Smart Structures Technologies and Earthquake Engineering –SE04, Osaka, Japan. July 6-9, 2004.

Eurocode 2: Design of concrete structures - Part 1-1: General rules and rules for buildings. BS EN 1992-1-1:2004.

Eurocode 4: Design of composite steel and concrete structures-Part 1.1: General rules and rules for buildings. BS EN 1994-1-1:2004.

Evans GR, Jones BC, McMillan AJ, Darby MI. A new numerical method for the calculation of impact forces. Journal of Physics D: Applied Physics 1991; 24:854-858.

Fang LX, Chan SL, Wong YL. Numerical analysis of composite frames with partial shear-stud interaction by 1 element per member. Engineering Structures 2000; 22(10): 1285-300.

Foundoukos N, Chapman JC. Finite element analysis of steel–concrete–steel sandwich beams. Journal of Constructional Steel Research 2008; 64(9):947–961.

Gambarova PG, Schumm C. Impulsive punching of fiber-reinforced concrete slabs. ASCE Structures Congress XII (Atlanta, Georgia, USA), pp. 252-257. 1994.

Goldsmith W. Impact, The theory and physical behaviour of colliding solids. London: Edward Arnold Publishers, 1960.

Gowda SS, Hassinen P. Behaviour of steel-concrete composite members for arctic offshore structures. The Proceedings of the First (1991) International Offshore and Polar Engineering Conference, Edinburgh, UK, August 11-16, 1991; Vol. 2, pp. 548-555.

Hallquist JO. LS-DYNA Keyword User Manual - Nonlinear dynamic analysis of structures. Livermore Software Technology Corporation, Livermore, California, 2006.

Hanson JA. Strength of structural lightweight concrete under combined stress. Portland Cement Association Research and Development Laboratories 1963;5(1):39-36.

Hazizan MA, Cantwell WJ. The low velocity impact response of foam-based sandwich structures. Composites: Part B 2002; 33(3): 193-204.

Hoo Fatt MS, Park KS. Dynamic models for low velocity impact damage of composite sandwich panels-Part A: Deformation. Composite structures 2001; 52:335-351.

Holt PJ. A procedure for assessment of steel structures subject to impact or impulsive loading. Structures under Shock and Impact III, Proceedings of the Third International Conference, June 1994, Madrid, Spain, pp. 157-164.

Hughes G, Beeby AW. Investigation of the effect of impact loading on concrete beams. The Structural Engineer 1982; 60B (3):45-52.

Hughes G, Speirs DM. An investigation of the beam impact problem. Technical Report 546, Cement and Concrete Association. 1982.

Johnson KL. Contact Mechanics. Cambridge University Press, 1985.

Johnson RP. Composite structures of steel and concrete: Beams, Slabs, Columns, and Frames for Buildings (3rd edition). Blakwell Publishing Ltd, UK. 2004.

Jones N. Structural impact. Cambridge: Cambridge University Press, 1989

Jones N. Plasticity methods in protection and safety of industrial plant and structural systems against extreme dynamic loading. Defence Science Journal 2008; 58(2):181-193

Keer LH, Woo TK. Low velocity impact on a circular plate. Advances in Aerospace Science and Engineering, ed U. Yuceoglu, R. Hesser., ASME, New York. 1984.

Kennedy SJ, Kennedy JL. Innovative use of sandwich plate system for civil and marine applications", International Symposium on Innovation and Advances in steel structures, 30 -31 August 2004, Singapore, pp. 175-185.

Koh CG, Ang KK, Chan PF. Dynamic analysis of shell structures with application to blast resistant doors. Shock and Vibration 2003;10(4):169-279.

Koller MG. Elastic impact on sandwich plates. Journal of Applied Mathematics and Physics 1986;37(2):256–9.

Kumar G. Double skin composite construction. M. Eng. Thesis, National University of Singapore, Singapore. 2000.

Lal KM. Low velocity transverse impact behavior of 8-ply, graphite-epoxy laminates. Journal of Reinforced Plastics and Composites 1983; 2(4):216–25.

Lahlou K, Lachemi M, Aı¨tcin P-C. Confined high-strength concrete under dynamic compressive loading. Journal of Structural Engineering 1999; 125(10):1100-1108.

Le JL, Koh CG, Wee TH. Damage modelling of lightweight high-strength concrete under impact. Magazine of Concrete Research 2006;58(6):343–355.

Lee EH. The impact of a mass striking a beam. J Appl Mech 1940; A129–38.

Lee SC. Finite element modeling of hybrid-fiber ECC targets subjected to impact and blast. Ph.D Thesis, National University of Singapore, Singapore. 2006.

Liang QQ, Uy B, Wright HD, and Bradford MA. Local and post-local buckling of double skin composite panels. Proceedings of the Institution of Civil Engineers: Structures and Buildings 2003; 156(2): 111-119.

Lim CT. Finite element modelling of impact damage on concrete by small hard projectiles. Master Eng. Thesis, Department of Mechanical Engineering, National University of Singapore. 1999.

Majdzadeh F, Soleimani SM, Banthia N. Shear strength of reinforced concrete beams with a fiber concrete matrix, Canadian Journal of Civil Engineering 2006;33(6):726-734.

Malek N, Machida A, Mutsuyoshi H, Makabe T. Steel-concrete sandwich members without shear reinforcement. Transactions of Japan concrete Institute 1993; 15(2):1279-1284.

Malvar LJ, Crawford JE, Wesevich JW, Simons D. A plasticity concrete material model for DYNA3D. International Journal of Impact Engineering 1997;19(9-10):847-873.

Malvar LJ, Ross CA. Review of strain-rate effects for concrete in tension. ACI Materials Journal 1998;95(6):735-739.

Malvar LJ. Review of static and dynamic properties of steel reinforcing bars. ACI Materials Journal 1998;95(5):609-616.

McKinley B, Boswell LF. Behaviour of double skin composite construction. Journal of constructional Steel Research 2002; 58(10): 1347-1359.

Mill F, Necib B. Impact behavior of cross-ply laminated composite plates under low velocities. Composite Structures 2001; 51:237–44.

Mindess S, Banthia NP, Bentur A. The response of reinforced concrete beams with fiber concrete matrix to impact loading. The international journal of cement composites and lightweight concrete 1986; 8(3):165-170.

Mindess S, Banthia NP, Yan C. The fracture toughness of concrete under impact loading. Cement and concrete research 1987; 17(2):231-241.

Mines RAW, Worrall CM, Gibson AG. The static and impact behaviour of polymer composite sandwich beams. Composites 1994;25(2):95–110.

Morison CM. Dynamic response of walls and slabs by single-degree-of-freedom analysis—a critical review and revision. International Journal of Impact Engineering 2006;32(8):1214-1247.

Mirsayah Amir A, Banthia N. Shear strength of steel fiber-reinforced concrete, ACI Material Journal 2002; 66(5):473-479.

Moyer ET, Gashaghai-Abdi. On the solution of Problems Involving Impact type loading. Advances in Aerospace Science and Engineering, ed U. Yuceoglu, R. Hesser., ASME, New York. 1984.

Naaman AE, Gopalaratnam VS. Impact properties of steel fibre reinforced concrete in bending. The International Journal of Cement Composite and Lightweight Concrete 1983; 5(4):225-233.

Narayanan R, Bowerman HG, Naji FJ, Roberts TM, Helou AJ. Application guidelines for Steel-Concrete-Steel sandwich construction-1: Immerses Tube Tunnels. SCI publication 132, The Steel Construction Institute, Ascot, Berkshire, UK. 1997.

Narayanan R, Roberts TM, Naji FJ. Design guide for Steel-Concrete-steel sandwich construction, Volume 1: General Principles and Rules for Basic Elements. SCI publication P131, The Steel Construction Institute, Ascot, Berkshire, UK. 1994.

Noble C, Kokko E, Darnell I, Dunn T, Hagler L, Leininger L. Concrete model descriptions and summary of benchmark studies for blast effects simulations. Lawrence Livermore National Laboratory, US Department of Energy. UCRL-TR-215024, LLNL, July 2005. <https://e-reports-ext.llnl.gov/pdf/322763.pdf>.

Oduyemi TOS, Wright HD. An experimental investigation into the behaviour of double skin sandwich beams. Journal of Constructional Steel Research 1989; 14(3):197-220.

Oehlers DJ, Bradford MA. Elementary behaviour of composite steel and concrete structural members. Butterworth-Heinemann publishing Inc. Oxford, Boston. 1999.

Olsson R, McManus HL. Improved theory for contact indentation of sandwich panels. AIAA Journal 1996; 34(6):1238–1244.

Onat ET, Haythornthwaite R M. The load-carrying capacity of circular plates at large deflection. Journal of Applied Mechanics 1956;23(1): 49-55.

Ong KCG, Basheerkhan M, Paramasivam P. Resistance of fibre concrete slabs to low velocity projectile impact, Cement & Concrete Composites 1999;21(5-6):391-401.

Parton GM, Shendy ME. Polystyrene bead concrete, properties and mix design. Int. J. Cement Composites & Lightweight Concrete 1982; 4(3):153-61.

Parton GM, Shendy ME. Polystyrene concrete beams, stiffness and ultimate load analysis. Int. J. CementComposites & Lightweight Concrete 1982; 4(4):199-208.

Perrone N, Bhadra P. Simplified large deflection mode solutions for impulsively loaded, viscoplastic, circular membranes. Journal of Applied Mechanics 1984;51(3):505–9.

Pryer JW, Bowerman HG. The development and use of British steel Bi-Steel. Journal of Constructional Steel Research 1998; 46(1-3):15.

Rabbat BG, Russell HG. Friction coefficient of steel on concrete or grout. Journal of Structural Engineering 1985; 111(3):505-515.

Radomski W. Application of the rotating impact machine for testing fibre reinforced concrete. International Journal of cement composites and Lightweight Concrete 1981; 3(1):3-12.

Rankin GIB, Long AB. Predicting the punching strength of conventional slab-column specimen. Proceedings of the Institution of Civil Engineers (London), part 1, 1987; 82:327-346.

Richardson MOW, Wisheart MJ. Review of low-velocity impact properties of composite materials. Composites Part A 1996;27A:1123-1131.

Roark RJ, Young WC. Formulas for stress and strain. 5th ed. London: McGraw- Hill; 1976.

Roberts TM, Edwards DN, Narayanan R. Testing and analysis of steel-concrete-steel sandwich beams. Journal of Constructional Steel Research 1996; 38(3):257-279.

Roberts TM, Helou AJ, Narayanan R, Naji FJ. Design criteria for double skin composite immersed tunnels. Proceeding of the third International Conference on Steel and Aluminium Structures, 24-26th May 1995, Istanbul.

Santosh S. Effect of hard impact on steel-concrete composite sandwich plates. PhD thesis, Civil Engineering Department, National University of Singapore. 2003.

Schrader EK. Impact resistance and test procedure for concrete. ACI Journal 1981; 78 (2):141-146.

Shah SP. Strain rate effects for concrete and fiber reinforced concrete subjected to impact loading. Prepared for U. S. Army Research Office, Metallurgy and Materials Science Division, Grant No. DAAG29-82-K-0171. October 1987.

Shanmugam NE, Kumar G, Thevendran V. Finite element modelling of double skin composite slabs. Finite Elements in Analysis and Design 2002; 38(7):579-599.

Shendy ME. A Comparative Study of LECA Concrete sandwich beams with and without core reinforcement. Cement & Concrete Composites 1991; 13(2): 143-149.

Shen WQ. Dynamic plastic response of thin circular plates struck transversely by nonblunt masses. International Journal of Solids Structructures 1995;32(14):2009–21.

Shivakumar KN, Elber W, Illg W. Prediction of impact force and duration due to low-velocity impact on circular composites laminates. Journal of Applied Mechanics 1985; 52:674–80.

Shukry MES, Goode CD. Punching shear strength of composite construction. ACI structural Journal 1990; 87(1):12-22.

Slobodan R, Dragoljub D. Static strength of the shear connectors in steel-concrete composite beams-Regulations and research analysis -UDC 624.072.2(045). FACTA UNIVERSITATIS Series: Architecture and Civil Engineering 2002; 2(4):251 – 259.

Sohel KMA, Liew JYR, Alwis WAM, Paramasivam P. Experimental investigation of low-velocity impact characteristics of steel-concrete-steel sandwich beams. Steel and Composite Structures- An International Journal 2003; 3(4):289-306.

Sohel KMA. Impact behaviour of Steel-Composite sandwich beams. M. Eng. Thesis, National University of Singapore. 2003.

Solomon SK, Smith DW, Cusens AR. Flexural tests of steel-concrete-steel sandwiches, Magazine of Concrete Research 1976; 28(94):13-20.

Soroushian P, Khan A, Hsu JW. Mechanical properties of concrete materials reinforced with polypropylene fibers or polyethylene. ACI Materials Journal 1992; 89(6):535-540.

Stronge WJ. Impact mechanics. Cambridge University Press, 2000.

Suaris W, Shah SP. Inertial effects in the instrumented impact testing of cementitious composites. J Cement Concrete Aggregates ASTM 1982;3(2):77–83.

Subedi NK, Coyle NR. Improving the strength of fully composite steel-concrete-steel beam elements by increased surface roughness-An experimental study. Engineering Structures 2002; 24(10):1349-1355.

Subedi NK. Double skin steel/concrete composite beam elements: experimental testing. The Structural Engineer 2003; 81(21):30-35.

Sun BJ. Shear resistance of Steel-Concrete-Steel beams. Journal of Constructional Steel Research 1998; 46 (1-3): 225.

Swamy RN, Jojagha AH. Impact resistance of steel fibre reinforced lightweight concrete. The international Journal of Cement Composite and Lightweight Concrete 1982; 4(4):209-220.

Thabet A, Haldane D. Three-dimensional numerical simulation of the behavior of standard concrete test specimens when subjected to impact loading. Computers and Structures 2001:79:21-31.

Thevendran V, Chen S, Shanmugam NE, Liew JYR. Nonlinear analysis of steel-concrete composite beams curved in plan. Finite Element in Analysis and Design 1999; 32(3):125–139.

Timoshenko S. Zur Frage Nach Der Wirkung Eines Stosses Auf Einen Balken. Z. Math. Phys 1913; 62:198-209.

Timoshenko SP, Goodier JN. Theory of elasticity. New York : McGraw-Hill. 1970.

Timoshenko S, Woinowsky-Krieger S. Theory of plates and shells. McGraw-Hill, New York; 1969.

Tomlinson M, Tomlinson A, Chapman M., Wright HD, Jefferson AD. Shell composite construction for shallow draft immersed tube tunnels. ICE International Conference on Immersed Tube Tunnel Techniques, Manchester, UK, April 1989.

Turk MH, Hoo Fatt MS. Localized damage response of composite sandwich plates. Composites Part B: Engineering 1999;30(2):157–165

US Dept. of the Army. Structures to resist the effects of accidental explosions. Technical manual 5-1300, Washington, DC; 1990.

Vincent LW. Functionally-graded cementitious panel for high-velocity small projectile. M.Eng. Thesis, National University of Singapore, Singapore. 2008.

Wang GH, Arita K, Liu D. Behavior of a double hull in a variety of stranding or collision scenarios. Marine Structures 2000;13(3):147–187.

Whirley RG, Engelmann BE. Slidesurfaces with adaptive new definitions (SAND) for transient analysis. New Methods in Transient Analysis, PVP-V246 / AMD-V143, ASME, New York. 1992.

Wright HD, Oduyemi TOS, Evans HR. The experimental behaviour of double skin composite elements. Journal of constructional Steel Research 1991; 19(2):97-110.

Wright HD, Oduyemi TOS, Evans HR. The design of double skin composite elements. Journal of Constructional Steel Research 1991; 19(2):111–132.

Xie M, Chapman JC. Development in sandwich construction. Journal of Construct-ional steel research 2006; 62(11):1123-1133.

Xie M, Foundoukos N, Chapman JC. Static tests on Steel–Concrete–Steel sandwich beams. Journal of Constructional steel research 2007; 63(6):735-750.

Yang SH, Sun CT. Indentation law for composite laminates. Composite Materials: Testing and Design (Sixth Conference), ASTM STP 787, I.M. Daniel Ed., American Society for Testing Materials, 1982: 425-449.

Zhao XL, Grzebieta RH. Void-filled SHS beams subjected to large deformation cyclic bending. J Struct Eng, ASCE 1999;125(9):1020-7.

Zhao XL, Grzebieta RH, Lee C. Void filled cold-formed RHS braces subjected to large deformation cyclic axial loading. J Struct Eng, ASCE 2002;128(6):746-53.

Zhao XL, Han LH. Double skin composite construction. Progress in Structural Engineering and Materials 2006; 8(3):93–102.

Zhou DW, Strong WJ. Low velocity impact denting of HSSA lightweight sandwich panel. International Journal of Mechanical Sciences 2006; 48(10):1031-1045.

Zollo RF. Fiber-reinforced Concrete: an overview after 30 Years of Development. Cement and concrete Composites 1997; 19(2):107-122.

Appendix A

A. 1 Static test for SCS sandwich slabs

SCS sandwich slab specimens same as slabs described in Chapter 6 were constructed for static test to obtain the load-deflection curves for impact analysis.

A.1.1 Sandwich slab specimens

A total of eight two SCS sandwich square slabs were cast and cured under laboratory conditions. All of the test slabs were same edge lengths 1200 mm, and had the core thickness 80 to 100 mm. All panels were fabricated with J-hook shear connectors. The diameter of J-hook connectors was 10 mm for six specimens and others contained 12 mm diameter connectors. The spacing of the connectors in both directions was 100 mm for all specimens. Lightweight concrete (density $\leq$ 1450 kg/m^3) with 1% of volume fraction of fibres (Dramix® RC-80/30-BP) were used as core material for three specimens. Plain light weight concrete (density $\leq$ 1420 kg/m^3) was used for one specimen. Ordinary Portland cement and expanded clay type of lightweight aggregate (LWA) (coarse and fine) with average particle density of 1000 kg/m^3 were used to produce the ultra lightweight concrete. The maximum size of the LWA was 8 mm. The remaining four specimens were casted with normal weight concrete (NWC) or normal weight concrete with fibres (NWFC). The details of the test specimens are

given in the Table A.1. The compressive strength of concrete was obtained by testing 100 mm dia and 200 mm long cylinders.

A.1.2 Experimental set-up

The experimental set-up is shown in Fig. A.1. The slab was simply supported on all four sides and subjected to a central concentrated load produced by a servo controlled Instron hydraulic actuator of capacity 2000 kN under displacement control mode. The loading area was 100 mm × 100 mm. All four support lines were 100 mm from the slab edges, so the effective span of the slab in both directions was 1000 mm. The central concentrated load was applied at increments of 0.1 mm/ min.

The applied load was measured using a calibrated load cell that was placed below the loading jack. The deflections at different positions were measured by linear displacement transducers which can measure maximum displacements ranged from 100 mm to 200 mm. The slip between bottom steel plate and concrete at each edge was measured by a displacement transducer. The strains of bottom steel plate were measured by strain gauges. The concrete core was painted white with a limewater mixture to enable the visual observation of the cracks in the concrete.

Prior to the application of any load on the specimen, all transducers and load cell were connected to a computer via data logger that recorded all data during testing. Load cell and transducer readings were monitored at each increment of loading and they were recorded in the computer. The load versus central slab deflection was monitored online to trace the progressive failure of the test specimens. Close observation was made to locate the loads associated with first crack and first yielding in the slab. The maximum

test load and the mode of failure for each specimen were recorded and the progressive cracking in the concrete were marked.

A. 2 Experimental results and observations

The test results for eight SCS sandwich slabs subjected to centrally concentrated load are given in Table A.2 and Fig. A.2.

The cracking could not be observed during the test for the SCS sandwich slab specimens because of the presence of steel face plates. A loud noise was heard when the maximum punching load was reached or flexural cracking of concrete core. In the post yield region, loud noise also occurred due to J-hook connector shear failure.

The load-deflections curves are given in Fig. A.2. In case of sandwich with normal weight concrete as the concentrated load increased, the tangent stiffness reduced until the load suddenly decreased with the occurrence of a local punching-shear failure within the concrete core around the loaded perimeter. After core punching failure, the SCS sandwich slabs were still able to take load due to the presence of steel face plates. The post punching (concrete punching) behaviour was dependent on thickness of the steel face plates and J–hook connectors' capacity. Due to membrane action of the steel plates, load was increasing with deflection. Slab SCS4-100 experienced steel plate punch at the same time of concrete core punching failure. For this reason the membrane cannot be developed and the load continuously going downward with displacement as seen in Fig. A.2(b).

In case of lightweight core, after yielding the load increasing due to membrane action of the steel plates and J-hook connectors. There was no significant reduction in load carrying capacity after yielding. This implied that flexural failure was governed over punching failure.

A3. Unit moment ca SCS sandwich slabs

For SCS sandwich slabs, the flexural capacity of the slab can be evaluated using the yield line theory. Fig. A.3 shows the fracture pattern of yield lines in a square slab, simply supported at four edges and subjected to a concentrated patch load. From the virtual work principle, the flexural capacity of the slab may be evaluated using the equation proposed by Rankin and Long (1987)

$$F_p = 8m_{pl}\left(\frac{L_s}{L-c} - 0.172\right)$$ as given in Eq. (6.16)

where m_{pl} is the plastic moment capacity per unit length along the yield line, c is the side length of the loading area, L_s is the dimension of the slab specimen; L is the span between the supports.

The plastic moment resistance of a fully composite SCS sandwich section can be determined by assuming a rectangular plastic stress block of depth x_c for the concrete as described in Chapter 3 (section 3.3.1.2**).** Normally, the number of welded J-hook connectors in the top and bottom plates is equal. If the two face plates are of the same thickness and strength, the value of 'x_c' in Eq. (3.16) should be taken as zero. Letting $t_c = t_t = t$ and the equation of moment capacity of the sandwich section of width '*XY*' in Fig. A.3 is from Eq. (3.16) as

$$M_{pl} = N_t\left(h_c + t\right) \qquad \text{(A1)}$$

Now consider a square SCS sandwich slab containing n_t pairs of J-hook shear connectors attached to the top and bottom plate as shown in Fig. A.3, the total number of J-hook connector in the bottom plate of a quarter section (XYZ) of the slab is $n_t/4$. For each yield line in the quarter section, the number J-hook connector is $n_t/8$. Therefore, the tensile or compressive force in the face plate along the yield line '*XY*' is

$$N_t = \frac{1}{8} n_t (P_R) \tag{A3}$$

Therefore, total moment capacity of the line '*XY*' is as following

$$M_{pl} = \frac{1}{8} n_t (P_R)\left(h_c + t\right) \tag{A4}$$

and the moment per unit width along the yield line is

$$m_{pl} = M_{pl} / l \tag{A5}$$

in which $l = L_s/(2\cos\theta)$. Substituting Eq. (A5) into Eq.(6.16), the load carrying capacity of the SCS slab for point load can be determined.

Table A.1 Properties of the SCS sandwich slab specimens for static test

Specimen ref.	t_s (mm)	d_j (mm)	h_c (mm)	Concrete type	f_c (MPa)	σ_y (MPa)
SCS4-100	4	10	100	NC	57.2	275.5
SCS6-100	6	10	100	NC	57.2	315.0
SLCS6-80	6	10	80	LC	27.0	315.0
SLFCS6-80	6	10	80	LFC	28.5	315.0
SLFCS6-100	6	10	100	LFC	28.5	315.0
SLFCS6-100(12)	6	12	100	LFC	28.5	315.0
SCFS6-100	6	10	100	NCF	59.0	315.0
SCFS8-100(12)	8	12	100	NCF	59.0	355.0

d_j = diameter of J-hook connector; NC = Normal weight concrete; LC = Lightweight concrete; NCF = Normal weight concrete with fibre; LFC = Lightweight concrete with fibre; t_s=steel face plate thickness, h_c= core thickness; S = spacing of J-hook connector; f_c = concrete cylinder strength; σ_y = yield strength of steel plate

Table A.2 Results of static test on SCS sandwich slabs

Specimen ref.	F_{cr} (kN)	F_u (kN)	w_e (mm)	F_{60} (kN)	Failure mode
SCS4-100	310	517.9	6.4	273.0	Punching-shear
SCS6-100	300	620.4	7.1	724.1	Punching-shear
SLCS6-80	150	252.2	4.1	465.5	Flexural
SLFCS6-80	184	302.4	5.5	529.3	Flexural
SLFCS6-100	213	363.9	6.0	600.1	Flexural
SLFCS6-100(12)	235	453.8	7.0	611.2	Flexural
SCFS6-100	325	728.8	8.7	740.2	Punching-shear
SCFS8-100(12)	550	891.7	8.5	863.9	Punching-shear

F_{cr}= Cracking load, F_u = experimental failure load, F_{60} = load at 60 mm deflection, w_e= central deflection at F_u

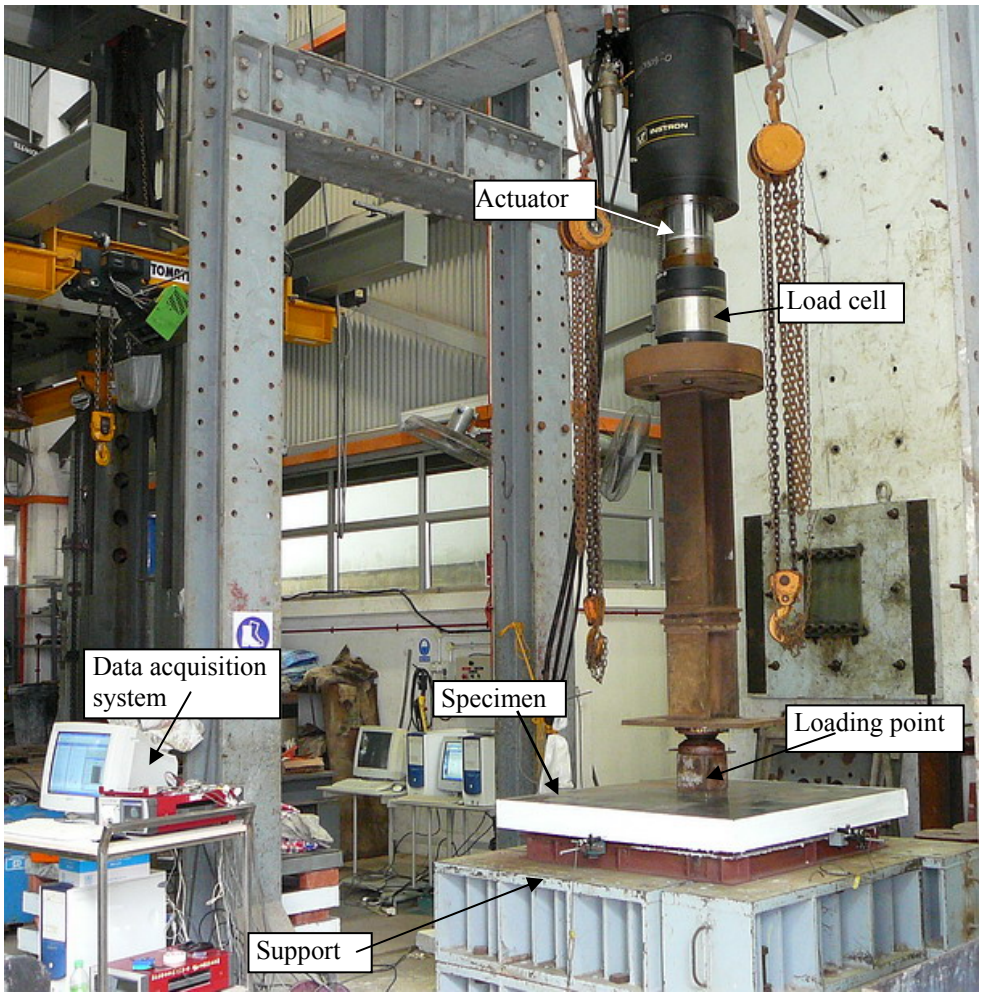

Fig. A.1 Static test set-up for SCS sandwich slabs

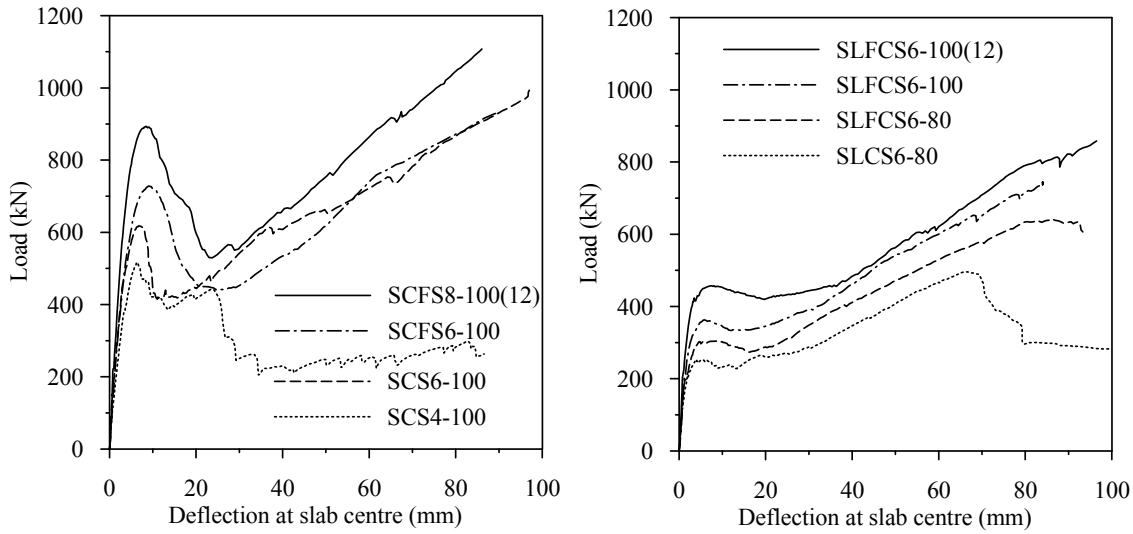

Fig. A.2 Experimental load-deflection curves: (a) sandwich slabs with light weight concrete core and (b) sandwich slabs with normal weight concrete core.

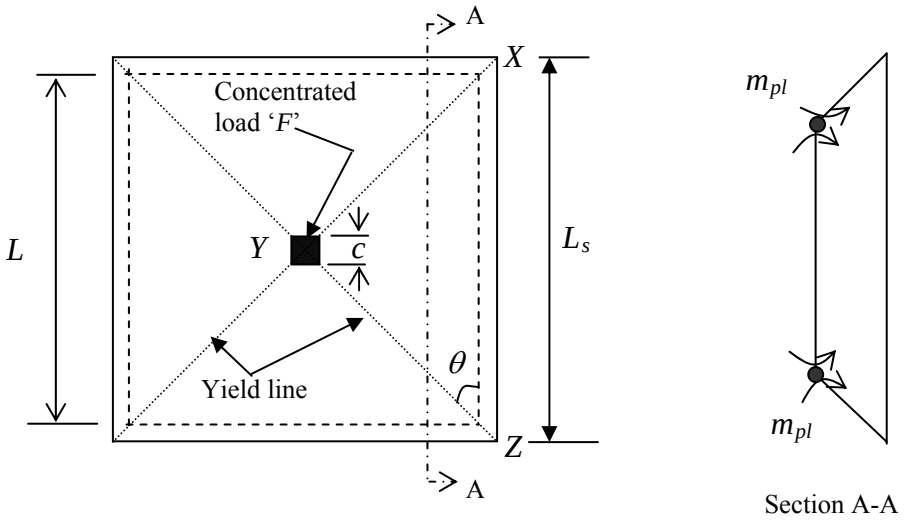

Fig. A.3 Yield-line mechanism of sandwich slab subjected to concentrated mid-point load

Appendix B

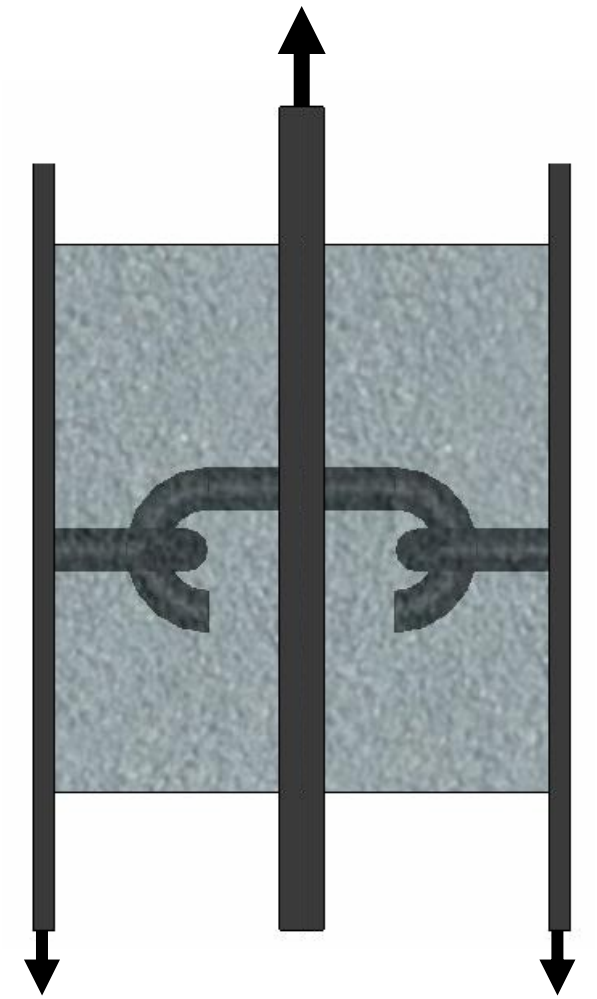

Fig. B.1 Modified push-out test set-up for J-hook connectors

Publications

Journal papers

Liew JYR, Sohel KMA. Lightweight Steel-Concrete-Steel Sandwich System with J-hook Connectors. Engineering Structures 2009, Vol. 31(5), pp. 1166-1178 .

Liew JYR, Sohel KMA, Koh CG. Impact tests on steel-concrete-steel sandwich beams with lightweight concrete core. Engineering Structures 2009. Aavailable in online.

Liew JYR, Sohel KMA. Structural Performance of Steel-Concrete-Steel Sandwich Composite Structures. Accepted for publication in Advances in Structural Engineering 2009.

Sohel KMA, Liew JYR. Steel-Concrete-Steel Sandwich Slabs with Lightweight Core – Part 1: Static Performance. To be submitted for publication in Journal of constructional steel Research.

Sohel KMA, Liew JYR, Koh CG. Steel-Concrete-Steel Sandwich Slabs with Lightweight Core – Part 2: Impact Performance. To be submitted for publication in Journal of constructional steel Research.

Sohel KMA, Liew JYR, Koh CG. Finite element analysis of Steel-Concrete-Steel sandwich composite beams subjected to impact. To be Submitted for publication in Finite elements in Analysis and Design.

Patent

Liew JYR, Wang TY, Sohel KMA. (2008). Separation Prevention Shear Connectors for Sandwich Composite Structures. US Provisional Patent Application No. 61/047,130.

Report

Liew JYR, Sohel KMA, Dai XX, Wang TY, Chia KS, Lee SC. Steel-Concrete-steel sandwich system for marine and offshore applications. Research project report 2008. MPA/Keppel/NUS Project, Singapore.

Conference papers

JYR Liew, SC Lee and KMA Sohel. Ultra-Lightweight Steel-Concrete-Steel Sandwich Composite Panels Subjected to Impact. Proceedings of the 5th International Symposium on Steel Structures March 12-14, 2009, Seoul, Korea. P.586-593.

Sohel KMA, Liew JYR, Lee SC, Koh CG. Numerical modelling of Steel-Concrete-Steel sandwich composite beams subjected to impact. Proceedings of the Twenty-First KKCNN Symposium on Civil Engineering, October 27–28, 2008, Singapore, p.121-124.

Lee SC, Sohel KMA, Liew JYR. Numerical Simulations of Ultra-Lightweight Steel-Concrete-Steel Sandwich Composite Panels Subjected to Impact. Proceedings of the Sixth International Conference on Engineering Computational Technology: ECT2008, Athens, Greece, 2-5 September 2008.

Liew JYR, Chia KS, Sohel KMA, Xiong DX. Innovation in Composite Construction – Towards the Extreme of High Strength and Lightweight. Proceeding of the Fifth International Conference on Coupled Instabilities in Metal Structures, Vol.1, ed by K. Rasmussen and T. Wilkinson, pp.19-33. Sydney, Australia, 23-25 June, 2008.

Dai XX, Sohel KMA, Chia KS, Liew JYR. Investigation of Fiber-Reinforced lightweight aggregate concrete for steel-concrete-steel sandwich structures. 5th International Conference on Advances in Steel Structures, Singapore, 5 – 7 December 2007, p 951-958.

Sohel KMA., Liew JYR, and Koh CG. Steel-Concrete-Steel sandwich structures subject to impact loads. Proceedings of the 6th International Conference on Steel and Aluminium Structures: ICSAS'07, Oxford, UK, 24th -27th July 2007, p 506-513.

Liew JYR, Sohel KMA, Chia KS, Lee SC. Impact behavior of Lightweight Fiber-reinforced Sandwich Composites. Proceedings of the 3rd International Conference on Steel and Composite Structures (ICSCS07), Manchester, UK, 30 July - 1 August 2007, p 873-878 .

Liew JYR, Koh CG and Sohel KMA. Development of composite sandwich structures for impact resistance. Proceedings of 8th Pacific Structural Steel Conference, Wairakei, New Zealand, 13-16 March 2007, p405-410.

Sohel KMA, Liew JYR, Koh CG. Impact performance of sandwich composite structures. Proceedings of the 4th Int. Symposium on Steel Structures:ISSS'06, Seoul, Korea, 16-17 November 2006; vol. 2: 593-603.

Liew JYR, Xiong D, Sohel KMA. Innovation in Composite Construction Using High Strength Materials. Proceeding of the Second International Symposium on Advances in Steel and Composite Structures 2007.